2005

Research Experience for Undergraduates Program, 2005

University of Arkansas, Fayetteville. Dept. of Chemistry and Biochemistry

Chemistry and Biochemistry
University of Arkansas

Research Experience for Undergraduates

2005

Table of Contents

Student Participant List

University of Arkansas

Quincy Anderson - Langston University

Bruce Atwater - Gustavus Adolphus College

Garen Holman - University of Central Arkansas

Abigail Hubbard - Kent State University

John-David McElderry - Brigham Young University

Danielle Reifsnyder - Duke University

Monique Robinson - Langston University

Lauren Rogers - Western Carolina University

Nicole Vanderbush - Shorter College

Melissa Weston - Colorado State University

Jamesha Wills - Grambing State University

Moscow Exchange

Evgenia Akhmetova - Moscow State University

Timothy Paslay - University of Tulsa

Ioana Peret - University of Arkansas

Anne St. Martin - Worcester Polytechnic Institute

Vitaly Vostrikov - Moscow State University, MITHT

Research Experience for Undergraduates
University of Arkansas

The University of Arkansas Department of Chemistry and Biochemistry hosted a National Science Foundation sponsored Research Experience for Undergraduates (REU) summer program for the 17th year. The department first hosted an REU in 1959. The 10-week summer program funded by the National Science Foundation allowed students an opportunity to gain hands-on experience in a chosen research area while introducing them to careers in scientific research in areas including analytical chemistry and sensor technology, biochemistry and protein dynamics, inorganic chemistry and nanotechnology, organic chemistry, and physical and theoretical chemistry.

Undergraduate chemistry majors, who were sophomores or juniors in fall 2005, applied to the program, which took place in the Ozark Mountain Plateau.

Outside the lab, students met each week to hear presentations from campus experts about topics ranging from how to get into graduate school and test-taking skills to ethics, and how to make a poster presentation. A number of social activities took place throughout the summer to give students a chance to interact.

Selected students received a scholarship to pay for room and board and an allowance to attend a regional or national chemical conference in 2005-2006 academic year. Students involved in the program were enrolled as students at the U of A and received one hour of research credit. The program was conducted from May 22, 2005 to July 29, 2005.

Tony Jude Award

The award recognizes a student for outstanding research in memory of a former REU student Tony Jude. Jude returned to the University of Arkansas to complete his doctorate in chemistry. At the time of his death, Dr. Jude was a faculty member in biochemistry at the University of Arkansas at Little Rock.

Above: The Tony Jude Award Winner, Abigail Hubbard with REU co-director David Paul.

REU 2005 Students

Evgenia Akhmetova
From: Moscow, Russia
Moscow State University
Mentor: Wilkins

Quincy Anderson
From: Oklahoma City, Okla.
Langston University
Mentor: Greathouse

Bruce Atwater
From: Edina, Minn.
Gustavus Adolphus College
Mentor: McIntosh

Aireal Haley
From: Springdale
University of Arkansas
Mentor: Vicic

Garen Holman
From: Russellville
UCA
Mentor: Gawley

Abigail Hubbard
From: New Philadelphia, Ohio
Kent State University
Mentor: Allison

John-David McEldery
From: Jacksonville
Brigham Young University
Mentor: Tian

Danielle Reifsnyder
From: New Canaan, Conn.
Duke University
Mentor: Peng

Monique Robinson
From: Okmulgee, Okla.
Langston University
Mentor: Stites

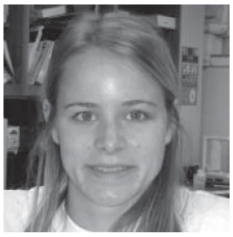

Lauren Rogers
From: Jamestown, N.C.
Western Carolina University
Mentor: Millett

Nicole Vanderbush
From: Peachtree City, Ga.
Shorter College
Mentor: Davis

Vitally Vostrikov
From: Moscow, Russia
Moscow State Academy of Fine Chemical Technology
Mentor: Paul

Melissa Weston
From: Thorton, Colo.
Colorado State University
Mentor: Fritsch

Jamesha Wills
From: Decatur, Ill.
Grambling State University
Mentor: Koeppe

REU Moscow

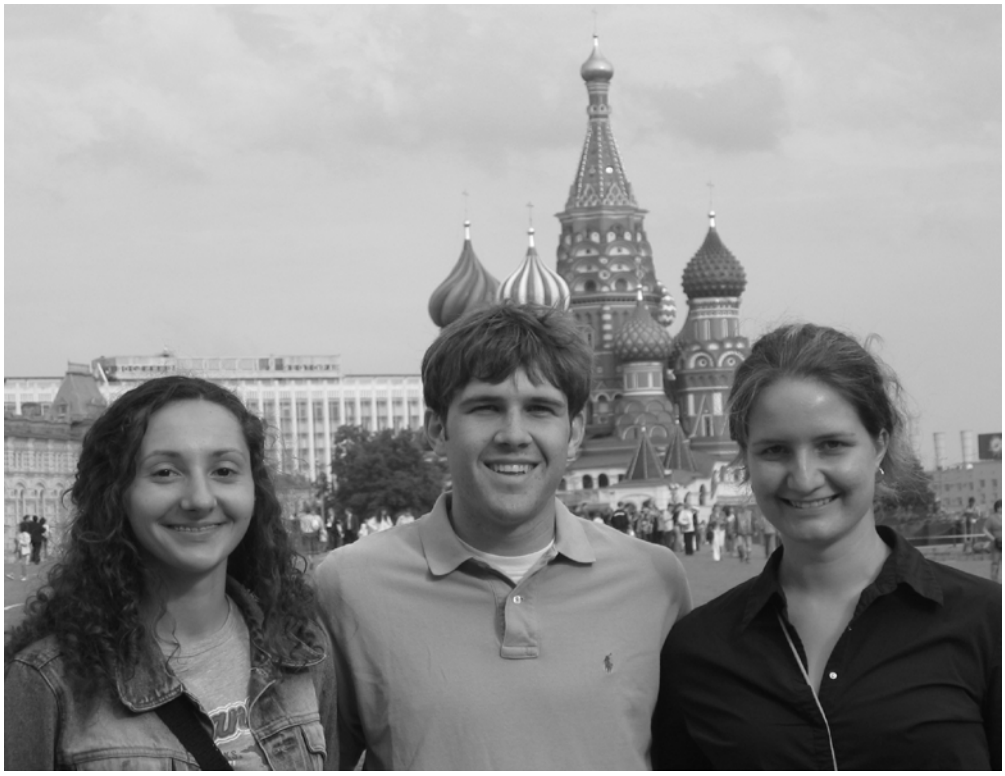

From left: Ioana Peret, Tim Paslay and Anne St. Martin

For the first time, the UA department of chemistry and biochemistry sponsored an international exchange program with Moscow State University and the Academy of Fine Chemical Technology in Moscow. The 10-week program was funded by the National Science Foundation as part of the chemistry and biochemistry Research Experience for Undergraduates program and provided students from both countries with a unique cultural and scientific experience.

Three U.S. students, Ioana Peret, Tim Paslay and Anne St. Martin, spent six weeks in Moscow where they were housed on the Moscow State University campus in the largest academic building in the world. The students were selected based on their chemistry background and interest in Russian language and culture. While the basic approach to scientific investigations is standard, differences in methodology exist, enhancing the education of students from both sides.

Peret is a UA junior chemistry major from Hot Springs. While abroad she studied organic synthesis in ionic liquids. Paslay is a 2003 graduate of Fayetteville High School and a junior at the University of Tulsa. He participated in carbon monoxide studies at both Moscow State University and Moscow State Academy of Fine Chemical Technology. St. Martin is a U.S. citizen currently living in Ottawa, Canada, and is pursuing degrees in chemistry and international studies at Worcester Polytechnic Institute. She focused her research on host-quest chemistry.

Two students from Moscow spent 10-weeks at the University of Arkansas as part of the REU in chemistry and biochemistry. Vitally Vostrikov is a fifth-year student at the Moscow State Academy of Fine Chemical Technology who was selected through a competitive process as the first exchange student from his academy to visit the U.S. since the dissolution of the Soviet Union. He measured the performance of chemical sensors for toxic gases under the direction of David Paul, associate professor and REU coordinator.

The other student was Evguenia Akhmetova, a fifth-year student at Moscow State University who worked with Distinguished Professor Charles Wilkins on developing mass spectral methods of analysis of polymer mixtures.

Faculty Project List

Neil Allison	Synthesis and Chemistry of Potential Organometallic Anticancer Drugs
Donald R. Bobbitt	Capillary Electrophoresis-based Micro-sequencing of Peptides and Proteins with "Ru(bpy)33+" Chemiluminescence Detection
Dan Davis	Protein-Protein Interactions in Photosynthesis: Structure-Function Relationships in Electron Transfer Proteins
Bill Durham	Electron-Transfer Reactions of Metalloproteins
Ingrid Fritsch	Microelectrochemical detection and microfluidics for lab-on-a-chip applications: protein, DNA, and microorganism analysis
Bob Gawley	Synthetic and Mechanistic Organ(ometall)ic Chemistry; or Chemosensors for Detection of Marine Toxins
Jim Hinton	Ultra High Magnetic Field NMR Study of Biological Channels
Roger Koeppe	Biophysical Studies of Single-Span Transmembrane Proteins and Membrane Channel Gating
Matt McIntosh	Total Synthesis of Biomedically Significant Complex Natural Products
Frank Millett	Biological Electron Transfer
David Paul	Development of Chemical Sensors for Clinical and Environmental Applications
Xiaogang Peng	Rational Synthesis and Manipulation of Colloidal Nanocrystals
Peter Pulay	Ab initio Calculation of the Vibrational and NMR Spectra of Protein Models
Joshua Sakon	Structure and function of drug-targets
Wes Stites	Exploring the influence of the denatured state upon protein stability, or Isolation, characterization, and impact upon blood clotting of human thrombomodulin in disease.
Z. Ryan Tian	Syntheses and applications of ordered and complex nanostructures
David Vicic	Synthesis, Structure and Reactivity of New Transition Metal Complexes
Charles Wilkins	Matrix-assisted Laser Desorption Fourier Transform Mass Spectrometry for Whole-Cell Bacteria and Polymer Analysis

Analysis of Poly(ethylene glycol) Mixtures by Matrix Assisted Laser Desorption/Ionization Fourier Transform Ion Cyclotron Resonance Mass Spectrometry

Eugenia Akhmetova, Moscow State University
Moscow, Russia

Abstract

The combination of matrix-assisted laser desorption/ionization (MALDI) with Fourier transform mass spectrometry (FTMS) is a powerful tool for characterizing synthetic polymers. MALDI permits the generation of intact, singly charged high-mass ions of polar and nonpolar analytes, whereas FTMS provides high resolution and mass accuracy. Once this combined technique was developed and applied to polymers and polymer blends, it became clear that optimization of experimental conditions is great interest. Two different ways to approach these problems are suggested in this research project: the first is to optimize ionization conditions by comparing different types of mass spectrometers. For this purpose, a comparison between external and internal ion source MALDI FT-ICR mass spectrometers was undertaken. The second approach involves use a new type of matrix: the ionic liquid matrix (ILM). In these studies we made a comparison with two commonly used matrices DHB and HABA. As a result of the research, it can be concluded that ion signal intensities obtained from both types of devices depends on the nature of the matrix and the matrix-to-analyte ratio and seems independent of the ion source type. There is also an obvious difference between external and internal source devices because of their different ionic molecular weight preference: in the case of the external source ions with low molecular masses are detected better than ones with high molecular mass. The opposite is true in the case of the internal source. In the three different matrices comparison experiments the considerable advantage of ionic liquid matrices was not found. The best results were obtained when the butyl amine-CHCA was used. In this case an acceptable ion signal was observed.

Introduction

Matrix assisted laser desorption/ionization (MALDI) is a relatively new soft ionization technique. This method is based on the using a solid solution of analyte molecules with a matrix which strongly absorbs laser irradiation. Figure 1 shows the MALDI ionization process details. Excitation of matrix molecules by means of a laser pulse results in the formation of a dense high-temperature plasma above the sample surface (the so-called gas phase plume [5]), containing matrix ions as well as both matrix and analyte molecules. Because the matrix absorbs mostly of the input photon energy, analyte molecules are desorbed with little fragmentation. Analyte ion formation occurs because of excited matrix-analyte interactions during the initial ionization (primary ionization). Secondary ionization is a result matrix-analyte interaction in the gas phase plume and the generated analyte ions possess moderate internal energy so their fragmentation is negligible.

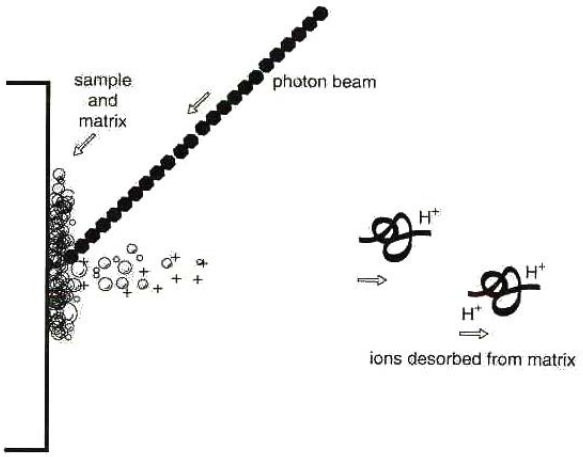

Figure 1: Ionization process in MALDI technique. Reprinted from [2]

Thus the great advantage of MALDI as a desorption/ionization method is that little or no fragmentation is observed during either desorption or ionization, and at least for lower molecular weight oligomers, only singly charged ions are observed [1, 3, 4, 5].

Fourier transform mass spectrometry (FTMS) based on ion cyclotron resonance principle. The cell, placed in a uniform magnetic field is the main element of a Fourier transform mass spectrometer. The cell can have different shapes [7] and simplest one is a cubic cell, shown in Figure 2. For magnetic field generation superconducting magnets are usually used. Ions, generated in the source, are directed to the analyzer cell and then undergo a cyclotron motion that keeps them orbiting in circular pathways that are perpendicular to the magnetic field [1, 3, 7]. The ions mass detection arises from measurement of their cyclotron frequencies which are independent of ions velocity and therefore of translational energy:

$$\nu_c = \omega_c / 2\pi = zeB / 2\pi m, \text{ or}$$

$\nu_c = 1.535611*10^7 B / (m/z)$ in which z and m are ionic mass and charge and B is the magnetic field strength [3, 7]. The exceptionally high resolving capabilities of this method results from the ability to trap and observe ions for long enough periods to measure their frequencies with extremely high accuracy.

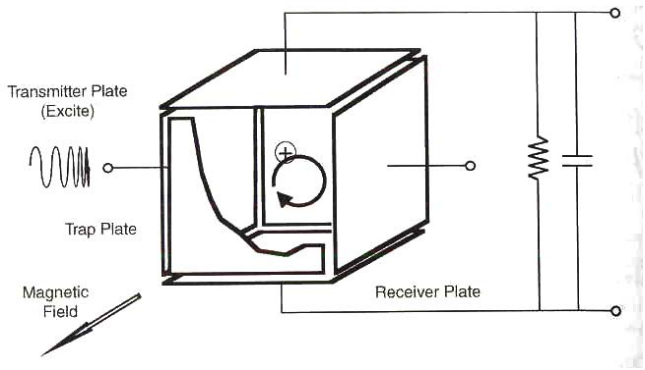

Figure 2: Diagram of FTMS cubic cell showing electrodes. Reprinted from [1]

The ions are trapped in the cell by means of electrostatic potentials applied to trapping plates on opposite ends of analyzing cell – positive potentials to trap positive ions and negative potentials to trap negative ions. The combination of magnetic and electrostatic fields creates three-dimensional

trap which can hold the ions during a long enough time to provide high accuracy measurements [3]. For analysis, a frequency-swept excitation is applied to transmission plates on opposite sides of the cell. As the orbiting ions become in phase with the applied excitation, they absorb the energy and accelerate to higher overall radii. The phase-coherent ion packets then induce an image current onto all plates, including the oppositely positioned detection plates. A sinusoidal image current is produced that exactly matches the frequency characteristics of the ions. Then the image current signal is amplified and digitized, followed by Fourier transformation to yield the individual ion frequencies that comprise the signal [1]. An additional advantage of this method is that it is nondestructive [1].

The combination of the MALDI ionization technique with FTMS is a powerful tool in characterizing different synthetic polymers. As described above, the main advantages of MALDI for polymer analysis are the limited fragmentation of ions, the formation almost exclusively of singly-charged ions and the ability to analyze polymers with high molecular weight (e.g. 10,000-15,000 daltons). Thus, the MALDI mass spectra are interpretable even if the polymer consists of a large number of oligomers with different masses [9]. An additional advantage is the recent development of MALDI methods that work with insoluble polymers [8, see references]. It was shown in different reviews [4, 6, 8], that MALDI is one the most popular ionization methods for polymer studies and that different problems can be solved: molecular weight measurements, end group determination, fragmentation investigations, copolymers and polymer blends studies. FT ICR-MS also has many advantages over conventional mass spectrometric techniques. For polymer studies, the most relevant advantages are high mass accuracy and high mass resolving power. This high mass accuracy can be used in determining the presence of impurities and specifically allows for the determination of end group functionality [11].

Once this method was developed and applied to synthetic polymers, the problem of optimization experiment conditions became in the focus of attention. The choice of matrix is critical to the success of polymer MALDI analysis, because the final role of the matrix is to provide a suitable ionization pathway for the polymer oligomers. The matrix also serves to minimize sample damage from the laser radiation by absorbing most of the incident energy. It is also believed that matrix promotes the ionization process [1, 3, 4]. It is easy to determine whether a potential matrix will absorb the laser wavelength efficiently. However, it is rather difficult to predict the formation of a homogeneous matrix-to-analyte mixture in the solid phase. That means that matrix selection and optimization for polymers is still often a trial and error process.

Within the limits of this project, two possible ways to solve this problem are suggested. The first approach uses a new type of matrix: the ionic liquid matrix (ILM). Ionic liquid matrices completely fulfill the MALDI-matrix requirements: electronic absorption at the employed laser wavelength, good vacuum stability and low vapor pressure. Moreover, in comparison with commonly used matrices (usually weak organic acids are used, such as 2,5-dihydroxybenzoic acid (DHB) and 2-(4-hydroxyphenylazo)benzoic acid (HABA)) they have obvious advantages. For example, a solvent is not required because ionic liquids are very good solvents by themselves for wide variety of substances, including polymers. Their acidity can be easily modified, which can be quite useful when MALDI experiments are carried out. Ionic liquids can also stabilize compounds, which are unstable in the usual molecular solvents. All these factors make ionic liquids very attractive to use as matrices for polymer MALDI analysis. It should be noted that in the literature applications ILMs to biopolymer mass-spectrometry analysis is described: specifically, the DNA were investigated [13], as well as proteins, peptides and oligodeoxynucleotides[14, 15, 16, 17]. However, there are only a few examples of similar polymer investigations [14]. The work described here was directed to comparisons well-known matrices like DHB and HABA with the new type of ionic liquid matrix discussed above.

Another way to improve MALDI-FTMS experiments is an optimization of sample ionization conditions. There are two types of ion sources, used in FT-ICR instruments – with external and internal ionization. External ionization (Figure 3) is observed when the ionization occurs away from the analyzer cell. Ions generated in this process must be transferred to the analyzer cell for the further detection. The advantage of this method is a possibility of tuning instrumental parameters independently, thus permitting optimization of the ion formation and detection events separately. Thereby, definite flexibility of the experiment is achieved. The disadvantage of this method is that the ions can undergo some unwanted fragmentation, such as water and amine losses [1, 3, 7].

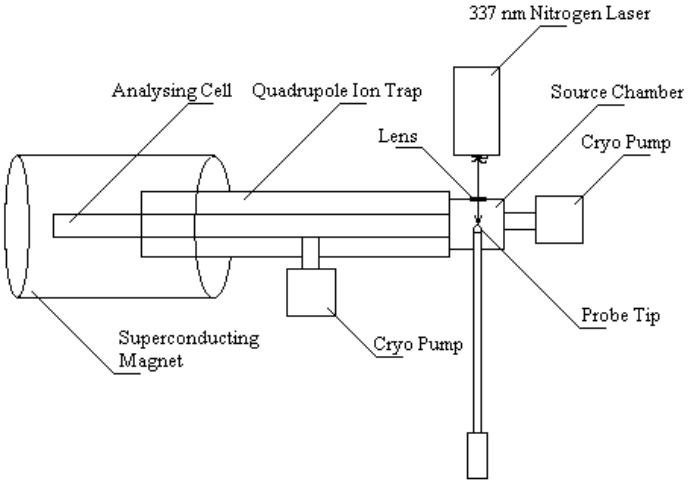

Figure 3: Block diagram for 3T Fourier transform external type ionization mass spectrometer

Internal ionization (Figure 4) occurs when the ions are generated directly in front of the analyzer cell. The main advantage of this technique is that ions can be detected very quickly, reducing the metastable decays observed in external ionization [1, 7].

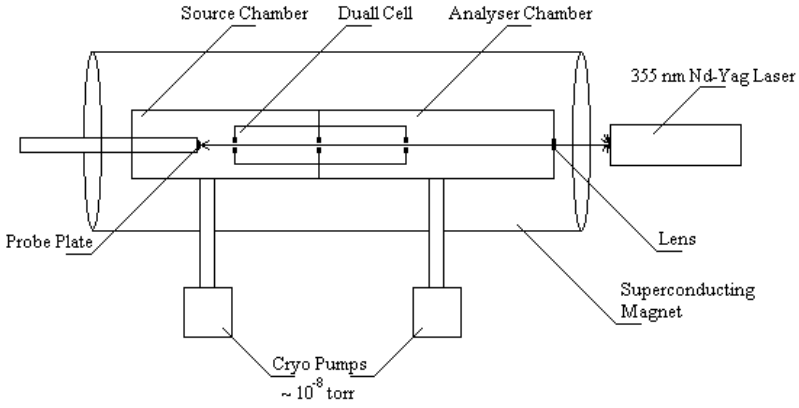

Figure 4: Block diagram for 7T Fourier transform internal type ionization mass spectrometer

The disadvantages of this technique are that the internal alignment of the lasers and the accumulation of matrix must be done the within magnetic field [1]. In our research, a comparison between external and internal ion source devices was undertaken.

Experimental Procedures

Chemicals

Polyethylene glycol (PEG) samples: PEG 1000, PEG 1500 and PEG 2000 were obtained from Fluka Chemicals (Buchs, Switzerland). The numbers in the names denote the average molecular weight of the sample. All samples were used without further purification. Matrix material substances 2,5-Dihydroxybenzoic acid (DHB) was obtained from Fluka Chemicals Co. (Buchs, Switzerland) and 2-(4-hydroxyphenylazo)benzoic acid (HABA) was obtained from Aldrich Chemical Co. (Milwaukee, WI). Ionic liquid matrices aniline-α-cyano-4-hydroxycinnamic acid (CHCA), diethyl aniline-CHCA and butyl amine-CHCA were synthesized in our laboratory with using preparation procedure described in [14] and were used without purification after the synthesis. Tetrahydrofuran (THF) was obtained from J.T. Baker and methanol from EM Science.

Sample preparation

THF was used as a solvent for the preparation of 0.5 M solution of HABA matrix, DHB was prepared as a 2.0 M solution in MeOH:H2O (90:10) mixture. A 0.005 M solution of each polymer was obtained by dissolving polymers in MeOH and then equimolar polymer mixture (1000, 1500, 2000) was prepared. For different matrix comparisons, samples were prepared with the same 400:1:1:1 molar ratio (matrix-to-analyte) by mixing DHB, HABA and IL matrices and polymer mixture solutions. For the different source type device comparison, samples were prepared with 400:1:1:1, 800:1:1:1, 2000:1:1:1, 4000:1:1:1 and 40000:1:1:1 molar ratios by mixing DHB and HABA matrices with polymer mixture solutions. Samples for the 7.2 Tesla FTMS were mixed and ~1.0 ml each was aerosprayed onto stainless steel probe plates uniformly to ensure homogeneity of the samples. Samples run on the 3.4Tesla FTMS were mixed and ~ 1.5-2.0 µl of each micro-pipetted onto the probe tip.

MALDI FTMS instrumentation

MALDI experiments with an internal ionization source were carried out using a 7.2 Tesla (Oxford Instrument, UK) Fourier transform mass-spectrometer equipped with a pulsed Nd-YAG laser operating at wavelength of 355 nm and a power of approximately 950 µJ. Each spectrum was taken using 20 individual transients. Experiments with external ionization source were run on a 3.4 Tesla (IonSpec, Lake Forest, CA) Fourier transform mass-spectrometer, equipped with a nitrogen laser operating at a wavelength of 337 nm and with full power >300 µJ. All spectra from the external source FTMS are result from a single laser shot and all detection was done in positive ion mode and 128K data points were collected at the rate of 2MHz.

Results and Discussion

In order to make a comparison between the internal and external ionization sources, the spectra must be normalized to a common scale factor. The amplitudes of the most abundant base peaks and scale factors for the spectra were recorded. Corrections are made based on the difference in the number of transients taken by the 3.4T and 7.2T FTMS, which are one and twenty, respectively. The 3.4T amplitudes were multiplied by the square root of 20 (because of different analyzing cell geometry: in 3.4T analyzing cell is cylindrical and in 7.2T it is cubic). The highest value for the corrected amplitudes was set at 1.00 and all other values were set as their proportional ratio. The recorded scale factors for each were multiplied by the corresponding ratio, which provides an "accepted" scale factor. This new scale was applied and graphs provided represent the overlaid spectra, and comparisons of observations can be made.

The following figures contain MALDI-FTMS spectra obtained with an equimolar mixture of PEG (1000, 1500, 2000) and with various matrix-to-analyte molar ratios. All experimental conditions with the exception of the difference in ratios were kept constant. In figure 5, the spectra from the PEG mix and DHB show distributions containing the same ions, but there is a clear distinction between the 3.4T and 7.2T results. The external ionization source discriminates against the high molecular weight ions, and the ion signal intensity of the 7.2T internal source is much higher than that of the 3.4T FTMS. With the internal source, there is also an apparent shift from high to low molecular weight distribution and an overall decrease in the observed intensities as the molar ratios are increased from 400:1:1:1 to 40000:1:1:1. Furthermore, if the detection of high molecular weights is desired, than a 400:1:1:1 ratio might be optimal and if the lower molecular weight ions are preferred, then a higher molar ratio might suffice. This trend is not observed so readily in the spectra from the external ionization source because no distinction between the intensities of either higher or lower MW ions is observed.

In Figure 6, the spectra from the PEG mix and HABA matrix show differences in the distributions, but the same molecular ions are obtained from both the internal and external ionization sources. The HABA matrix allows for large differences between the molecular weight ranges of the highest intensity peaks. The external source clearly favors the lower molecular ions and the peak intensities are greatest from the range of 1000-1700 m/z. In contrast, the internal source ions are generated at a higher range with the greatest intensity from 2000-2500 m/z. Unlike the spectra with the DHB, the graphs from the PEG mix and HABA as the matrix do not show a shift in molecular weights of the detected ions as the molar ratios are increased. The external source FTMS provides higher signal intensities when using HABA as a matrix rather than DHB. By looking at the 400:1:1:1 and 800:1:1:1 molar ratios, the spectra clearly shows that equivalent intensities are observed between the internal and external ionization sources but in contrasting m/z ranges. In addition, the 3.4T FTMS detected a larger amount of ions than the 7.2T when using HABA with at high molar ratios. This is not the case when DHB was used as a matrix because there is no substantial difference in the number of ions detected in the 4000:1:1:1 or 40000:1:1:1 spectra.

A comparison between different matrices using the 3.2T FTMS was also examined in this experiment. Figure 7 shows the overlaid spectra of DHB, HABA, and the ionic liquid matrices which were adjusted to have the same scale factors. The same molecular ions are present in each of the matrices, but the HABA and DHB have higher intensities. With the aniline-CHCA and diethyl aniline-CHCA matrices, there is a lower intensity of ions detected and from the shape of the distributions; one observes that there is no preference given to either high or low end molecular ions. On the contrary, the butyl amine-CHCA matrix shows comparable intensities and molecular weight distribution with that of the DHB matrix.

Conclusions

The comparison procedure between two different ion source type MALDI FT ICR mass spectrometers was developed and applied to two experiment series using different matrices. It can be concluded from the results of the comparison conducted that in case when the DHB matrix was used, the signal intensity of the 7.2T internal source is much higher than that of the 3.4T FTMS for the high molecular weight ions. The optimal molar matrix-to-analyte ratio if the detection of these ions is desired was also ascertained.

When the HABA was used as a matrix the higher molecular weight ions preference was also shown in case of internal source device. But the essential distinction between experiments with two different matrices is that external source experiment with HABA clearly favors the lower molecular

ions but that the different instrument intensities were comparable. In the three different matrix comparison experiments no considerable advantage for ionic liquid matrices was found. The best result was obtained when the butyl amine-CHCA was used: in this case an acceptable ion signal was observed.

Acknowledgments

I would like to gratefully acknowledge Dr. Anthony Maksimov, Prof. Edward Karakhanov and Prof. Valery Lunin for offer me to join this summer research program, Prof. David Paul, Prof. Anatoly Ishchenko for my trip organization and help, Prof. Charles Wilkins and members of his research group for support and patience during all my work. My participation in this program was financially provided by National Science Foundation (special international supplement to grant number US/NSF/CHE-0243978/REU) and Department of Chemistry and Biochemistry at the University of Arkansas.

References

1. Montaudo, G.; Lattimer, R. *Mass Spectrometry of Polymers.* CRC Press LLC: Florida, **2002**.
2. Siuzdak, G. *Mass Spectrometry for Biotechnology.* Academic Press, Inc.: California, **1996**.
3. Lebedev, A. *Mass Spectrometry for Organic Chemistry.* Binom: Moscow, **2003**.
4. Hanton, S. *Chemical Reviews.* **2001**. 101, 527-569.
5. Dreisewerd, K. *Chemical Reviews.* **2003**. 103, 395-425.
6. Nielen, M. *Mass Spectrometry Reviews*. **1999**. 18, 309-344.
7. Marshall, A.; Hendrickson, C.; Jackson, G. *Mass Spectrometry Reviews*. **1998**. 17, 1-35.
8. McEwen, C.; Peacock, P. *Analytical Chemistry.* **2002**. 74, 2743-2748.
9. Dey, M.; Castoro, J.; Wilkins, C. *Analytical Chemistry.* **1995**. 67, 1575-1579.
10. Maziarz, E.; Baker, G.; Lorenz, S.; Wood, T. *Journal of American Society for Mass Spectrometry.* **1999**. 10, 1298-1304.
11. Koster, S.; Duursma, M.; Boon, J.; Heeren, R. *Journal of American Society for Mass Spectrometry.* **2000**. 11, 536-543.
12. Pastor, S.; Wilkins, C. *Journal of American Society for Mass Spectrometry.* **1997**. 8, 225-233.
13. Carda-Broch, S.; Berthod, A.; Armstrong, D. *Rapid Communications in Mass Spectrometry.* **2003**. 17, 553-560.
14. Armstrong, D.; Zhang, L.; He, L.; Gross, M. *Analytical Chemistry.* **2001**. 73, 3679-3686.
15. Mank, M.; Stahl, B.; Boehm, G. *Analytical Chemistry.* **2004**. 76, 2938-2950.
16. Zabet-Moghaddam, M.; Heinzle, E.; Tholey, A. *Rapid Communications in Mass Spectrometry.* **2004**. 18, 141-148.
17. Li, Y.; Gross, M. *Journal of American Society for Mass Spectrometry.* **2004**. 15, 1833-1837.

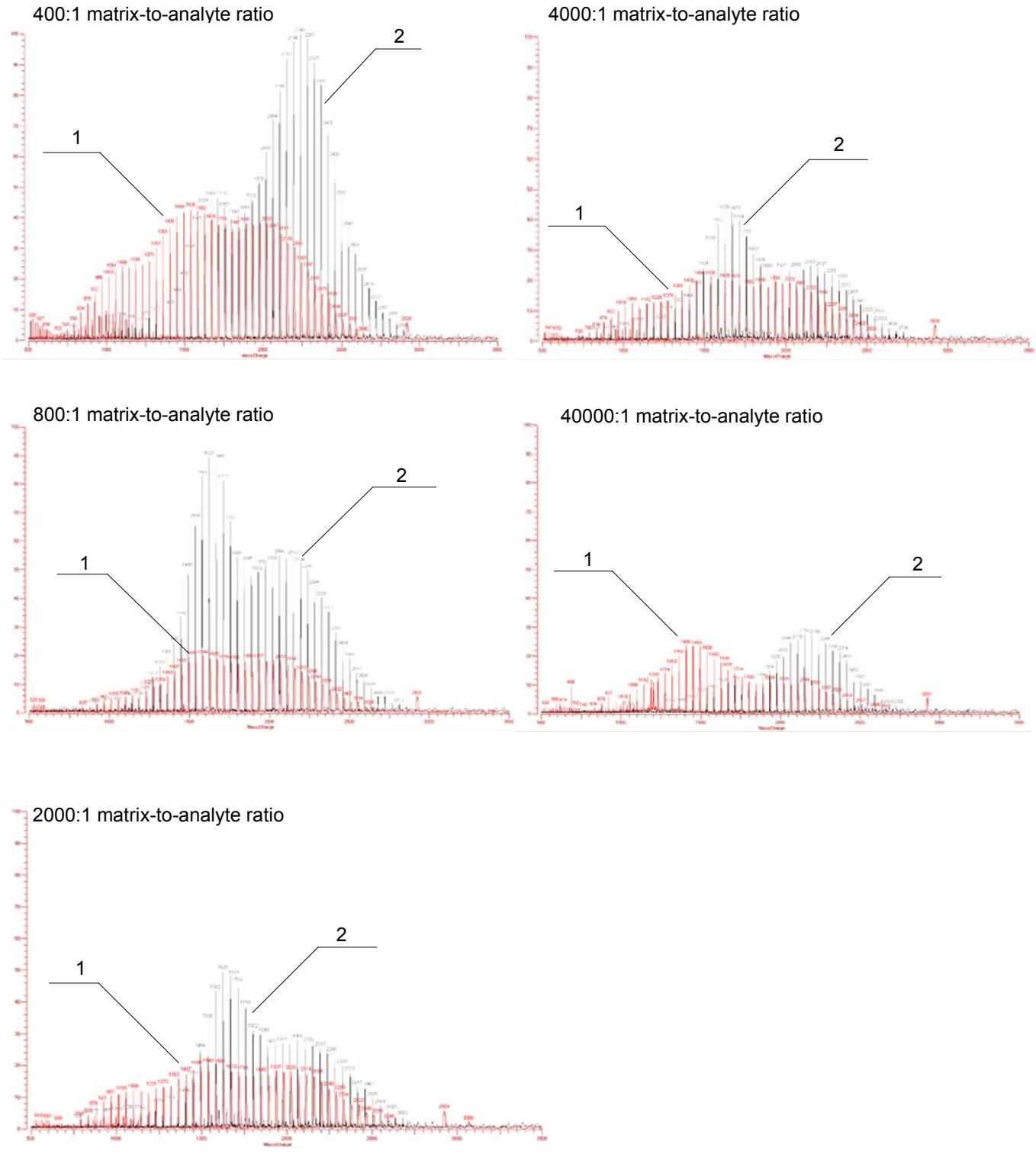

Figure 5: Comparison of 3T (1) and 7T (2) FTMS 2M DHB and 0.005M PEG mixture (1000, 1500, 2000)

400:1 matrix-to-analyte ratio

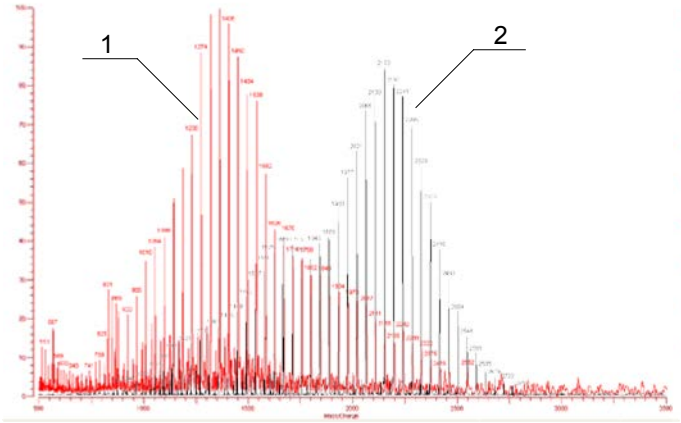

40000:1 matrix-to-analyte ratio

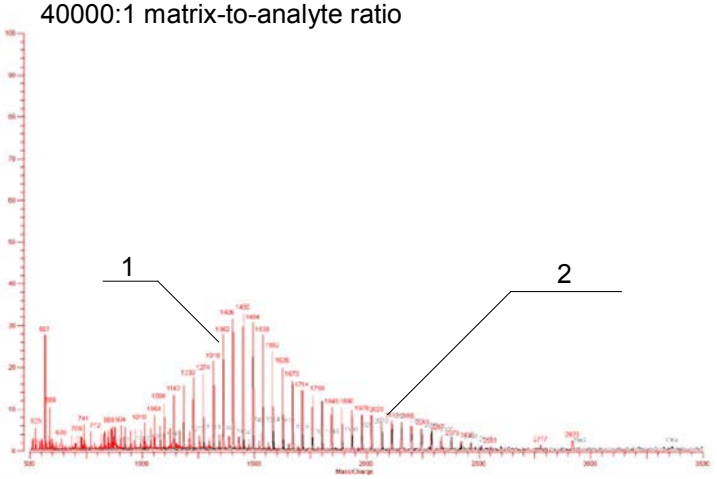

800:1 matrix-to-analyte

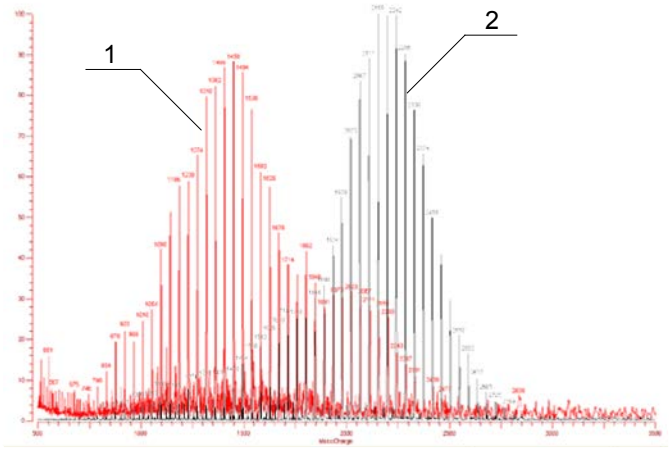

4000:1 matrix-to-analyte

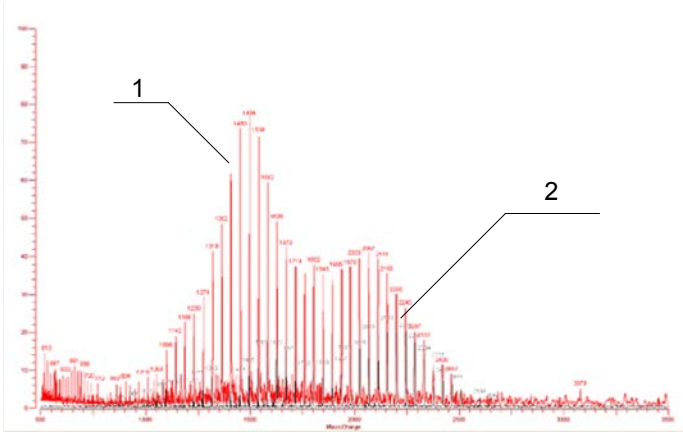

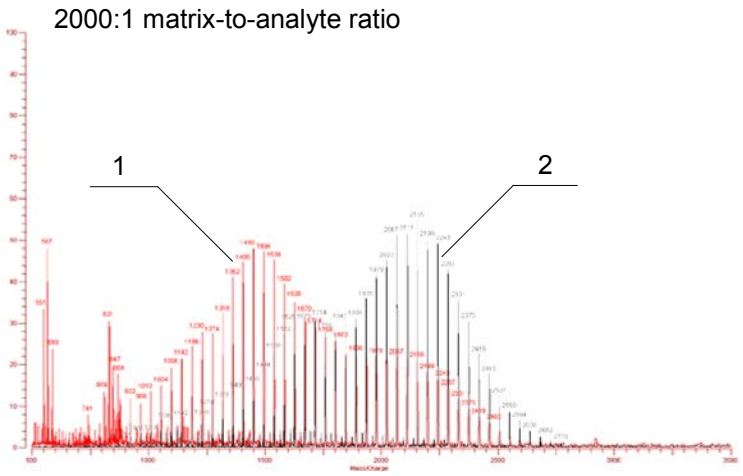

Figure 6: Comparison of 3T (1) and 7T (2) FTMS 0.5M HABA and 0.005M PEG mixture

(1000, 1500, 2000)

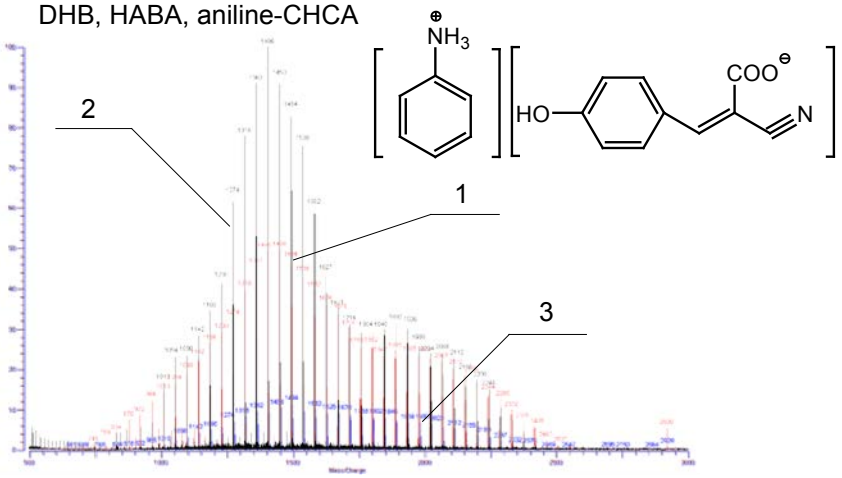

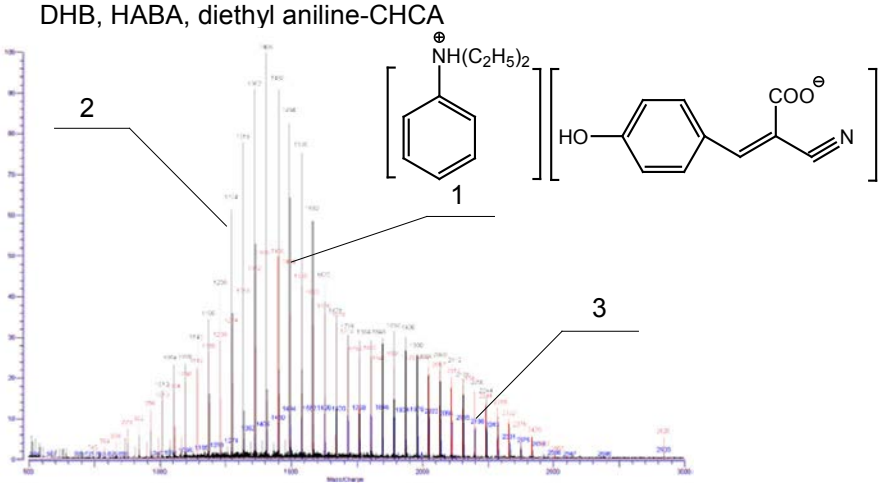

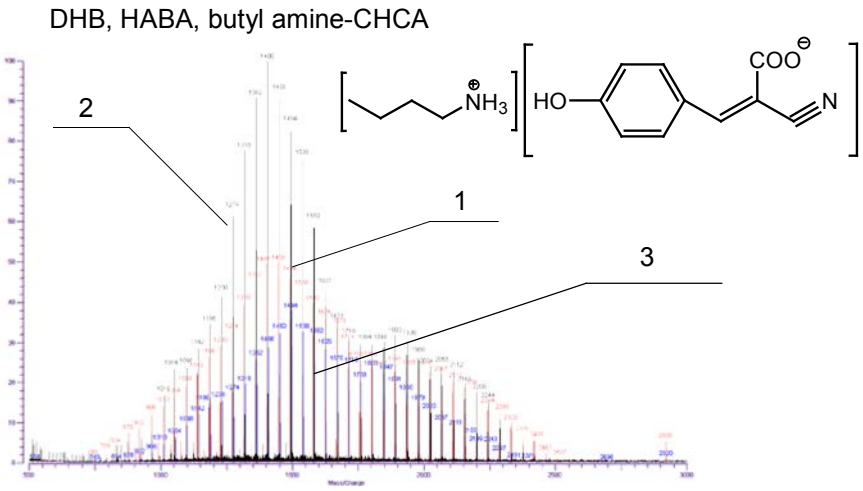

Figure 7: Comparison of 2.0M DHB (1), 0.5M HABA (2) and three ionic liquid matrices (3) used in 3.2T PEG mixture (1000, 1500, 2000) analysis

Synthesis and Comparison of Thiol vs. Non-Thiol Cleavages of Bovine Lactoferricin Peptides

Quincy Anderson, Langston University
Langston, Oklahoma

Abstract

With the increase in multidrug resistant bacteria there is a need to understand the properties of natural occurring antimicrobial peptides. Antimicrobial peptides are future candidates for newly made antibiotics. Lactoferricin Bovine (20-25), an antimicrobial hexapeptide, is believed to exert its effect directly on bacterial cellular membrane lipids. In order to learn more about these interactions three derivatives of Lactoferricin B were synthesized by Solid Phase Peptide Synthesis (SPPS) and cleaved with Thiol and Non-Thiol (TIPS) cleavage cocktails. The qualities of the peptides were analyzed by HPLC and MS and the peptide/lipid interaction was observed through NMR. Non-Thiol cleavages produced better yields of peptides and more consistent results.

Abbreviations

LF - Lactoferrin; Lf - Lactoferricin; LfB- bovine lactoferricin; R - Arginine; W - Tryptophan; Q - Glutamine; 1 MeW - 1 Methyl Tryptophan; FMOC-ONSu - 9-Florenylmethoxycarbonyloxy; DME - Dimethoxyethane; NM P- Npmethylpyrrolidone; DCM - Dichloromethane; HBTU - [2-(1 H-benzotrazol-1-yl)-1,1,2,3-tetramethyluronium hexafluorophosphate]; HOBT - [1-hydroxybenzotriazole]

Introduction

In the world of medicine there is a need for the discovery of new antibiotics. Since the 1940's antibiotics have been available as protection against bacterial infections. However, many bacteria have become resistant to specific antibiotics so that they won't work against them. This means that the increase of multidrug resistance bacteria surely exceeds that of new antimicrobial agents. Antimicrobial peptides, produced in all animal kingdoms and vital for the innate immune response, have considerable potential as new antibiotic drug candidates against increasingly prevalent multiresistant pathogens[1]. Time is of the essence to do research in discovering new antibiotics to treat illness and hopefully save lives.

Bacterial membranes are organized in such a way that the outer-most leaflet of the bilayer, the surface exposed to the outer world, is heavily populated by lipids with the negatively charged phospholipids headgroups [3]. Most antimicrobial peptides are positively charged and have a high solubility in water; hence they are attracted and will approach the surface of the bacterial cell1. It can be expected that the positively charged peptides bind strongly to negatively charged lipids. The relationship between the bacterial membrane and antimicrobial peptide is still not completely understood. It is often

suggested that most antimicrobial peptides act solely by binding to and perturbing the cytoplasmic membrane that surrounds the bacterial cell[4]. However, it is also thought that some antimicrobial peptides enter the cell and bind to and upset intracellular targets[4]. The more research being performed by observing the two and monitoring the effects the more we can understand.

All antimicrobial peptides are derived from larger precursors. The peptide for our interest of study is Lactoferricin. Lactoferricin is a twenty-five amino acid antimicrobial peptide derived from the gastric pepsin cleavage of Lactoferrin (LF) (amino acids 17-41 of LF). Lactoferrin is an iron-binding protein that is secreted in mammalian milk and in most exocrine fluids such as tears, saliva, bile, and pancreatic juice [3]. Not only does the peptide Lactoferricin have significantly higher antimicrobial potency, which draws most of the attention of researchers to date, but it is smaller in size which makes it much easier to synthesize and therefore a more suitable drug candidate.

Our research focuses on the six amino acid lactoferricin B20-25 (RRWQWR-NH2) derivative of the twenty-five amino acid peptide. LfB 20-25 retains significant activity, suggesting that it may constitute a core active region or perhaps even the antimicrobial active-site [1]. Antimicrobial peptides rich with tryptophan (Trp) and arginine (Arg) residues are endowed with unique properties. Previous studies have found that the Arg and Trp residues are of particular importance in giving stronger binding and more significant membrane perturbations [2].

In order to gain more knowledge about the function of Trp and Arg in the hexapeptide LfB we synthesized several derivatives to see what kind of effects the modified peptides would have on the bacterial membrane.

Table 1. Amino Acid sequence of modified Lactoferricin

	Syn #		**1**	**2**	**3**	**4**	**5**	**6**	
AC Lfb 20-25 1 MeTrp3	637a	Ac	R	R	MeW	Q	W	R	NH
Lfb 20-25 (Native)	639		R	R	W	Q	W	R	NH
Lfb 1 Me Trp3	641		R	R	MeW	Q	W	R	NH

Synthesizing these peptides was achieved through a process called Solid Phase Peptide Synthesis (SPPS) which is a standard method used today for producing peptides and small proteins with both high fidelity and yield. To protect the alpha amino group of the amino acids during synthesis we use the base-labile group Fmoc. To protect the side chains we use acid labile groups Boc, Pbf, and Trt.

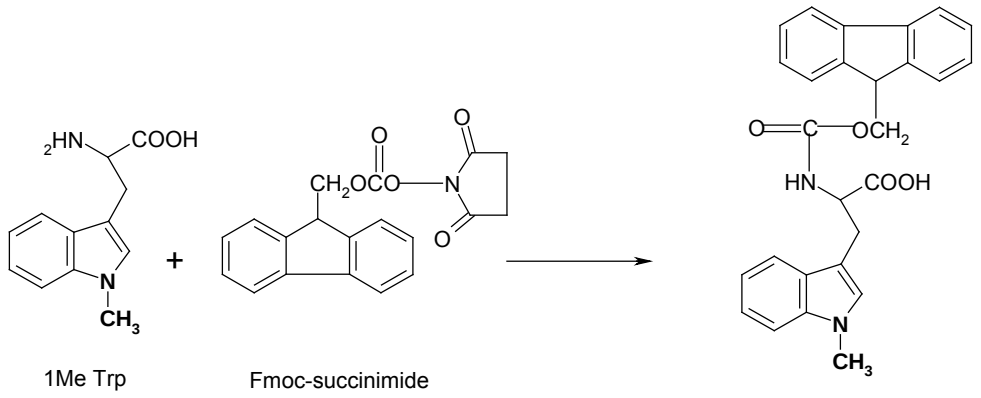

Figure 1. Formation of an FMOC Protecting group on 1Me Trp

In order to synthesize amino acids into a complete peptide the Fmoc group on the first amino acid is removed with 20% piperdine. The second amino acid can be attached to the first only when its alpha carboxyl group is activated with HBTU. This process continues for the attachment of the rest of the amino acids. Peptides are synthesized in the C to N terminal direction.

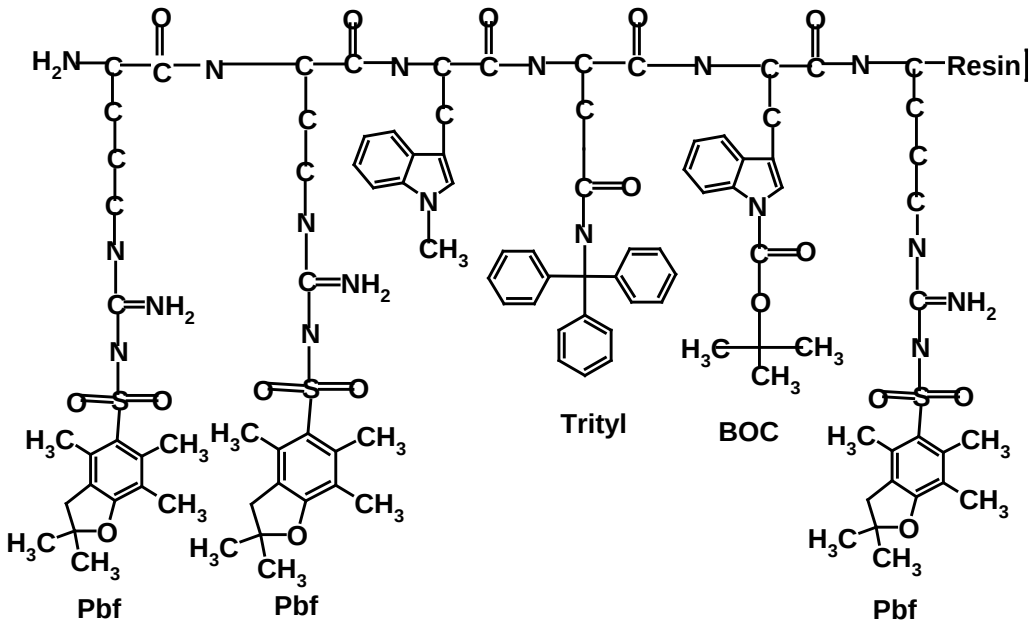

Figure 2. Lactoferricin B 20-25 1MeTrp3 shown with protecting groups

Experimental Procedures

Chemicals and Abbreviations

1-Methyl-L-Trp, Dimethoyethane (DME), Triisoproplysilane (TIPS), Fmoc-ONSu: N-(9-Fluorenylmethoxycarbonyloxy)-succinimide were from Sigma Aldrich Company. Amino acids were purchased from NovaBiochem (EMD BioSciences, San Diego, CA) Bachem (King of Prussia, PA) and Advanced Chem Tech (louisville, KY). The Rink Amide AM resin, substitution 0.63 mmol/gram, was from Novabiochem. N-Methylpyrrolidone, (NMP) from Burdick and Jackson. Methyl t-Butyl Ether (MtBE) from Burdich and Jackson. Deuterium oxide (D20) from Cambridge Isotope Laboratories. Trifluoroacetic acid (TFA) from Pierce Chemical. Phenol, ethanedithiol (EDT), and thioanisol were obtained from Sigma-Aldrich Chem. Co. Dimyristolyphosphatidylcholine (DMPC), and dimyristoylphosphatidylglycerol (DMPG) were obtained from Avanti Polar Lipids (Alabaster, GA).

FMOC ADDITION TO L 1-METHYL-TRP NH GROUP

Procedure 1:
In a 500 ml round bottom flask (RBF) we dissolved 2.5 grams of Fmoc-ONSu in 30ml of DME. Then we dissolved 1 gram of L 1-Methyl-Trp in 30 ml of 10% Na_2CO_3. We added the cloudy N-Methyl-Trp solution to the Fmoc solution dropwise while stirring. After a white precipitate formed almost immediately the pH was checked and recorded at pH 10 which was okay. 15 ml DME was added, and then after one hour 15 ml of acetone was added. The recommended pH is 8-10, if not adjust with 10% Na2CO3. If the solution were to become too thick DME/acetone (50/50) was added so that it could mix easily with stir bar.
We continued to stir at room temperature overnight.

Procedure 2 Extraction:
We filtered the solution with a Buchner funnel using Whatman ashless filter paper (#44) and discarded the precipitate. The RBF was rinsed with acetone and ethyl acetate and the filtrate was returned to the RBF. We checked the pH of the filtrate with pH strips and neutralized it to pH 7.0 with several drops of concentrated HCl. The liquid was concentrated under reduce pressure to dryness with a BUCHI RE111 Rotavapor. At this time the product (white precipitate) precipitated out with some contaminants. The neck of the RBF was wiped to remove any vacuum grease and about 20 to 30 mls of MtBE was added to precipitate the product. This was mixed well and sonicated to remove residual white material from sides of RBF. Filtration was done with a Buchner funnel and the solid material was washed with cold MtBE several times. The top of the glass filter was covered with aluminum foil with a few poked holes and the white material was dried on the vacuum line for 15 to 30 minutes to remove residual MtBE. The white precipitate was transferred to a 500 ml RBF and then 80 ml of ethyl acetate and 80 ml 0.1 N HCL were added (2 layers formed).We then mixed until the precipitated material completely dissolved. An HCL extraction was performed by transferring the ethyl acetate/ aqueous

HCL solution to a large enough separatory funnel and waiting for the two layers to separate. We then discarded the aqueous bottom layer and added 60ml more of 0.1 M HCL to the funnel. This was mixed well and bottom layer was discarded again. The ethyl acetate layer was transferred to a beaker and several scoops of MgSO4 powder was added to remove excess water. The solution was stirred and filtered as above and the 500 ml RBF was rinsed with MeOH and ethyl acetate, and then the filtrate was transfered back to the RBF. The filtrate was evaporated on the rotovap and dried over night on the vacuum line.

Procedure 3 Crystallization:
30 ml of ethyl acetate was added in 5 ml increments while stirring in a 50 °C bath water. The filtrate did not completely dissolve so another 30 ml was added. The filtrate was transferred to a crystallization jar and the volume reduced with N_2, and the jar was placed in the freezer over night. Several days later no crystals had formed so the solution was filtered again to remove a small amount of precipitate that had formed, and it was placed back in the freezer. Two days later crystals formed at the bottom. Glass filtration was performed and the filter containing the product was wrapped with foil then placed on the vacuum line.

Solid Phase Peptide Synthesis

Test for Resin Loading Efficiency: FMOC Removal
Before we synthesized our peptides we loaded our first amino acid to the Rink Amide AM resin using a 433A Peptide Synthesizer and tested the loading efficiency by Fmoc removal. The loaded resin was dried on the vacuum line overnight and the next day 1 ml of 20% piperidine(800 µl NMP + 200 µl piperidine) was prepared fresh. 500 µl of 20% piperidine was added to 3.5 mgs of resin in a pre weighed test tube and mixed for 15 minutes. The other 500 µl was used as a blank on the Diode array spectrometer,set to scan between 250-350 nm. After blanking the spectrometer the resin sample was scanned and its absorbance was measured at 301 nm. With the recorded absorbance we calculated the loading percent using equation 1 below.

Equation 1.

Moles Fmoc AA/gram resin =

$$(Abs301)(50 \times 10^{-3} \text{ liters})/(7{,}800 \text{ liters mole}^{-1} \text{ cm}^{-1})(\text{grams resin})(1\text{cm})$$

The value was at least 60% of the substitution value, which meant the loading was good. Next the unreacted functional groups on the resin were capped, and then we proceeded to synthesizing the rest of the peptide.

TIPS and Thiol TFA Cleavages

TIPS and Thiol cleavages were performed to remove protecting groups and the resin from the peptide. The first peptide cleaved, Ac LFB 1 MeTrp3, was cleaved and deprotected with TIPS on a small scale to get an understanding of the best method for other peptides. The small scale was performed by mixing 10 mg of resin with 500 µl of the specified Cleavage Cocktail. Table 2 below shows the TIPS and Thiol TFA cleavage cocktail solutions. Once the resin and Cleavage cocktail were mixed, at each specific hour (1hr, 2hr, 3hr, 4hr, 6hr, and 24hr), 5µl were removed and diluted into 250 µl of 50/50 H_2O/TFE.

On the Large scale all three peptides were cleaved with both TIPS and Thiol deuterated TFA cleavage cocktails. 2ml of fresh TFA-d cleavage cocktail was added to 100 ml of resin in a RBF. The RBF was flushed with N_2 and the seal was covered with parafilm. After mixing on the orbital shaker in the dark (covered with foil) for 3 hr a plastic pipette was use to transfer the resin to be filtered in a glass pipette with glass wool plug. The empty RBF was rinsed with 1 ampule of deuterated TFA to collect any residual resin and then filtered again. The filtrate was collected in a 50 ml centrifuge tube, the volume was reduced with N_2, and the peptide was precipitated with 25ml of cold 50/50 MTBE/ Hexane and cooled on ice for 30 minutes. The sample was then centrifuged with the Heraeus Labofuge 400 R centrifuge at 4 degrees Celsius for 15 min at 2500 rpm. The supernatant was poured off and we added another 25 ml. The 50/50 MTBE/Hexane, ice, and centrifuge process were repeated 3 times. After pouring off the supernatant for the last time the pellet in the centrifuge tube was dissolved with 50/50acetonitrile/dH_2O,and frozenwith liquid N_2. the frozen sample was lyophilized on the vacuum line overnight to a white powder. A 1 mg/ml sample of the peptide was prepared in either dH_2O (639 and 641) or dH2O/Acetonitrile (50/50) (637), and the concentration of a 1:10 dilution was measured at 280 nm on a Hewlett Packard Diode Array Spectrometer using an extinction coefficient of 5600 cm^{-1} M^{-1} per Trp.

Table 2. Cleavage Cocktails

Small Scale	Large Scale	
Reagent 1	Reagent 2	Reagent 3
88% TFA (880µl)	88% TFA-D1 (2ml)	82.5% TFA (1.75µl)
5% dH2O (50 µl)	5% TIPS (125µl)	5% dH2O (100µl)
2% TIPS (20 µl)	5% dH2O (125µl)	5% Thioanisole (100µl)
5% Phenol (50µl)	5% Phenol (125mg)	2.5 EDT (50µl)
		5% Phenol (100mg)

High performance Liquid Chromatography (HPLC)

3µl of the ~1mg/ml cleaved peptide were injected on to the HPLC. The HPLC used was the Hitachi L-7100 HPLC pump and Zorbax C_8 reversed phase column (SB_{80} 4.6 x 50mm, 3.5 um particle size) with a gradient file 5 as seen in table 3. The peptides were

also analyzed by MALDI/TOF MS (University of Arkansas, Statewide Mass Spectrometry Facility)

Table 3. Gradient File 5

Minutes	MeOH + 0.1% TFA	dH_2O + 0.1% TFA
0	10	90
2	10	90
10	60	40
15	60	40
15.1	10	90
23	10	90

Preparation of Oriented samples for solid state ^{31}P and ^{2}N NMR

Lipid only

Fifty glass slides were arranged in a radial position at the bottom two Petri dishes. With a small conical bottom flask we added 3:1 mixture of DMPC:DMPG (75 μmol DMPC:25 μmol DMP) and dried under stream of N2 to remove solvent. Figure 3 shows lipid structures. We dissolved lipid mixture in 400μl of MeOH, 50μl of distilled water, and 400 ul of chloroform. With a glass syringe 10μl of solution was applied to each slide and reapplied until the solution was all used up. Petri dishes were air dried for approximately for 15 minutes then placed in a desiccator under vacuum for 48 hours. After 48 hours 1μL of 100 mm phosphate was applied to each slide with a glass syringe. Slides were stacked in a cuvette and if cuvette was not full additional black slides were added. The cuvette was sealed with a glass cap and epoxy glue and placed in a heating block at 45^{o} C for about one week so sample can become transparent.

Figure 3. Structure of Lipids

DMPG

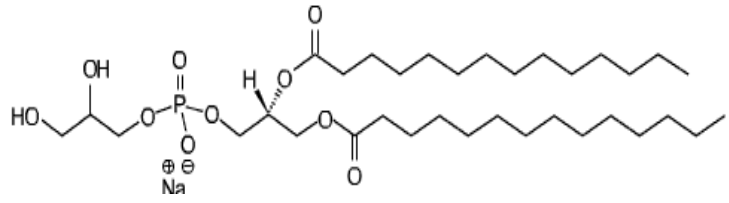

DMPC

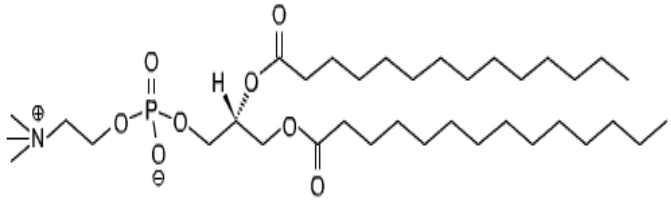

Lipid and peptide

The same procedure was used as above for lipids only with the exception of adding peptide #641 Lfb 1MeTrp. The small conical bottom flask contained 1:50 peptide:lipid (2 μmoles peptide:100 umoles lipid mixture). The mixture was dissolved with the help of a sonicator.

Figure 4. shows an illustration of oriented samples are prepared.

Figure 4.

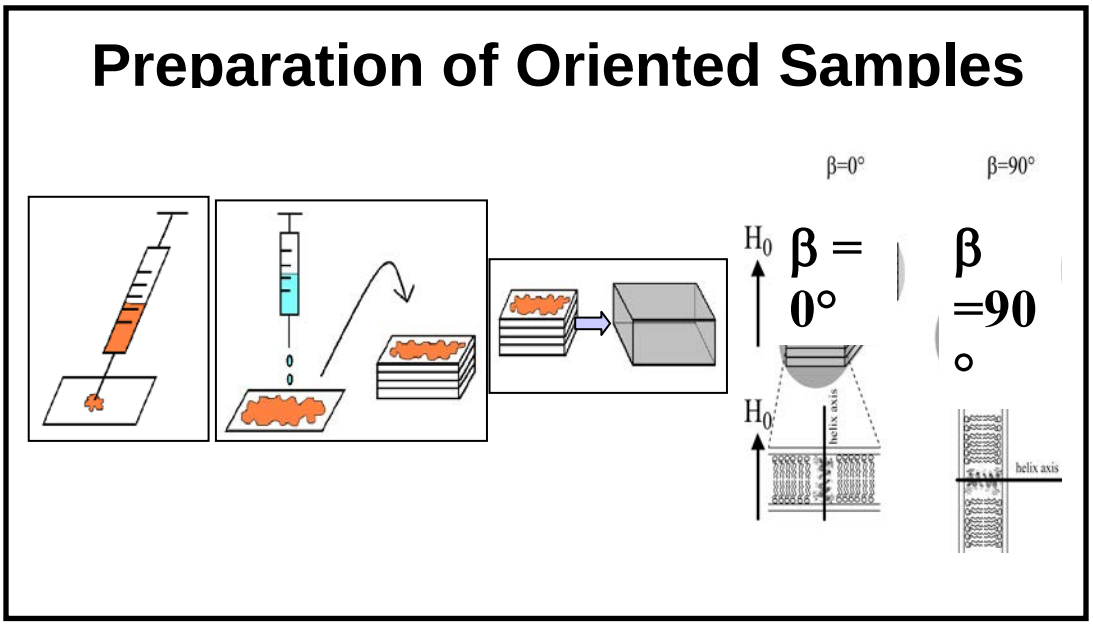

2H NMR and ^{31}P NMR

The sample was analyzed with ^{2}H NMR to look for signals from deuterated 1MeTrp and analyzed with ^{31}P NMR to check for alignment of lipids.

Results and Discussion

The HPLC and the mass spectrometry were used to test the quality of the peptides. The HPLC data revealed more than one peak for each peptide which possible suggested unsuccessful peptides were synthesized, incomplete cleavage from the resin, or reaction of side chains. All chromatograms, however, do indicate one prominent peak which is believed to be the desired peptide.

Figure 5. HPLC analysis of Ac LfB 1MeTrp3 Small scale TIPS

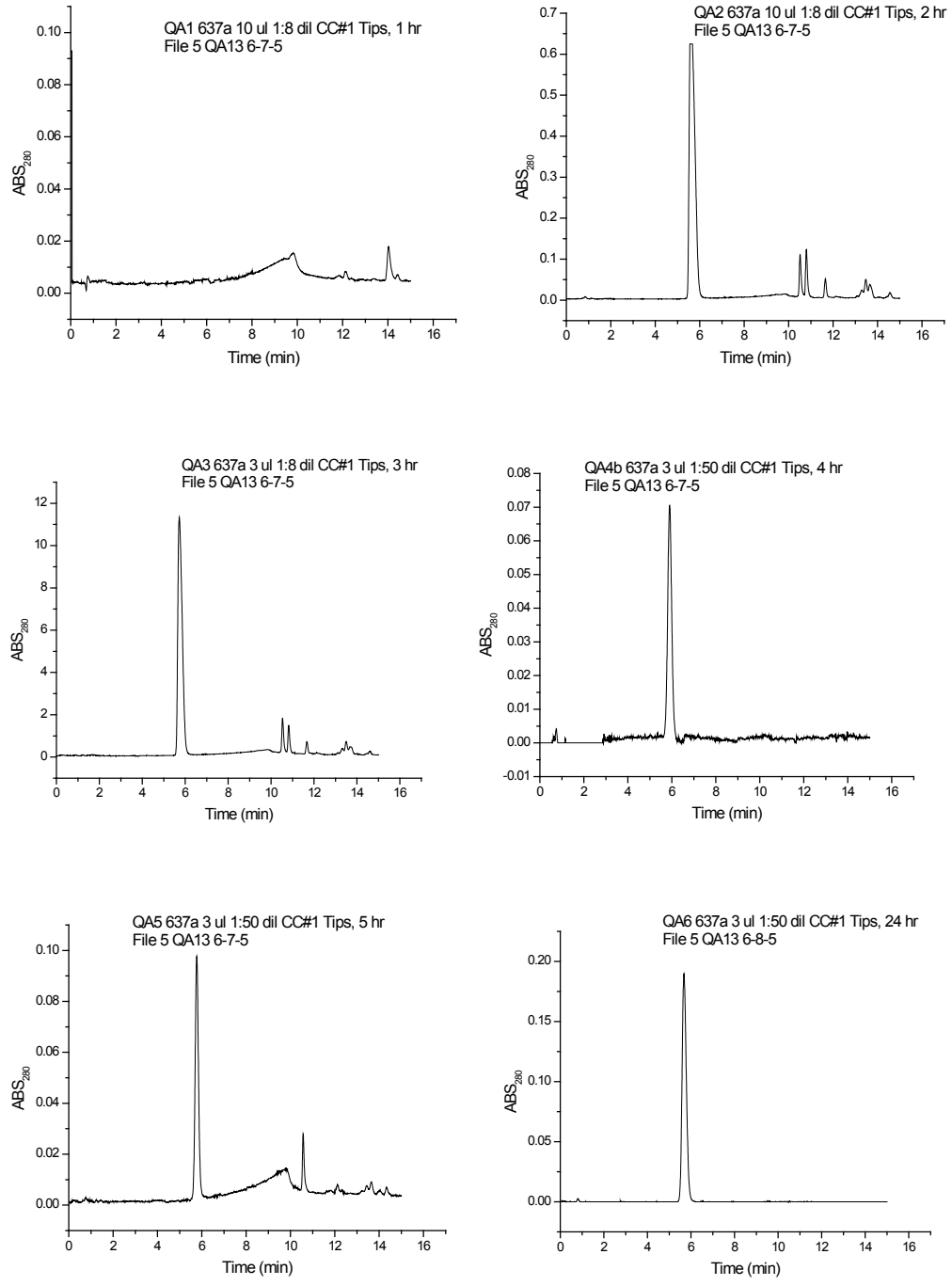

Figure 5 shows Ac LfB 1MeTrp3 small scale after 1,2,3,4,6, and 24 hour TIPS cleavage times. Chromatogram 4 shows the best cleavage time due to one large peak which is believed to be the desired product with minimum shoulder peaks. The 24 hour chromatogram looks good, but the base line is below the baseline which gives difficult data to read.

Figure 6. Ac LfB 1MeTrp3 Large Scale TIPS Before Lyophylization

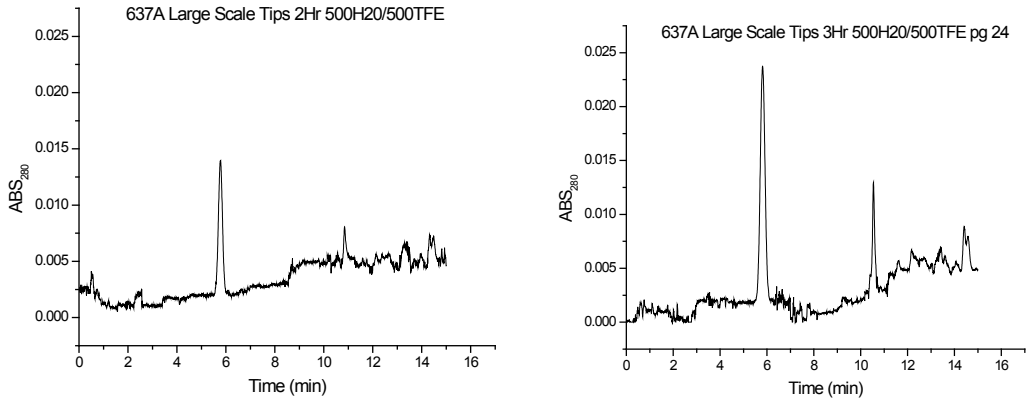

Figure 6 shows Ac LfB 1MeTrp3 Large Scale TIPS cleavage before Lyophylization. The 3 hour chromatogram seems to show more product than the 2 hour which is good but it also shows a second peak eluting at about 10.5 minutes.

Figure 7. Ac LfB 1MeTrp3 Large Scale TIPS/Thiols after Lyophylization

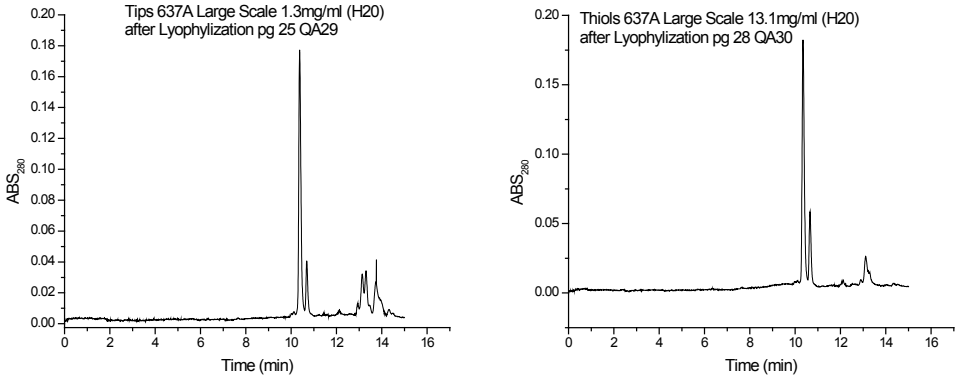

Figure 7 shows a cleavage of TIPS and Thiols after lyophylization.

Figure 8. LfB Native Large Scale TIPS/Thiols after Lyophylization

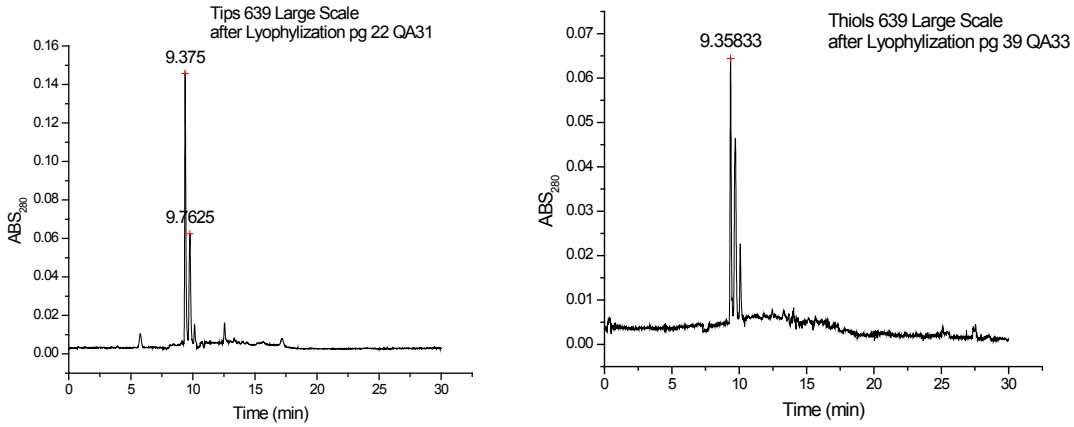

Figure 7 shows large scale LfB Native cleaved with TIPS and Thiols then lyophylized. TIPS seem to be the better cleaving mixture because it shows less shoulder peaks

Figure 9. LfB 1MeTrp Large Scale TIPS/Thiols after Lyophylization

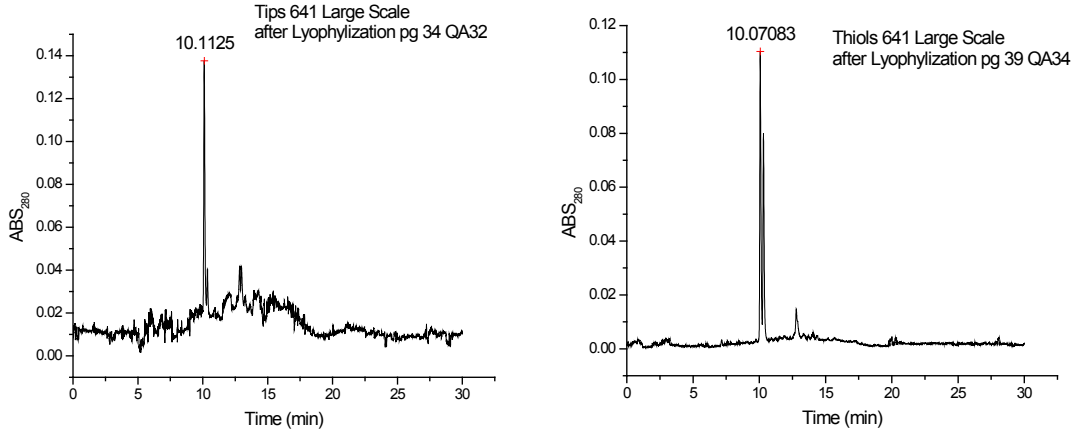

Figure 8 shows large scale with TIPS and Thiols of 1MeTrp after lyophylization.

HPLC analysis of the small scale cleavages was performed by diluting the cleavage solutions after specified time intervals (1, 2, 3, 4, 6 and 24 h), making a 1:50 dilution into trifluoroethanol, and injecting approximately 3 µl onto the column. This was done to reduce the time and number of samples required for analysis. Chromatograms of the small scale cleavage of peptide #634 AcLfB 1MeTrp with TIPS (shown in figure 5) revealed single peaks, suggesting that the method worked well. To confirm these results, the same peptide was cleaved again on a larger scale for 2 and 3 hours, with both TIPS and Thiols. All large scale cleavages were performed with deuterated TFA-d so the peptides could be used to prepare oriented solid state NMR samples. Preliminary results,

obtained from diluting the cleavage reactions as above, revealed a single major peak at about 5.8 minutes, and a second peak around 10.5 minutes, which was larger after 3 hours. The peptides were then precipitated from the cleavage solution, washed with MtBE and lyophilized overnight to a white powder. A ~1mg/ml solution of the lyophilized peptide was then analyzed. These results (shown in figure 7) showed a major peak at ~ 10 minutes with a second smaller peak at about 10.25 min. This indicated that the small-scale cleavage tests did not accurately predict the quality of the peptide after lyophilization. Therefore, all future cleavages were performed on a larger scale, and were analyzed only after lyophilization.

Figures 8 and 9 show the results of large scale TIPS and thiol cleavages of native and 1MeTrp3 LfB. All show a single major peak, with a smaller shoulder peak(s), however the secondary peaks are larger, and sometimes increased in number for the thiol cleavages compared to the TIPS cleavages. These results suggest that cleavage with TIPS is superior to thiols.

Figure 9. Mass Spectrometry of Lfb 1Me Trp3 (Thiols)

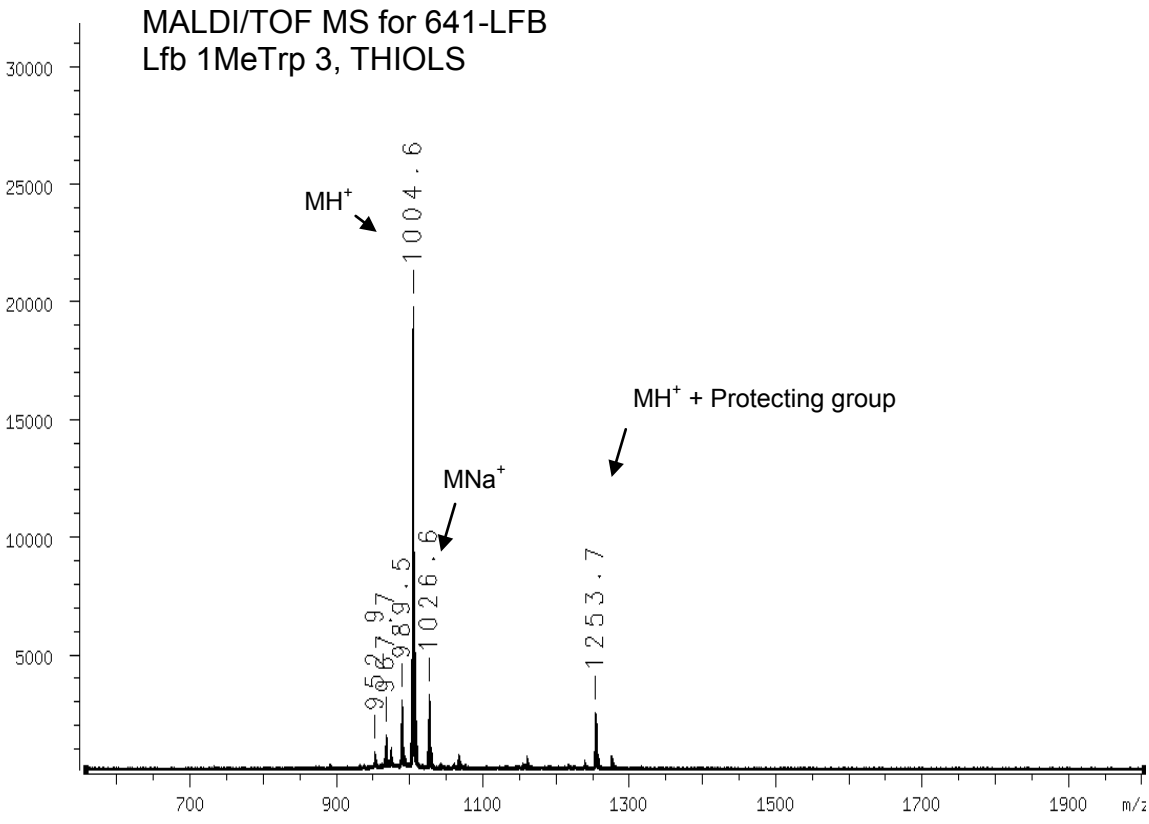

Figure 9 shows the MS of LfB 1Me Trp3

The mass spectrum of LfB 1Me Trp3, shown in Figure 9, confirms the correct mass, plus 4 deuterons which were expected due to cleavage with TFA-d. Previous results have shown that the 4 deuterons are present on the MeTrp (Gu, 2005). The peak at 1253.7 is due to peptide with residual Pbf protecting group present (mass 254).

Figure 10. Mass Spectrometry of Lfb Native (Tips)

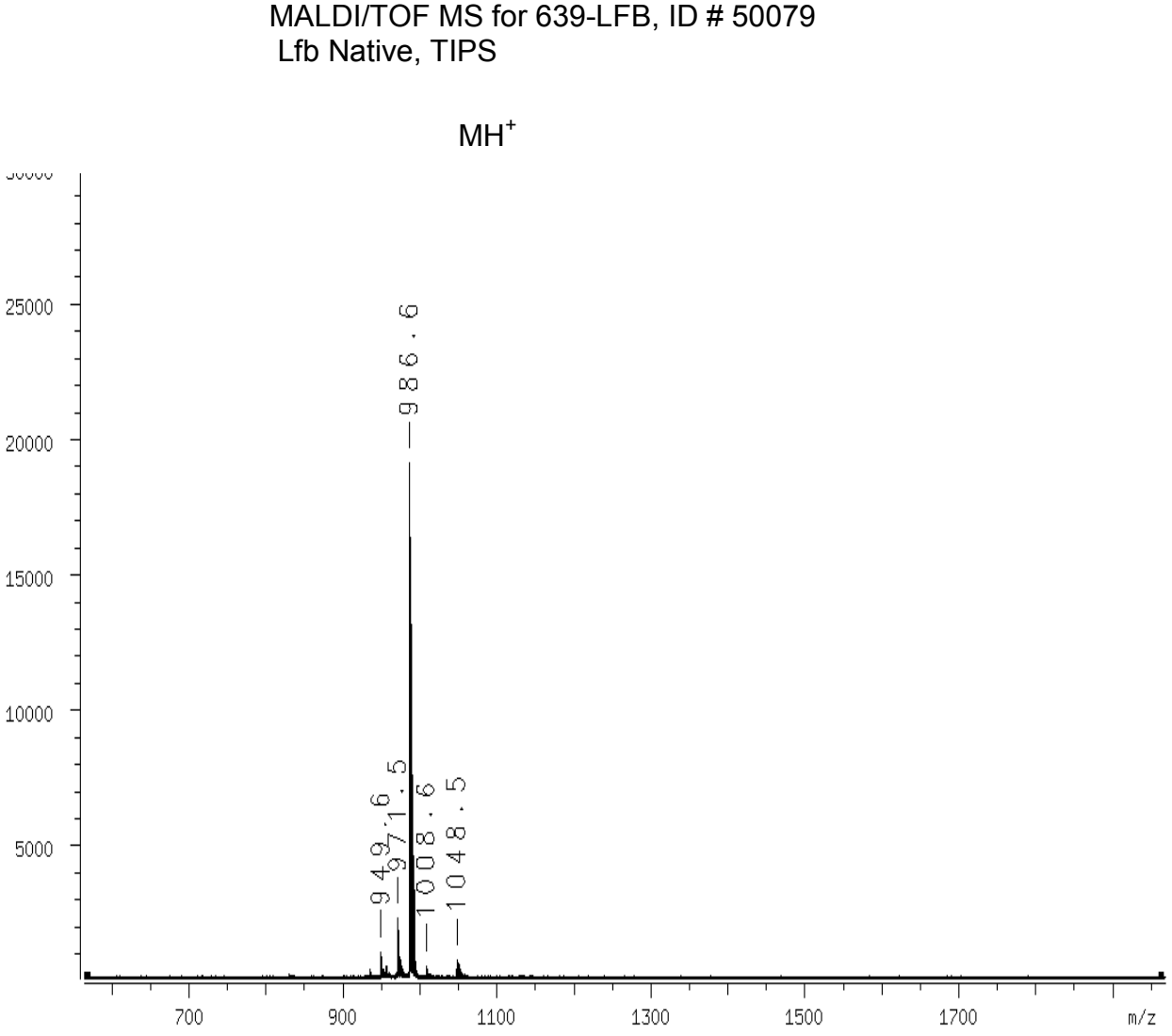

The mass spectrum of LfB native cleaved with TIPS, shown in Figure 10, confirms the correct mass. In this case no deuteration occurred, despite cleavage with TFA-d, as no MeTrp was present. Due to the presence of the Boc protecting group, the 2 Trp residues are not deuterated. No residual protecting group is present in the peptide cleaved with TIPS.

Figure 11. Mass Spectrometry of Lfb Native (Thiols)

MALDI/TOF MS for 639-LFB-7/20/05
Lfb Native, Thiols

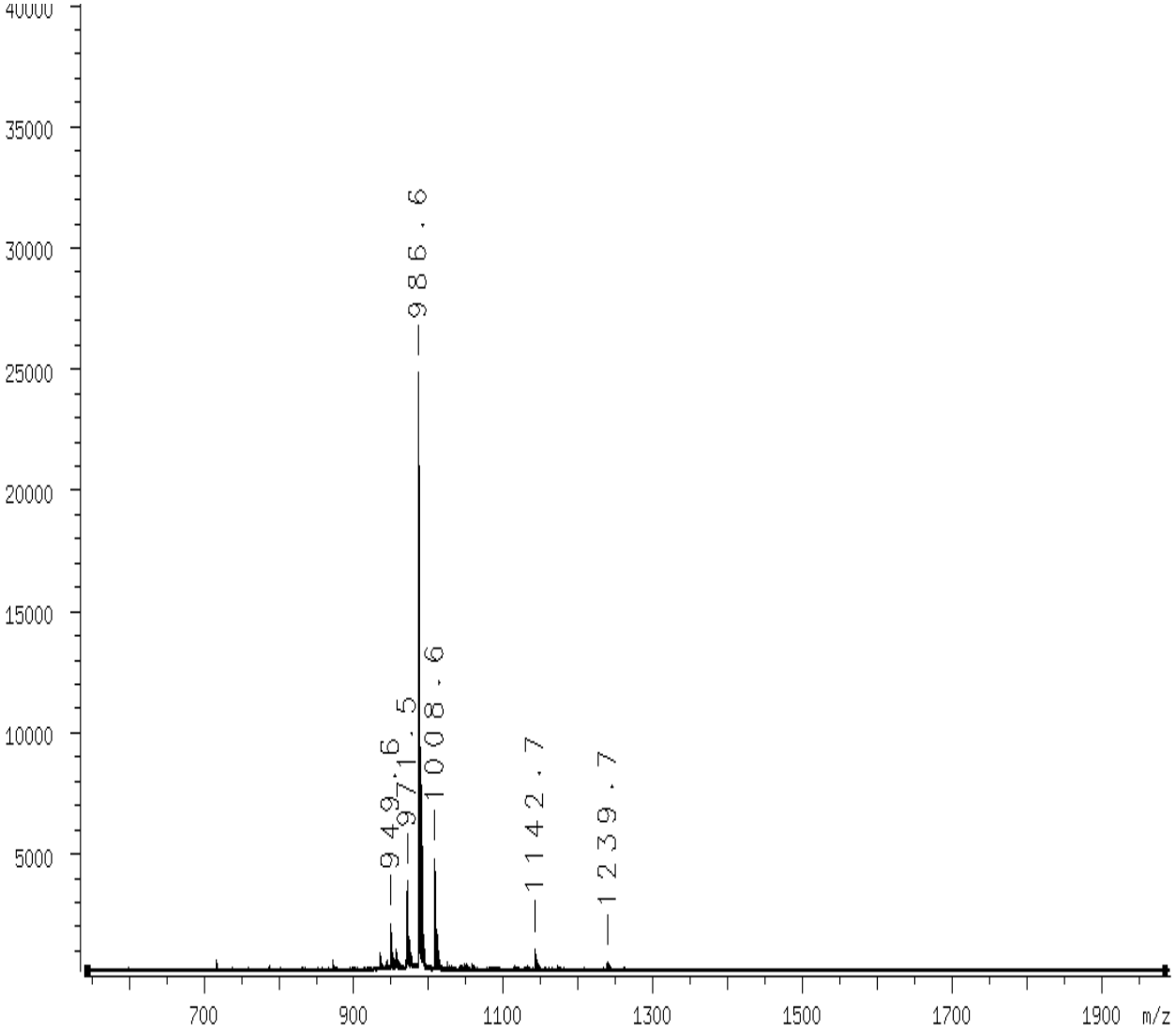

Figure 12. 2H NMR

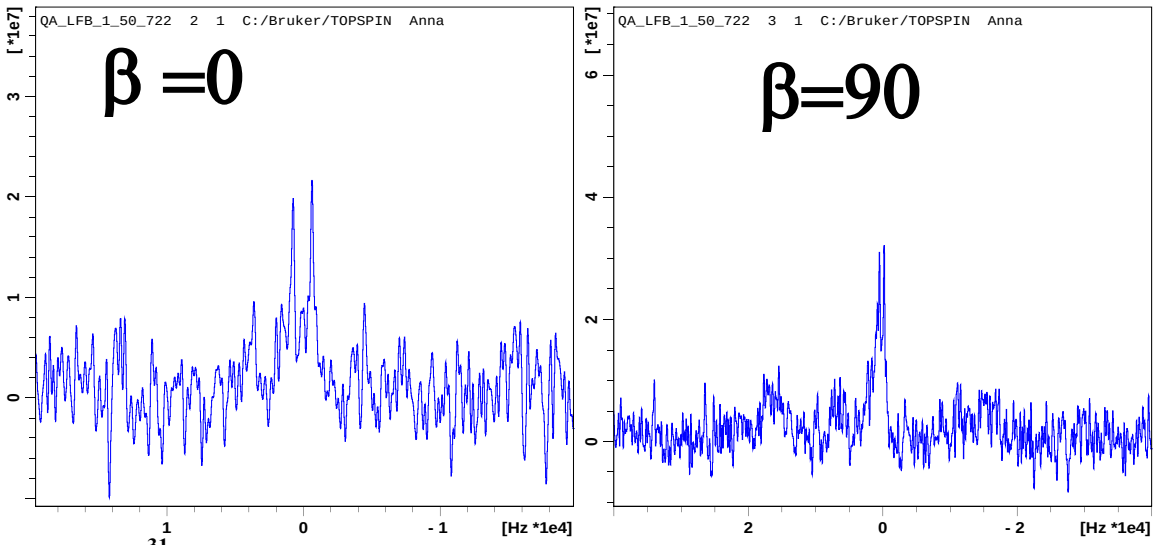

Figure 13. ^{31}P NMR

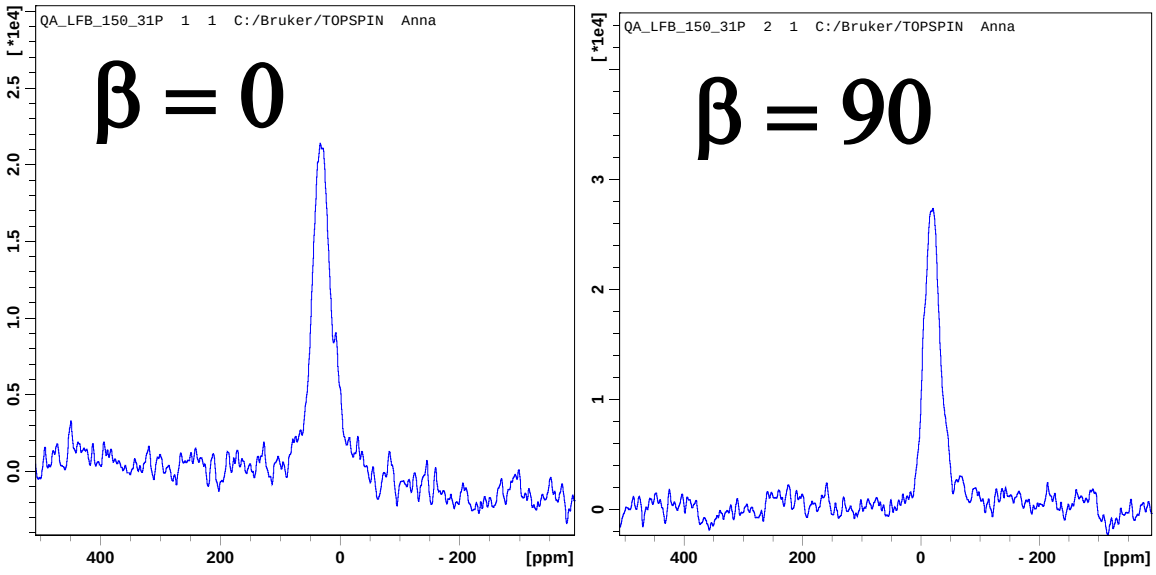

Figure 12 shows 2H NMR of peptide # 641 1MeTrp LfB in oriented samples of DMPC:DMPG (3:1), at a 1:50 peptide:lipid ratio.
Figure 13 shows ^{31}P NMR of the same sample

Conclusion

Synthesis of the 3 peptides was successful. HPLC and MS analysis indicates TIPS is the better cleavage cocktail. Peptides were cleaved with TFA-D in attempt to selectively deuterate the indole ring of 1 MeTrp. 2H NMR Spectra indicated a specific ring orientation, with two positions labeled. More spectra are needed to complete the analysis. 31P NMR showed that the lipids retain a bilayer phase and are well oriented with respect to the magnetic field.

Acknowledgements

I would like to thank the National Science Foundation, Langston Integrated Network College (Linc), Undergraduate Biomedical Education Program at Langston University (UBEP), and the National Science Foundation. I would also like to highly thank Dr. Denise V. Greathouse and the Koeppe Research Group for being patient with me and providing plenty of assistance.

References

1. Greathouse, D.V., Doeppe, R.E., II, Providence, L.L., Shobana. S., and Andersen, O.S. (**1999**) *Methods in Enzymology*. 294, 525-550.
2. Fields, G.B, (**1997**) *Methods in Enzymology*. 289, 505.
3. Mechael Zasloff. (**2002**) *Nature*. 415
4. Erik Strandberg, Anne S. Ulrich., (**2004**) *Concepts in Magnetic Resonance Part A*. 23A, 89-120
5. Vogel, H.J., Schibli, D.J., Jing. W., Lohmeier-Vogel, E.M., Epand, R.F., Epand, R.M. (**2002**) *Biochem. Cell Biol*. 80, 49-63

Steps Toward the Synthesis of Caulerpenynol

Bruce A. Atwater, Gustavus Adolphus College
St. Peter, Minnesota

Abstract

The natural product caulerpenyne has shown great potential as an anticancer drug. This paper discusses advances towards the synthesis of a derivative of caulerpenyne using alkyne cross dimerization reactions with palladium (II) acetate.

Introduction

Caulerpenyne (1) is a natural product isolated from *Caulerpa taxifolia*, a tropical seaweed, which is currently invading the Mediterranean Sea.[1,2] Barbier et al have reported that caylerpenyne is cytotoxic against multiple cell lines and have investigated its toxicological effects on the neuroblastoma cell line known as SK-N-SH.[1] They reported that caulerpenyne increased the rate of cell death in the neuroblastoma cells and also inhibited cell proliferation by interfering with the microtubule network.[1] As a result of its potential uses in fighting cancer the McIntosh group has designed a synthesis (Scheme 1) for a derivative of caulerpenyne known as 7,7-C-didehydro-6-hydroxy-6,7-dihydrocaulerpenyne, or caulerpenynol (2). One of the major reasons for choosing to use this route is that the alkyne cross dimerizations using catalytic amounts of palladium have been shown to add in a stereospecific depending on the ligand you choose.[3] This thereby allows us the potential to generate many derivatives of caulerpenyne.

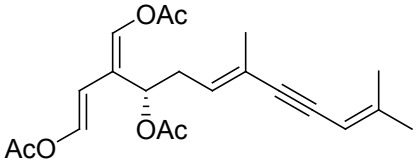

1

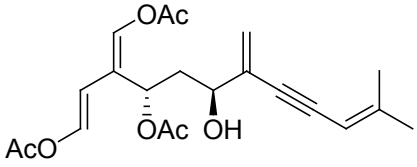

2

Scheme 1

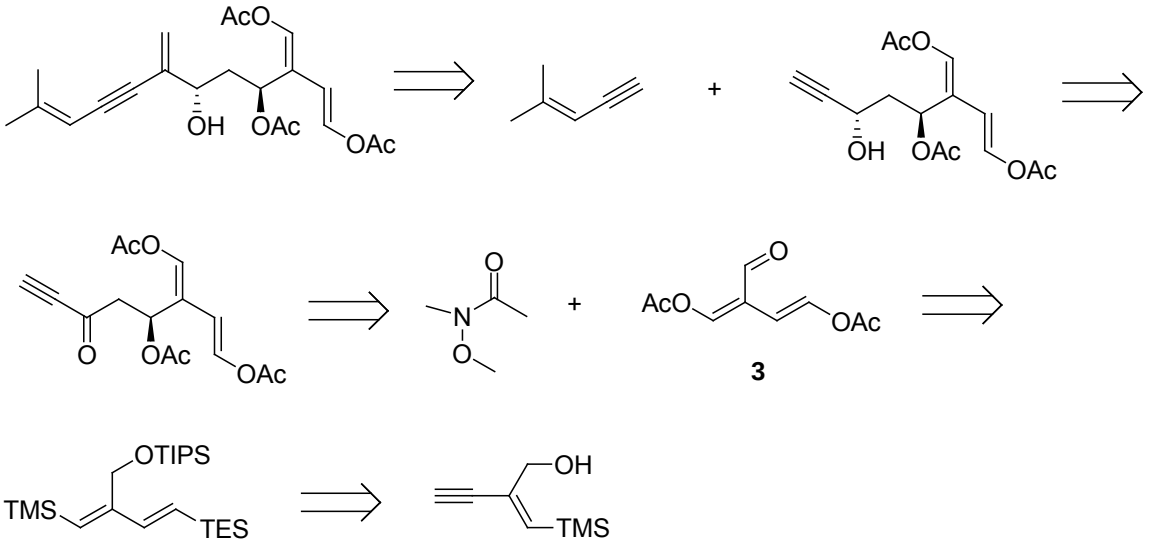

In this paper we report advances towards the synthesis of bis-enol acetate 3, using a more detailed retrosynthesis (Scheme 2), which will serve as the precursor for further work on the synthesis of caulerpenynol.

Scheme 2

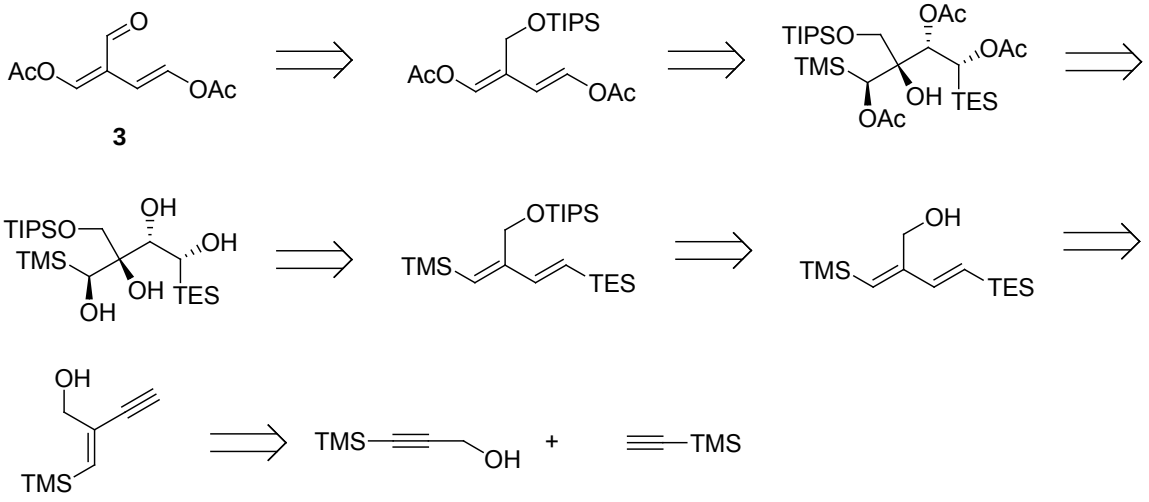

Results and Discussion

The first step in the synthesis of bis-enol acetate 3 involved the addition of *para*-formaldehyde to deprotonated (trimethylsilyl) acetylene, TMS acetylene (4), at –78 °C (Scheme 3). This gives a fairly good yield of 3-(trimethylsilyl)-2-propyn-1-ol, TMS propynol (5), which was identified using ^{1}H NMR.[2]

Scheme 4

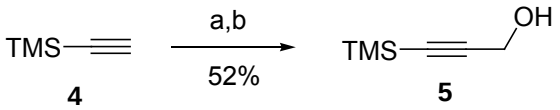

4 **5**

Conditions: (a) Bu-Li, THF, -78 ^{o}C;
(b) p-formaldhyde, rt, 4 h

Purified alkyne **5** was added to palladium (II) acetate along with tris(2,6-dimethoxyphenyl) phosphine (TDMPP) and TMS-acetylene (**Scheme 4**). This reaction mixture gave poor yields of enynol **6** due to a large amount of polymer being formed in the distillation flask during the vacuum distillation of the crude reaction mixture.[3] After unsuccessfully trying to purify **6** using flash column chromatography on Florisil we decided to use the crude mixture of **6** in the subsequent hydrosilylation step using chloroplatinic acid (H_2PtCl_6) and triethylsilane (TES-H) (**Scheme 4**). This provided a 10-20% overall yield after two steps of the desired *trans*-vinylsilane **7** along with the isomeric product **8**. This mixture of products was inseparable by flash column chromatography on silica gel. We did not attempt to separate the products by distillation due to concerns about the thermal stability of the diene.

Scheme 5

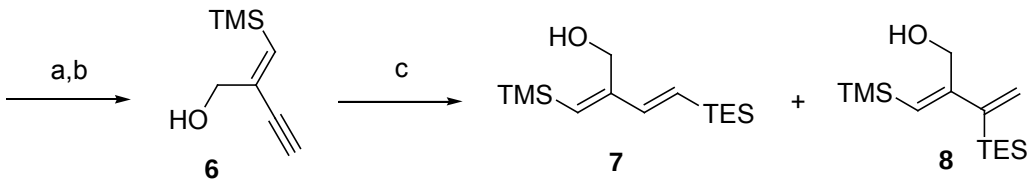

6 **7** **8**

Conditions: (a) TMS-acetylene, $Pd(OAc)_2$, TDMPP, rt, 48 h;
(b) K_2CO_3, MeOH, 4 h; (c) H_2PtCl_6, TES-H, PhH, rt, 16 h.

Protection of the hydroxyl group of the mixture of **7** and **8** using triisopropylsily-trifluromethanesulfate (TIPSOTf) yielded TIPS dienes **9** and **10** in acceptable yield (**Scheme 5**). Compound **9** was purified at this point by flash column chromatography on silica gel.

Scheme 6

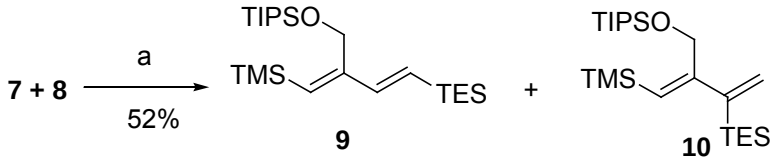

Conditions: (a) TIPSOTf, 2,6-lutidine, CH_2Cl_2, rt, 1.5 h

Trost and McIntosh have found that compound **7** could be dihydroxylated to yield *cis*-diol of **11a**.[3] Using this as a precedent we are currently attempting to dihydroxylate **9** to yield the diol **11b** using Sharpless asymmetric dihydroxylation conditions. As expected, the dihydroxylation occurred preferentially at the more substituted alkene.[3,4] Once this compound has been isolated, we will acylate it to yield acetate **12**.

Scheme 7

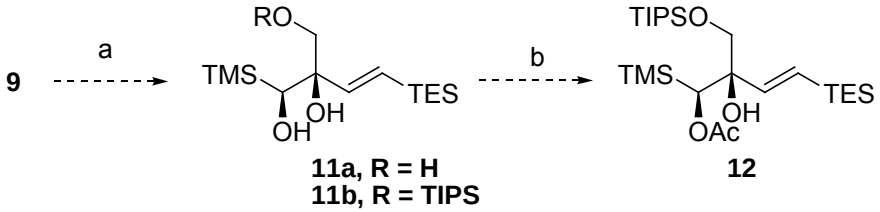

Conditions: (a) OsO_4, NMO; (b) Ac_2O

Conclusion

During the course of the summer we have made good progress towards the synthesis of diene **3**. We have currently built a stockpile of diene **9** which will be used to carry out further work on the synthesis of diene **3**. Hopefully, we will shortly have diene **3** prepared which will allow us to press on in the synthesis of caulerpenynol.

Experimental Procedures

TMS Propynol 5. n-BuLi (303 mL, 2.93 M in hexane, 303 mmol) was added in a drop wise fashion to a solution of TMS acetylene (42.4 mL, 29.5 g, 300 mmol) in THF (900 mL) at –78 °C. After 20 min, a slurry of *p*-formaldehyde (18 g, 600 mmol) in THF (150 mL) was added. The reaction mixture was allowed to come to room temperature and the mixture was stirred for 4 h. Glacial acetic acid (21 mL) was then added followed by H_2O (500 mL). The reaction mixture was then added to a seperatory funnel followed by another aliquot of H_2O (500 mL) and it was then extracted by with three time with ether. The organic phases were combined and then washed three times with saturated $NaHCO_3$ solution. The organic phase was then dried over $MgSO_4$ and concentrated in

vacuo. The reaction mixture was then purified by vacuum distillation (2.25 mmHg, 56-57°C) to yield alcohol **5** as a clear liquid (20.07g, 52%). The purity was verified by ^{1}H and ^{13}C NMR and the spectra were compared with the commercially available material. ^{1}H NMR (300 MHz, $CDCl_3$) δ 0.163 (s, 12H), 2.61 (s, 1H), 4.27 (s, 2H); ^{13}C NMR (67 MHz, $CDCl_3$) δ 0.14, 51.59, 90.61, 103.88.

Enynol 6. To a flame dried flask with $Pd(OAc)_2$ (0.101 g, 0.45 mmol) and TDMPP (0.199 g, 0.45 mmol) in benzene (50 mL) at room temperature, TMS propynol (2.22 mL, 1.924 g, 15 mmol) and TMS acetylene (3.18 mL, 2.21 g, 22.5 mmol) were simultaneously added. The reaction mixture was allowed to stir for 4 h and then another aliquot of TMS acetylene was added (3.18 mL, 2.210 g, 22.5 mmol). The reaction mixture was allowed to stir for another 18 h (22 total) and another aliquot of TMS acetylene (3.18 mL, 2.210 g, 22.5 mmol) was then added. The reaction mixture was then allowed to stir for another 26 h. After a total of 48 h the reaction mixture was concentrated in vacuo and then run through a plug of Florisil which was eluted with ether. The resulting blood red solution was then again concentrated in vacuo and the resulting solution was then added to methanol (50 mL) and K_2CO_3 (7 g, 50.65 mmol) and allowed to stir for 4 h. After 4 h H_2O (400 mL) was added to the reaction mixture which was then extracted three times with ether, dried over $MgSO_4$, and concentrated in vacuo. The resulting semi-crude reddish-brown colored mixture was then used directly in the next step without further purification.

Diene 7. To a flame dried flask with H_2PtCl_6 (0.0777 g, 0.15 mmol) in benzene (40 mL) the semi-crude mixture of enynol **6** was added (2.314 g, 15 mmol) (100% yield assumed) triethylsilane (3.59 mL, 2.616 g, 22.5 mmol) was added. The reaction mixture was allowed to stir for 16 h. The reaction mixture was then concentrated in vacuo and then run through a plug of Florisil. This was done first by running through hexane until the first colored band had run through the plug of Florisil. The plug of Florisil was then rinsed with ether. The ether extract was then concentrated in vacuo. The resulting brownish solution was then purified by flash column chromatography on silica gel with 98/2 hexane/ethyl acetate with 1% triethylamine to yield diene **7** along with the isoproduct **8** in a 6:1 mixture as a yellow liquid (0.8706 g, 10.8%). Purity was confirmed by ^{1}H and ^{13}C NMR and compared with values reported by Trost and McIntosh.[3] ^{1}H NMR (300 MHz, $CDCl_3$) δ 0.145 (s, 12H), 0.584 (q, J=7.95 Hz, 8H), 0.93 (t, J=7.62, 12H), 4.36 (s, 2H), 5.78 (s, 1H), 6.01 (d, J=19.39 Hz, 1H), 6.59 (d, J=19.46 Hz, 1H); ^{13}C NMR (67 MHz, $CDCl_3$) δ 0.27, 3.43, 7.40, 30.92, 61.35, 126.64, 148.07, 153.41.

TIPSdiene 9. TIPSOTf (1.91 mL, 2.17 g, 7.09 mmol) was added to a solution of diene **7** and the isodiene **8** (1.5320 g, 5.67 mmol) along with 2,6-lutidine (3.51 mL, 3.25 g, 30.3 mmol) in CH_2Cl_2 (25 mL) in a dropwise fashion. The reaction mixture was monitored by TLC and once it was complete the reaction mixture was quenched with H_2O (100 mL) and the mixture was extracted three times with CH_2Cl_2. The organic phases were combined and dried with $MgSO_4$ before being concentrated in vacuo. The resulting solution was then purified by flash column chromatography on silica gel with 98/2 hexane/ethyl acetate with 1% triethylamine. The resulting solution was yellow liquid (1.265 g, 52.2%): ^{1}H NMR (300 MHz, $CDCl_3$) δ 0.18 (s, 12H), 0.62 (q, J=8.12 Hz, 8H),

0.98 (t, J=7.85 Hz, 9H), 1.11 (d, J=4.29 Hz, 19), 4.50 (s, 2H), 5.79 (s, 1H), 6.18 (d, J=19.28 Hz, 1H), 6.61 (d, J=19.28 Hz, 1H); ^{13}C NMR (67 MHz, $CDCl_3$) δ 0.28, 3.48, 7.38, 12.12, 18.14, 62.99, 126.76, 131.59, 147.70, 154.03.

References

1. *Caulerpenyne from Caulerpa taxifolia has an antiproliferative activity on tumor cell line SK-N-SH and modifies the microtubule network* Barbier, P.; Guise, S.; Huitorel, P.; Amade, P.; Pesando, D.; Briand, C.; Peyrot, V. *Life Sciences* **2001**, *70*, 415 – 429.

2. *Caulerpenyne, an unusual sequiterpenoid from the green alga Caulerpa prolifera* Amico, V.; Oriente, G.; Piattelli, M.; Tringali, C. *Tetrahedron Lett.* **1978**, *38*, 3593 – 3596.

3. Trost, B.M.; McIntosh, M.C. unpublished results.

4. *Catalytic Asymmetric Dihydroxylation* Kolb, H.C.; VanNeuiwenhze, M.S.; Sharpless, K.B. *Chem. Rev.* **1994**, *94*, 2483 – 2547.

Towards The Synthesis of A Chiral Alkyl Bromide For Cross-Coupling Studies

Aireal D. Haley, University of Arkansas
Fayetteville, Arkansas

Abstract

Progress towards the synthesis of a chiral alkyl bromide has been made using chemical procedures. This synthesis consists of a Diels-Alder addition of 2-chloroacrylonitrile to cyclopentadiene followed by hydrolysis of the resulting chloronitrile with potassium hydroxide in aqueous dimethyl sulfoxide. Then the resulting ketone is reduced with Super Hydride in THF resulting in *endo*-norborn-2-en-5-ol which is a key intermediate in the total synthesis.

Introduction

Chemokines are a form of cytokines that are released by a variety of cells in order to attract T-Cells, macrophages, eosinophils, basophils, and neutrophils to sites of inflammation.[1,2] The chemokines bind to cell-surface receptors that belong to the family of G-protein-coupled seven-transmembrane-domain proteins[3] which are called "chemokine receptors." HIV-1 infection of macrophages, monocytes, and T-Cells is mediated by the β-chemokine receptor CCR5.[4-6] Absence of CCR5 appears to protect from infection by HIV-1.[7] An agent which could block chemokine receptors in humans could prevent infection in healthy individuals and slow or halt viral progress in those infected with HIV. Inhibition of chemokine receptors by small molecules may be a viable method for the prevention or treatment of infection by HIV in the future.[8] Data from lead compounds suggest that piperidine based molecules that are substituted at the sp^3-piperidyl 4-position show selective binding to CCR5 protein.[9] Models suggest that the nitrogen binds to the acidic Glu residues in proteins anchoring the small molecules to the active sites.[10]

The Vicic group is going to use Negishi-like cross-coupling reactions to synthesize differing piperidine subunits with varying alkyl and aryl groups (Figure 1). These subunits in turn will be attached to the active core units found on lead antagonists.

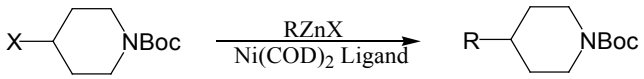

Figure 1

The Vicic library is going to be based upon active core unit **2** (Figure 2). Compound **2** will be synthesized by the reductive amination of **1** with derivatized piperidines.

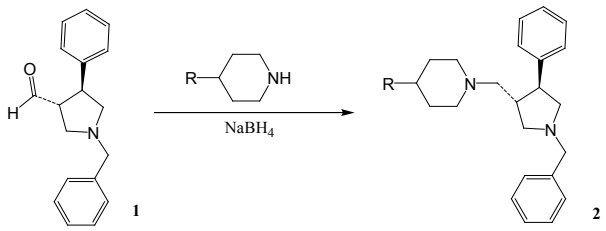

Figure 2

Derivatives of **3** (Figure 3) will be synthesized to study the effects of an all carbon subunit core. A *trans* arrangement of the aryl and piperidine groups is important because it has been shown that the *trans* stereochemistry exhibits more biological activity than *cis* stereochemistry.[11]

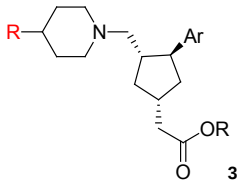

Figure 3

The goal of this project is to synthesize a precursor to **3** and determine if stereocontrolled additions of alkyl and aryl groups are possible (**4**, Figure 4). Under Negishi like conditions a new library with the general structure of **5** will be synthesized. This will be combined with the library of piperidines to prepare bifunctionalized compounds similar to **7**. These compounds will be screened for anti-HIV activity.

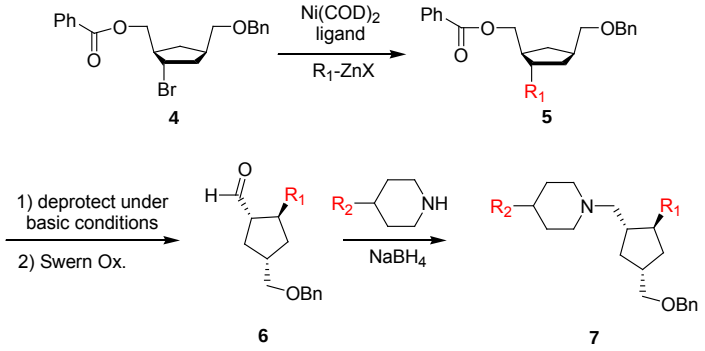

Figure 4

Compound **4** can be synthesized by following a known procedure for the synthesis of the known compounds, carba-5-iodo-2'-deoxyuridine and carba-(E)-5-(2-bromovinyl)-2'-deoxyuridine until about the 6th synthetic step.[12] Another published procedure will be used to generate the chiral alkyl bromide from the chiral alkyl alcohol (Figure 5).[13]

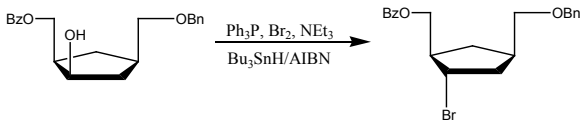

Figure 5

The synthesis begins with *endo*-norborn-2-en-5-ol which is not commercially available and must be synthesized chemically or enzymatically. Two different schemes have been used so far to synthesize *endo*-norborn-2-en-5-ol.

Experimental Procedures

The synthesis was begun by taking commercially available 1,3-dicyclopentadiene and combining it (0.11 mol) with 2-chloroacrylonitrile (0.11 mol) to make 5-chloro-5-cyano-bicyclo[2.2.1]hept-2-ene (Figure 6).[14] This was accomplished by heating the dicyclopentadiene past its boiling point and collecting the cracked cyclopentadiene once the distillate's temperature reaches 40 ºC. Monomeric cyclopentadiene was added drop-wise to a stirred mixture of the 2-chloroacrylonitrile in about 60 mL anhydrous benzene at room temperature. This reaction mixture was refluxed at 85 ºC for three hours under a nitrogen atmosphere until the reaction was complete. Benzene was removed by distillation and the solid product was dried under high vacuum (.4 mbar). Tan colored crystals were obtained.

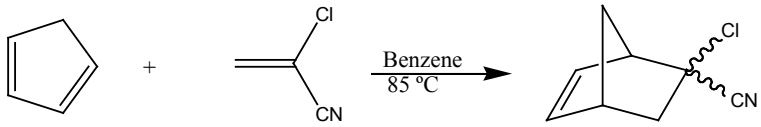

Figure 6

5-chloro-5-cyano-bicyclo[2.2.1]hept-2-ene (0.03 mol) was dissolved in about 40 mL dimethyl sulfoxide, and 8 M 85 % potassium hydroxide (0.08 mol) was added to the stirred mixture at room temperature (Figure 7).[15] The reaction mixture immediately turned a dark color. The reaction mixture is stirred for 24-36 hours. Dehydronorcamphor is obtained by distilling the reaction mixture under partial vacuum (vacuum created by a water aspirator) and collecting the product distillate between 30-40 ºC. The distillate is extracted with ether three times and dried with magnesium sulfate. The ether was removed by a rotary evaporator, and the clear oil was dried under high vacuum (.4 mbar).

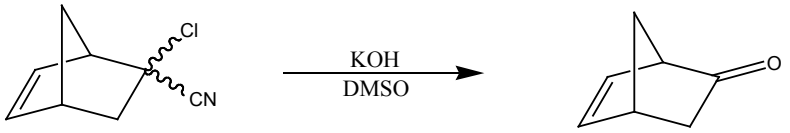

Figure 7

Reduction of dehydronorcamphor was achieved by dissolving dehydronorcamphor (2.7 mmol) in about 25 mL of anhydrous THF and cooling to -70 ºC under a nitrogen atmosphere (Figure 8).[16] A 1 M solution of (3 mmol) Super Hydride in THF was added to the stirred reaction mixture at -70 ºC. The reaction mixture is stirred at -70 ºC for three hours in an acetone and dry ice bath and then -20 ºC in an ethylene glycol

and dry ice bath for 1 hour. The reaction mixture was quenched by adding about 10 mL of water. The quenched reaction mixture was then extracted with ether three times and washed with water and a saturated sodium chloride solution. The extract was dried with magnesium sulfate, and the ether was removed with a rotary evaporator. Further purification of the product, norborn-2-en-5-ol, was achieved by column chromatography (dichloromethane). The product at room temperature takes form of colorless crystals.

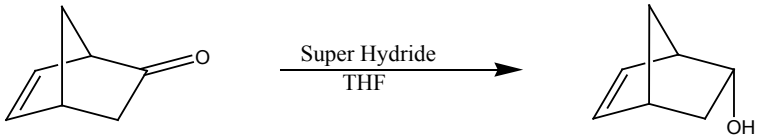

Figure 8

During the course of these reactions a few alternate synthetic routes were attempted. The first of which is synthesis of *endo*-norborn-2-en-5-ol by enzymatic hydrolysis using lipase from *Candida Cylindracea* (Figure 9).[17] The reaction was attempted twice, once at room temperature and the second time at 4 ºC. The reaction was monitored by gas chromatography. The first time a 1 M phosphate buffer solution was used, and the reaction was carried out at room temperature. This was done by making a 1 M solution of monobasic sodium phosphate monohydrate and a 1 M solution of dibasic sodium phosphate heptahydrate. 80 mL of the monobasic 1 M solution was combined with 420 mL of the dibasic 1 M solution to make a 1 M buffer solution. The pH was adjusted to 7.5. Lipase (4g) was added to the buffer. 5-norbornene-2-carboxylic acid methyl ester (10g) was added to the stirred buffer/enzyme solution and the reaction mixture was monitored by gas chromatography. It was determined by gas chromatography that the reaction was unsuccessful. The next time the reaction was attempted, a .5 M buffer solution was used instead of the 1 M buffer solution and the reaction was done at 4 ºC. All other procedure was identical. It was confirmed that the reaction was unsuccessful by gas chromatography.

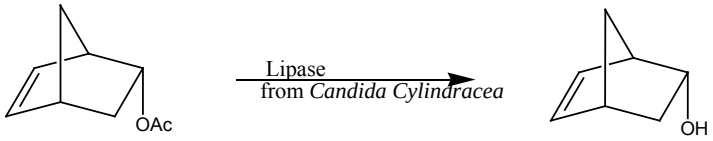

Figure 9

Results and Discussion

The first step of the synthesis yields 5-chloro-5-cyano-bicyclo[2.2.1]hept-2-ene in about a 75 % yield. The yield is just outside of 15 % of what the yield was of the known procedure. The isomers are present in about a 3:1 ratio. It is believed that the 5-*exo*-chloro-5-*endo*-cyano-bicyclo[2.2.1]hept-2-ene is the dominant stereoisomer for steric reasons. These results were confirmed by NMR and GC-MS analysis. ^{13}C APT NMR results are as follows for the dominant stereoisomer: ($CDCl_3$, 21.8 ºC) δ 42.49, 45.21, 48.08, 54.95, 56.44, 120.79, 131.48, 139.12. ^{1}H NMR results are as follows for the dominant stereoisomer: ($CDCl_3$, 21.8 ºC) δ q 6.33, q 6.0, s 3.68, s 2.98, dd 2.58, qd 2.15, m 1.63, dd 1.55.

The synthesis of dehydronorcamphor was confirmed by the change in NMR. The percent yield (5 %) is less than originally calculated because of the presence of unremoved solvents. There is also a solid byproduct that forms in the course of the reaction. Efforts are still being made to characterize it, but according to the procedure that was followed for this reaction, the byproduct makes up about 42 % of the product mixture. The percent yield could possibly be so low because the base concentration was possibly not high enough. The original procedure used about a 45 M concentration of base. The higher concentration of base could possibly push the reaction in favor of the dehydronorcamphor product. The reaction could possibly be more successful if it were refluxed for a period of time, as the base that the procedure added was hot. ^{1}H NMR results are as follows: ($CDCl_3$, 21 ºC) δ dd 6.56, m 6.1, s 3.18, q 3.0, m 2.2, d 1.97, dd 1.87.

The synthesis of norborn-2-en-5-ol was confirmed by IR and NMR analysis. Sometimes after the reaction was done, the *exo* stereoisomer was present in small amounts. The percent yield is estimated to be about 20 % after column chromatography. However, it has recently been discovered that norborn-2-en-5-ol can possibly be purified by sublimation. The *endo* isomer forms most of the time. It may be that lower temperatures favor the formation of the *endo* isomer.

The enzymatic hydrolysis scheme would seem to be the best method by which to synthesize the *endo*-norborn-2-en-endo-5-ol stereoisomer. However, this synthetic scheme has been largely unsuccessful. The first time the reaction was tried there was a problem with the phosphate salt concentration in the buffer. Initially the 1 M dibasic phosphate salt solution was not made properly. When the 1 M buffer solution was made part of the salt precipitated out changing the salt concentration in the buffer. The pH was also adjusted with pH paper instead of an electronic pH meter. This first attempt could have been unsuccessful because the enzyme might have become inactive at room temperature. It was probably unsuccessful because the salt concentration was not correct for the lipase. The second attempt at the reaction took place in 4 ºC. The monobasic and dibasic salt solutions were a .5 M concentration instead of a 1 M concentration. There were no initial precipitation problems. However the solution might not have totally been cooled to 4 ºC before the lipase was added. Additionally after a few hours of stirring and monitoring the reaction it was noticed that part of the salt had precipitated out because of the colder temperatures. These problems have yet to be addressed.

The reduction of dehydronorcamphor by using sodium borohydride was attempted twice. It was also done according to a known procedure of a nearly identical molecule.[18] It was initially thought that the reaction was unsuccessful because it was done in methanol instead of anhydrous methanol. The second time the reaction was attempted it proved untrue as anhydrous methanol was used. If the reaction using sodium borohydride did work, the Super Hydride is the better choice because super hydride is so much more sterically hindered than the sodium borohydride therefore favoring the formation of the *endo*-norborn-2-en-5-ol.

Data Collection

All experimental data was collected with a 300 MHz Bruker NMR and a 270 MHz JEOL NMR. Infrared spectra were collected with a Nicolet Impact 410 FT-IR spectrometer. Gas Chromatography data was collected with a GC-17A Shimadzu unit. Mass spectrometry data was collected with an Agilent Technologies GC-MS system.

Conclusions

Synthesis of *endo*-norborn-2-en-5-ol is the start of the synthesis of the chiral alkyl bromide. There are still a few problems in the synthetic steps that have already been completed. Improvement of the yield of dehydronorcamphor is one of the first things that need to be completed. The enzyme reaction also needs to be investigated further. Another problem to soon be worked out in the future is the problem of the formation of *exo*-norborn-2-en-5-ol. This problem can possibly be resolved using chiral solvent such as tartaric acid. Beyond these problems, the future involves going to the next few steps in the synthesis.

Chemicals

Dicyclopentadiene –Alfa Aesar
2-Chloroacrylonitrile – TCI
Sodium Phosphate Monobasic monohydrate – Sigma Aldrich
Sodium Phosphate Dibasic heptahydrate – Sigma Aldrich
5-Norbornene-2-carboxylic Acid Methyl Ester (*endo*- and *exo*- mixture) – TCI
Super Hydride (1M in THF) – Sigma Aldrich
Lipase from *Candida Cylindracea* - Fluka

Acknowledgements

NSF-REU
University of Arkansas
Bill Durham, Ph. D.
David Paul, Ph. D.
David Vicic, Ph. D.
Chris McFarland, Ph. D.
Gavin D. Jones
Marv Leister

References

1. Murphy, P. M. "The Molecular Biology of Leukocyte Chemoattractant Receptors." *Ann. Rev. Immun.* **1994,** *12*, 593-633.
2. Schall, T. J. "Biology of the rantes/sis cytokine family." *Cytokine* **1991,** *3*, 165-183.
3. Horuk, R. "Molecular properties of the chemokine receptor family." *Trends Pharm. Sci.* **1994,** *15*, 159-165.
4. Dragic, T.; Litwin, V.; Allaway, G. P.; Martin, S. R.; Huang, Y.; Nagashima, K. A.; Cayanan, C.; Maddon, P. J.; Koup, R. A.; et al. "HIV-1 entry into CD4+ cells is mediated by the chemokine receptor CC-CKR-5." *Nature* **1996,** *381*, 667-673.
5. Deng, H.; Liu, R.; Ellmeier, W.; Choe, S.; Unutmaz, D.; Burkhart, M.; Di Marzio, P.; Marmon, S.; Sutton, R. E.; et al. "Identification of a major co-receptor for primary isolates of HIV-1." *Nature* **1996,** *381*, 661-666.
6. Fauci, A. S. "Host factors and the pathogenesis of HIV-induced disease." *Nature* **1996,** *384*, 529-533.
7. Hill, C. M.; Littman, D. R. "Aids: Natural resistance to HIV?" *Nature* **1996,** *382*, 668-669.
8. Seibert, C.; Sakmar, T. P. "Small-molecule antagonists of CCR5 and CXCR4: A promising new class of anti-HIV-1 drugs." *Current Pharm. Design* **2004,** *10*, 2041-2062.
9. Dorn, C. P.; Finke, P. E.; Oates, B.; Budhu, R. J.; Mills, S. G.; MacCoss, M.; Malkowitz, L.; Springer, M. S.; Daugherty, B. L.; Gould, S. L.; DeMartino, J. A.; Siciliano, S. J.; Carella, A.; Carver, G.; Holmes, K.; Danzeisen, R.; Hazuda, D.; Kessler, J.; Lineberger, J.; Miller, M.; Schleif, W. A.; Emini, E. A. "Antagonists of the human CCR5 receptor as anti-HIV-1 agents. Part 1: Discovery and initial structure-activity relationships for 1-amino-2-phenyl-4-(piperidin-1-yl)butanes." *Bioorg. Med. Chem. Lett.* **2001,** *11*, 259-264.
10. Mirzadegan, T.; Diehl, F.; Ebi, B.; Bhakta, S.; Polsky, I.; McCarley, D.; Mulkins, M.; Weatherhead, G. S.; Lapierre, J. M.; Dankwardt, J.; Morgans, D., Jr.; Wilhelm, R.; Jarnagin, K. "Identification of the binding site for a novel class of CCR2b chemokine receptor antagonists: binding to a common chemokine receptor motif within the helical bundle." *J. Biol. Chem.* **2000,** *275*, 25562-71.
11. Hale, J. J.; Budhu, R. J.; Mills, S. G.; MacCoss, M.; Malkowitz, L.; Siciliano, S.; Gould, S. L.; DeMartino, J. A.; Springer, M. S. "1,3,4-Trisubstituted pyrrolidine CCR5 receptor antagonists. Part 1: discovery of the pyrrolidine scaffold and determination of its stereochemical requirements." *Bioorg. Med. Chem. Lett.* **2001,** *11*, 1437-1440.
12. Balzarini, J.; Baumgartner, H.; Bodenteich, M.; Clercq, E.; Griengl, H. *J. Med. Chem.***1989**, 32, 1861-1865.
13. H.; Bodenteich, M.; Griengl, H. *Tetrahedron Lett*. 1988, 29, 5745-5746.
14. Krieger, H. *Suomen Kemistilehti.* **1963**, *36, B*, 68.

15. Balls, D.; Brown, D.; Freeman, P. *JOC*. **1968**, *33*, 2211-2214.
16. Mayo, P.; Tam, W. *Tetrahedron*. **2002**, *58*, 9513-9525.
17. Eichberger, G.; Penn, G.; Faber, K.; Griengl, H. *Tetrahedron Lett.* **1986**, *27*, 2843- 844.
18. Chapuis, C.; Dupuis, D.; Guo, M.; Oppolzer, W. *Helvetica Chimica Acta*. **1985**, *68*, 2100-2114.

Synthesis of 3rd Generation Dendrimers as Chemosensors

Garen Holman, University of Central Arkansas
Conway, Arkansas

Abstract

The synthesis of a 3rd generation dendrimer can be attached to a fluorescent chemosensor that is selective to the marine biotoxin saxitoxin. The chemosensor must have minimum fluorescence when unbound to saxitoxin and must have significantly increased fluorescence that is not in the background fluorescence[1] region of saxitoxin when bound to the toxin. The binding constant for our sensor and saxitoxin should be $>10^5$.

Introduction

Saxitoxin (STX) (**1**) is a marine biotoxin produced by dinoflagellates. When shellfish consume the dinoflagellates, the toxin becomes concentrated within the shellfish. This is especially common during the more frequently occurring red tides, in which the algal species grow rapidly. The shellfish are then caught and brought to markets for human consumption. When ingested, the toxin causes paralytic shellfish poisoning (PSP). Approximately 0.2 mg of STX is enough to kill an average weight human and because it is so toxic, it is necessary to test for STX concentration in shellfish before they are shipped out for consumption[2].

STX 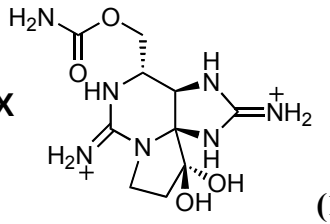

(1)

The only approved method for STX detection is mouse bioassay. Other methods have been developed but are expensive and not practical for in-field detection of saxitoxin. The goal is to develop a chemosensor that is cheap and efficient, and which avoids the ethical problems of mouse bioassay.

STX works as a sodium channel blocker. The STX is in solution when it is digested. When it binds in the sodium channel, the STX is in a solvent excluded region. I am trying to synthesize a 3rd generation dendrimer, and then attach anthracene diaza-crown ether to the dendrimer. The dendrimer will act to mimic the solvent excluded region surrounding the binding site. The diaza-crown ether will be our binding site, and the anthracene acts as our fluorescent sensor.

Results and Discussion

My dendrimer has three generations. We begin by making our first building block (Scheme 1), H_2N-G1$(COtBu)_3$ **2** in 50 % yields, which has three *tert*-butyl ester termini. In order to proceed with the process, it is necessary to protect the primary amine with an Fmoc protecting group (Scheme 2), using standard Fmoc protection/deprotection methods to form Fmoc-G1$(COtBu)_3$ **3** in 75 % yield. After deprotecting the t-butyl groups (Scheme 3), there are three carboxylic acid branches forming Fmoc-G1-triacid **4** in 78 % yield. Then we condense the triacid with three **2** molecules. The dendron is now in its second generation and is called Fmoc-G2$(COtBu)_9$ **5** and is obtained in 69% yield. We then add three equivalents of an Fmoc deprotected H_2N-G2$(COtBu)_9$ **6** to one equivalent of **4** to obtain our third generation dendrimer called Fmoc-G3$(COtBu)_{27}$ **7** (Scheme 4). After we obtain **7**, we remove the Fmoc protecting group from the amine, H_2N-G3$(COtBu)_{27}$ **8**, and then we will then attach the anthracene diaza-crown ether **9** sensor to our dendrimer[3]. At this stage (Scheme 5), we would have our final chemosensor **10**, which would be tested with saxitoxin samples.

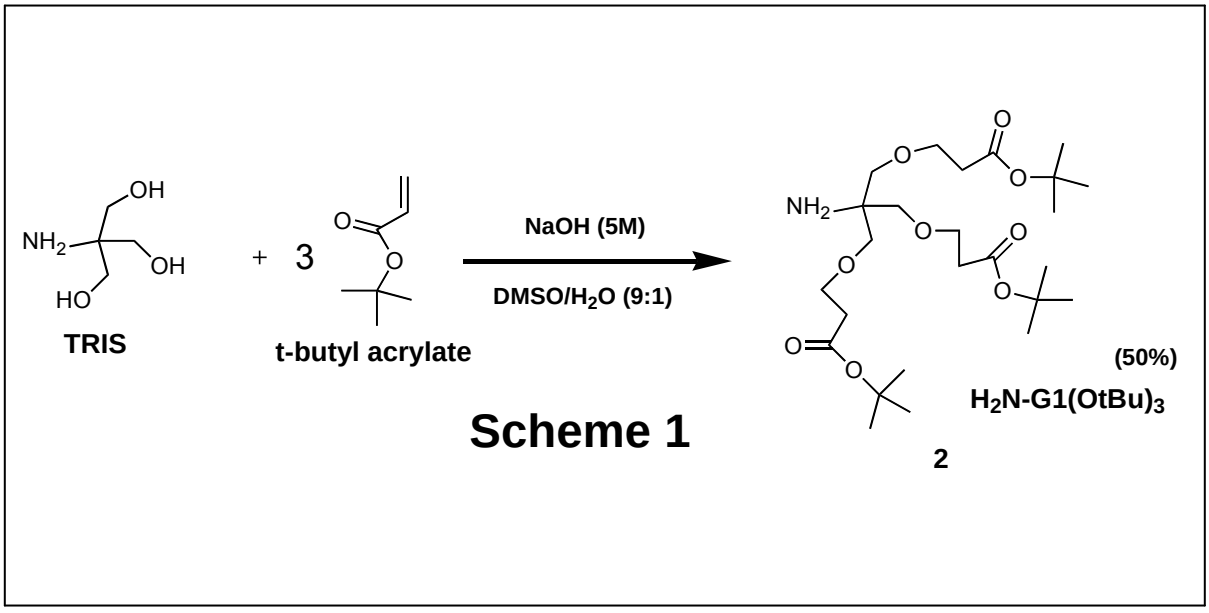

Scheme 1

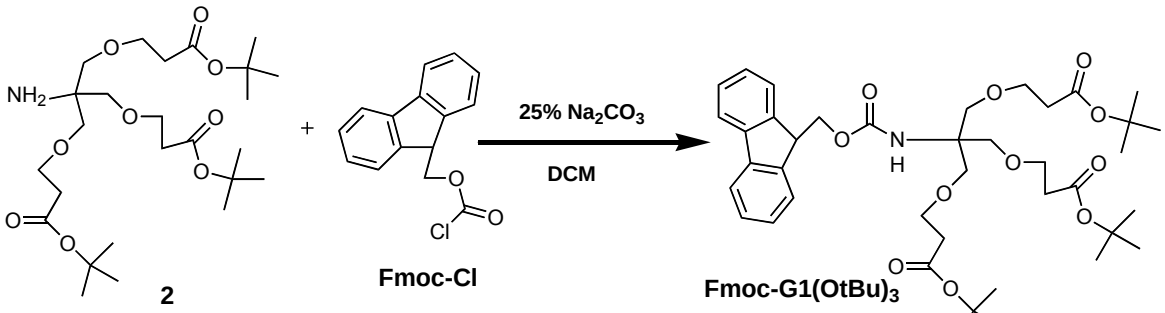

Scheme 2

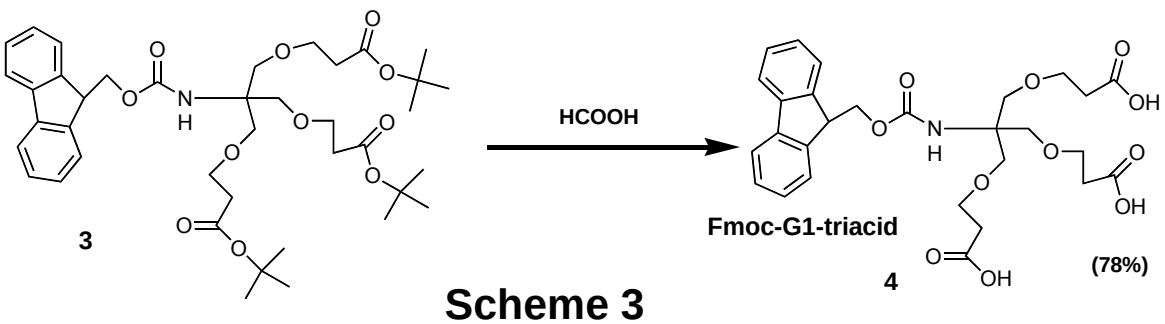

Scheme 3

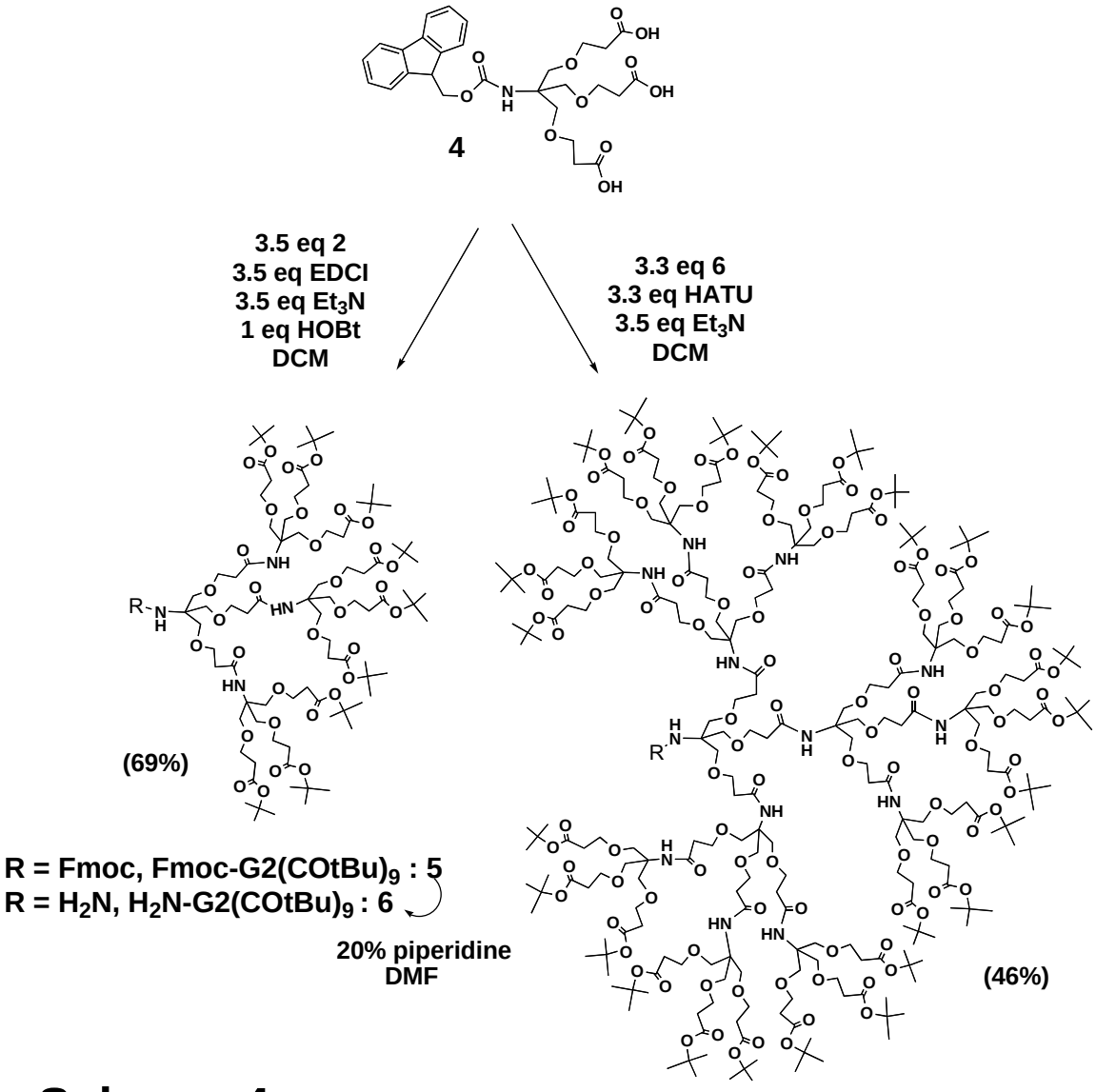
4
3.5 eq 2
3.5 eq EDCI
3.5 eq Et3N
1 eq HOBt
DCM
3.3 eq 6
3.3 eq HATU
3.5 eq Et3N
DCM
(69%)
R = Fmoc, Fmoc-G2(COtBu)9 : 5
R = H2N, H2N-G2(COtBu)9 : 6
20% piperidine
DMF
(46%)
R = Fmoc, Fmoc-G3(COtBu)27 : 7
R = H2N, H2N-G3(COtBu)27 : 8
20% piperidine
DMF

Scheme 4

Scheme 5

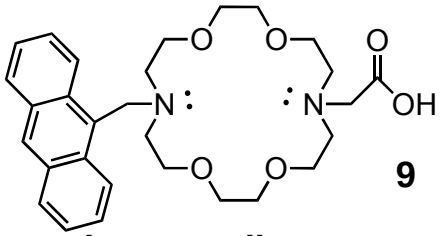

9

anthracene diaza-crown

8, Et_3N, HATU, DCM

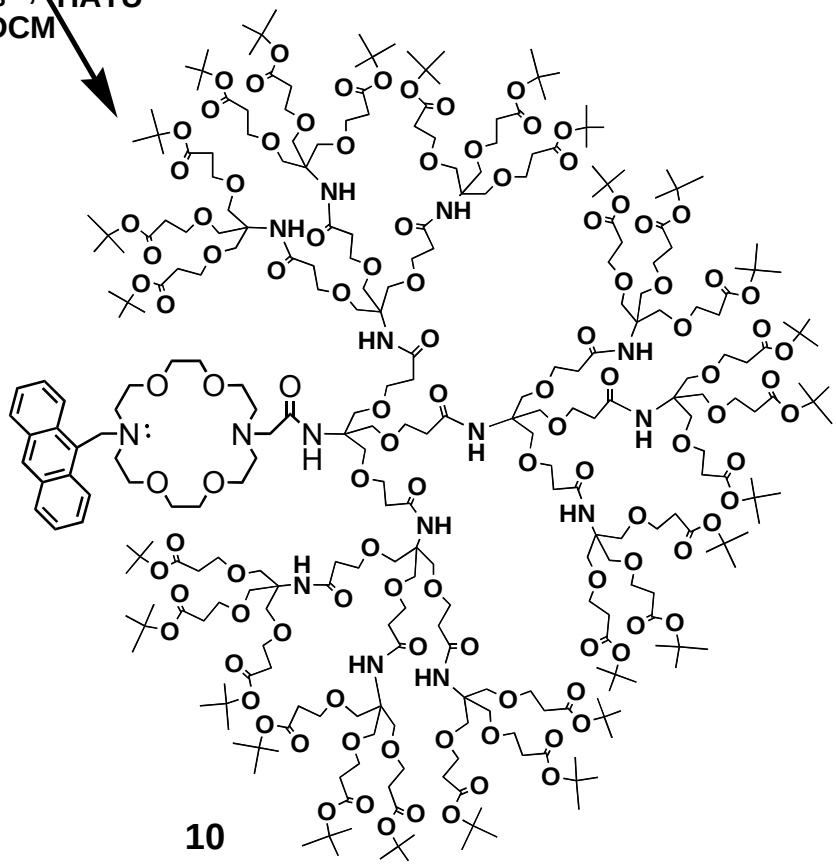

10

G3($COtBu)_{27}$-anthracene diaza-crown

Anthracene diaza-crown (Scheme 5) is our fluorescent sensor attached to the binding site. The sensor works through a process known as photo-induced electron transfer (PET). The molecule absorbs a photon of UV light, which excites an electron to the lowest unoccupied molecular orbital (LUMO). When STX is not bound to the diaza-crown, the nitrogen adjacent the anthracene sensor contributes an electron to the highest occupied molecular orbital (HOMO) before the excited electron can relax. This results in the release of energy in the form of heat, resulting in decreased fluorescence. This process is known as PET (Figure 1).

If STX is bound to the diaza-crown, then the relative energies of the HOMO and nitrogen lone pair orbitals are reversed. When the STX and sensor complex is excited with UV light, the electron in the LUMO relaxes back down to the HOMO. The release of the energy is in the form of light, resulting in increased fluorescence. This process occurs with no PET (Figure 2).

PET: ***(Decreased Fluorescence)***

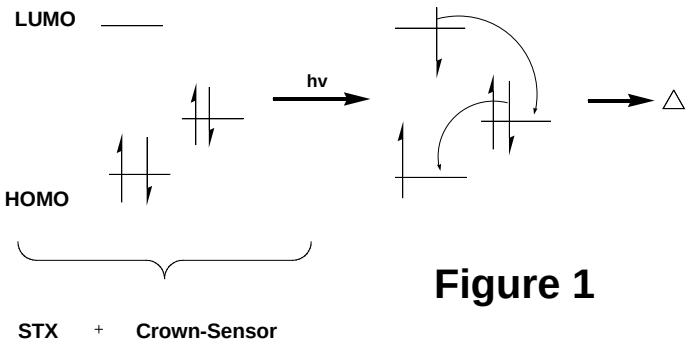

Figure 1

No PET: ***(Increased Fluorescence)***

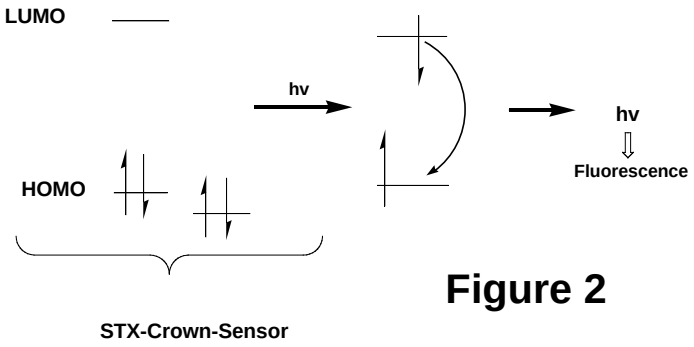

Figure 2

Conclusion

With each addition of a generation to the previous, the coupling became increasingly difficult. This was especially evident in the formation of the 3rd generation dendron, which took five days for the reaction to finish. Each generation was obtained, and during purification, a few of the test tubes that were found to be without impurities were collected for the NMR and Mass Spec samples. It was observed that the purity of the starting generation is crucial for a complete reaction. When the reaction proceeds with impure starting materials, di-substituted dendrons were sometimes observed, either by GPC or Mass Spec.

Experimental Procedures

General Methods. All reagents were commercially available and used without further purification. THF was dried over sodium benzophenone. Column chromatography was performed on either silica gel grade 62 (60-200 mesh) or aluminum oxide standard grade (~150 mesh) accordingly. TLC was carried out using aluminum-backed plates coated with silica gel 60 (F-254) or aluminum-backed plates coated with aluminum oxide 60 (F-254) respectively. Mass Spec is electrospray ionization (ESI) ion trap detection. NMR chemical shifts (δ) are reported in ppm using a residual solvent as an internal reference.

Tris{[2-(*tert*-butoxycarbonyl)ethoxy]methyl}methylamine (2). The TRIS (3.0 g, 24.76 mmol) was added to 5.0 mL of DMSO/H_2O (9:1). Then 0.5 mL 5.0M NaOH was added while stirring, followed by *tert*-butyl acrylate (12.38 mL, 85.29 mmol). The reaction was left stirring for 26 h. NH_4Cl was then added to the reaction mixture, and the organic layer was separated 3x using DCM in a separatory funnel. The product was then dried over $MgSO_4$ for 15 min then filtered. The solvent was then evaporated on a rotovap. The residue was purified by column chromatography (SiO_2, 8:2 EtOAc/hexane) to yield a colorless oil (6.8142 g, 50%). ^{1}H NMR ($CDCL_3$, 300 MHz): δ 1.407 (s, (CH_3)$_3$C, 27H); δ 2.412 (t, CH_2CH_2O, J = 6.3 Hz, 6H); δ 3.273 (s, CCH_2O, 6H); δ 3.604 (t, CH_2CH_2O, J = 6.3 Hz, 6H). ^{13}C NMR ($CDCL_3$, 300 MHz): δ 28.06 ((CH_3)$_3$C); δ 36.27 (CH_2CH_2O); δ 55.91 (CCH_2O); δ 67.08 (CH_2CH_2O); δ 72.81 (CCH_2O); δ 80.36 ((CH_3)$_3$*C*); δ 170.88 (*C*OOt-Bu). Ms: 506 (MH^+).

9-Fluorenylmethyl *N*- Tris{[2-(*tert*-butoxycarbonyl)ethoxy]methyl}-methylcarbamate (3). The amine (**2**) (3.4382 g, 6.827 mmol) was dissolved in 20 mL DCM and 20 mL 25% Na_2CO_3 was added while stirring. Then 9-fluorenylmethyl chloroformate (2.6500 g, 10.2435 mmol) was added to the reaction mixture and was allowed to stir for 21 h. NH_4Cl was then added to the reaction mixture, and the organic layer was separated 3x using DCM in a separatory funnel. The product was then dried over $MgSO_4$ for 15 min then filtered. The solvent was then evaporated on a rotovap. The residue was purified by column chromatography (SiO_2, 2:8 EtOAc/hexane) to yield a colorless oil (3.7388 g, 75%). ^{1}H NMR ($CDCL_3$, 300 MHz): δ 1.466 (s, (CH_3)$_3$C, 27H); δ 2.470 (t, CH_2CH_2O, J = 6.3 Hz, 6H); δ 3.668 (m, CCH_2O, CH_2CH_2O, 12H); δ 4.230 (m, $CCHCH_2$, $CHCH_2O$, 3H); δ 7.33 – 7.78 (m, C*H* aromatic, 8H). ^{13}C NMR ($CDCL_3$, 300 MHz): δ 28.11 (((CH_3)$_3$C); δ 36.23 (CH_2CH_2O); δ 47.24 ($CCHCH_2$); δ 58.78 (CCH_2O); δ 66.37 (CH_2CH_2O); δ 67.07 ($CHCH_2O$); δ 69.33 (CCH_2O); δ 80.47 ((CH_3)$_3$*C*); δ 119.90, 125.22, 127.06, 127.60 (*C*H aromatic); δ 141.27 (*C*CH); δ 144.13 (CH*C*CH); δ 170.85 (*C*OOt-Bu). Ms: 750 (MNa^+).

9-Fluorenylmethyl *N*- Tris[(2-carboxyethoxy)methyl]-methylcarbamate (4). Tri-*tert*-butyl ester (**3**) (3.7388 g, 5.1366 mmol) was stirred in 20 mL 96% HCOOH for 22 h. Then the reaction mixture was placed on a rotovap to remove the HCOOH, and then was placed on a vacuum overnight. The residue was purified by column chromatography (SiO_2, EtOAc) to produce a slight yellow oil, which when dried by vacuum was crystalline (2.2300 g, 78%). ^{1}H NMR (CD_3COCD_3, 300 MHz): δ 2.549 (t, CH_2CH_2O. J = 5.77 Hz, 6H); δ 3.701 (m, CCH_2O, CH_2CH_2O, 12H); δ 4.246 - 4.259 (m, $CCHCH_2$, $CHCH_2O$, 3H); δ 5.955 (NH amide, 1H); δ 7.35 - 7.87 (m, C*H* aromatic, 8H). ^{13}C NMR

(CD_3COCD_3, 300 MHz): δ 34.23 (*C*H_2CH_2O); δ 47.15 (*C*HCH_2O); δ 59.77 (*C*CH_2O) δ 65.73 (*C*H_2 benzylic); δ 66.79 (CH*C*H_2O); δ 69.00 (C*C*H_2O); δ 119.89, 125.31, 127.09, 127.58 (*C*H aromatic); δ 141.21 (C*C*CH); δ 144.33 (CH*C*CH; δ 155.10 (*C*ONH); δ 171.94 (*C*OOH). Ms: 560 (MH^+), 582 (MNa^+), 1119 (M_2H^+), 1141 (M_2Na^+).

9-Fluorenylmethyl *N*-Tris[(2-{[(tris{[2-(*tert*-butoxycarbonyl)ethoxy]-methyl}methyl)amino]carbonyl}ethoxy)methyl]methylcarbamate (5). The HOBt (0.2736 g, 1.7871 mmol), Et_3N (0.8718 mL, 6.2549 mmol), and EDCI (1.1991 g, 6.2549 mmol) were added to fmoc-triacid (**4**) (1.0000 g, 1.7871 mmol) and dissolved in 5 mL THF/DCM (1:1) and stirred for 30 min. Then the amine (**2**) (3.1628 g, 6.2549 mmol) was dissolved in 5 mL THF/DCM (1:1) and added to the reaction mixture to stir for 24 h. NH_4Cl was then added to the reaction mixture, and the organic layer was separated 3x using DCM in a separatory funnel. The product was then dried over $MgSO_4$ for 15 min then filtered. The solvent was then evaporated on a rotovap. The residue was purified by column chromatography (SiO_2, 6:4 EtOAc/hexane) to yield a slight yellow oil (2.4802 g, 69%). ^{1}H NMR ($CDCL_3$, 300 MHz): δ 1.450 (s, (C*H*$_3$)$_3$C, 81H); δ 2.443 (m, C*H*$_2$CH$_2$O, gen. 1 & 2, 24H); δ 3.633-3.700 (m, CH$_2$C*H*$_2$O gen. 1 & 2, CC*H*$_2$O gen. 1 & 2, 48H); δ 4.237-4.316 (m, CC*H*CH$_2$, CHC*H*$_2$O, 3H); δ 6.185 (NH amide, 1H); δ 7.33 – 7.77 (m, C*H* aromatic, 8H). ^{13}C NMR ($CDCL_3$, 300 MHz): δ 28.11 ((*C*H$_3$)$_3$)C); δ 36.13 (*C*H$_2$CH$_2$O gen. 2); δ 37.31 (*C*H$_2$CH$_2$O gen. 1); δ 47.26 (*C*HCH$_2$O); δ 59.77 (*C*CH$_2$O gen. 1 & 2); δ 67.03 (CH$_2$ benzylic); δ 67.57 (CH$_2$*C*H$_2$O gen. 2); δ 69.12 (C*C*H$_2$O gen. 2); δ 69.32 (C*C*H$_2$O gen. 1); δ 80.43 ((CH$_3$)$_3$*C*); δ 119.89,127.11, 127.61 (*C*H aromatic); δ 141.26 (C*C*CH); δ 144.14 (CH*C*CH); δ 170.82 (*C*ONH amides); δ 170.89 (*C*OOt-Bu). Ms: 2022 (M^+), 2044 (MNa^+).

***N*-Tris[(2-{[(tris{[2-(*tert*-butoxycarbonyl)ethoxy]-methyl}methyl)amino]-carbonyl}ethoxy)methyl]methylamine (6).** Nano-*tert*-butyl ester (**5**) (0.6564 g, 0.3646 mmol) was stirred with 40 mL 20% piperidine in DMF for 3 h. NH_4Cl was then added to the reaction mixture, and the organic layer was separated 3x using DCM in a separatory funnel. The product was then washed with water 3x to remove the DMF, then another 3x with DCM. The product was then dried over $MgSO_4$ for 15 min then filtered. The solvent was evaporated on a rotovap. The residue was purified by column chromatography (SiO_2, 5:95 MeOH/DCM) to yield a slight yellow oil (0.6425 g., 98%). ^{1}H NMR ($CDCL_3$, 300 MHz): δ 1.462 (s, (C*H*$_3$)$_3$C, 81H); δ 2.462 (m, C*H*$_2$CH$_2$O, gen. 1 & 2, 24H); δ 3.654 – 3.707 (m, CH$_2$C*H*$_2$O gen. 1 & 2, CC*H*$_2$O gen. 1 & 2, 48H); δ 7.282 (NH_2 amine, 2H). ^{13}C NMR ($CDCL_3$, 300 MHz): δ 28.12 ((*C*H$_3$)$_3$)C); δ 36.11 (*C*H$_2$CH$_2$O gen. 1 & 2); δ 59.82 (*C*CH$_2$O gen. 2); δ 67.02 (CH$_2$*C*H$_2$O gen. 2); δ 67.60 (CH$_2$*C*H$_2$O gen. 1); δ 69.09 (C*C*H$_2$O gen. 2); δ 80.48 ((CH$_3$)$_3$*C*); δ 170.94 (*C*OOt-Bu). Ms: 901.0 (MH_2^{+2}), 1800.0 (MH^+)^4.

Fmoc-G3(COtBu)$_{27}$ (7). Fmoc-triacid(**4**) (0.0226 g, 0.0404 mmol), HATU (0.0507 g, 0.1333 mmol), and Et_3N (0.0198 mL, 0.1414 mmol) were dissolved in 5.0 mL DMF while stirring. Then nano-*tert*-butyl ester (**6**) (0.2400 g, 0.1333 mmol) was added and allowed to stir for 114.5 h (monitored by gas phase chromatography (GPC) (Figure 19)) (0.1048 g.,46%). Ms: 5929.0 (MNa^+), 1477.7 (MH_4^{+4}).

Data Collection

Figures 3-20 are the ^{13}C NMR, ^{1}H NMR, and Mass Spec data to show we have obtained the dendron to its corresponding generation. Figures 3-5 suggest the synthesis of G1(OtBu) was a success. Figures 6-8 confirm the addition of the amine protecting group Fmoc-Cl, to produce Fmoc-G1(OtBu). Figures 9-11 show that the Ot-Bu protecting group has been removed, leaving three carboxylic acid branches corresponding to Fmoc-triacid. Figures 12-14 show that the G1 amine successfully coupled to the Fmoc-triacid to form the 2nd generation dendron Fmoc-G2(OtBu). Figures 15-17 again show the removal of the Fmoc protecting group was successful, resulting in G2(OtBu). Figures 18 & 19 confirm the final coupling to produce our 3rd generation dendron Fmoc-G3(OtBu). Figure 21 is a GPC graph confirming that the reaction to make Fmoc-G3(OtBu) has finished, shown by a large single peak. NMR data has not yet been obtained for the 3rd generation dendrimer, but because of the single product shown by GPC and Mass Spec data, it can be currently assumed that Fmoc-G3(OtBu) has been obtained.

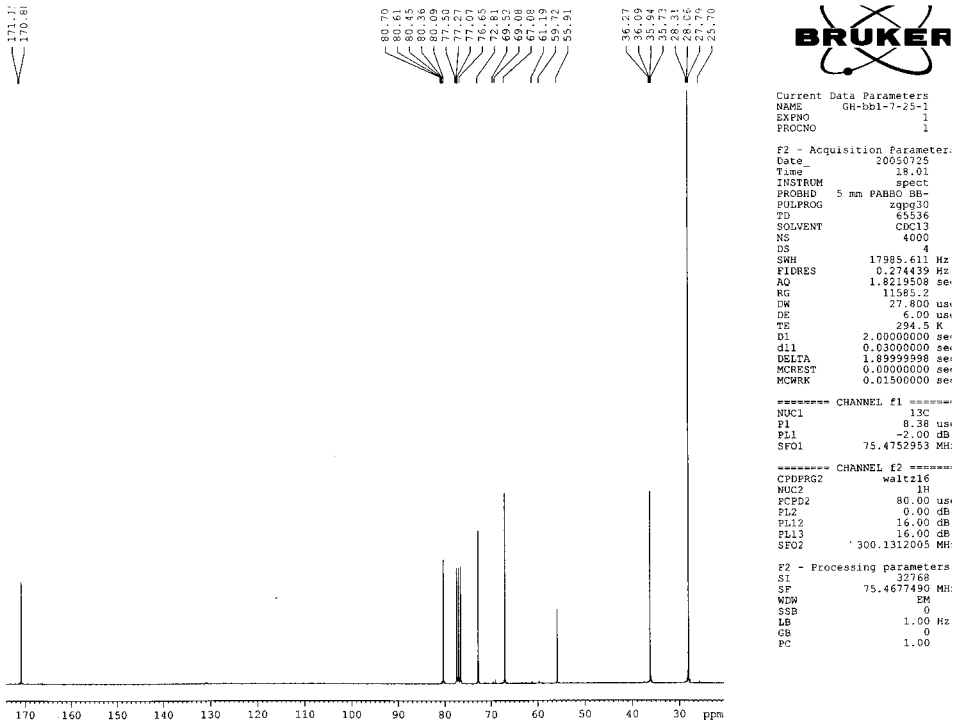

Figure 3: H_2N-G1$(COtBu)_3$ ^{13}C NMR

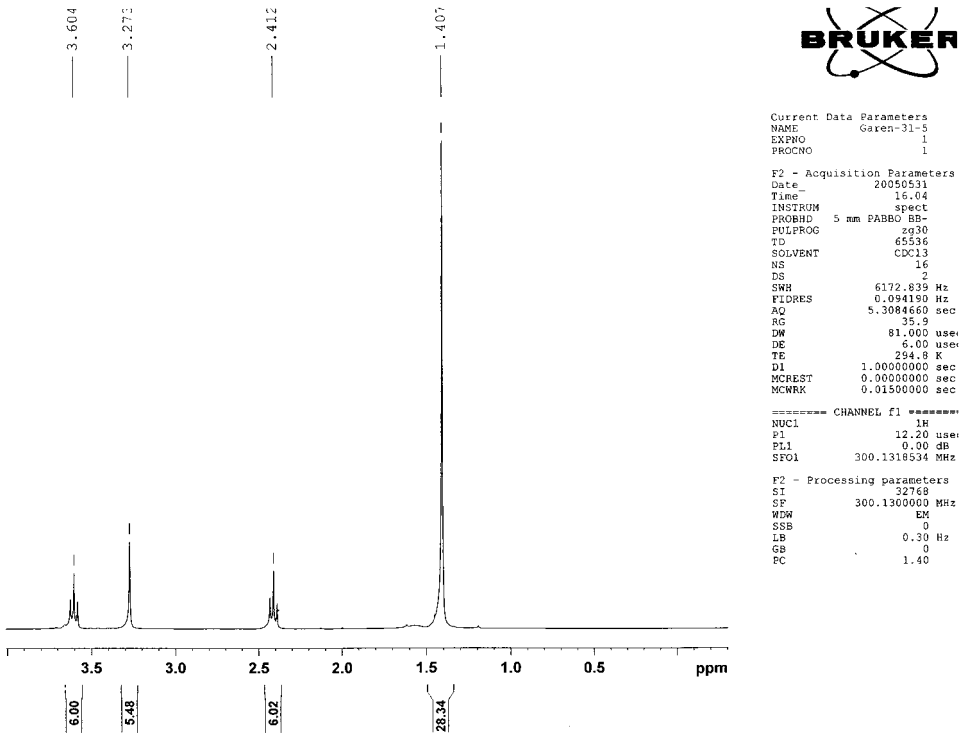

Figure 4: H_2N-G1$(COtBu)_3$ ^1H NMR

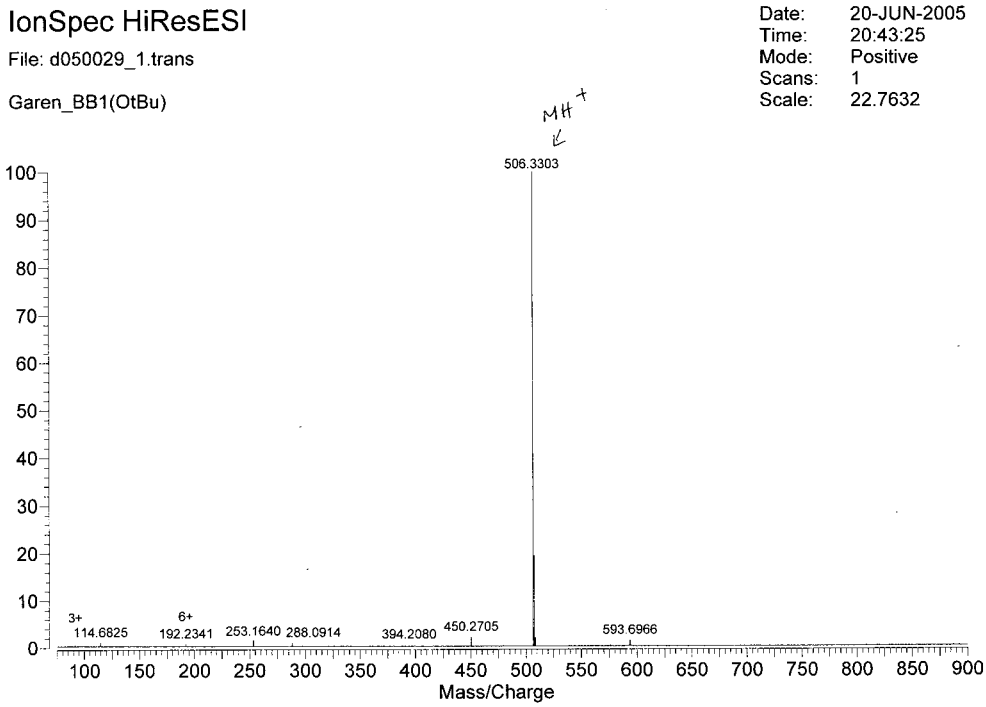

Figure 5: H_2N-G1$(COtBu)_3$ Mass Spec

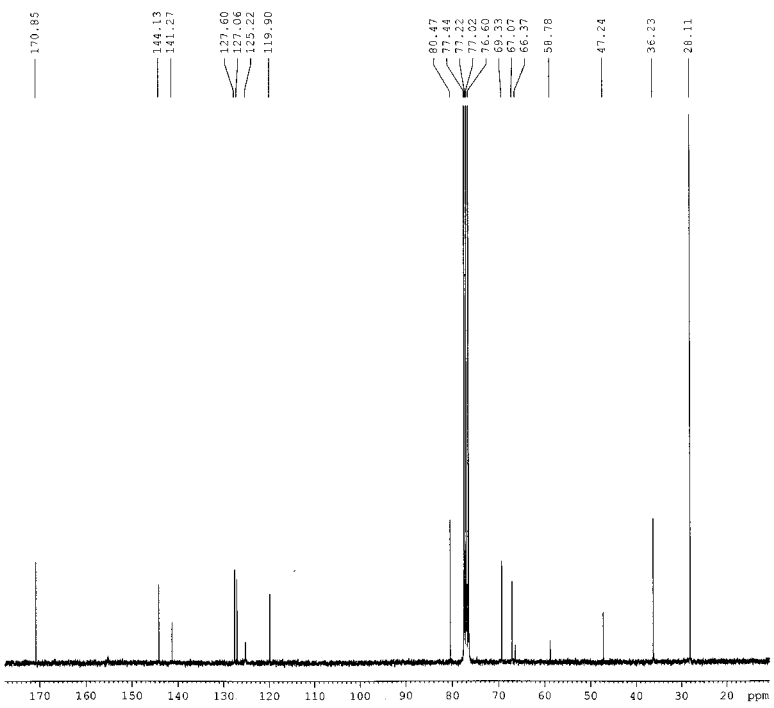

```
Current Data Parameters
NAME      GH-fmocbb1-7-25-1
EXPNO                    1
PROCNO                   1

F2 - Acquisition Parameters
Date_             20050725
Time                 22.28
INSTRUM              spect
PROBHD   5 mm PABBO BB-
PULPROG           zgpg30
TD                 65536
SOLVENT            CDCl3
NS                  6000
DS                     4
SWH            17985.611 Hz
FIDRES          0.274439 Hz
AQ              1.8219508 sec
RG                23170.5
DW                27.800 usec
DE                 6.00 usec
TE                295.1 K
D1           2.00000000 sec
d11          0.03000000 sec
DELTA        1.89999998 sec
MCREST       0.00000000 sec
MCWRK        0.01500000 sec

======== CHANNEL f1 ========
NUC1                 13C
P1                  8.38 usec
PL1                -2.00 dB
SFO1         75.4752953 MHz

======== CHANNEL f2 ========
CPDPRG2          waltz16
NUC2                 1H
PCPD2             80.00 usec
PL2                0.00 dB
PL12              16.00 dB
PL13              16.00 dB
SFO2        300.1312005 MHz

F2 - Processing parameters
SI                  32768
SF           75.4677490 MHz
WDW                    EM
SSB                    0
LB                  1.00 Hz
GB                     0
PC                  1.40
```

Figure 6: Fmoc-G1(COtBu)$_3$ ^{13}C NMR

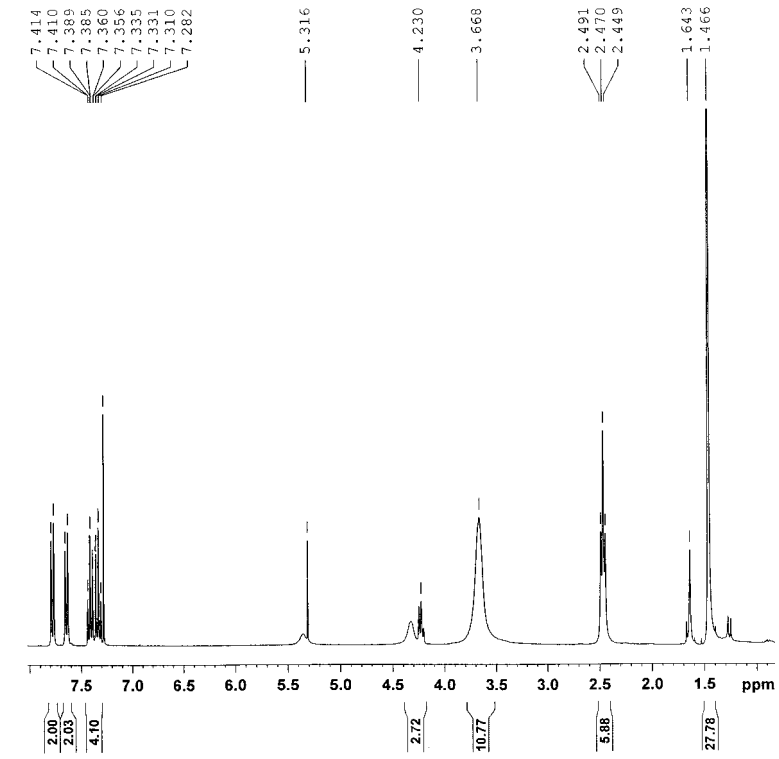

```
Current Data Parameters
NAME      Garen-6-8-05-1
EXPNO                   1
PROCNO                  1

F2 - Acquisition Parameter
Date_             20050608
Time                 14.41
INSTRUM              spect
PROBHD   5 mm PABBO BB-
PULPROG              zg30
TD                 65536
SOLVENT            CDCl3
NS                    16
DS                     2
SWH             6172.839 Hz
FIDRES          0.094190 Hz
AQ              5.3084660 se
RG                 203.2
DW                81.000 us
DE                 6.00 us
TE                301.0 K
D1           1.00000000 se
MCREST       0.00000000 se
MCWRK        0.01500000 se

======== CHANNEL f1 ======
NUC1                 1H
P1                12.20 us
PL1                0.00 dB
SFO1        300.1318534 MH

F2 - Processing parameters
SI                  32768
SF          300.1300000 MH
WDW                    EM
SSB                    0
LB                  0.30 Hz
GB                     0
PC                  1.00
```

Figure 7: Fmoc-G1(COtBu)$_3$ ^{1}H NMR

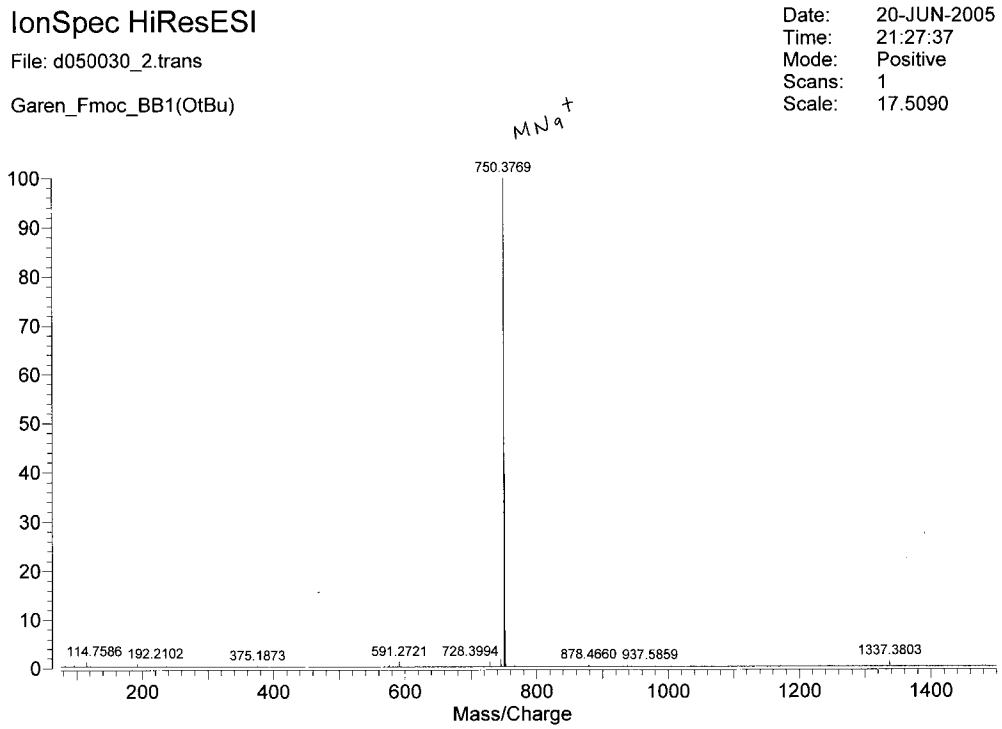

Figure 8: Fmoc-G1(COtBu)$_3$ Mass Spec

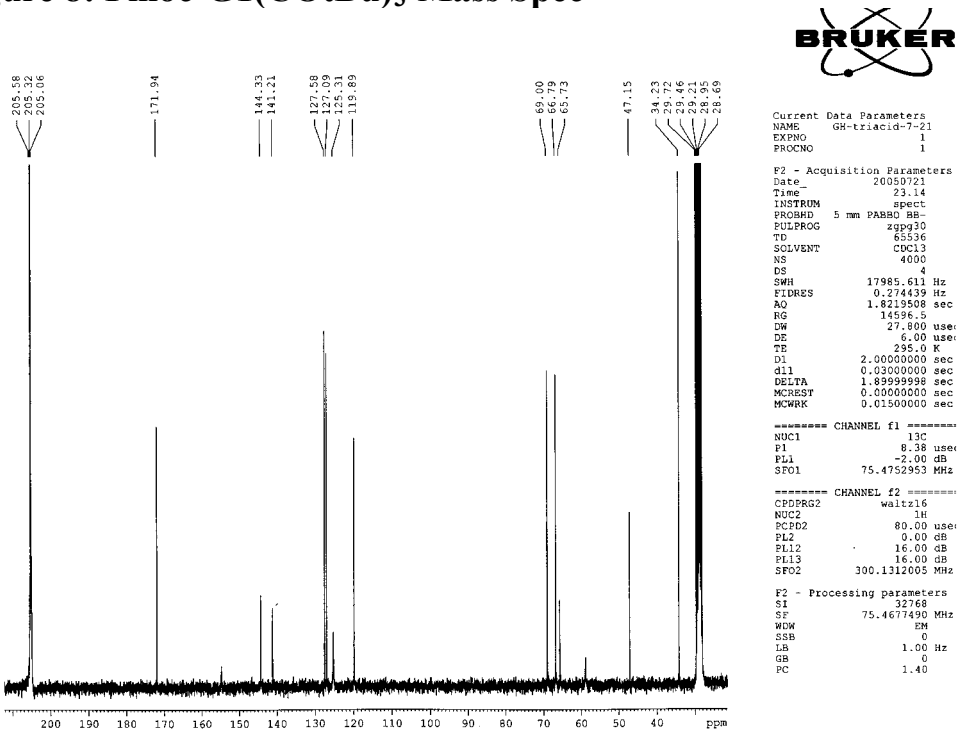

Figure 9: Fmoc-G1-triacid ^{13}C NMR

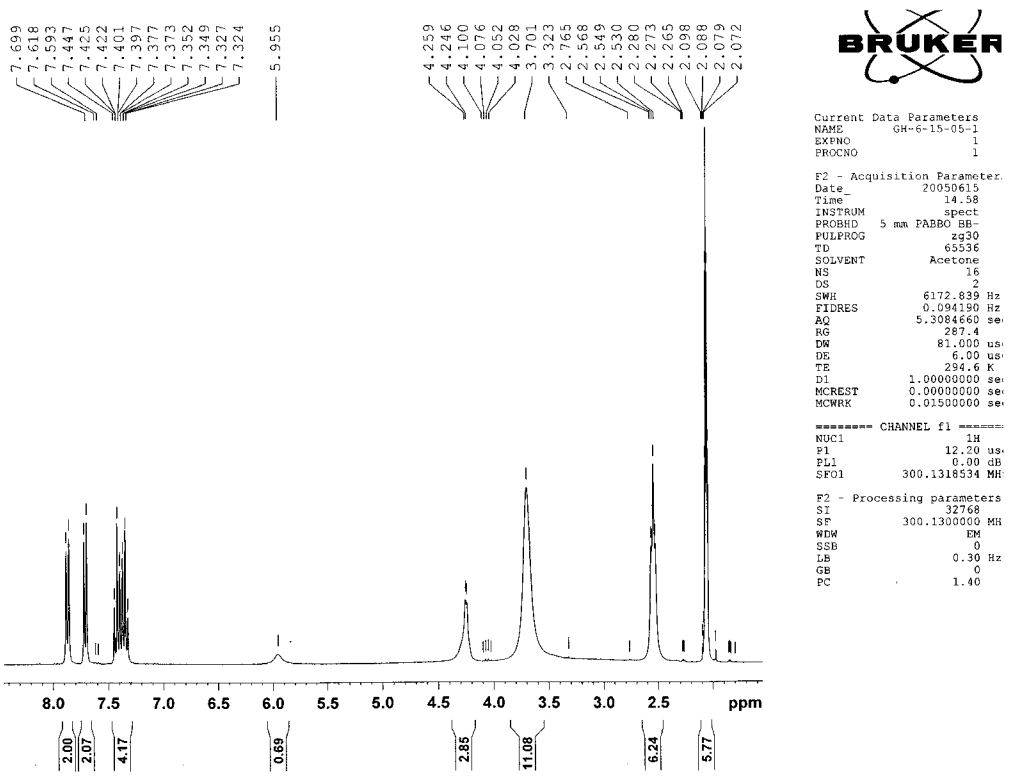

Figure 10: Fmoc-G1-triacid ^{1}H NMR

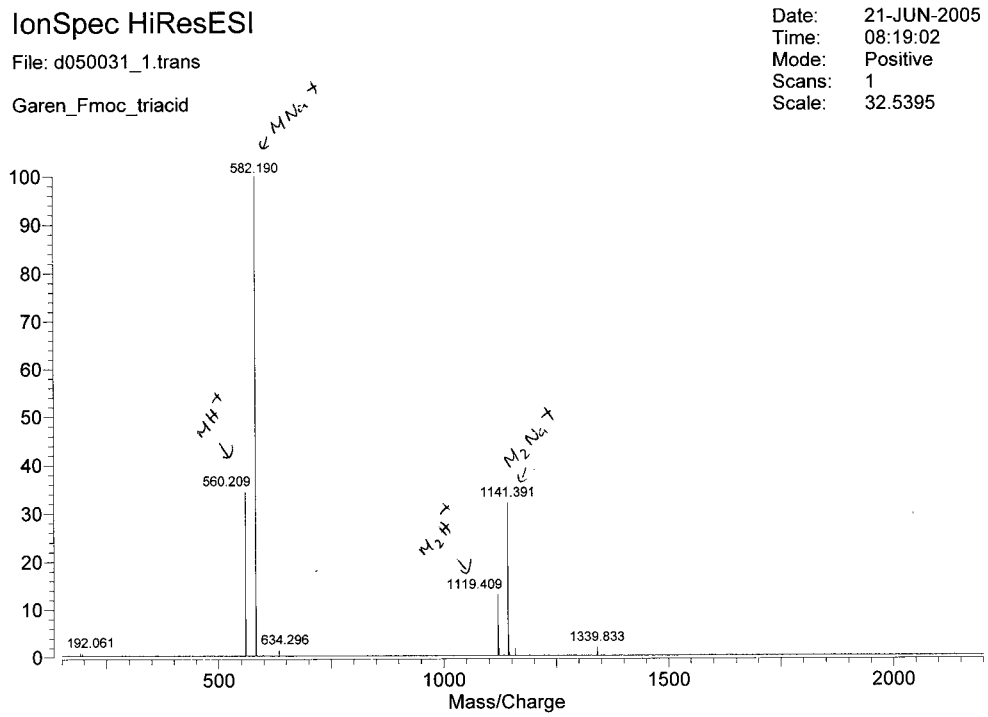

Figure 11: Fmoc-G1-triacid Mass Spec

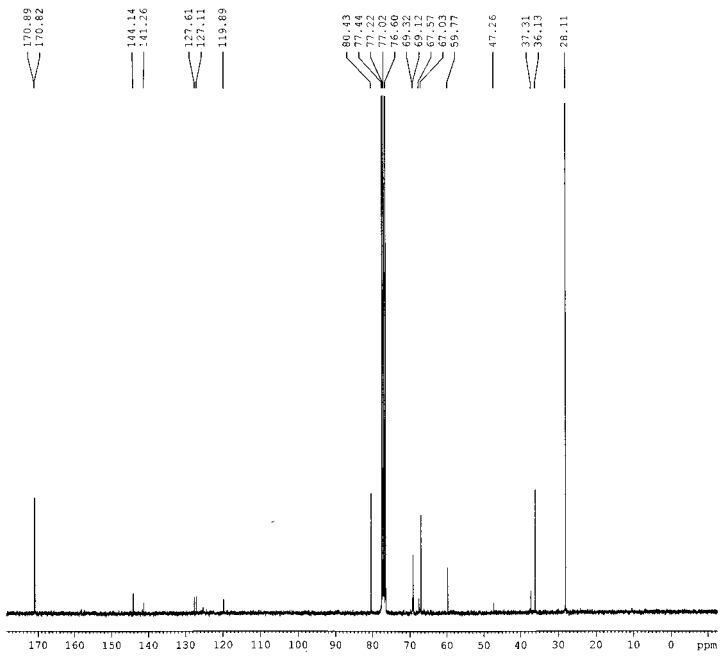

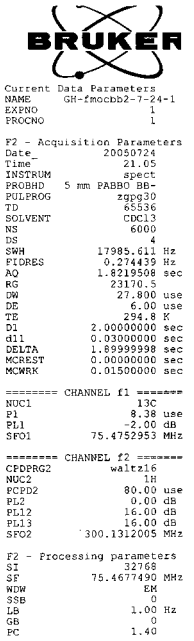

Figure 12: Fmoc-G2(COtBu)$_9$ ^{13}C NMR

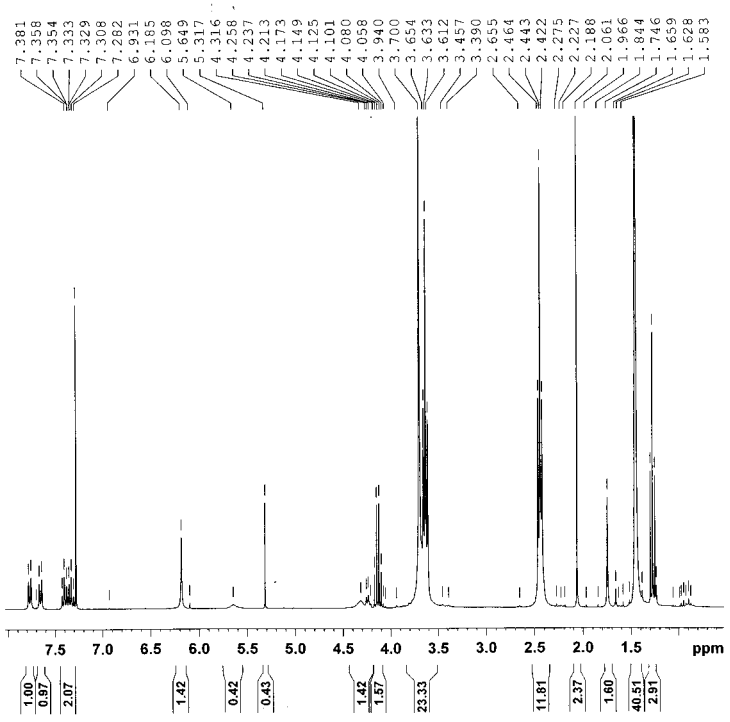

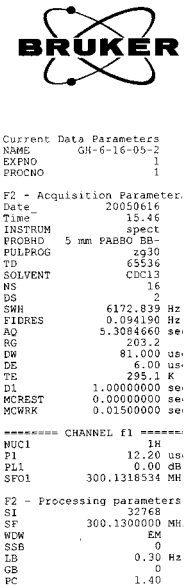

Figure 13: Fmoc-G2(COtBu)$_9$ ^{1}H NMR

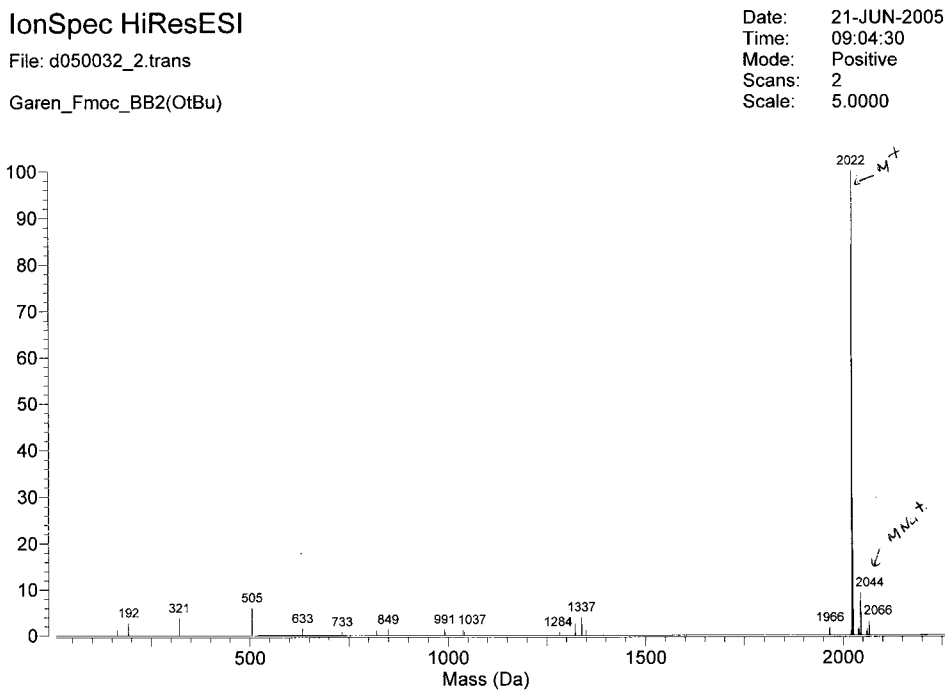

Figure 14: Fmoc-G2(COtBu)$_9$ Mass Spec

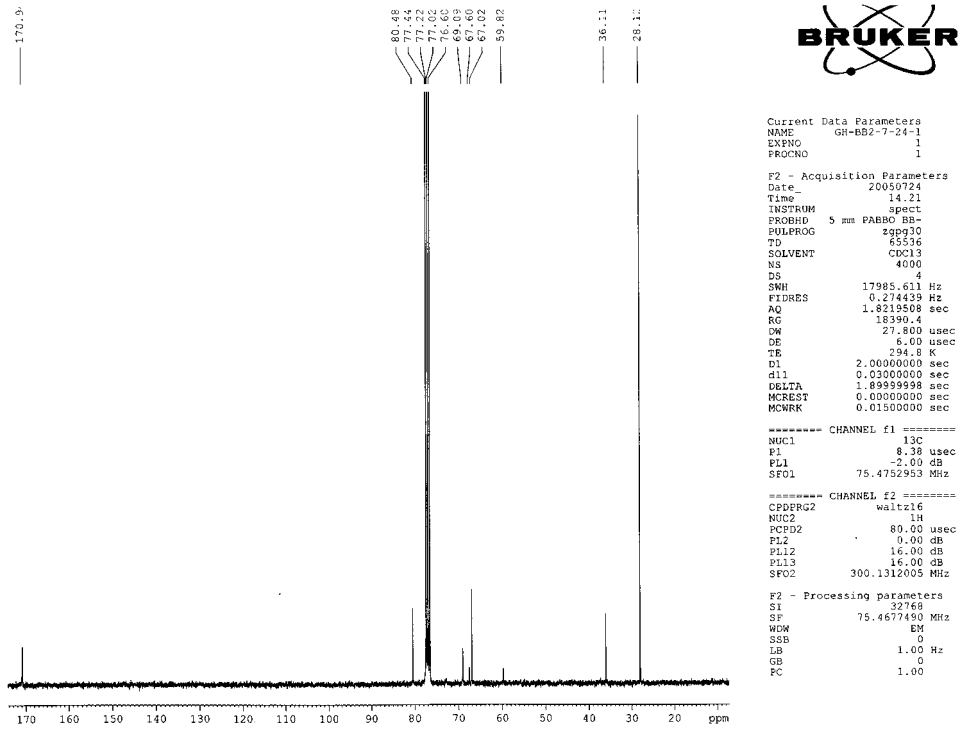

Figure 15: H_2N-G2(COtBu)$_9$ ^{13}C NMR

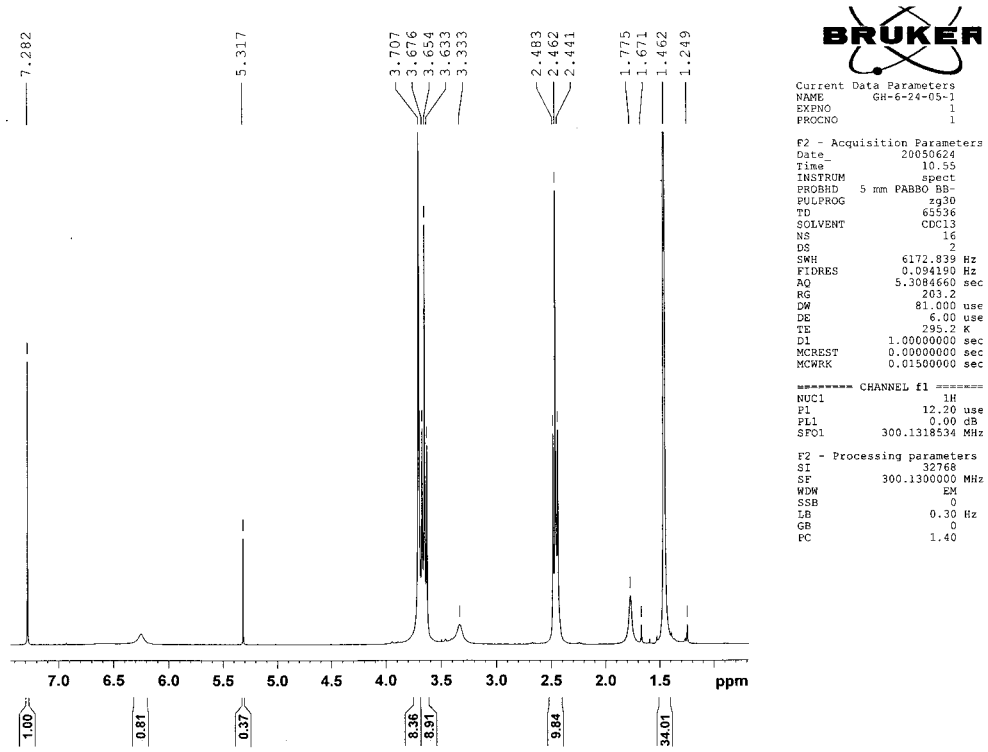

Figure 16: H_2N-G2(COtBu)$_9$ ^{1}H NMR

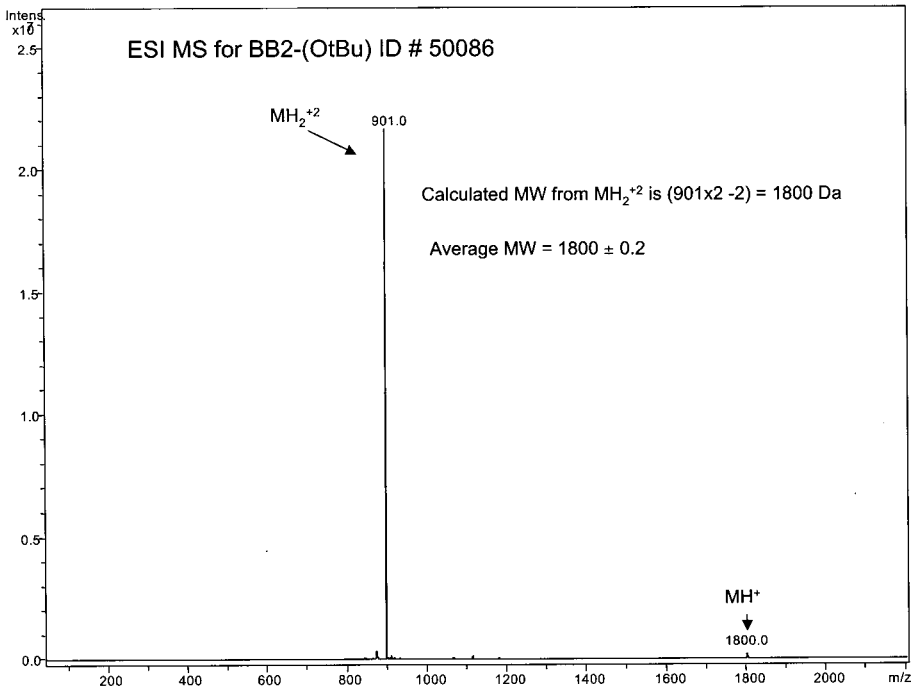

Figure 17: H_2N-G2(COtBu)$_9$ Mass Spec

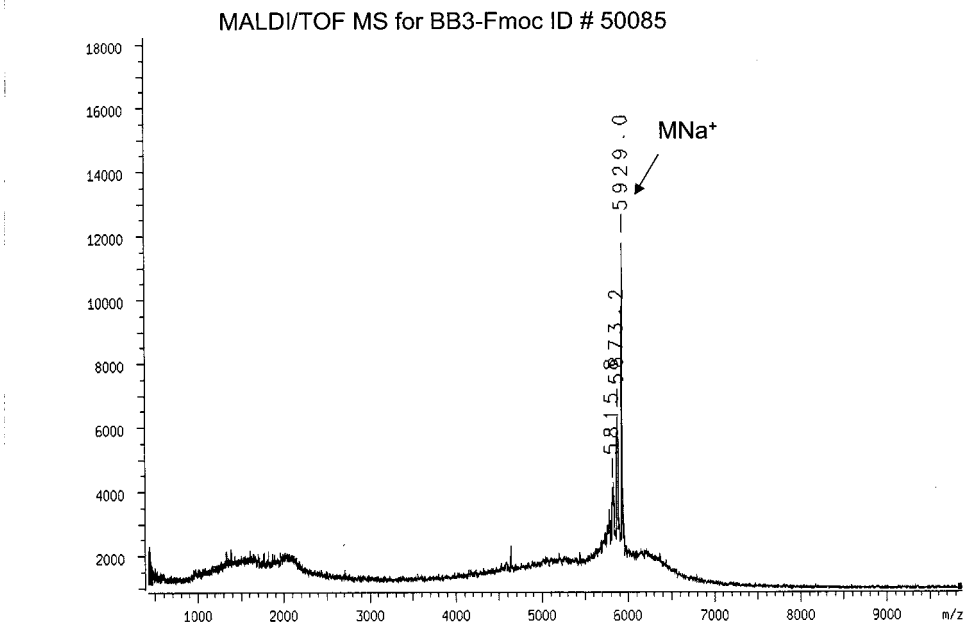

Figure 18: Fmoc-G3(COtBu)$_{27}$ Mass Spec

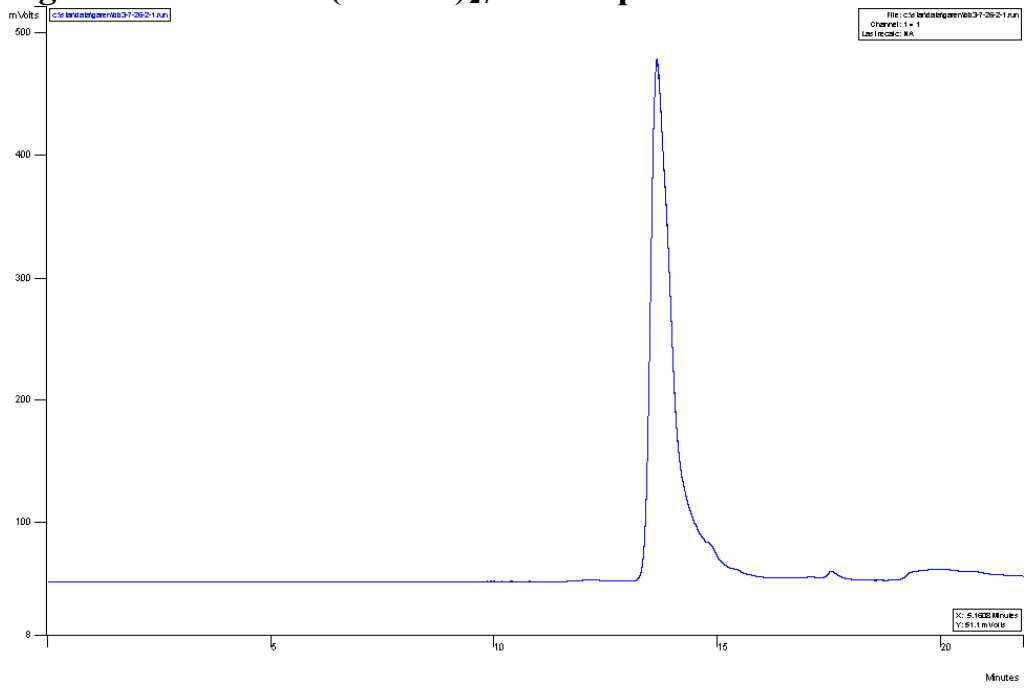

Figure 19: Fmoc-G3(COtBu)$_{27}$ GPC

References

1. Gawley, Robert E.; et al. *Toxicon*. **2005**. 45, 783-787.

2. Edwards, Neil. Saxitoxin. 18 Aug. 1998. School of Chem., Phys., & Env. Sci., U. of Sussex at Brighton. 20 June 2005 <http://www.chm.bris.ac.uk/motm/stx/saxi.htm>.

3. Cardona, Claudia M.; et al. *Helvetica Chimica Acta*. **2002**. 85, 3532-3558.

4. Cardona, Claudia M.; and Robert E. Gawley. *J. Org. Chem*. **2002**. 67, 1411-1413.

Acknowledgements

I would like to thank Dr. Gawley and the Gawley Group for all of their help and support with this project. I would like to thank Hua Mao for taking the time to help and show me many different aspects involved in this research. Without the funding from the National Science Foundation and the acceptance of the University of Arkansas into this program, none of this experience would have been possible. I appreciate the letters of recommendation sent by Dr. R. Tarkka and Dr. L. Isom of the University of Central Arkansas in Conway. I would also like to thank the National Institutes of Health (NIH P20 R15569), Arkansas Bioscience Institute, and the Environmental Protection Agency (EPA STAR R8295990) for there funding of our project.

The Progress on the Synthesis of Transition Metal Complexed 5-Member Ring Quinone Methide Analogs

Abigail Hubbard, Kent State University
Kent, Ohio

Abstract

Quinone Methides (QM) are a class of compounds whose reactivity includes DNA alkylation and hetero-Diels-Alder reactions. They are the reactive intermediate in numerous biological and synthetic processes, including an important class of chemotherapy drugs known as anthracyclines. However, the extreme reactivity of QM causes instability and prohibits their study. By synthesizing a metal-stabilized analog, it is hoped that QM chemistry could be studied in detail and lead to the synthesis of faster-acting, better-working anti-cancer agents. The focus of the Allison group is the synthesis of an o-QM analog via hydroxyferrocene chemistry.

Introduction

The Allison group's research is focused on a synthetic pathway for transition metal complexed five-membered ring quinone methide analogs. Quinone methides and their analogs have both a nucleophilic and an electrophilic center due to resonance:

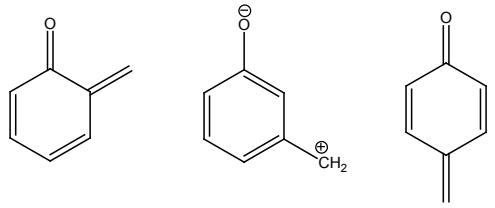

As a result, QM are an extremely reactive class of compounds and are thus unstable and difficult to isolate. Those which have been isolated were done so at very low temperatures as transition metal complexes:

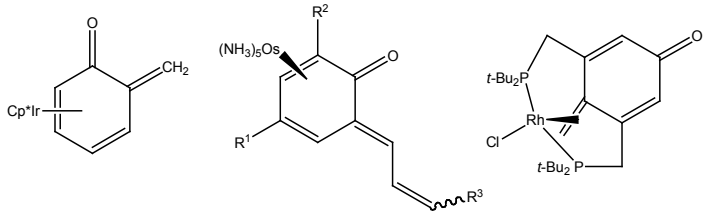

The reactivity of QM includes hetero-Diels-Alder reaction and DNA alkylation. These reactive characteristics make QM an important intermediate in numerous biological processes. QM have the ability to alkylate adenosine, guanine, and cytosine. Following are the reactive orientations of an o-QM with those nucleosides (1) and a hetero-Diels-Alder (2):

1.)

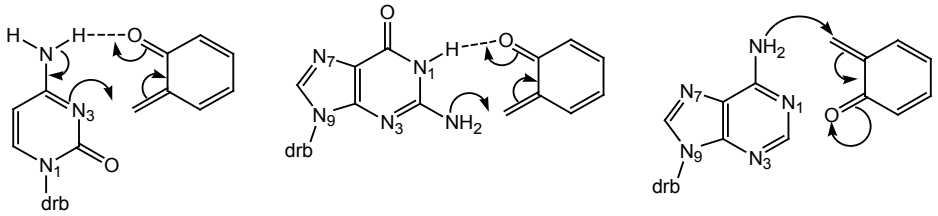

dC **dG** **dA**

2.)

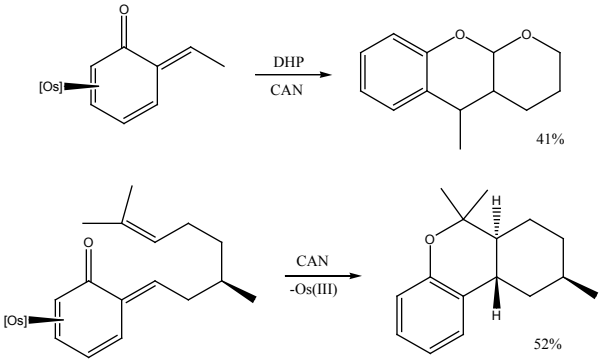

In order to study the chemistry of this very reactive molecule, the Allison group has developed a synthetic pathway for a transition metal stabilized QM analog, which takes the general form:

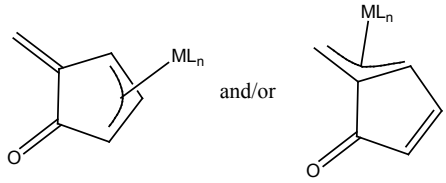

The synthetic strategy utilizes the stability of the pentadienyl ligand and hydroxyferrocene chemistry. The pentadienyl ligand is exceptionally stable due to multi-center metal bonding and resonance:

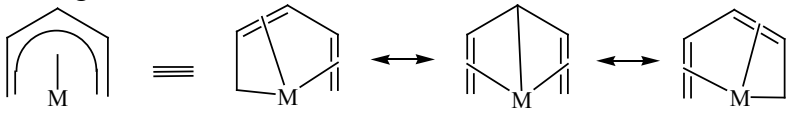

Placing a terminal carbonyl on such a ligand allows for rapid electrocyclic ring closure upon exposure to light and heat. In the same manner, a butadienyl metal complex may cyclize to a hydroxyferrocene:

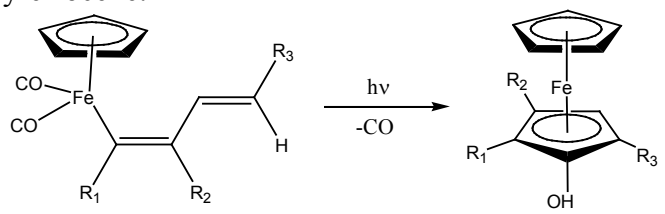

It is hoped that a pentatrienyl system may undergo a photolytic ring closure to yield a quinone methide analog in a manner analogous to the formation of the hydroxyferrocene via butadienyl complex cyclization:

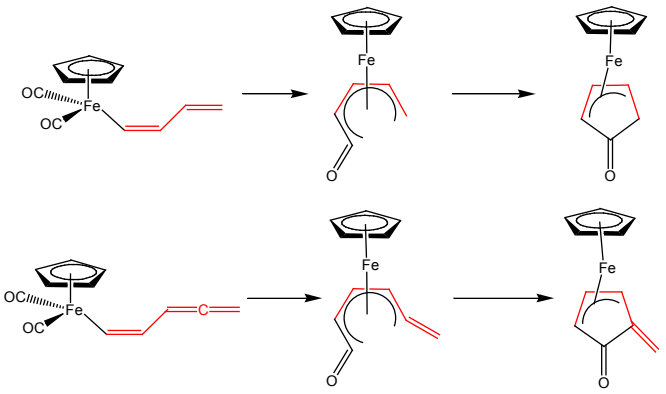

Thus, our synthetic strategy will form the allene via a metal-halogen exchange. A dihalocyclopropane will be attached to the metal with a metal-halogen exchange of a vinyl halogen. The retrosynthetic analysis is as follows:

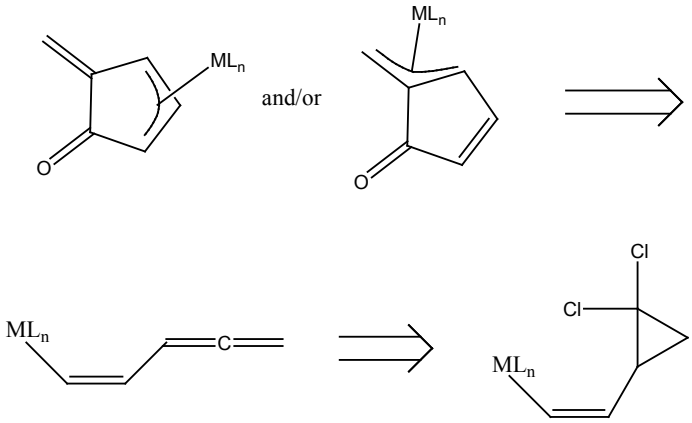

The vinyl halogen will be generated by a Corey-Fuchs reaction followed by a Wittig reaction and the dihalocyclopropane will be generated via carbene addition. The retrosynthetic analysis is as follows:

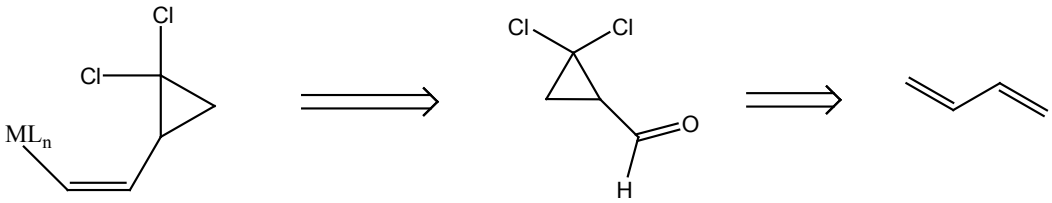

In this way, our research group hopes to efficiently synthesize a QM analog with enough stability to isolate and study.

Results and Discussion

Dichlorocarbene addition to butadiene using chloroform and K-t-butoxide will afford the vinyl dichlorocyclopropane. Ozonolysis will give the corresponding aldehyde which will then be converted to the dichloride/dibromide using a Corey-Fuch/Wittig reaction series. Loss of a single bromide using tributyltin hydride will yield the cis dichlorobromide which will be treated with n-butyl lithium to exchange the last bromine. This vinyllithium compound can be metallated with FpI and will lose lithium chloride to yield the desired vinylallene sigma complex. This product will then be prepared for photolytic ring closure to yield the quinone methide analog. The synthetic pathway is diagrammed below:

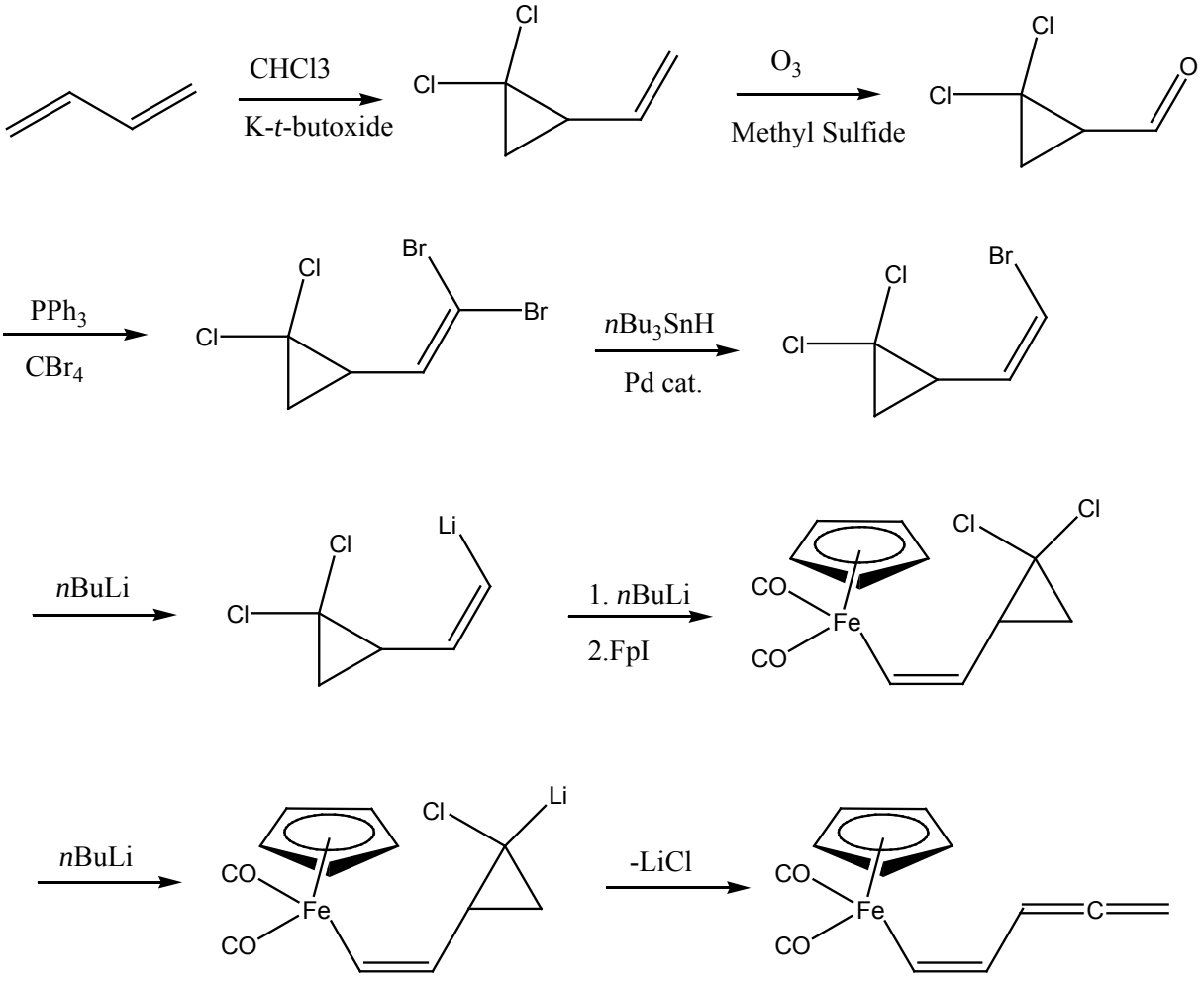

During my time here I have achieved the dichlorocarbene addition in a 23.7% yield. A proton NMR is located in the appendix as Figure 1 and peak designation is located below. The ozonolysis was completed in a 62.2% yield. A proton NMR is located in the appendix as Figure 2 and peak designation is given below. The Corey-Fuch/Wittig reaction series received a 37.7% yield. A proton NMR is located in the appendix as

Figure 3 and peak designation is located below. The reaction of tributyltin hydride proved to be a significant stumbling block in the synthesis. Initially, the Pd catalyst was synthesized in our research lab unsuccessfully. It was also purchased and found to be massively impure and unusable and was then placed on backorder by the chemical manufacturer. These events resulted in the loss of nearly a month's research time. In the meantime, I conducted the reaction at very low temperatures (-100ºC) with n-butyl lithium and no catalyst. I achieved significant conversion but with no stereospecificity in a 57.9% yield. A proton NMR located in appendix as Figure 4 and peak designation is located below. When the Pd catalyst was finally available, the reaction was achieved with superb stereospecificity to the cis conformation in a crude yield of 50.0%. A proton NMR is located in the appendix as Figure 5 and peak designation is given below. The product was, however, wrought with a significant impurity in the form of unreacted tributyltin hydride. Multiple attempts confirmed the excess reagent could not be separated from the product in a column. The dichloride/bromide could not be distilled due to instability resulting in decomposition with heat exposure. The synthesis could not continue without greater purity because of the very reactive nature of tributyltin hydride.

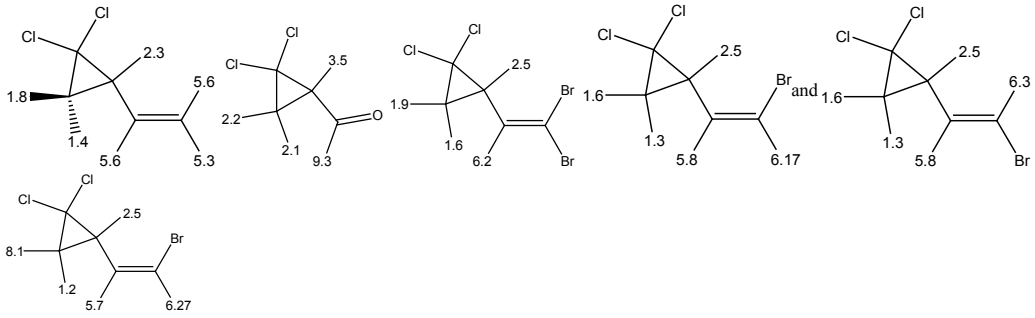

Figure 1 Figure 2 Figure 3 Figure 4 Figure 5

Experimental Procedure

Materials: Bruker 300 Ultra Shield used for all spectral data. All chemicals and solvents purchased from VWR. Carbon tetrabromide used in the C/F/W reaction was sublimed for purity. Dichloromethane in the C/F/W reaction and THF/ether in the tributyltin hydride reaction used as dry solvents after purification on an alumina column. All other chemicals were obtained in the highest commercial grade available and used without further purification.

1,1-Dichloro-2-vinylcyclopropane[1]: Chloroform (56.25 g, 37.7 ml) was added dropwise over three hours to a stirred slurry of 1,3-butadiene (37.50 ml, 23.25 g), pentane (125 ml), and potassium t-butoxide (37.50g) in a three-necked roundbottom flask equipped with a nitrogen inlet, mechanical stirrer, dry ice/isopropanol condenser and dropping funnel, cooled to -15 to -10ºC in an external salted ice bath. The slurry was stirred at 0ºC overnight (13 hr) and then allowed to warm to room temperature. Distilled water (125 ml) was added and the mixture was stirred for 20 minutes. The pentane solution was separated, washed with water (62.5 ml x 7) and saturated sodium chloride solution (62.5

ml x 1), dried over magnesium sulfate, and concentrated on the rotovap. Crude dibromide was purified via vacuum distillation through a Vigreaux column (0.5mm Hg, heated flask at 35ºC, receiving flask cooled with dry ice).

2,2-dichlorocyclopropylcarbaldehyde[2]: Ozone enriched oxygen was passed into a solution of methanol (10.5 ml) and dichloromethane (31.5 ml) with 1,1-dichloro-2-vinylcyclopropane (7.111g) at -78ºC until a faint blue color persisted. Nitrogen was then swept into the solution until no ozone could be detected. A solution of methyl sulfide (3.8 ml, 0.0525 mol) and dichloromethane (5.25 ml) was added dropwise. The solution was allowed to slowly attain room temperature and distilled for purification.

Corey-Fuchs Olefination of 2,2-dichlorocyclopropylcarbaldehyde[3]: Triphenylphosphine (525 mg), in dichloromethane (5 ml) was added to a mixture of tetrabromide (663 mg) and zinc powder (131 mg) in dichloromethane (3 ml) under nitrogen. After the mixture was stirred at room temperature for 30 minutes, the aldehyde (1.0 mmol) in dichloromethane (5 ml) was added and the suspension was stirred at room temperature for 14-17 hr. The crude reaction mixture was passed through a short pad of silica gel using dichloromethane, the solution was evaporated, and the residue was chromatographed on silica to get the product.

Uncatalyzed Hydrogenolysis: The dibromide/dichloride compound (250 mg) was diluted with dry THF and ether (15 ml ea.) and cooled to -100ºC in a hexane/liquid nitrogen slurry bath. N-butyl lithium (75% stoichiometric excess) was added dropwise over 15 minutes. The solution was stirred for 15 minutes and then quenched with a 4:1, THF:water solution (5 ml). The flask was stirred at -100ºC for 30 minutes and then slowly warmed to 0ºC over 1 hour. The aqueous layer was washed with ether and the organic layer was then dried over magnesium sulfate. The product was purified on a silica column with hexanes.

Stereoselective Hydrogenolysis with Pd Catalyst[3]: A Schlenk flask was charged with dichlorovinyl derivative (0.800 mmol) and $Pd(PPh_3)_4$ (46.2 mg) and flushed with nitrogen. Toluene (8 ml) was added and the solution was treated with tributyltin hydride (0.958 mmol) under stirring at room temperaturefor 0.2-3.0 hours until the reaction composition did not change (as monitored by TLC). The reaction mixture was diluted with brine and extracted with dichloromethane (3 x) and dried over magnesium sulfate. The solvents were evaporated and the residue was chromatographed on silica gel to the product.

Conclusions

Once the QM analogs have been successfully synthesized, their chemistry can be investigated by changing the substituents R_1-R_4 and thereby varying the reactivity of the molecule.

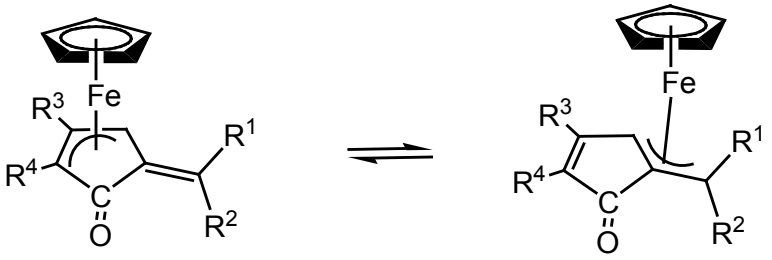

Such substituent variation should greatly alter the reactivity towards hetero-Diels-Alder reactions by directing the approach of the dienophile electronically or sterically. In addition to this research, the stabilizing metal could also be varied to observe different chemical reactivity. Strategic substituent manipulation of quinone methide analogs promises much new knowledge on the chemistry of this important and reactive class of compounds.

Appendix

Figure 1

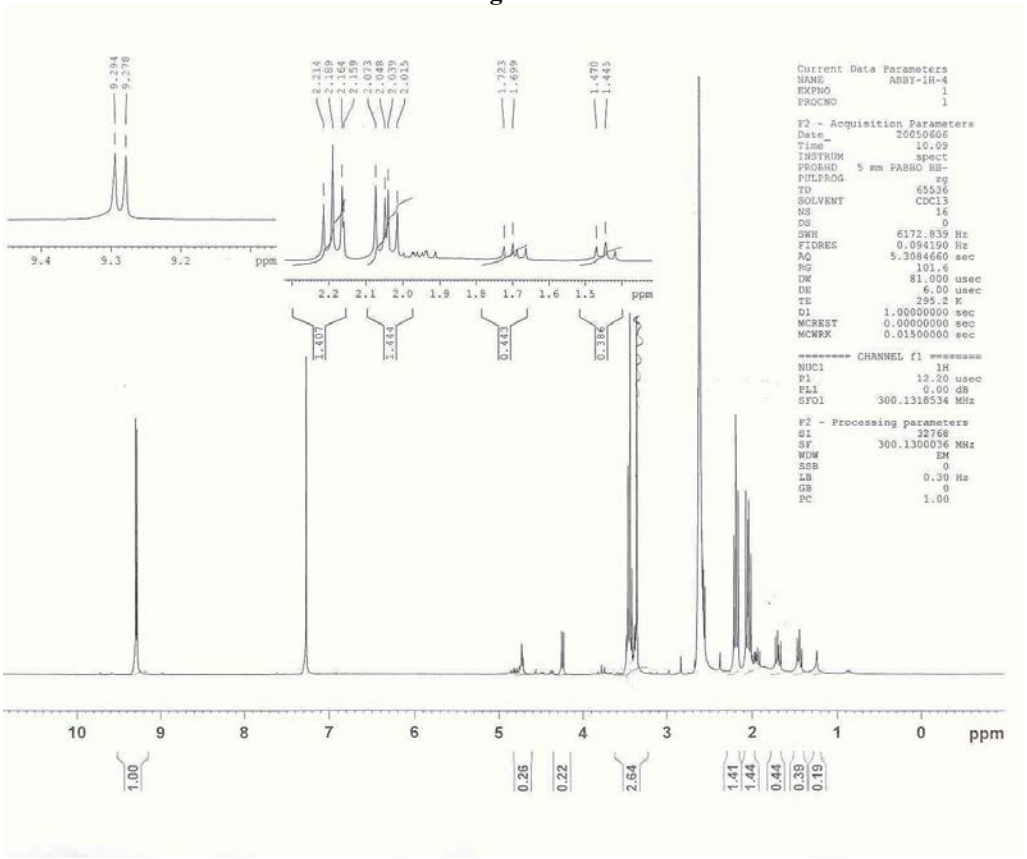

Figure 2

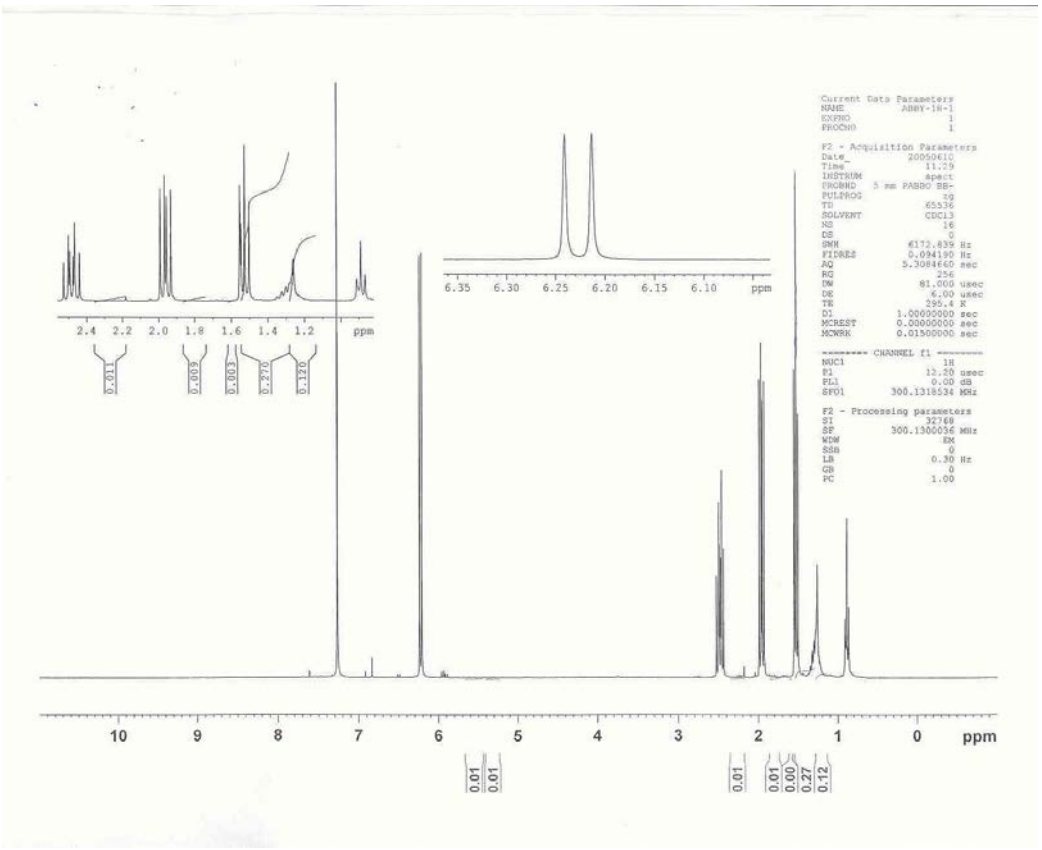

Figure 3

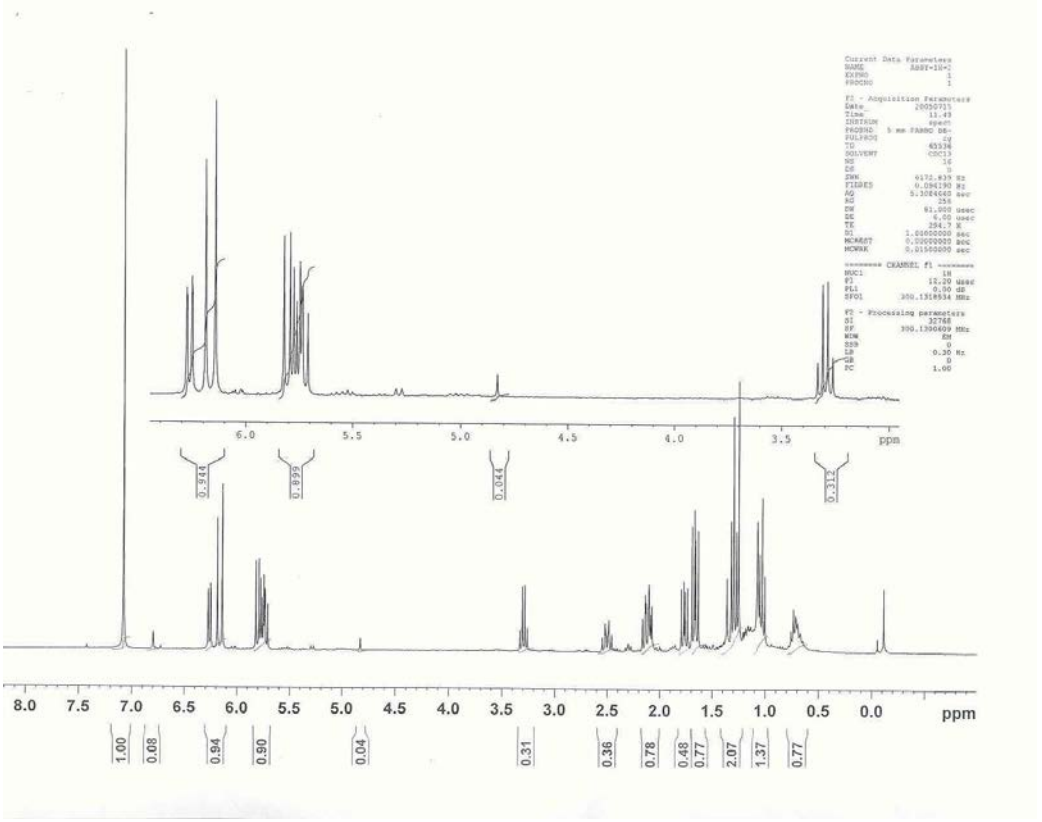

Figure 4

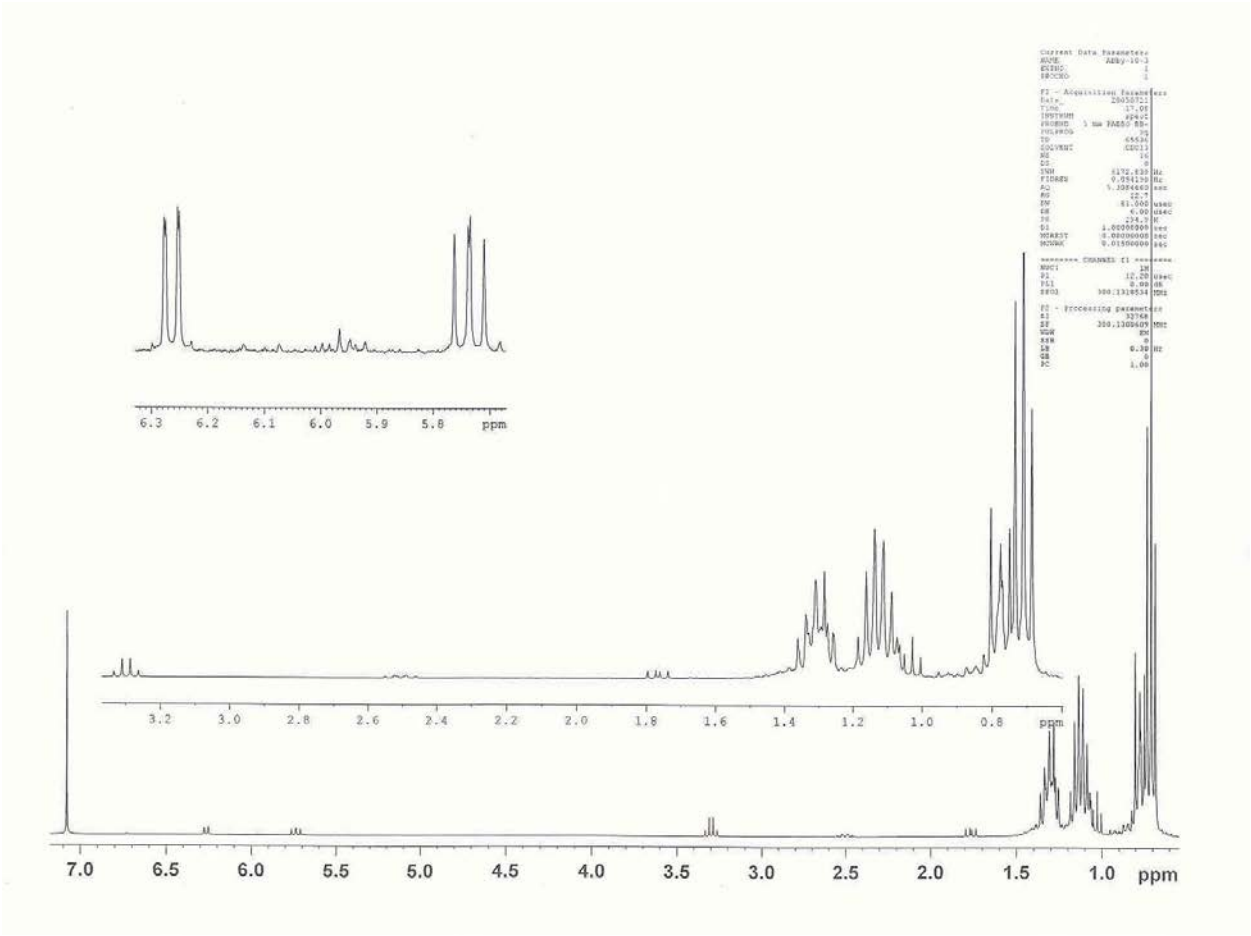

Figure 5

Acknowledgements

I would like to extend my sincere thanks and appreciation to the National Science Foundation Research Experience for Undergraduates for providing this incredible opportunity and to Dr. Neil Allison and the Allison Research Group for their guidance, support, and inspiration.

References

1. Miller, Ronald. *Synthesis and Reactions of Selected Potential Synthons of an Iron Complexed Vinylcyclopropyldiene*. University of Arkansas Department of Chemistry. 1984.

2. Holm, Kjell H.; Lee, Donald G.; Skattebol, Lars. *Preparation of gem-Dibromocyclopropyl Aldehydes and Acids from Conjugated Dienes*. University of Oslo Department of Chemistry. 1978.

3. Fiedler, Pavel; Teply, Filip; Stara, Irena G.; Stary, Ivo; Kollarovic, Adrian; Saman, David; Rulisek, Lubomir. *Synthesis of [5]-, [6]-, and [7]Helicene via Ni(0) – or Co(I)-Catalyzed Isomerization of Aromatic cis, cis-Dienetriynes*. Academy of Sciences of the Czech Republic. 2002.

Fabrication and Applications of Colorful Diffraction from Ordered Arrays of Colloidal SiO_2

John-David McElderry, Brigham Young University
Provo, Utah

Abstract

Crystalline colloidal arrays were formed from SiO_2 particles with diameters ranging from 262-389nm in both 2 dimensional thin films and 3 dimensional suspensions showing brilliant diffraction of color. By grafting sulfonyl groups onto the surface of the SiO_2 spheres the surface charge was enhanced thus creating a suspension of particles in water that repel each other by electrostatic repulsion. Such highly charged spheres configure themselves into low energy structures which resemble crystalline lattices that show Bragg diffraction properties.

Introduction

Fabrication of polystyrene (PS) crystalline colloidal arrays (CCA) has many applications in the materials sciences. Due to its optical properties of light diffraction[1] it has drawn much attention in the nanoscience and materials science field. With a wide variety of compounds that can be grafted onto the surface of PS spheres more applications are being found that involve anything from light filters to trace detection of metal ions[2,3]. Much of the current experimentation being performed with CCA's is focused on control of the crystalline formation in both 3D[3-5] and 2D[4-7]. For instance, the formation of a consistent monolayer on a given substrate is of enormous use. Multilayers of alternating sphere diameter monolayers is only one example of what is being done in the study of light diffraction on a 2D surface[7]. Crown ethers grafted onto the PS spheres in a 3D lattice have shown to be sensitive to select ions even in ppb concentrations[3].

More recently, Wei Wang has taken much of what S. A. Asher has done with PS and used silicon dioxide spheres utilizing a technique by Stober et al.[8] With the diversity of sphere materials more can be done in the way of surface modification. Possible applications that are being researched is the grafting of DNA onto SiO_2 spheres with the hopes of creating a CCA that is sensitive to certain cancer antigens up-regulated in the body during early stages of cancer[9]. Other novel ideas for control of the crystalline formation are being researched such as a photopolymerization of acrylic groups attached to the surface of the SiO_2 spheres with the expectation of creating a substrate-free monolayer at the interface of two immiscible liquids.

Much of the difficulty in the fabrication and application of the SiO_2 CCA is that there is lower surface charge on the SiO_2 spheres than the PS spheres and therefore has less repulsive force in the 3D crystalline structure. It is necessary to produce spheres with a surface modification that will enhance the surface charge enough to form a crystalline lattice that has interplanar spacing that is much greater than the sphere diameter[4]. SiO_2 spheres have been created with an enhanced surface charge which allows the formation of CCA's in water that Bragg diffracts light as has previously been done with PS colloidal spheres.

Experimental Procedures

Materials. Tetraethoxysilane (TEOS, 98%) and 2-(4-chlorosulfonylphenyl) ethyltrimethoxy-silane (50% in dichloromethane) were purchased from Acros Organics. NH_4OH (28-30%), propanol, absolute ethanol, and chloroform were purchased from VWR. SnakeSkin pleated dialysis tubing (MW 10,000) was purchased from Pierce Scientific. Mixed bed ion exchange resin was purchased from J.T. Baker. Ultrapure water was obtained from a Millipore-Q Plus water purifier with a resistivity of 18 MΩ was used throughout the experiment.

Synthesis. Two techniques were used in the synthesis of the silicon dioxide spheres. The method established by Stober et al. created spheres with a diameter between 200-300nm. Two solutions of 100ml each were made separate, one containing NH_4OH and H_2O in alcohol and the other containing TEOS in alcohol. The two were mixed together having combined concentrations of 1.63M NH_4OH, 17M H_2O, and .05-.3M TEOS. The concentration of TEOS was varied while water and ammonia concentrations were held constant. About two minutes after the solutions were mixed the resulting solution turned turbid white.

The second technique developed by Wang et al. is a modification of the Stober method used to create larger spheres with a low polydispersity. Spheres with a diameter of 300-450nm were synthesized using the following technique. The two solutions were made just as before with moderate stirring. More TEOS is then added 1ml/min in its concentrated form twenty minutes after the start of the reaction. This allows the first addition of TEOS to "seed" the reaction and therefore the second addition of TEOS does not form new spheres but rather adds to the size of the original spheres.

The grafting of CSPETMOS occurred after 6h of moderate mixing. 1ml of CSPETMOS in 5:2 alcohol/chloroform was added dropwise at a rate of about 1ml/min. The final solution was then allowed to spin rigorously for 12h. The solution was then dialyzed against ultrapure water for three days. The water was changed twice a day. After the dialysis process little or no precipitate was found to drop out of solution. For further purification, the solution was then mixed at low speed with a mixed bed ion exchange resin. Any ions remaining in the solution would shield the electrostatically charged surface of the spheres and would "melt" out of the CCA structure. The solution was then centrifuged at 4000rpm for 30 min. The precipitate was then rediluted into about 5ml of ultrapure water. Diffracted light could be seen coming from the milky solution after only a few minutes.

Measurements. Scanning Electron Microscopy (SEM) images were taken at 10.0kV at a magnification of 5,000-50,000x on a glass slide coated with gold sputtering. A straight filament lamp type 1003, 12V was used in Bragg diffraction measurements along with a diffraction grating with a slit density of 15,000in^{-1}.

Results and Discussion

These highly charged spheres when placed in water arrange themselves into a lattice structure which reduces the free energy of the system. Calculations suggest that a face centered cubic lattice structure is slightly more favorable[4]. The interplanar distances

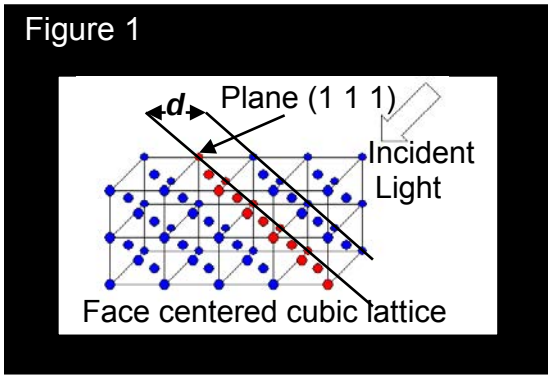

Figure 1 Charged SiO2 spheres organize themselves into a highly ordered 3 dimensional lattice structure in solution

of the 2D dried thin film is about the size of the sphere diameter[4,5]. However, the 3D CCA forms a lattice structure with interplanar distances that are much greater than the sphere diameter[1]. Because of the order of the spheres both the 2D and 3D CCA's obey the Bragg Equation:

$$m\lambda = 2nd\sin\theta$$

where d is the interplanar distance, λ is the wavelength that is diffracted, θ is the angle of the incident light, and n is the refractive index of the solution. The interplanar spacing for CCA's can be calculated by using the equation :

$$d = a/(h^2 + k^2 + l^2)^{1/2}$$

a being the lattice constant and (h k l) corresponding to the miller indices for crystalline structures. The spheres either formed an fcc structure with the (1 1 1) plane horizontal or a bcc structure with the (1 1 0) plane horizontal[1]. The polydispersity of the solution is defined by Wang[4] as σ/D where D is the diameter of the spheres and σ is the standard deviation of the distribution of a sample of 100 spheres as measured from an SEM photograph. The polydispersity indicates how uniform the sphere diameters are for a given sample. A low polydispersity is necessary in order to achieve more efficient diffraction.

Synthesis. In order to control the sphere size the conditions must be manipulated accordingly. The two step process created spheres that were about 450nm in diameter. Due to a larger surface area the spheres formed into a larger lattice structure causing much of the diffraction to occur in the near-IR. For a more colorful diffraction the sphere diameter was reduced to about 262nm which still only displayed slight visible diffraction in solution. By using the one step process smaller spheres were created and proved to be

the easier process. Adjusting the TEOS concentration also changed the sphere diameter.

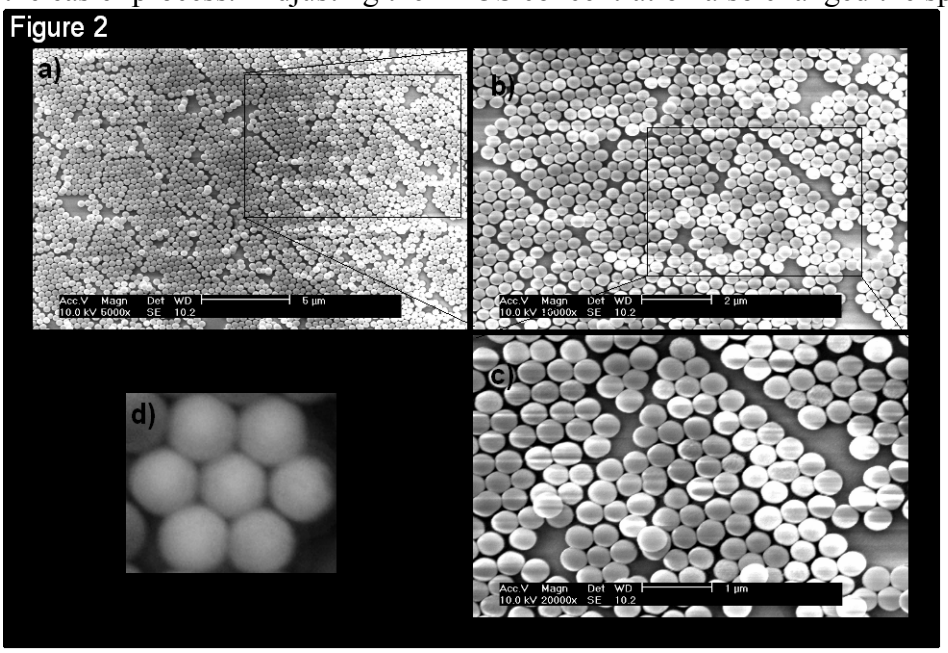

Figure 4 shows pictures taken from a SEM. Sample diameter is 389nm (a-c) with a polydispersity of 7.0%. Hexagonal close packing can be seen clearly in d.

Concentrations ranged from .3M to .05M and created spheres with diameters of 345nm to 262nm with a polydispersity of 5.4-14.2%. Other published results have indicated polydispersity of SiO_2 particles as low as 3.4%. Sphere diameter was found to increase as TEOS concentrations increased during synthesis. The polydispersity was found to decrease as TEOS concentrations increased. Concentrations below .05M formed so few spheres that it was difficult to recover after dialysis and centrifugation. Solvent seemed to have an affect on sphere diameter as well. Absolute ethanol allowed for larger growth of spheres whereas isopropanol solvent caused slightly smaller diameters.

2 Dimensional Arrays. The colloidal solution of SiO_2 spheres was collected on a glass slide and allowed to drip off as the slide was inclined to a near vertical position. Only a thin layer of residue was left on the slide and was then air dried until a colorful coating formed out of the residue. This film showed highly ordered planes in close packing on the surface of the slide. Pictures were taken on an SEM after gold coating. This array is very similar to the PS array formed by Asher et al. and also allows for the

Bragg diffraction of light. As the light incident angle on the thin layer increased the

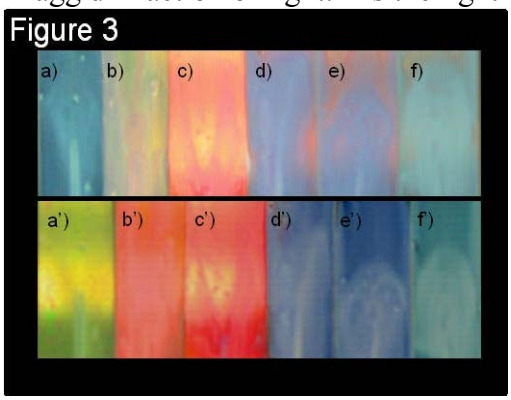

Figure 3 a-f were taken at about 60o to the right. a'-f' were taken about 60o to the left. a) 262nm b) 294nm c) 320nm d) 345nm e) 346nm f) 389nm

wavelength of diffracted light also increased. Wavelengths were measured from 500nm-719nm. Much success was met with the fabrication of the 2D thin layer diffraction such that brilliant colors were observed coming from the samples. With this optical property observed and easily reproduced, the next step is to manipulate the formation of monolayers such that they are substrate free. By cross-linking the spheres to each other with robust polymers, thin layers might possibly be formed that are sturdy enough to be handled without the glass substrate which has been used up to the present.

3 Dimensional Arrays Spheres synthesized using the Wang et al. process were able to organize themselves in water much like as in the two dimensional thin layer but with a non-close packing allowing for higher wavelength diffraction. This diffraction disappointingly showed little visible color diffraction possibly due to too large of an interplanar spacing. More study of the diffraction of radiation in the near-infrared is necessary to fully describe the phenomenon observed from the CCA's low output of diffracted light. Also, the manipulation of the conditions of synthesis is necessary to draw better conclusions as to the fabrication of CCA's using SiO_2 that diffracts in the visible spectrum. Some of the advantages of using SiO_2 as a basis for CCA fabrication stems from their "stability in a wide range of solvents and their chemical and thermo resistance"[4].

References

1. Liu, L.; Li, P. Asher, S. A. *J. Am. Chem. Soc.*, **1997**, 119, 2729-2732
2. Asher, S. A. Crystalline narrow band radiation filter.U.S. Patent No. 4,632,517
3. Holtz, J.; Asher, S. A. *Nature*, **1997**, 389, 829-832
4. Wang, W.;Gu, B.; Liang, L.; Hamilton, W. A. *J. Phys. Chem. B,* **2003**, 107, 12113-12117
5. Wang, W.; Gu, B.; Liang, L.; Hamilton, W. *J. Phys. Chem. B*, **2003**, 107, 3400-3404.
6. Li, H. L.; Marlow, F.; *Chem. Mater.*,**2005**, 17, 3809-3811
7. Masse, P.; Ravaine, S. *Chem. Mater.*, **2005**, ASAP article.
8. Stober, W.; Fink, A.; Bohn, E. Journal *of Colloid and Interface Science*, **1968**, 26, 62-69.
9. O'Brien, T. J.; Beard, J. B.; Underwood, L. J.; Dennis, R. A.; Santin, A. D.; York, L. *Tumor Biol.* **2001**, 22, 348-366.

The Production of Oxidation Catalyst

Timothy J. Paslay, University of Tulsa
Tulsa, Oklahoma

Abstract

The development of an catalyst to oxidize carbon monoxide to carbon dioxide utilizing palladium and copper salts on an activated carbon cloth carrier. The most effect layering technique tested came very close to lowering the CO concentration to safe levels. The most effective ratio of $PdCl_2$ and $CuCl_2 - 2H_2O$ that we tested was 0.1227 g $PdCl_2$ to 0.2254 g $CuCl_2 - 2H_2O$ and allowing the cloth to impregnate for 24 hours before drying at 80º C for 2 hours produced the greatest conversion.

Introduction

Carbon monoxide (CO) has been identified as one of the most common air pollutants. It is colorless, odorless, tasteless, and toxic, because of its ability to create a complex with hemoglobin in human blood. This CO-hemoglobin complex is 250 times more stable than the oxygen hemoglobin which is an integral part of hemoglobin's ability to transport oxygen in human blood. The CO-hemoglobin complex limits hemoglobin's ability to function and in high concentrations can be fatal. CO is a produced when not enough oxygen is present to complete combustion. The largest contributor to CO pollution is by far the transportation industry. Consequently the highest outdoor ambient CO concentrations are found at street level near high traffic regions in cities. CO concentrations are relatively high and accordingly its concentration is expressed in mg/m^3, where as most all other pollutants are measured in terms of $\mu g/m^3$. Various palladium and copper salts have been used to oxidize carbon monoxide. These catalysts have been supported on alumina pellets, metallic fibrous materials, or carbon fibrous materials. The goal of this research is to analyze the efficiency of these catalytic materials at various concentrations, under various conditions, and impregnated on different carriers in an effort to develop a mask that could be manufactured to minimize exposure to lethal CO concentrations.

Experimental Procedure

Data Collection

Before the beginning of each experiment gas flow rate and CO concentration must be regulated. The experiment begins with the cycle where the CO concentration is measured before the reactor. After 5 minutes the valve system is arranged to measure CO concentration after exiting the reactor and continues for 15 minutes before returning the system to measure pre-reactor concentrations. This pattern is repeated for the entire duration of the experiment, 2 hours. During the 5 minute cycle the CO concentration, gas flow, temperature, and humidity data is collected, in contrast to the 15 minute cycle where the CO concentration and gas flow rate are recorded.

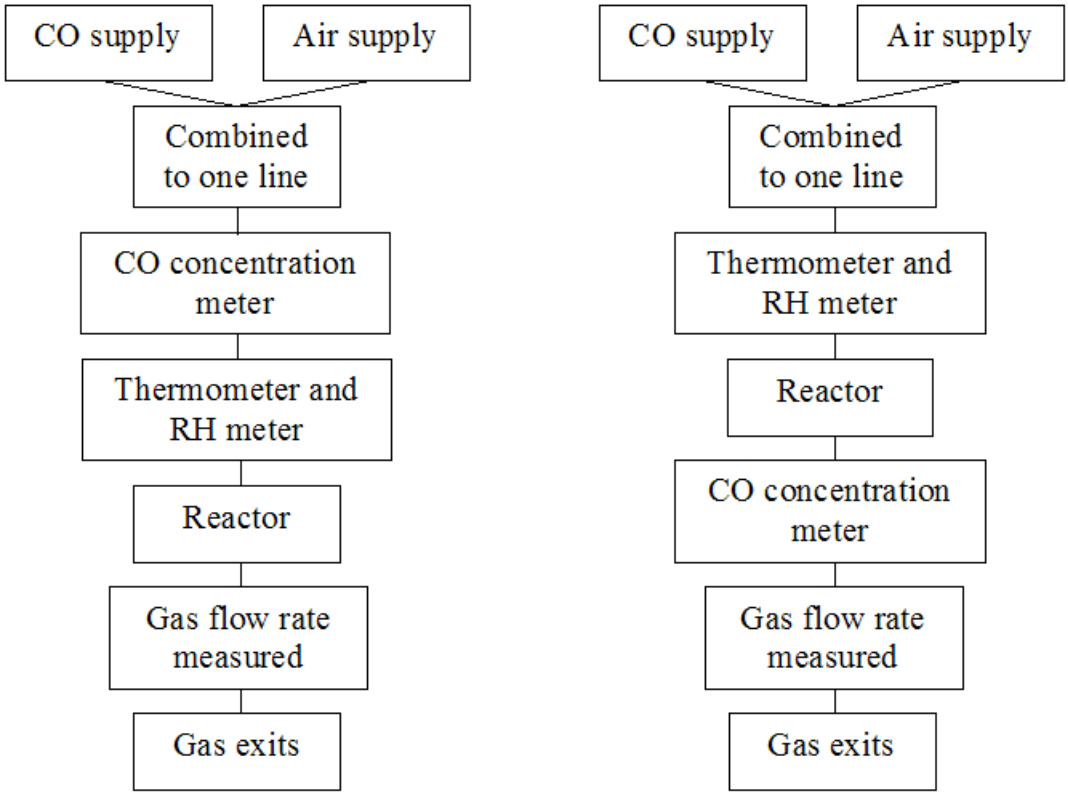

Preparation of the catalyst

Thirteen different catalysts were created during this study and the preparation of each is as follows.

Catalyst 1

0.0575 g $PdCl_2$ and 0.2160 g $CuCl_2 - 2H_2O$ were dissolved in 6.3 mL of water by stirring and heating at 70º C while refluxing via a condenser for 20 minutes. This solution was allowed to cool before being added to 5 mL (2.3 g) γ-alumina pellets (Al_2O_3). The solution was allowed to impregnate the carrier for 24 hours before being separated by vacuum filtration and then dried at 100º C for 1.75 hours.

Catalysts 2-7, Variations to preparation and supports

0.0621 g $PdCl_2$ and 0.2332 g $CuCl_2 - 2H_2O$ were dissolved in 7 mL of water by stirring and heating at 70º C while refluxing via a condenser for 20 minutes. This solution was allowed to cool to room temperature (10 min). 1 mL of this solution was then added to each carrier to allow impregnation. In catalysts 2-4 the carrier was Kynol ACC-507-15, while catalysts 5-7 were supported on Kynol ACC-5092-15. Catalyst 4 and 7 were allowed to air dry after 6 hours of impregnation. Catalyst 2,3,5, and 6 were each allowed to impregnate for 24 hours before catalyst 2 and 5 were dried at 100 C for 2 hours, and catalyst 3 and 6 dried at 80 C for 2 hours.

Catalysts 8-10

0.1227 g $PdCl_2$ and 0.2254 g $CuCl_2 - 2H_2O$ were dissolved in 7 mL of water by stirring and heating at 70º C while refluxing via a condenser for 20 minutes, and allowed to cool

to room temperature (10 min). 1 mL of this solution was then added to Kynol ACC-5092-15. Each of the catalyst was allowed to impregnate for 24 hours. Catalyst 8 and 9 were then dried at 80º C for 2 hours.

Catalysts 11-13

0.2477 g $PdCl_2$ and 0.4673 g $CuCl_2 - 2H_2O$ were dissolved in 7 mL of water by stirring and heating at 70º C while refluxing via a condenser for 20 minutes. This solution was allowed to cool to room temperature (10 min). 1 mL of this solution was then added to Kynol ACC-5092-15. Each of the catalyst was allowed to impregnate for 24 hours. Catalyst 11 and 12 were then dried at 80 C for 2 hours.

To analyze the effectiveness of the various catalysts and preparation procedures, an apparatus had been developed which is capable of measuring CO levels present in the air mixture both before and after contact with the catalyst in the reactor. This apparatus must utilize two separate cycles to most effectively accomplish this goal. Both cycles employ separate compressed air and CO supplies which can be regulated and controlled independently of one another.

Measuring CO levels before Reactor

The air and CO are mixed at the specified amounts and then moved through the CO concentration detector followed by measurement of temperature and humidity. Next the mixture passes through the reactor, which contains the catalyst, and finally exits the system via a gas volume recorder.

Measuring CO levels after Reactor

The air and CO mixture first pass the thermometer and humidity gauge before entering the reactor. After contacting the catalyst in the reactor the CO concentration is measured just before the mixture exits the system via the gas volume recorder.

A system of valves was utilized to switch between cycles while maintaining a constant gas flow to the reactor. In each of the experiments the CO concentration before contact with the catalyst was regulated at 100 mg/m^3. The temperature during experiments was room temperature, approximately 23 ^oC. All of the experiments were preformed at a humidity regulated at 40%, except for catalyst 1 where the humidity level was near 63% . Care was taken to insure that the gas flow during experiments for catalyst 2-13 remained close to 11 L/h and for 3 separate experiments involving catalyst 1, gas flows of 60 L/h, 80 L/h, and 100 L/h were maintained.

Data Analysis

The most important aspect of this study is the rate of conversion from carbon monoxide to carbon dioxide.

Catalyst	% Conversion	Temperature	Humidity	Gas Flow	Carrier
1A	97.00%	23.3	64.0%	62.00	Alumina
1B	95.20%	21.8	65.0%	82.00	Alumina
1C	94.90%	22.4	65.0%	100.00	Alumina
2	6.86%	23.2	39.0%	11.04	Single Layer ACC
3	6.86%	22.6	39.0%	11.64	Single Layer ACC
4	7.48%	22.6	37.0%	11.76	Single Layer ACC
5	7.41%	22.2	40.0%	11.32	Single Layer ACC
6	9.72%	23.7	41.0%	11.44	Single Layer ACC
7	11.54%	22.1	37.0%	9.96	Single Layer ACC
8	66.98%	22.0	35.0%	10.76	Single Layer ACC
9	63.55%	24.2	34.0%	11.96	Single Layer ACC
11	22.91%	22.7	39.0%	10.32	Single Layer ACC
12	10.37%	25.4	40.0%	12.00	Single Layer ACC
5 and 6	13.21%	23.1	42.0%	10.44	Double Layer ACC
8 and 9	80.00%	25.0	32.0%	12.00	Double Layer ACC

This is calculated and analyzed by taking the difference of the CO concentrations before and after the reactor as a percentage of the CO concentration before the reactor.

Results and Discussion

The γ-alumina pellets produce the highest conversion percentage, but also require that significantly more catalyst be impregnated onto the carrier. The ACC catalyst do not convert at as high a percentage as one would like, but the cloth nature of this catalyst permits multiple layers to be used. The most effect layering technique tested came very close to lowering the CO concentration to safe levels. The most effective ratio of $PdCl_2$ and $CuCl_2 - 2H_2O$ that we tested was 0.1227 g $PdCl_2$ to 0.2254 g $CuCl_2 - 2H_2O$ and allowing the cloth to impregnate for 24 hours before drying at 80º C for 2 hours produced the greatest conversion.

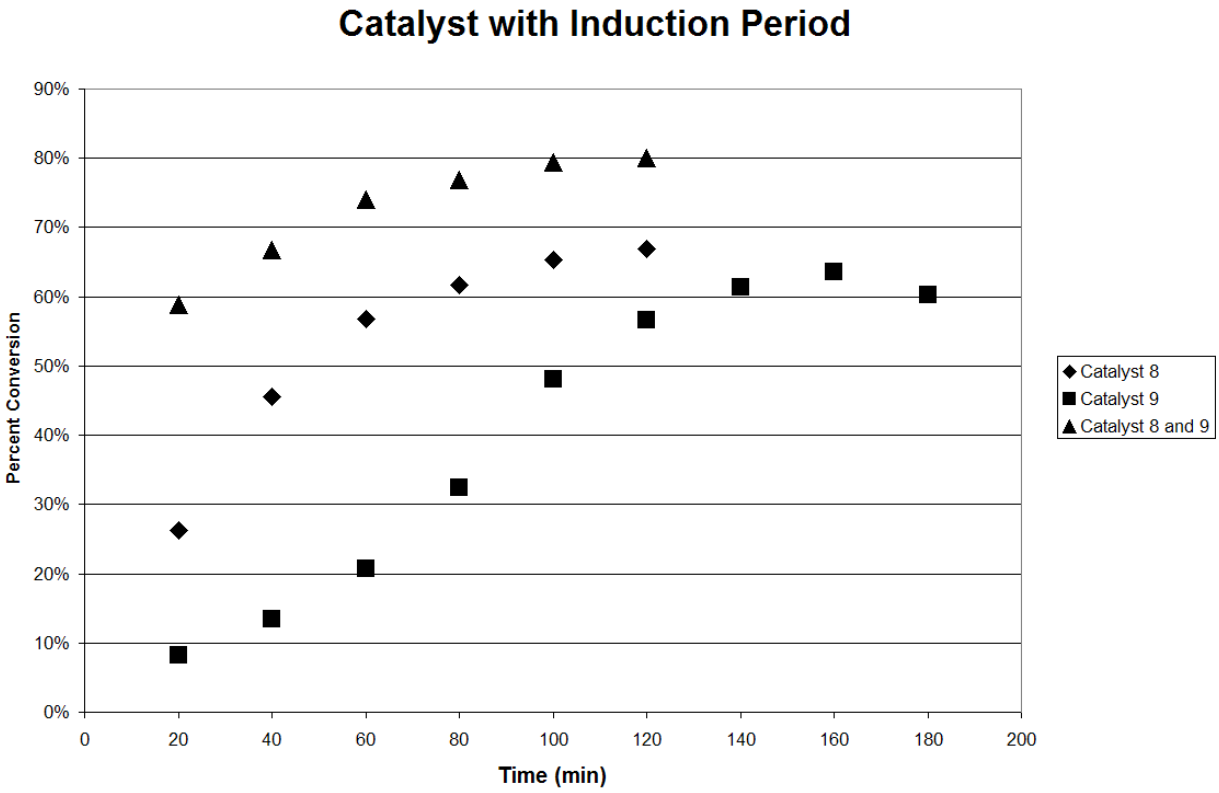

This graph shows a phenomenon that we observed in our experiments with catalyst 8 and 9. The test of catalyst 8 had to be extended to allow the conversion percentage to stabilize.

Conclusion

The catalyst utilizing the activated carbon cloth possesses promise and seems capable of reaching the necessary percent conversion requirements, but more investigation is needed to prove stability of conversion. The induction period phenomenon that appeared in catalyst 8 and 9 is not fully understood and further investigation is needed to know the cause.

Acknowledgements

The National Science Foundation sponsored this trip and research. My research abilities and techniques improved immensely, because of this trip, but even more importantly I now have some understanding of how science carries around the world. The University of Arkansas was tremendous arranging the logistics of our trip and I appreciate their efforts allowing me to worry about my work rather than any annoyances that world travel can sometimes produce. Moscow Lomonosov State University and the Moscow Lomonosov State Academy of Fine Chemical Technology were great host and I appreciate the guidance and educated provided by my mentors, Dr. Savilov, Dr. Bruk, and Dr. Oshanina.

References

1. Lloyd, Gilber W. and Rowe, Donald R. Palladium Compositions Suitable as Oxidation Catalyst. Larox Research Corporation. Patent 1,438,557. July 19, 1973.
2. Matatov-Meytal, Yu. and Sheintuch, M. Catalytic fibers and cloths. Applied Catalysis A: General. November 11, 2001.
3. Sinha, Rabindra K.Catalytic Carbon for Oxidation of Carbon Monoxide in the presence of sulfur dioxide. Calgon Corporation, assignee. Patent 4,158,643. June 19, 1979.
4. Sinha, Rabindra K.Preparation of Active-Carbon-Supported Oxidation Catalyst. Calgon Corporation, assignee. Patent 1,498,572. March 9, 1976.

Complexation of Resorcin[4]arene with Ionic Liquids and Tetrahydropyrimidine Compounds

Ioana Peret, University of Arkansas
Fayetteville, Arkansas

Abstract

We synthesized two supramolecular resorcinarene ligands as well as six guest molecules: four tetrahydropyrimidine derivatives using two distinct methods of one-pot reactions and two 1-ethyl-3-methylimidazolium ionic liquids. The stability constants of host-guest complexes were determined by ^{1}H NMR titration. The constants are in the range of 1.1 ± 0.2 for resorcinarene-ethyl 4-ethyl-6-methyl-2-thioxo-1,2,3,4-tetrahydropyrimidine-5-carboxylate complexes and 11 ± 1.5 for resorcinarene-1,3-dialkylimidazolium ionic liquids. Constants are dependant on the size, nature, position and quantity of substituents in the guest molecules. Complexation was also studied using mass spectrometry for all six guest molecules with a resorcin[4]arene host. Work remains to be done on the stability constants of other host-guest complexes of synthesized molecules.

Introduction

Resorcinarenes

In 1872, during the synthesis of phenol-based dyes, Adolf von Baeyer synthesized a red-coloured product from concentrated sulfuric acid added to a mixture of benzaldehyde and resorcinol.[1] In 1883, the molecular formula of the crystalline product $(C_{13}H_{10}O_2)_n$ and its acetyl derivative $(C_{13}H_8(OCOCH_3)_2)_n$ suggested that the product is formed from an equal number of benzaldehyde and resorcinol molecules with the equal loss of water molecules. [1] The 1883 suggested structure of the crystalline product (**1**) was supported in 1922 by Fabre. [1] Niederl and Vogel, in 1940, concluded that the ratio between aldehyde and resorcinol products should be 4:4 from molecular weight determinations of several condensation products between aldehydes and resorcinol and should resemble cyclic tetramers often found in nature such as porphyrins. [1] The structure of the acetyl derivative (**2**) was finally proven in single crystal X-ray anaylsis in 1968 by Erdtman and coworker.[1]

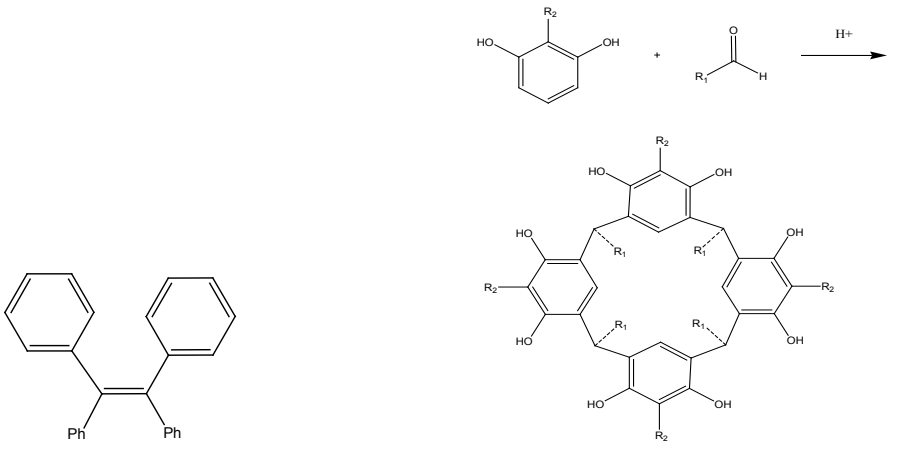

Figure 1: Molecule 1 shows the crystalline product of benzaldehyde and resorcinol. Molecule 2 shows the formation of the tetracyclic-resorcinarene ring.

Compound 2's IUPAC name is 2,8,14,20-tetra-alkylpentacyclo[19.3.1.1^{3,7}.1^{9,13}.1^{15,19}]octacosa-1(25),3,5,7(28),9,11,13,(27),15,17,19(26),21,23-dodecaene-4,6,10,12,16,18,22,24-octol (R1=aliphatic, R2=H), although the compound is often referred to by such trivial names as calix[4]resorcinarenes, resorcinol-derived calix[4]arenes, Hogberg compounds, octols, or more often, resorcinarenes.[1]

Resorcinarenes are generally synthesized in a one-pot synthesis with acid-catalyzed condensation of resorcinol and an aliphatic or aromatic aldehyde.[1,3] In a mixture of ethanol and concentrated HCl, the reaction is refluxed several hours depending on the aldehyde used.[1,3] The synthesis is initiated by dimethyl acetal which forms from the aldehyde. The electrophilic dimethyl acetal then attacks C4 of resorcinol which studies have shown to be particularly reactive in resorcinols.[1] The cyclotetramer may crystallize from the reaction mixture or water may be necessary to form crystals.[1] Almost all variations of aliphatic and aromatic aldehydes can be used except sterically crowded aldehydes such as 2,4,6-trimethyl-benzaldehyde or aliphatic aldehydes with functional groups too close to the reaction center like $ClCH_2CHO$ or glucose.[1] Most resorcinols can also be used to form cyclotetramers except those with electron withdrawing functional groups such as NO_2 or Br at the 2-position or those with alkylated hydroxyl groups.[1]

Resorcinarenes are included in a family of cavitands that often complex via hydrogen bonding of the alcohol groups and CH-π interaction of the aliphatic moiety in the guest and the electron-rich aromatic rings in the host. The importance of the CH-π interaction increases with longer guest alkyl chains.[1] Cavitands are a class of synthetic organic compounds that contain a concave cavity that accommodates other molecules or ions.[1] The rims of the cavitand bowls can be varied by changing the R_2 and R_3 functional groups, manipulating the solubility and functionality of the catalyst.[1] Because of the nanosized cavity and ease of molecular specification, resorcinarenes are being complexed with guest molecules to act as catalytic, carrier, and purification complexes.

Ionic Liquids

Due to a recent chemical move towards using more environmentally friendly solvents, researching the potential of ionic liquids for catalytic and organic reactions has become an important area of study.[2,4]

Water emerged in the last twenty years as a preferable solvent in biphasic industrial metal-catalyzed reactions.[2] However, water is a poor solvent for organic substrates because of poor misibility in protic, coordinating water.[2] On the other hand, protic water can react with organometallic complexes by halide-carbon bond protolysis or metal-carbon bond splits indicating that water can be utilized for organic reactions only if modified to better interact with hydrophobic molecules.[2]

Three solvents have been suggested for organic and catalytic reactions. Chemically, perfluorinated solvents seem to be ideal for a number of catalytic and organic reactions, but the solvents' use is limited by the toxic byproducts and the requirement of specific ligands to solubilize catalysts in the perfluorinated solvents.[2] Supercritical solvents have also been proposed as ideal green, environmentally friendly, solvents due to physical and chemical stability, but the solvents require critical conditions not suitable for most reactions.[2] Features of ionic liquids include very low vapor pressure which can take the place of volatile organic solvents and a large, thermally stable operating range (-40ºC to 200ºC).[2] Ionic liquids thus far are the most likely candidates for future green solvents.[2]

First developed by electrochemists for batteries, ionic liquids today are applied to electrolytes for electrochemical devices and processes, solvents for organic and catalytic reactions, new material production, solvents for separation and extraction processes, and enzyme catalysis or in multi-phase bio-process operations.[2,4] In catalytic chemistry, the main benefits of ionic liquids is enhancement of reaction rates and improvement of chemo- and regioselectivities compared to other organic solvents.[2] In microwave enhanced reactions, only a small amount of ionic liquids absorb much microwave energy, distributing energy throughout the reaction and making the reaction time extremely short.[2] Reactions carried out in microwaves can shorten the reaction rate from a few hours to mere minutes when heating in refluxing solvent, thus making reactions more economic.[2]

A further benefit of using ionic liquids is the potential of synthesizing biphasic systems that allow products to be easily separated from its catalyst.[2] An ideal system would dissolve the catalyst and be partially miscible with the substrate, but would be immiscible with the product so that it can be easily removed without removing the catalyst.[2] This system would not require heating so that energy would be conserved and would better preserve ionic liquids which are susceptible to thermal decomposition.[2] Extraction with CO_2 has great potential for extracting solely products and not catalysts because $ScCO_2$ dissolves quite well in ionic liquids but ionic liquids do not dissolve in CO_2, so pure products can be extracted with carbon dioxide.[2]

Ionic liquid cations are typically bulky, organic, and asymmetric molecules.[2] Widely studied cations include the N,N-dialkylimidazolium cations, which have diverse physio-chemical properties.[2] Easy substitutable, imidazolium halide precursors can undergo anion exchange to give various liquid imidazolium salts with a wide range of characteristics. Upon studying assymetrical N,N-dialkylimidazolilum cations, which have lower melting point salts, it was discovered that 1,3-dialkylimidazolium

hexafluorophospates with dibutyl, dipentyl, dioctyl, dinonyl, and didecyl substituents are found to be liquid at room temperature. [2] The addition of functional groups to imidazolium leads to specialized ionic liquids specific for the intended task. The viscosity of 1-alkyl-3-methylimidazolium salts can be decreased by varying the anion with viscosity decreasing from $Cl^- > PF_6^- > BF_4^- \sim NO_3^- > NTF_2^-$.[2] Viscosity can also be decreased by using highly branched and compact alkyl chains. [2]

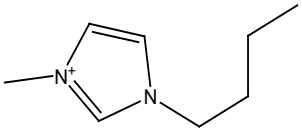

Figure 2: 1-butyl-3-methylimidazolium cation

Ionic liquids can be synthesized to undergo versatile changes in various conditions to give an assortment of compositions in different temperatures. For example, for the 1-butyl-3-methylimidazolium cation [BMI], the BF_4^-, $CF_3SO_3^-$, $CF_3CO_2^-$, NO_3^-, and halide salts are completely miscible in water at room temperature. [2] However, at 4ºC, the [BMI][BF4]/water solution separates into a water-rich phase. [2] A cation similar to [BMI] but with a larger alkyl group shows a low co-miscibility with water at room temperature. [2] Furthermore, changing the anion to PF_6^-, SbF_6^-, NTF_2^-, or BR_4^- shows extremely low solubility in water. [2] However, a short alkyl chain, symmetric 1,3-dimethylimidazolium replacement of BF_4^- with PF_6^- is water soluble. [2] These various miscibilities allow efficient catalytic reactions with the substrate that can be removed from the product by changing the reaction conditions.

Other characteristics affected by alkyl chain length and anion are viscosity, surface tension, melting point, and thermal stability. [2] Anions play a more significant role in determining the characteristics of ionic liquids than the imidazolium side chain length. [2] On the other hand, the alkyl chain length from butyl to octyl largely increase the hydrophobicity and viscosity of imidazolium ionic liquids, but decrease densities and surface tension values making the ionic complex tunable to different reactions. [2]

Table 1: Some physical characteristics of more currently used 1-butyl-3-methylimidazolium ionic liquids[2]

Anion	Melting Pt (ºC)	Density (g/cm)	Viscosity (mPas)	Conductivity(S/m)
BF4-	-82/-83	1.17 (30 ºC)	233 (30 ºC)	0.173 (25 ºC)
PF6-	-61	1.37 (30 ºC)	312 (30 ºC)	0.146 (25 ºC)
CF3SO3-	16	1.290 (20 ºC)	90 (20 ºC)	0.37 (20 ºC)
CF3CO2-	-50/-30	1.209 (21 ºC)	73 (20 ºC)	0.32 (20 ºC)
NTf2-	-4	1.429 (19 ºC)	1.429 (19 ºC)	0.39 (20 ºC)

Two types of anions exist. The first anions, those sensitive towards air and water, are polynuclear including $Al_2Cl_7^-$, $Al_3Cl_{10}^-$, $Au_2Cl_7^-$, $Fe_2Cl_7^-$, and $Sb_2F_{11}^-$ formed by the reaction of a Lewis Acid such as $AlCl_3$ with a mononuclear anion in this case $AlCl_4^-$.[2] The second type of anion is mononuclear which forms neutral stoichiometric ionic liquids for example BF_4^-, PF_6^-, SbF_6^-, $ZnCl_3^-$, $CuCl_2^-$, $SnCl_3^-$, $N(CF_3SO_2)_2^-$, $C(CF_3SO_2)_3^-$, $CF_3CO_2^-$, $CF_3SO_3^-$, $CH_3SO_3^-$, etc. [2]

Zwitterionic-type ionic liquids consisting of imidazolium cations covalently bound to anionic sites such as sulfonate or sulfonamide exhibit unique properties including very high ion densities so that component ions cannot migrate. [2] The ions form a matrix in which only added ions can move through the system. [2]

We synthesized two N-1-ethyl-3-methylimidazolium salts, one with ethyl sulfate anions and the other with hexafluorophosphate anions using methods based on Holbrey, etal's previous studies on 1,3-dialkylimidazolium salts.[5]

Biginelli Tetrahydropyrimidines

Biginelli compounds, generally derivatives of 5-acyl-1,2,3,4-tetrahydropyrimidine-2-thiones/ones, first synthesized by Pietro Biginelli in 1893, were largely ignored until the early 1980's when scientists discovered the pharmaceutical potential of the compounds as antimicrobial drugs, calcium channel modulators, α_{1a}-adrenergic receptor antagonists, anticarcinogens, and HIV therapy.[6,8] Biginelli compounds were synthesized in a one pot cyclocondensation reaction of β-ketoesters, aromatic aldehydes, and urea or thiourea.[8] To improve the yields, the present reaction requires an ethanol solvent, a catalytic amount of HCl, and a thermal driving force.[8]

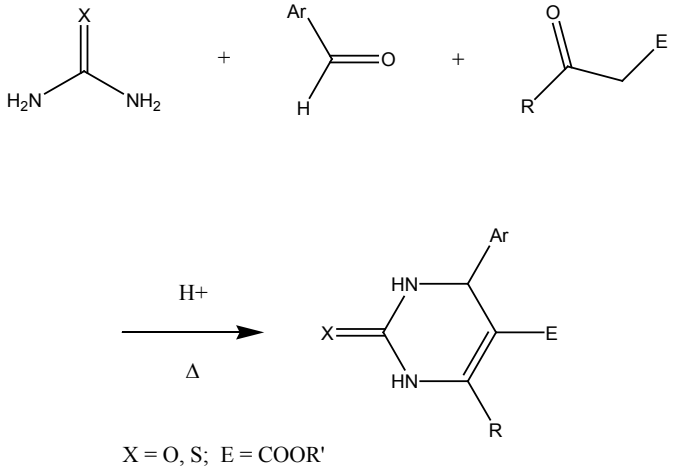

Figure 3: *The traditional reaction scheme of Biginelli compounds.*

Initial research of the tetrahydropyrimidine compounds carried out reactions similar to that of Biginelli but with variations of the initial reagents.[6] The products of this research led to large tetrahydropyrimidine libraries whose biological activities were tested. An example of the biological relevance of a tetrahydropyrimidine is monastrol, a cell permeable molecule that inhibits the mitotic kinesin Eg5 motor protein and causes cell arrest, useful as an anticancer drug.[6] Moreover, many natural products similar to Biginelli compounds have been found in nature including batzelladine alkaloids A and B which inhibit the binding of HIV envelope protein gp-120 to human CD4 cells.[6]

Besides the Biginelli synthesis scheme, two other significant tetrahydropyrimidine synthesis methodologies have been proposed: the Atwal and Shutalev approach. Atwal's synthesis is currently more widely accepted because of its broad application. It requires the condensation of an enone with a suitable protected urea or thiourea derivative in the presence of $NaHCO_3$ in DMF solvent.[8] The product later requires deprotection by HCl or TFA/EtSH.[8]

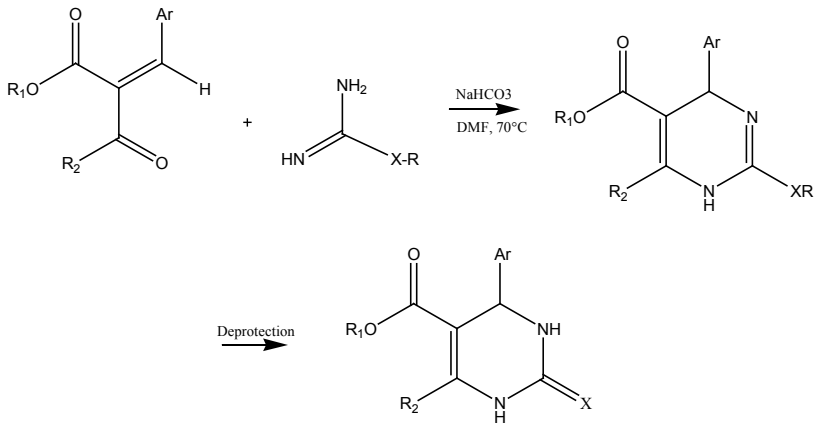

Figure 4: *Atwal's reaction scheme using the condensation of enone.*

Shutalev utilizes α-tosyl-substitutes (thio)ureas with enolates of β-ketoesters or 1,3-dicarbonyl compounds.[6] Advantages of Shutalev's synthesis include the use of readily available α-tosyl-substitutes (thio)ureas whereas Atwal's enones must be synthesized. Also Atwal's synthesis is more expensive and labor intensive as a protecting group must be removed, and the synthesis requires the use of DMF.[8] Shutalev's method also results in higher yields than both Biginelli's and Atwal's synthesis.

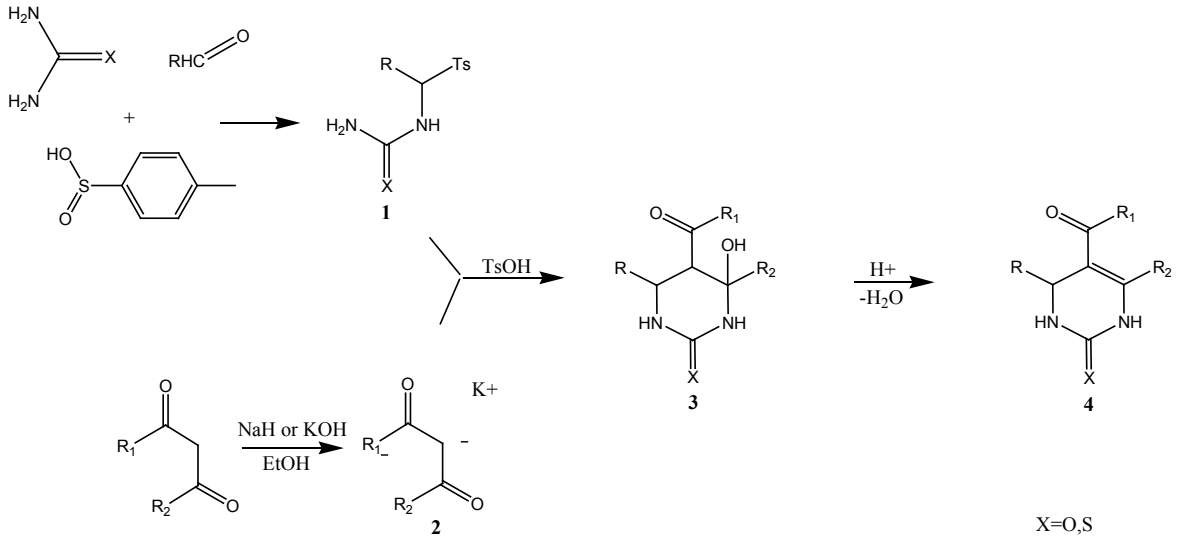

Figure 5: *Shutalev's reaction scheme used to successfully synthesize four tetrahydropyrimidines.*

Four tetrahydropyrimidines were synthesized using Shutalev's methods. First, N-(1-tosylpropyl)urea, N-(1-tosylpropyl)thiourea, and ethyl-2-thioureido-2-tosylacetate were synthesized leading to product **1.** Then tetrahydropyrimidines (**4**), ethyl 4-ethyl-6-methyl-2-oxo-1,2,3,4-tetrahydropyrimidine -5-carboxylate, ethyl 4-ethyl-6-methyl-2-

thioxo-1,2,3,4-tetrahydropyrimidine-5-carboxylate, and 5-acetyl-4-ethyl-6-methyl-1,2,3,4-tetrahydropyrimidine-2-thione were produced using Shutalev's method with the base KOH. 5-acetyl-4-ethyl-6-methyl-1,2,3,4-tetrahydropyrimidine-2-one used NaH in its synthesis. A final synthesis of 4,5-Diacetyl-6-methyl-1,2,3,4-tetrahydropyrimidine-2-thione from ethyl-2-thioureido-2-tosylacetate failed using KOH, leaving no product to analyze.

Mass Spectroscopy

Potential host-guest complexes were tested on mass spectrometry where variations in the mass of ionized particles gives the mass of complexation. All synthesized tetrahydropyrimidines were complexed with resorcinarenes. The two synthesized imidazolium ionic liquids were also complexed with resorcinarenes and analyzed using mass spectroscopy. A catalytic amount of copper was added to the tetrahydropyrimidine ethyl 4-ethyl-6-methyl-2-thioxo-1,2,3,4-tetrahydropyrimidine-5-carboxylate to induce complexation. Further studies of seen oligomers and metallic complexes must be studied.

^{1}H NMR Host-Guest Titrations

Because of the potential use of ionic liquids as environmentally friendly solvents, the complex formation of resorcin[4]arene with 1,3-dialkylimidazolium ionic liquids was of particular interest to us so ^{1}H NMR titrations were performed on resorcinarene complexation with the synthesized ionic liquids. Resorcinare-tetrahydropyrimidine complexes were also analyzed using ^{1}H NMR. Titration conditions and calculations were based on previous work by Cao, etal. who usually held the host concentration constant and varied the guest concentration for a series of samples.[9] Cao, etal determined the association constants (K_a) of the host-guest complexes by titration ^{1}H NMR, in conjunction with the nonlinear least-square fit of the data to 1:1 models.[9] The association constant (K_a) as well as the chemical shifts of the □ bonds are describe

$$G + H = C$$

$$\delta = \delta_H(1 - \chi) + \delta_C\chi \quad \text{where } \chi = [C]/[H]_1$$

$$[H]_1 (\delta - \delta_H) = [C](\delta_G - \delta_H)$$

$$K_a = \frac{[C]}{[H][G]}$$

$$[H]_1 = [H] + [C]$$

$$[G]_1 = [G] + [C]$$

where H, G, and C represent the host, guest and the complex; $[H]_1$ is the total concentration of the host molecule at initial state: $[G]_1$ is the total concentration of guest molecules at the initial state; [H], [G], [C], are the concentrations of host, guest, and complex at the finals states. δ_H, δ_G, and δ represent the chemical shift of host, complex, and observed chemical shift, respectively. K_a is the association constant.

$$K_a = \frac{[C]}{([H]_1 - [C])([G]_1 - [C])}$$

$$[C] = \frac{([H]_1 + [G]_1 + 1/K_a) \pm \sqrt{([H]_1 + [G]_1 + 1/K_a)^2 - 4([H]_1[G]_1)}}{2}$$

Then,

$$(\delta - \delta_H) = \frac{(\delta_G - \delta_H)}{2}\left\{ \frac{[G]_1}{[H]_1} + 1 + \frac{1}{K_a[H]_1} + \sqrt{\left(\frac{[G]_1}{[H]_1} + 1 + \frac{1}{K_a[H]_1} \right)^2 - 4\frac{[G}{[H}} \right\}$$

By plotting chemical shifts against [host]/[guest] mole ratio, computer software with Cao's pre-programmed equation determined the complexation constant K_a.

Experimental Procedures

2-Methylresorcin[4]arene

Resorcin[4]arene (2,8,14,20-tetramethyl-5,11,17,23-tetramethyl-pentacyclo[19.3.1.1^{3,7}.1^{9,13}.1^{15,19}]octacosa-1(25),3,7(28),9,13,(27),15,19(26),21-octaene-4,6,10,12,16,18,22,24-octol) by addition of acetaldehyde ***(1)***

To a round bottom flask with a stir bar, 90% 2-methylresorcinol (5.774g, 0.04mol) was added to 50mL ethanol, 50mL H_20, and 25mL concentrated aqueous 37% HCl while stirring. 2.3mL (1.8g) acetaldehyde diluted with 10mL ethanol was then added dropwise over a period of 20min. The reaction continued 48 hours with alternating periods of stirring. The product was then dried on a vacuum line, and the filtrate was placed on a rotoevaporator to remove ethanol. H_2O remaining in the filtrate was poured into a separate vial so that both the water and oily residue could be evaluated on mass spectrometry. Tetrahydrofuran was used twice while heating to wash the oily residue away from the wanted precipitate, but the powdery precipitate could not be separated from the residue leaving product of 1.219g from pre-rotovap filtration.
ESI MS: 599.3 $[RA]^-$.

Resorcin[4]arene by addition of acetaldehydediethyl acetal ***(2)***

In a 3-neck flask, 50mL H_2O, 50mL ethanol, 25mL 37% aqueous concentrated HCL, and 5.774g 90% 2-methylresorcinol (0.04mol) were added. A yellow product formed. 5.7mL acetaladehyde diethyl acetal diluted with 10mL ethanol was added dropwise into the flask while stirring. The reaction was allowed to react 4 days and the precipitate was collected in a Buchner funnel.

Bromination of Resorcin[4]arene (2,8,14,20-tetramethyl-5,11,17,23-tetramethylenebromine-pentacyclo[19.3.1.1^{3,7}.1^{9,13}.1^{15,19}]octacosa-1(25),3,7(28),9,13,(27),15,19(26),21-octaene-4,6,10,12,16,18,22,24-octol) ***(3)***

A solution of resorcinarene **(1)** (1.22g, 2.03mmol), recrystallized NBS (1.624g, 9.09mmol), and a catalytic amount of AIBN was refluxed in 71mL CCl_4 for 5h. The reaction mixture was allowed to cool to room temperature, the precipitate was removed by filtration, and the organic layer was washed with H_2O (2x20mL) and dried over $MgSO_4$. The red product that formed was removed with several filtrations because of small molecular size. Evaporation of the solvent provided the crude product which was recrystallized from CH_2Cl_2/EtOH to make a yellowish powder. Yield: 1.379g (75%). ESI MS: 675.3 $[RA*1Br]^-$, 755.0 $[RA*2Br]^-$, 833.0 $[RA*3Br]^-$, 914.9 $[RA*4Br]^-$.

*Bromination of pre-prepared Resorcin[4]arene **(4)***
A solution of preprepared resorcinarene(2.00g, 2.42mmol), recrystallized NBS (1.94g, 10.8mmol), and a catalytic amount of AIBN was refluxed in CCl_4 (84.3mL) for 5h. The reaction mixture was allowed to cool to room temperature, and the precipitate was removed by filtration. The organic layer was washed with H_2O (2 x 20mL) and dried with $MgSO_4$. The crude product was collected by evaporation of the solvent to give a yellowish powder.

Ionic Liquids
*Methylimidazolium ethyl sulfate **(5)***
Diethyl sulfate (29mL, 0.221mol) was added dropwise to a solution of 1-methylimidazole (18.146g, 0.221mol) in 100mL dry toluene. Reaction proceeded in an ice water bath to maintain temperature below 40 ºC. The ionic liquid product formed immediately and caused the solution to become opaque, followed by a biphasic solution and formation of a denser IL phase. The reaction mixture was stirred for 1h after the addition of diethyl sulfate and allowed to sit overnight in separate phases. The upper organic phase was decanted and the lower IL phase was washed with 50mL of toluene, then dried by heating at 75 ºC under reduced pressure to remove the residual organic solvents. The final product was dried on a vacuum line to give a colorless liquid 1-ethyl-3-methylimidazolium ethyl sulfate.

*N-3-Methyl-1-ethylimidazolium hexafluorophosphate **(6)***
To a solution of 3-methyl-1-ethylimidazolium methyl sulfate (45.85g, 0.194mol) in 171mL H_2O was added 28mL 64% solution hexafluorophosphoric acid while stirring. Then was added a solution of NaOH (7.695g, 0.19mol) in 85.5mL H_2O. The colorless 1-ethyl-3-methylimidazolium hexaflourophosphate crystals formed on cooling to 4ºC, and the precipitate was collected by filtration.

Toluenesulphinic Salts
*p-Toluenesulfinic Acid **(7)***
p-Toluenesulfinic acid salt hydrate (30.590g, 0.172mols) along with 120mLs H_2O was dissolved. In a separate flask, 20% excess 36% HCl (17.7mLs, 0.206mols) was added to equal volumetric amounts of H_2O and cooled for 20 minutes. While stirring, cold, dilute HCl was placed into the *p*-toluenesulfinic acid flask. The mixture was cooled to 0ºC and washed and filtered three times with 4mL ice cold H_2O and twice with 4mL hexane. The product was dried in a vacuum dessicator over phosphorous pentoxide giving 19.450g, 72.5% product.

N-(1-Tosylpropyl)urea ***(8)***
In a round bottom flask, propionaldehyde (1.480g, 25.48mmol) was allowed to react 10 minutes with 30mLs H_2O and *p*-toluenesulfinic acid (3.970g, 25.45mmol). Then a threefold excess of urea (4.591g, 76.45mmols) was added as well as 10mL H_20. The flask was shaken every 10 minutes for 2h 40min. The precipitate was then filtered, washed in cold water and hexane and a yield of 5.33g, 82% resulted.

N-(1-Tosylpropyl)thiourea ***(9)***
Propionaldehyde (1.550g, 26.69mmol) was stirred for 1h with 7mL H_2O, thiourea (2.033g, 26.71mmols), and *p*-toluenesulfinic acid (4.163g, 26.69mmols). A coagulation formed which was refrigerated for 2 hours and was later crushed into small pieces with a spatula. The mixture was stirred for 15h. After this period, the crystals were still large so they were again crushed into smaller pieces. Additional stirring was applied and the precipitate was filtered. Yield: 5.685g, 78%.

Ethyl 2-thioureido-2-tosylacetate ***(10)***
Ethyl 2-ethoxy-2-hydroxyacetate (0.684g, 4.61mmol) was added to a round bottom flask with *p*-toluenesulfinic acid (0.636g, 4.08mmol) and 5mL H_2O, allowing to react 10min. Then thiourea (0.260g, 3.41mmol) was added and the reaction mixture was shaken periodically for 6h. A yellow precipitate formed with a large, hard clump which had to be broken up. The reaction was then cooled to 0ºC, the precipitate was filtered and washed with ice water. The product was dried overnight in a dessicator over phosphorous pentoxide to give 0.439g of product (87%). NOTE: Unknown reagents were used so mmols used of each reagent were recalculated and show thiourea to be the limiting reagent when it should be in 10% excess with respect to the *p*-toluenesulfinic acid.

Pyrimidines
Ethyl 4-ethyl-6-methyl-2-oxo-1,2,3,4-tetrahydropyrimidine-5-carboxylate ***(11)***
KOH (0.300g, 5.34mmol) was dissolved in 5mL ethanol on a stirring plate in a round bottom flask. Weigh 0.698g (5.34mmol) ethyl acetoacetate into a glass bottle. Add 2.5mLs ethanol to the bottle and add dropwise to the dissolved KOH. Add 2.5mLs ethanol to the bottle and add to the RBF. After 2 minutes, added 1.143g (4.460mmol) N-(1-tosylpropyl)urea, and the reaction was allowed to stir for 5h. TsOH (0.341g, 1.79mmol) was then added and the reaction was refluxed for 1h. The product was cooled to 0 ºC overnight. The solvent was then evaporated using a rotovap and the oily product was washed twice with 4mL portions of hexane which was stirred with the product and poured into waste receptacle. 1ml of saturated water solution $NaHCO_3$ was added to the solution and the mixture was heated 40 ºC for 1.3h to cause reaction progression. The precipitate was filtered and washed with 0 ºC H_2O, then dried in a vacuum dessicator phosphorous pentoxide. TLC testing on Silufol UV254 plates with 9:1 $CHCl_3$:CH_3OH and iodine dessicator revealed some impurity so another 1mL portion of $NaHCO_3$ was added to the dried product and left for three days at 30 ºC. Yield: 0.557g, 65%.
H NMR, δ_H (400MHz, DMSO-d_6) 0.79 (3H, t, 7.45 Hz, $CH_2C\mathit{H}_3$), 1.18 (3H, t, J=7.07Hz, $OCH_2C\mathit{H}_3$), 1.42 (2H, m, $NHCHC\mathit{H}_2$), 2.16 (3H, s, $NHCC\mathit{H}_3$), 4.00-4.15

(1H, m, NC*H*), 4.05 (2H, q, J=7.07Hz, OCH_2), 7.24 (1H, s, N*H*), 8.87 (1H, s, N*H*). ^{13}C NMR, δ_H (400MHz, DMSO-d_6), 8.45 (CHCH$_2$*C*H$_3$), 14.19 (OCH$_2$*C*H$_3$), 17.67 (NHC*C*H$_3$), 29.59 (NHCH*C*H$_3$), 51.33 (NH*C*H), 58.99 (O*C*H$_2$*)*, 98.77 *(C*COO*)*, 148.36 (NH*C*CH$_3$), 152.77 (HN*C*ONH), 165.49 (*C*OO). ESI MS: 234.8 [Pyr*Na]$^+$, 423.0 [2Pyr]$^+$, 446.9 [2Pyr*Na]$^+$.

Ethyl 4-ethyl-6-methyl-2-thioxo-1,2,3,4-tetrahydropyrimidine-5-carboxylate ***(12)***
KOH (0.298g, 5.30mmol) was dissolved in 5mL ethanol and a mixture of ethyl acetoacetate (1.204g, 5.32mmol) and 5mL ethanol was added dropwise while stirring. After 7 minutes, *p*-tosylpropylthiourea (1.204g, 4.42mmol) was added along with 5mL ethanol and the mixture was allowed to stir for 4h. TsOH (0.281g, 1.478mmol) was then added and the reaction was refluxed for 1h. The cooled mixture was placed on a rotoevaporator. The residue was treated twice with 5mLs of hexane. 1mL of saturated water solution $NaHCO_3$ was added to the flask and left overnight. The product was then filtered, washed with 0 ºC H_2O, and dried in a vacuum desiccator. Yield: 0.6739g, (55%). 207mg of crude product were recrystallized with 1mL ethanol giving 54.2mg of recrystallized product with a yield of 26%.
^{1}H NMR, δ_H (400MHz, DMSO-d_6), 0.78 (3H, t, J=7.45Hz, CHCH$_2$C*H*$_3$), 1.19 (3H, t, J=7.07Hz, OCH$_2$C*H*$_3$), 1.43 (2H, m, NHCHC*H*$_2$), 2.21 (3H, s, NHCC*H*$_3$), 4.01-4.16 (1H, m, NHC*H*), 4.08 (2H, q, J=7.07Hz, OC*H*$_2$CH$_3$), 9.18 (1H, s, *H*N Ar CH$_3$), 10.03 (1H, s, *H*N Ar CH$_2$CH$_3$). ^{13}C NMR, δ_H (400MHz, DMSO-d_6), 8.12 (CHCH$_2$*C*H$_3$), 14.12 (OCH$_2$*C*H$_3$), 17.04 (NHC*C*H$_3$), 29.19 (NHCH*C*H$_2$), 51.65 (NH*C*H), 59.41 (O*C*H$_2$CH$_3$*)*, 100.08 *(C*COO), 145.29 (NH*C*CH$_3$), 165.25 (*C*OO), 175.07 (*C*S). ESI MS: 519.0 [2Pyr*Cu]$^+$.

5-Acetyl-4-ethyl-6-methyl-1,2,3,4-tetrahydropyrimidine-2-thione ***(13)***
KOH (0.403g, 7.184mmol) was dissolved in 5mLs ethanol and placed on a stirring plate. (0.725g, 7.246mmol) acetyl acetone was weighed into a glass bottle. N-(1-Tosylpropyl)thiourea (1.631g, 5.99mmols) was also weighed before acetylacetone was added to the KOH solution along with 5mL ethanol. After 2 minutes, the pre-weighed N-(1-tosylpropyl)thiourea was added. Round precipitate balls formed that were later dissolved as the mixture became cloudy and yellow with precipitate. The reaction was stirred at room temperature for 4h, then 0.384g (2.02mmols) TsOH was added and the mixture was refluxed in 1h. The solvent was removed using a rotoevaporator, the residue treated with hexane, and then with saturated water solution $NaHCO_3$ (1mL)in a 50ºC water bath for 9h. The obtained solid was filtered out, washed three times with 0ºC water and hexane and then dried in desicator. Yield: 0.789g (66%). 0.203g crude product was purified by recrystallization from ethanol (5.2mL) giving 137mg pure product (68%).
^{1}H NMR, δ_H (400MHz, DMSO-d_6), 0.78 (3H, t, J=7.33Hz CH$_2$C*H*$_3$), 1.37 (2H, m, NHCHC*H*$_2$), 2.21* (3H, s, NHCC*H*$_3$), 2.22* (3H, s, COC*H*$_3$), 4.13 (1H, m, NHC*H*), 9.27 (1H, s, *H*N Ar CH$_3$), 10.00 (1H, s, *H*N Ar CH$_2$CH$_3$). ^{13}C NMR, δ_H (400MHz, DMSO-d_6), 8.34 (CH$_2$*C*H$_3$), 18.09 (NHC*C*H$_3$), 29.03* (NHCH*C*H$_2$), 30.20* (CO*C*H$_3$), 51.78 (NH*C*H), 110.73 *(C*CO*)*, 144.07 (NH*C*CH$_3$), 174.92 (*C*S), 194.87 (*C*OCH$_3$). ESI MS: 458.9 [2Pyr*Cu]$^+$.

5-Acetyl-4-ethyl-6-methyl-1,2,3,4-tetrahydropyrimidin-2-one ***(14)***
NaH (0.183g, 7.63mmol) was added to a round bottom flask along with 10mL dry acetylnitrile. Over an ice-water bath, a mixture of 4mL acetylnitrile and acetylacetone (0.763g, 7.63mmol) was added to the flask dropwise during a period of 10min. The total amount of CH_3CN added to the entire reaction should equal 2.5mL CH_3CN per mmol sulfone added. Allow the reaction to stir for 10 minutes. N-(1-Tosylpropyl)urea (1.629g, 6.36mmol) was added and the mixture stirred at room temperature for 6 hours. White foam precipitate forms. TsOH (0.483g, 2.54mmol) was added and the mixture was refluxed for 1.5h, cooled to r.t. and evaporated on the rotovap. The residue was treated twice with 5mL hexane, then 1mL $NaHCO_3$ was added and the mixture was left overnight at r.t., and then in 40ºC water bath, stirring occasionally. The mixture was cooled to 0ºC and the solid was collected by filtration, washed with ice water and hexane, dried in dessicator to give product (0.753g, 65%). The recrystallization of 0.286g of product from 7mL CH_3CN gave 0.140g (49%) of pure product.
^{1}H NMR, δ_H (400MHz, DMSO-d_6), 0.80 (3H, t, J=7.33Hz, CH_2CH_3), 1.37 (2H, m, $NHCHCH_2$), 2.17* (3H, s, $NHCCH_3$), 2.19* (3H, s, $COCH_3$), 4.07 (1H, m, NHCH), 7.34 (1H, s, HN Ar CH_3), 8.88 (1H, s, HN Ar CH_2CH_3). ^{13}C NMR, δ_H (400MHz, DMSO-d_6), 8.70 (CH_2CH_3), 18.78 ($NHCCH_3$), 29.47* ($NHCHCH_2$), 30.12 ($COCH_3$), 51.55 (NHCH), 110.12 *(CCO)*, 147.40 (CCH_3), 152.77 (HNCONH), 194.24 ($COCH_3$). ESI MS: 204.8 $[Pyr*Na]^+$, 386.9 $[2Pyr*Na]^+$.

Diethyl-6-methyl-2-thioxo-1,2,3,4-tetrahydropyrimidine-4,5-dicarboxylate ***(15)***
In a solution of KOH (0.323g, 5.75mmol) dissolved in 5mL ethanol was added dropwise ethyl acetoacetate (0.721g, 5.54mmol) into a vial along with 4mL ethanol. After 7min, ethyl-2-thioureido-2-tosylacetoacetate (0.354g, 1.12mmol) was added to the flask along with 2.5mL ethanol. The reaction was stirred at room temperature for 4h. A yellow, slightly cloudy solution forms. After adding TsOH (1.140g, 5.993mmol) the mixture was refluxed for 1h, and then the solvent was removed with a rotoevaporator. The residue was treated 7 times with hexane. A saturated water solution of $NaHCO_3$ was then added, the remaining oily precipitate was filtered and washed with water after which most of the product was washed away as salt and did not leave enough product for analysis.

Data Collection

TLC was performed with a 9:1 $CHCl_3$:CH_3OH mobile phase on Silufol UV254 plates from Czechoslovakia and a iodine dessicator. HPLC was performed using Gilson equipment with Dynamic Mixer 811C, Pump 305 805 Manometric Module Max Pressure: 60MP, and Model 131 Refractive Index Detector. Capillary used was Zorbax 3.5µm SB-C18, 4.6x75mm, PN 888953-902, Sn:US02007750. LCMS used was Agilent 1100 Series LC/MSD. NMR used Bruker Avance 400 operating on 400 MHz with a TMS internal standard.

Data Analysis

The mass spectrum of the formed resorcinarene shows many impurities from resorcinarene intermediates. According to Timmerman's review of resorcinarenes, the sequential coupling arises from the electrophilic dimethyl acetal reacting with resorcinol units to form di-, tri-, tetra-, and higher oligomers of the resorcinol monomers.[1] At intermediate reaction times, higher oligomers are present in concentrations as large as 45%, but concentrations decrease significantly at the end of the reaction time as the condensation reaction is reversible. Dimers and trimers can be isolated, but tetramers cyclise too quickly to be isolated in significant proportions due to a folded rather than linear conformation. The folded conformation allows strong hydrogen bonds to form between phenolic hydroxyl groups of adjacent resorcinol units. [1]

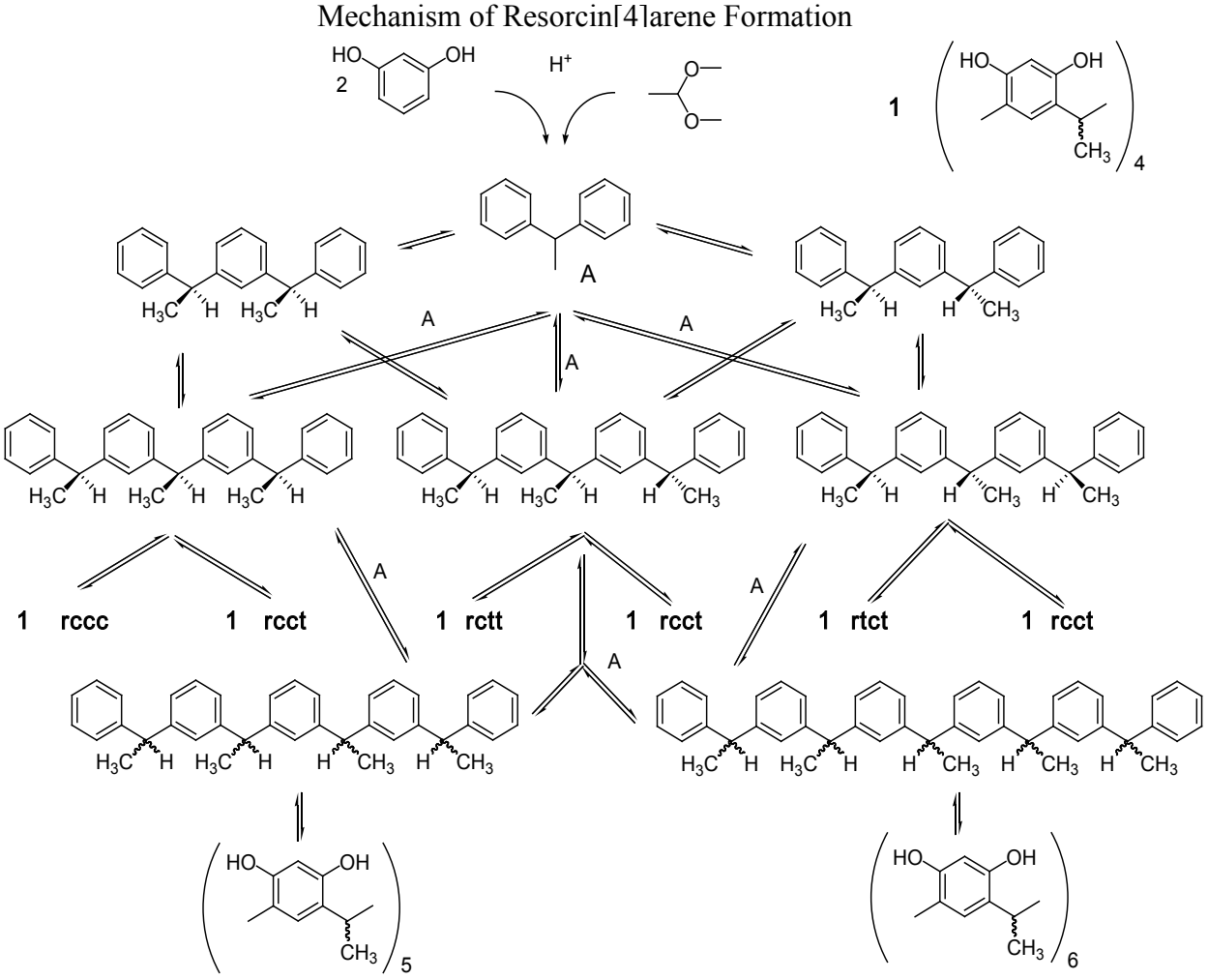

Figure 6: The reaction of resorcinarene from aldehydes and resorcinols.

As can be seen, the bromination of resorcinarene shows many impurities in mass spectrometry including mono-, di-, tri-, and tetra-bromination.

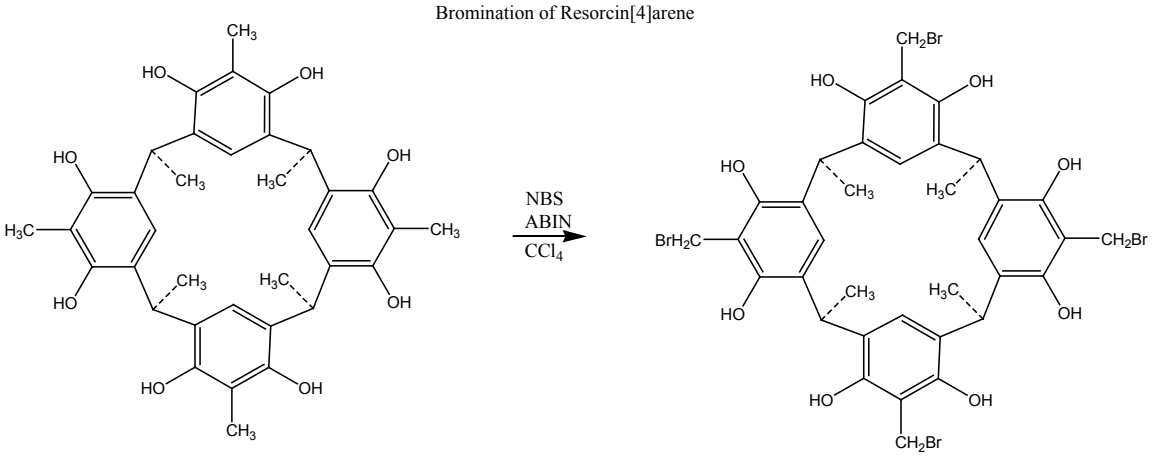

ESI MS: 675.3 $[RA*1Br]^-$, 755.0 $[RA*2Br]^-$, 833.0 $[RA*3Br]^-$, 914.9 $[RA*4Br]^-$.

Figure 7: The bromination of resorcinarene along with mass spectroscopy that showes partial bromination.

Mass spectroscopy data for complexes of host/guest molecules can be found at the end of the report. Complexation of 1-ethyl-3-methylimidazolium ethyl sulfate shows a significant peak at 834.0 which corresponds to 1-ethyl-3-methylimidazolium complexed with ethyl sulfate (236.3) and resorcinarene (600.6). Two protons are lost during ionization for mass spectroscopy analysis. Impurities can also be seen of various complexes. Mass spectrometry of 1-ethyl-3-methylimidazolium hexafluorophosphate shows the resorcinarene-imidazolium peak (711.5) almost exclusively at 710.8 with a proton lost during ionization.

Complexes of synthesis **(11)** show the most significant peak at 817.8 which corresponds to the dehydration of resorcinarene complexed with pyrimidine **(11)** and Na^+. Impurities seem to correspond to previous analyses with a peak at 710.3 corresponding to resorcinarene with 1-ethyl-3-methyl-imidazolium. The peak at 730.6 is also seen in previous analyses. Mass spectroscopy of pyrimidine **(12)** would not show significant complexes with resorcinarene until copper chloride was added in a test analysis. While copper induced complexation, it did not form a complex with the pyrimidine and resorcinarene. Data from the test is inconclusive. The peak at 849.7 for **(12)** corresponds to complexation of resorcinarene with the pyrimidine and Na+ with the loss of two protons. Pyrimidine **(13)** shows a peak at 819.8 which shows again complexation of resorcinarene with the pyrimidine and Na^+. With almost no impurities, pyrimidine **(14)** gives a peak at 803.9 along with the nearby peaks of isotopes. Pyrimidine **(14)**, Na^+, and resorcinarene have predicted masses of 805.4 showing partial ionizations, with definite complexation.

No data is available for 4,5-Diacetyl-6-methyl-1,2,3,4-tetrahydropyrimidine-2-thione. We do not believe ethyl 2-thioureido-2-tosylacetate was synthesized. Product

from the reaction **(15)** completely dissolved upon washing so we hypothesize a salt formed from the added ingredients.

Upon plotting chemical shift differences in comparison to [host]/[guest] molar ratios, computerized calculations using Cao's equations, the complexation constant of resorcinarene with1-ethyl-3-methylimidazolium ethyl sulfate was calculated as 11 ± 1.5mol^{-1}.

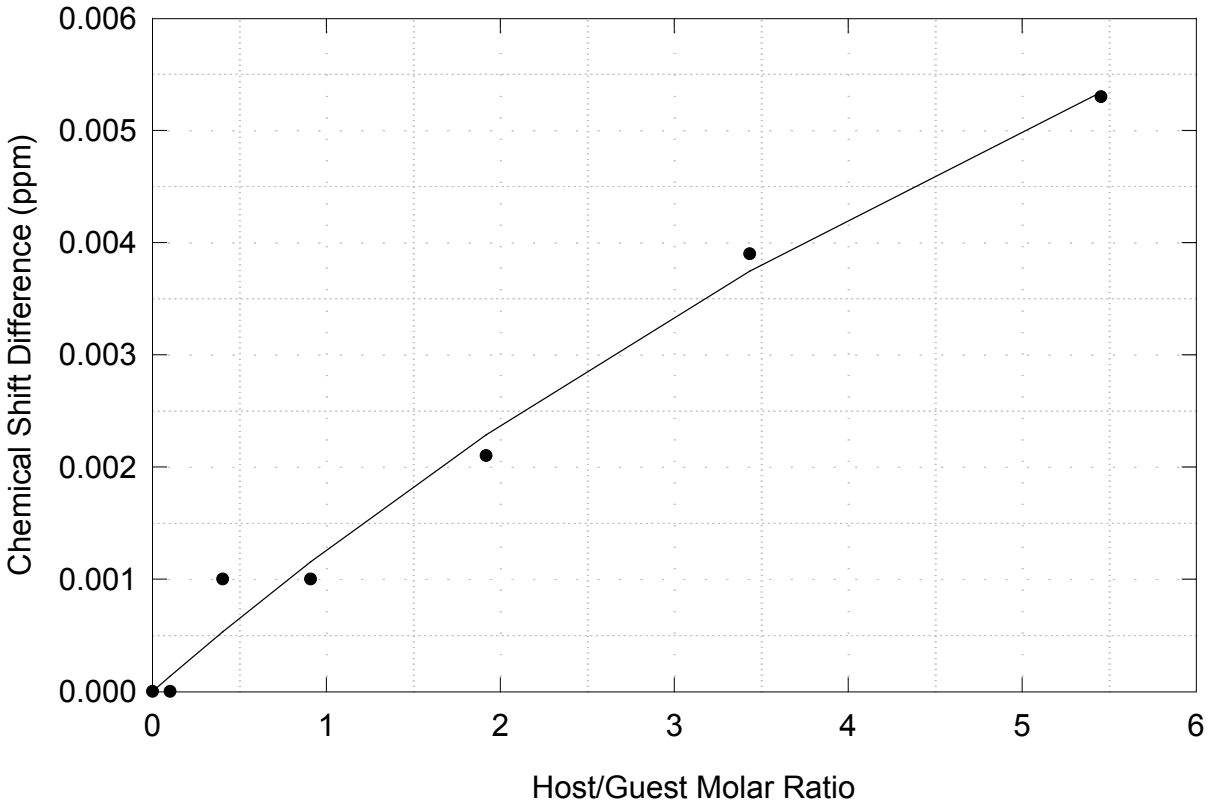

Figure 8: Chemical shift changes of the resorcinarene methylene bridge compared to the 1-ethyl-3-methylimidazolium ethyl sulfate/host concentration.

The complexation constant determined in a similar manner for the interaction between resorinarene and ethyl 4-ethyl-6-methyl-2-thioxo-1,2,3,4-tetrahydropyrimidine carboxylate was 1.1 ± 0.2mol^{-1}.

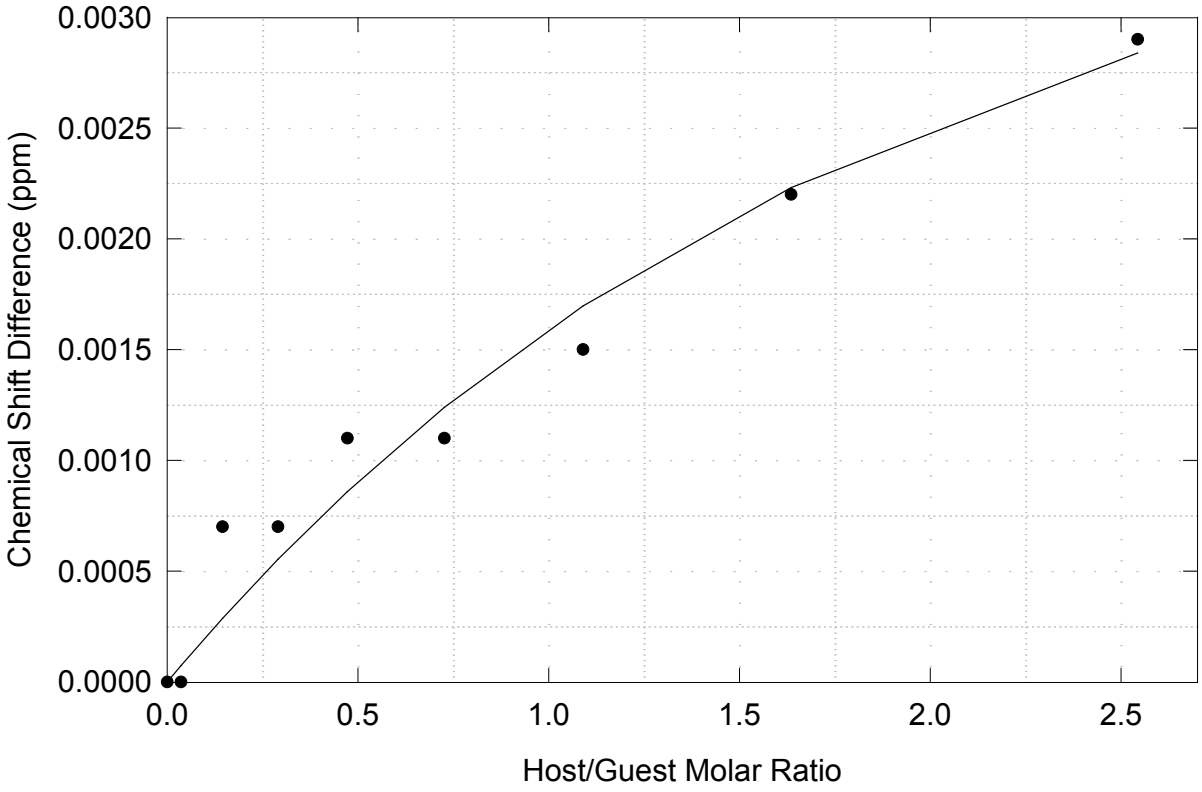

Figure 9: Chemical shift changes of the resorcinarene methylene bridge compared to the ethyl 4-ethyl-6-methyl-2-thioxo-1,2,3,4-tetrahydropyrimidine carboxylate/host concentration.

Results and Discussion

Mass spectrometry shows the loss of more than one electron in complexes of resorcinarene with pyrimidines. Resorcinarene in fact can be easily oxidized by loss of a proton from an alcohol group because of resonance stabilization from the phenol groups. Resorcinarene, however, only shows proton loss in interactions with pyrimidines. The ionic liquid complexes show only the ionization of one molecule which we believe is the ionic liquid.

Because resorcinarenes can be engineered to specify the shape of the rim, they can be specialized to act as catalysts, carriers, or purifying agents. The rim of the resorcinarene can have functional groups that react with the guest molecules to give specific isomers. The studies of complexation with ionic liquids further improves our understanding of the interactions between a resorcinarene catalyst and ionic liquids which form matrices to stabilize transition states. Furthermore, the addition of reacting

functional groups can change Biginelli compounds which as far as we know have never been complexed with resorcinarene.

Resorcinarene can also be used as a carrier. The functional groups can be engineered to target receptor molecules, carrying tetrahydropyrimidines among other biological molecules into specific cell membranes where the biological molecules can alter cell function. As mentioned earlier Biginelli compounds have a wide array of biological functions so that its complexation with resorcinarene can provide a wide range of pharmaceutical possibilities.

By synthesizing resorcinarenes specific for only one or a few molecules, the supramolecule can be used to extract molecules from reactions or natural sources. Perhaps resorcinarene's use as an environmental cleaning agent can be investigated.

The two determined complexation constants showed a much higher constant for 1-ethyl-3-methyl-imidazolium ethyl sulfate. We believe that the size and bond tension along with ionic bonding greatly affected the constants seen by ^{1}H NMR titration. We would like to continue our work on other host/guest complexes to determine if the trend can be seen in all ionic liquid and pyrimidine complexation constants.

Using the following graph, the oxidation constant for resorcinarene-ionic liquid complexes was determined as 11 ± 1.5. The graph also shows predicted ranges for future titration work.

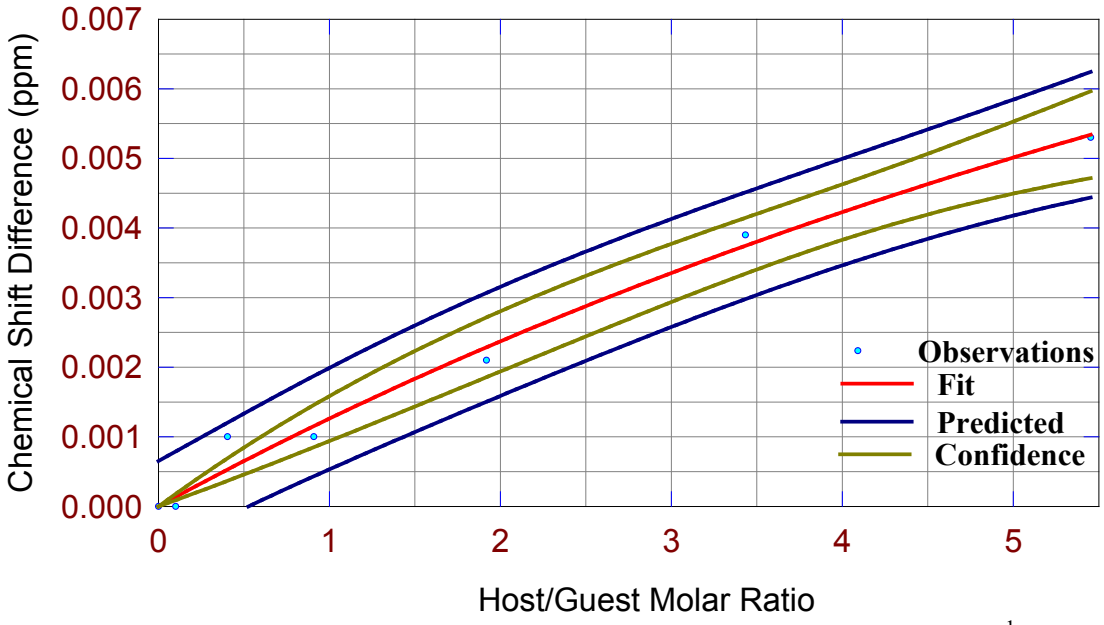

Figure 10: Data plot of the observations, predictions, and confidence of the ^{1}H NMR titration of resorcinarene with 1-ethyl-3-methylimidazolium ethyl sulfate.

The oxidation constant for the resorcinarene-ethyl 4-ethyl-6-methyl-2-thioxo-1,2,3,4-tetrahydropyrimidine-5-carboxylate was found to be 1.1 ± 0.2 using the following graph and the before mentioned Cao ^{1}H NMR titration equation. The graph also shows predicted values for future work and our margin of error.

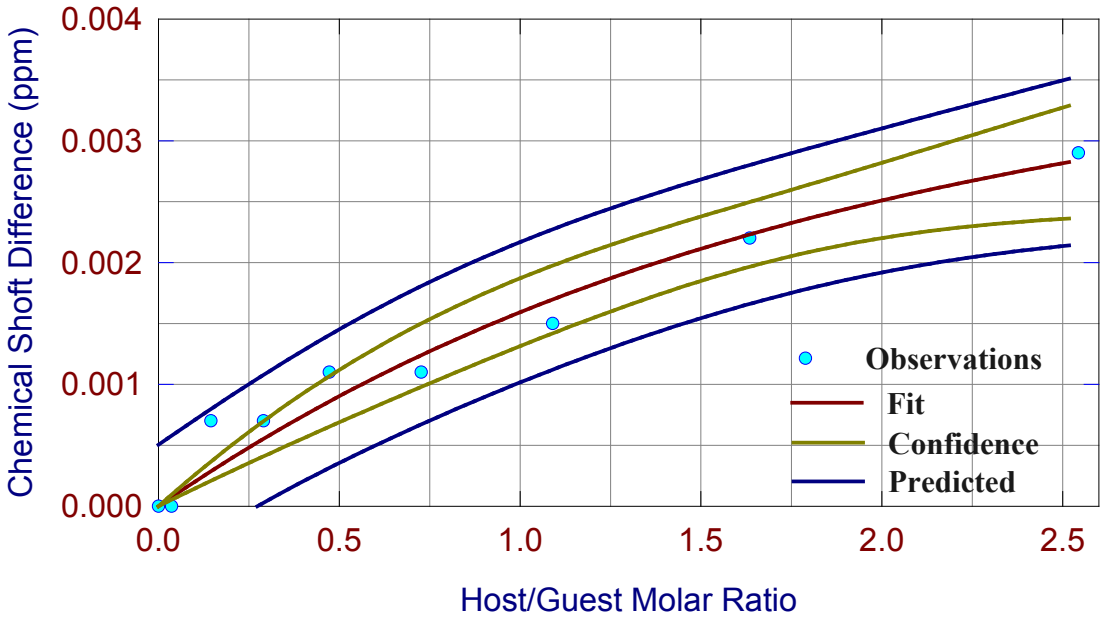

Figure 11: Data plot of the observations, predictions, and confidence of the ^{1}H NMR titration of resorcinarene with ethyl 4-ethyl-6-methyl-2-thioxo-1,2,3,4-tetrahydropyrimidine-5-carboxylate.

Conclusion

We synthesized two host molecules, brominated and unbrominated resorcin[4]arene. Unfortunately only the unbrominated resorcin[4]arene could be used for complexation studies because the MS SPEC of the brominated resorcin[4]arene showed impurities of all partially brominated cyclotetramers. Six guest molecules were also synthesized including two ionic liquids (1-ethyl-3-methylimidazolium ethyl sulfate and 1-ethyl-3-methyimidazolium hexafluorophosphate). The other four guest molecules were tetrahydropyrimidines synthesized using two variations of Shutalev's reaction method. ^{1}H NMR titration was used to find the complexation constant of the resorcin[4]arene host with 1-ethyl-3-methylimidazolium ethyl sulfate to be 11 ± 1.5 mol^{-1}. A complexation constant of 1.1 ± 0.2 mol^{-1} was also found using ^{1}H NMR titration for resorcin[4]arene with ethyl 4-ethyl-6-methyl-2-thioxo-1,2,3,4-tetrahydropyrimidine-5-carboxylate. Mass spectrometry showed complexation of resorcin[4]arene with all four tetrahydropyrimidines as well as complexation with both ionic liquids. The complexation occurred by the binding of the guest molecule in the cavity of the host. We believe that the pyrimidine complexation constant was lower than the constant for the ionic liquid because of the smaller size of the ionic liquids. Pyrimidine functional groups along with the hexacyclic structure caused the molecule to strain in its formation of complexes.

Acknowledgements

I would first like to acknowledge the National Science Foundation whose support for research not only allowed this amazing new program to Moscow, but also supports hundreds of undergraduates to experience research every summer. Russia helped me realize how fortunate students in the United States are to have the support of such a wonderful foundation. My unending appreciation also goes to Dr. David Paul from the University of Arkansas, Dr. Lunin from Moscow State University, and Dr. Ishenko from the State Academy of Fine Chemical Technology for their organization of the program. The years of collaboration and hard work ensured the success of the program. Dr. Paul went far beyond his obligations as program leader and put every effort possible into making the REU program through the University of Arkansas the best possible program. I would also like to thank Dr. Maksimov whose teachings went far beyond organic chemistry. He helped me to understand the role of chemistry on a global level including its environmental and social significance. Dr. Shutalev also influenced my growth as a chemist and allowed me to better understand the difficulties facing scientists in countries where research lacks governmental support. He also spent hours teaching me mechanisms and showing me research projects in various fields of chemical research. Furthermore, I would like to thank my mentors at both institutes in Moscow Pavel Soloviev and Dimitri Sakharov. Finally I would like to thank Iulia Fyodorovna our Russian teacher who gave us foundational Russian which allowed us to have a smooth transition into Russian life. She empowered us to travel throughout Russia without a feeling of helplessness. My sincerest thanks to you all.

References

1. Timmerman, P; Verboom, W; Reinhoudt, D. Resorcinarenes. *Tetrahedron*. **1996.** 52:8, 2663-2704.
2. Olivier-Bourbigou, H.; Magna, L. Ionic Liquids: perspectives for organic and catalytic reactions. *Journal of Molecular Catalysis A: Chemical.* **2002.** 182-183, 419-437.
3. Boerrigter, H.; Verboom, W.; Reinhoudt, D. Novel Resorcinarene Cavitand-Based CMP(O) Cation Ligands: Synthesis and Extraction Properties. *J. Org. Chem.* **1997**. 62, 7148-7155.
4. Welton, T. Ionic Liquids in Catalysis. *Coordination Chemistry Reviews.* **2004.** 248, 2459-2477.
5. Holbrey, J. D.; Reichert, W. M.; Swatloski, R. P.; Broker, G. A.; Pitner, W. R.; Seddon, K. R.; Rogers, R. D. Efficient, halide free synthesis of new, low cost ionic liquids: 1,3-dialkylimidaziolium salts containing methyl- and ethyl-sulfate anions. *Green Chemistry*. **2002**. 4, 407-413.
6. Kappe, O. C. Biologically Active Dihydropyrimidones of the Biginelli-type—a Literature Survey. *Eur. J. Med. Chem.* **2000**. 35, 1043-1052.
7. Shutalev, A. D.; Kishko, E.; Sivova, N.; Kuznetsov, A. Y. A New Convenient Synthesis of 5-Acyl-1,2,3,4-tetrahydropyrimidine-2-thiones/ones. *Molecules.* **1998.** 3, 100-106.

8. Kappe, Oliver C. Recent Advances in the Biginelli Dihydropyrimidine Synthesis. *Acc. Chem. Res.* **2000**. 33, 879-888.
9. Cao, Y.; Xiao, X.; Lu, R.; Guo, Q. ^{1}H NMR titration and quantum calculation for the inclusion complexes of styrene and □□ methyl styrene with cyclodextrins. *Journal of Molecular Structure.* **2003.** 660: 73-80.

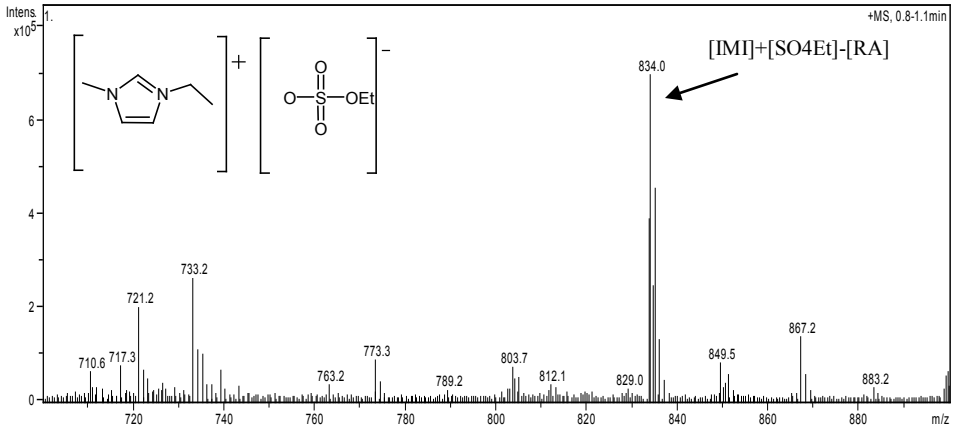

(5)

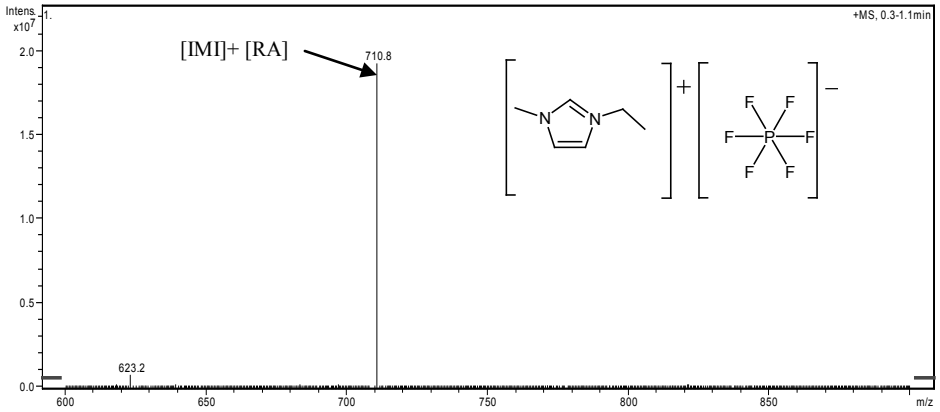

(6)

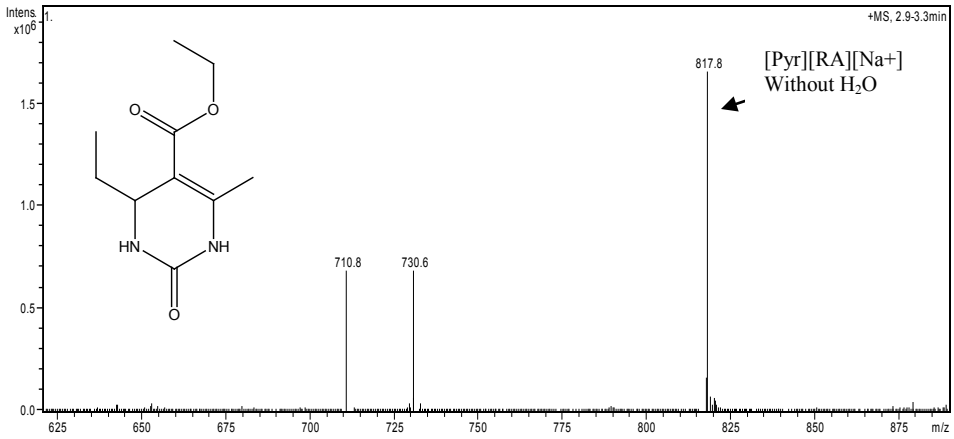

(11)

Figure 12: Mass spectroscopy complexation of resorcinarene with **(5)**, **(6)**, and **(11)**.

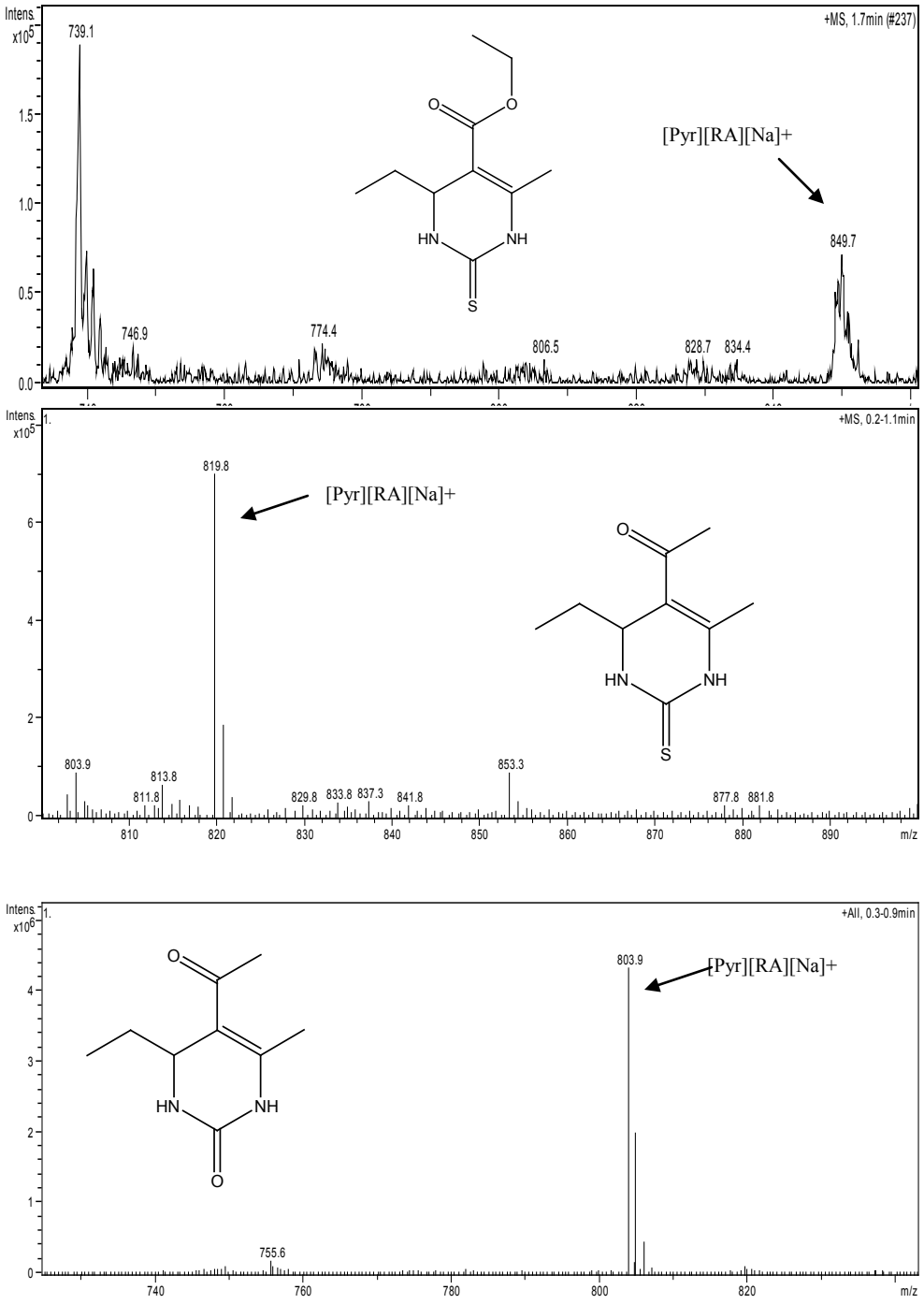

Figure 13: Mass spectroscopy complexation of resorcinarene with syntheses **(12)**, **(13)**, and **(14)**.

Growth Rates of CdSe Nanocrystals with Surface Ligand Mobility

Danielle Reifsnyder, Duke University
Durham, North Carolina

Introduction

Fluorescing semiconductor nanocrystals (NCs), widely known as quantum dots (QDs), are currently in the forefront of research because of their potential applications as light-emitting diodes (LEDs), lasers, biomedical tags, etc.[1] A huge amount of project funding from NSF and other agencies is currently in place to bring these nanotechnologies to everyday life. In Dr. Peng's lab, the basic research goals are to design simpler and greener approaches to the synthesis of high quality NCs and to improve their effectiveness in biosensors, solar cells, and LEDs.

A number of synthetic methods have been developed for inorganic NCs. However, many are extremely expensive or dangerous. Dr. Peng's group strives to improve upon established methods by designing greener processes, which use environmentally safe, easy to handle, and inexpensive materials. In order to create such methods, studies of NC growth mechanisms are especially important due to the limited knowledge on crystallization in literature.

Controlling the rate of NC growth at different stages is central to synthesizing high quality NCs. When growth rate can be controlled, the properties of NCs can be manipulated. As an example, controlling the growth rate of semiconducting CdSe NCs controls the emission color of the NCs. Because of quantum size effects, decreasing size corresponds to increasing band gap, which means that as size decreases, NC photoluminescence (PL) shifts continuously from red to blue (650 nm to 450 nm). Thus, if NC size can be controlled, emission can be also. [1] Consequently, if growth rates are known and can be altered, CdSe NCs can be tuned to emit specific wavelengths of light.

NCs, defined by their size, lose their quantum properties when they agglomerate, so ligands are required to stabilize them in solution.[2] Ligands that bind to the surface of growing NCs are known as a capping agent. Ligand binding, however, has been thought to be dynamic during the growth of nanocrystals. Ligands exist both on the NC surface and as bulk in solution. As temperature rises, these ligands gain kinetic energy and continuously make and break bonds with the NCs. When they leave the NC surface, they allow monomers that are in solution to react with the NC surface, causing growth. Higher temperature means a higher growth rate due to either the increased motion of the monomers for diffusion-controlled growth or increasing the reactivity of the monomers and nanocrystal surface atoms for reaction-controlled growth .

Long-chain amines are good capping agents, hence they have often been used in NC synthesis.[3] Amines must be primary in order to grow NCs with a high PL efficiency.[1] In noncoordinating solvents, amines help control the size and size distribution of growing NCs by helping to balance nucleation (the formation of new CdSe crystals) and growth. Ligands in solution are widely thought to control NC size and shape, but it is unknown whether they do this only by working on the NC surface, as some propose, or also by

affecting the reactivity of the monomers, as a conflicting theory proposes. In the growth stage, ligands may act similarly on NC surfaces and ligands, but in the nucleation stage during which NCs are absent, ligands should be acting on monomers alone. The ability to act on monomers suggests that monomer activity, or "effective monomer concentration," is more important than simply monomer concentration. It is possible to tune monomer reactivity in noncoordinating solvents by varying the ligand chain length.[4]

For years it has been believed that high quality semiconductor NCs, such as CdSe NCs, can only be synthesized at high temperatures (250ºC-350ºC). However, as nanoscience develops, new synthetic opportunities may be realized, which require significantly lower temperature and are thus simpler and greener from a manufacturing point of view. Such developments will benefit greatly from a clear understanding of the dynamic nature of the ligands on the surface of nanocrystals during growth. This research project intends to initiate such efforts.

Amines of different chain lengths were used in the growth of CdSe. With the help of these amines, synthesis at various temperatures was studied. Emphasis was placed on growth rates around the amine boiling point. The zero order consideration made us think that the bonding nature of ligands on the surface of nanocrystals may change around the boiling point.

Experimental Procedures

Cd-TDPA (tetradecylphosphonic acid), dodecylamine (C-12 amine), and octadecene (ODE) were loaded into a three-neck flask. After flushing the system with argon, it was heated to 190°C under Ar flow. At 190°C, TBP-Se (tributylphosphine-Se) was injected into the colorless solution. After injection, aliquots were taken every 2 min for 9 min and placed in a cuvette filled with chloroform. UV-visible spectra were then obtained. Except for one reaction that ran at 190°C until 35min, all the these reactions were heated, beginning at 10 min. Different reactions were heated to 220°C, 150°C, 165°C, and 180°C.

A similar system was run for decylamine (C-10 amine). Cd-TDPA, dodecylamine, and ODE were loaded into a three-neck flask. After flushing the system with argon, it was heated to 170°C so that it became clear. It was then cooled to 150°C and TBP-Se was injected. After injection, aliquots were taken every 2 min for 29 min and placed in a cuvette filled with chloroform. UV-visible spectra were obtained and, except for one trial that remained at 150°C, the reaction flask was heated, beginning at 30 min. The reaction was run until 51 min. Different reactions were heated to 165°C, 180°C, 210°C, 225°C and 240°C.

Data Collection

Absorbance measurements were taken on a HP UV-Visible spectrometer. A sample UV-Vis spectrum can be found below in Figure 1.

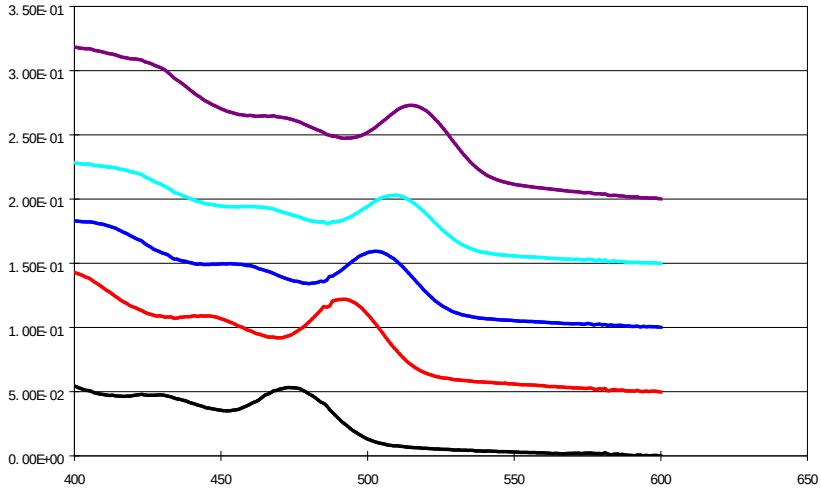

Figure 1. Temporal evolution of UV-Vis spectra of CdSe nanocrystals during growth. Successive UV-vis spectra taken at 3, 5, 7, 9, & 11 min in a reaction with dodecylamine. 3 min is shown at the bottom, and time follows sequentially upward to 11 min on the top. This reaction was injected at 190°C and heated to 280°C beginning at 10 min.

UV-vis data was recorded as the wavelength of the peak position corresponding to the first exciton peak. Two plots of this (one for decylamine and the other for dodecylamine), Figures 2 & 3, show the wavelength of absorbance vs. time collected.

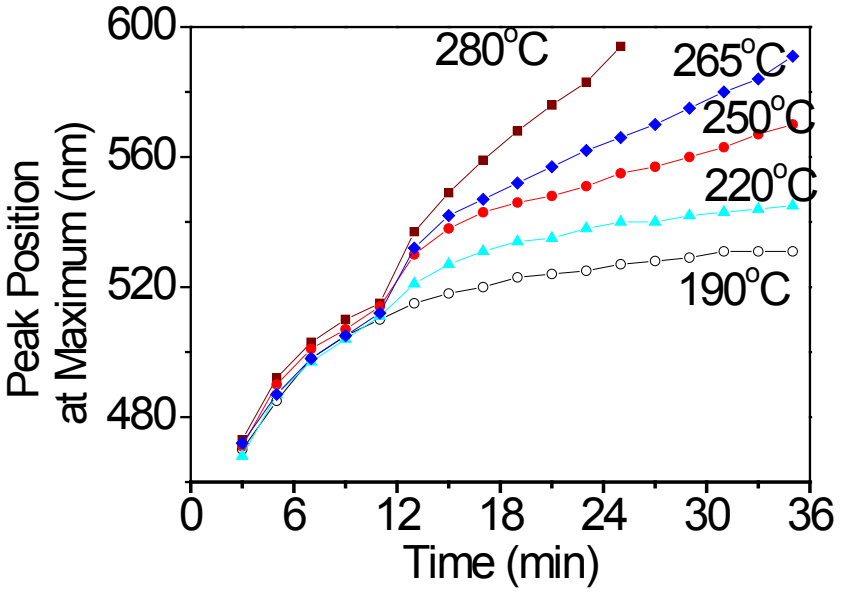

Figure 2. CdSe formation and growth with dodecylamine. 10 min after injection of the Se solution, heating to various temperatures was begun.

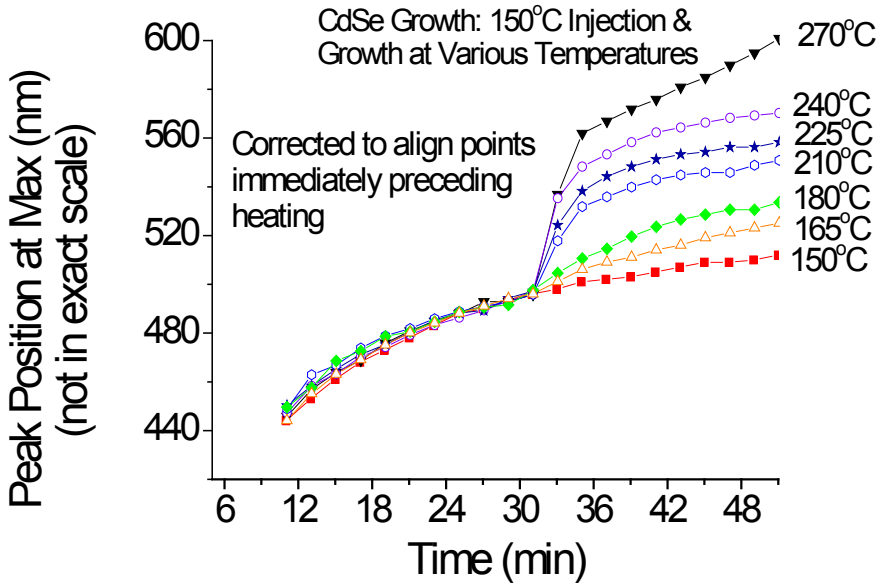

Figure 3.CdSe formation and growth with decylamine. 30 min after injection of the Se solution, heating to various temperatures was begun. Plotted lines have been shifted vertically slightly to align the points preceding heating.

Data Analysis

In the two model systems studied (dodecyl- and decylamine), heating to higher temperatures partway through the reaction time increased the rate of reaction. This increase displayed a trend: below the boiling point of the amine the increase was gradual, while above the amine's boiling point, the increase was sharp. In order to view this better, the volume of the growing NCs was calculated by using Figure 4, and the growth rate of volume vs. temperature was plotted. This was done by considering the amount of growth that took place in the four minute window just after heating where the slope of the graphs in Figures 2 & 3 is greatest, as shown in Figures 5 & 6 below.

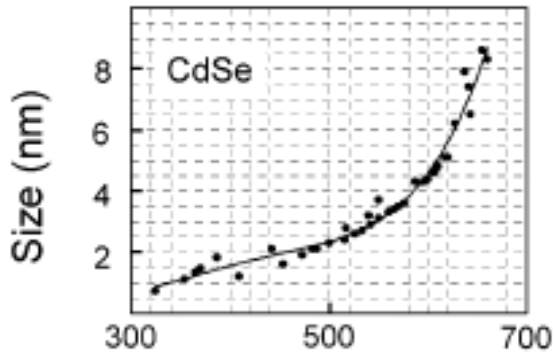

Figure 4. Correlation between wavelength of peak absorbance and NC diameter.

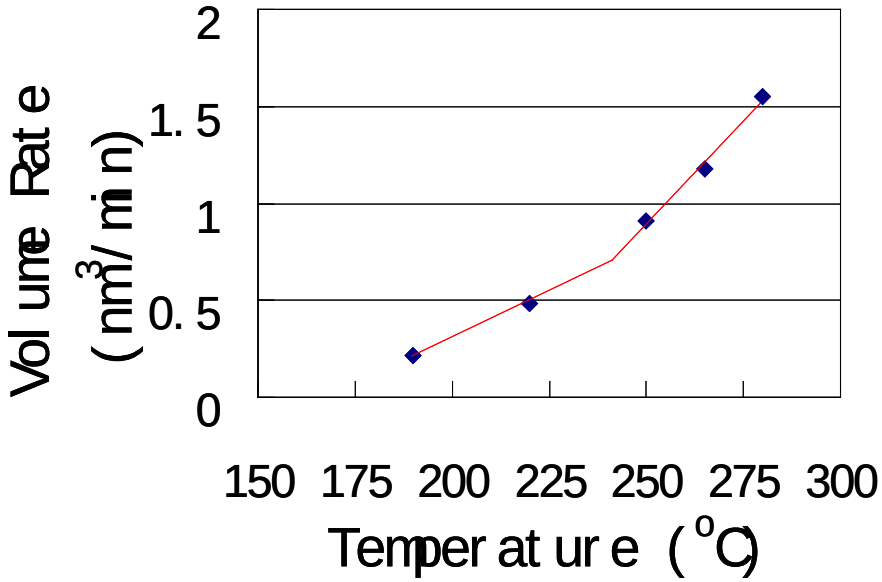

Figure 5. Rate of change of volume vs. temperature for dodecylamine. Two distinct slopes are present.

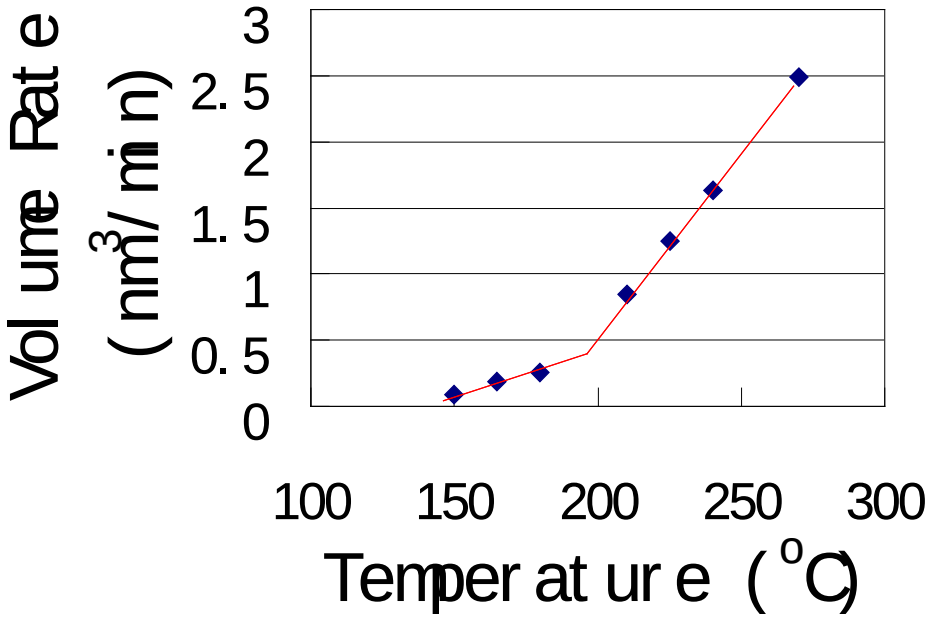

Figure 6. Rate of change of volume vs. temperature for decylamine. Two distinct slopes are present here, also.

Both Figures 5 & 6 show two distinct slopes, which approximately correspond to before and after the boiling points of the amine. The transition point for both cases was about 10 degrees below the boiling point for the given amine. In Figure 5, the slope change happens at 240°C, immediately preceding dodecylamine's boiling point of 247°C-249°C. In Figure 6, the slope change again occurs just before the boiling point of the amine. Decylamine boils at 216°C-218°C and shows its change in slope around 200°C. Both before and after this change, both plots display linearity.

Discussion

Evidence in literature has suggested that growth of nanocrystals in current systems should be diffusion-controlled. The linear relationship between the growth rate and growth temperature shown in Figures 5 and 6 is consistent with diffusion-controlled growth. For a diffusion controlled reaction, when two reactant molecules come within a distance R* of each other, the rate constant is[7]

$$k_d = 4\pi R^* D N_A$$

where D is the sum of the diffusion coefficients for the two reactant species in solution. For each species, the diffusion coefficient is[8]

$$D = RT/N_A 6\pi\eta r$$

where η is the viscosity of the liquid and r is the radius of the spherical particle. Therefore,

$$k_d = 2R^* RT/3\eta r$$

which demonstrates that rate is directly proportional to temperature ($k_d \alpha T$).

Figures 5 & 6 show an unusual trend. Because in each case rate follows linear slopes as temperature increases, the criteria for diffusion-controlled growth are satisfied. However, each plot does not display just one linear slope but two. The temperature increases steadily while the rate jumps, so another variable in the rate equation must be different below and above the boiling point of each amine. Two possibilities exist, and both can be explained by the dynamic binding of ligands to surfaces.

Since the concentration of amines was chosen to be relatively low, about 5% in mass of the total solution, the bulk viscosity should be mostly determined by the solvent, in this case ODE. The transition temperatures observed in Figures 5 and 6 were significantly below the boiling point of ODE. Therefore, the bulk viscosity in the solution should not have dramatic and sudden changes at the transition points observed. The transition temperatures should also not be associated with the reactivity of the precursors, Cd-TDPA and Se, because these chemicals were the same for the two model systems in Figures 5 and 6.

The local viscosity around each nanocrystal, however, could be different below and above the boiling point of the ligands on the surface of the nanocrystals. Monomers and NCs must come into contact for growth to occur. When the temperature is below the boiling point, ligands are tightly capping the NC/monomer surfaces. This can cause a situation similar to that encountered in the "hole theory."[8] According to the hole theory, liquids contain vacancies into which molecules move, thus shifting the hole locations. As pressure is increased, the viscosity of a liquid increases because the number of holes decreases. When this happens, molecules move around each other with less ease. Tightly capping ligands have the same effect; they reduce the mobility of molecules around surfaces, which is precisely where mobility is critical for growth. Because rate is inversely proportional to viscosity, this increased viscosity due to tight capping decreases the rate. Conversely, ligand mobility above its boiling point gives a lower viscosity, which in turn gives a faster rate.

Conclusion

A method for studying growth kinetics of nanocrystals upon changing the reaction temperature has been established. The results obtained indicate that two different diffusion modes exist for the growth of CdSe nanocrystals with amines as the ligands. The transition point between the two modes is found to be slightly below the boiling point of the ligands but significantly below the boiling point of the solvent/solution. Above the boiling point, a fast diffusion rate was observed, which is consistent with a dynamic bonding nature between the ligands and the nanocrystals, as suggested in literature. Below the boiling point, the ligands were likely significantly more tightly bonded on the surface of the nanocrystals, which resulted in a slow reaction rate as observed.

Acknowledgements

1. Dr. Peng, Dr. Pradhan, and the Peng group
2. National Science Foundation
3. University of Arkansas

References

1. Qu, L.; Peng, X. *J. Am. Chem. Soc.* **2002**, *124*, 2049-2055.
2. Thomas, P.J.; Kulkarni, J.U. *Current Science*. **2003**, *85*, 1760-1766.
3. Kulkarni, G.U.; Thomas, P.J.; Rao, C.N.R. *Pure Appl. Chem.* **2002**, *74*, 1581-1591.
4. Yu, W.W.; Wang, Y.A.; Peng, X. *Chem. Mater.* **2003**, *15*, 4300-4308.
5. Peng, X. *Adv. Mater.*, **2003**, 15, 459.
6. *Aldrich Handbook of Fine Chemicals and Laboratory Equipment*.
7. Atkins, Peter. *Physical Chemistry*. New York: W.H. Freeman and Company, 1998.
8. Silbey, Robert J. and Robert A. Alberty. *Physical Chemistry: Third Edition*. New York: John Wiley & Sons, Inc., 2001.

Cloning Various Fragments of the Human Gene for Thrombomodulin and Expressing Them in Pichia Pastoris

Monique Robinson, Langston University
Langston, Oklahoma

Abstract

Cardiovascular disease is the most common cause of death in smokers. The thrombotic arterial occlusive diseases are the most common. The blood of smokers is much more prone to clot than that of non-smokers. It is hypothesized that the level of oxidation of methionine 388 in thrombomodulin, a key regulatory protein in blood coagulation, is elevated in smokers and in various diseases, which impose oxidative stress. It is further hypothesized that this oxidation is a key molecular cause of the prethrombotic state in individuals with these diseases and in smokers and thus a critical factor in the development of thrombosis and premature death in these populations. Cloning various fragments of the human gene for thrombomodulin and expressing them in Pichia Pastoris will facilitate in further work. This research, if correct, could eventually lead to treatments alleviating some the consequences of smoking and these other diseases, thus dramatically reducing the risk of heart attack and stroke for millions of Americans (Stites).

Introduction

Cloning various fragments of the human gene for thrombomodulin, a protein important in regulation of blood clotting, and expressing them in yeast, Pichia Pastoris, will help facilitate further work. After the protein is expressed it will be used in the development of immunoassays specific for oxidized and non-oxidized thrombomodulin. The protein will also be helpful in the development of a protocol using recombinant protein for the quantification of the level of methionine 388 oxidation in the thrombomodulin of diabetics and non-diabetics using chromatography and mass spectroscopy of proteolytic fragments and confirmation of the immunoassay (Stites).

Human Thrombomodulin

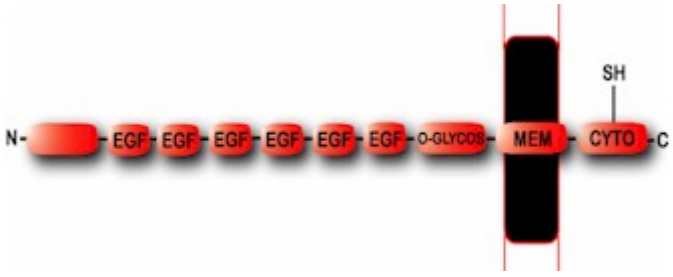

Experimental Procedures

Buccal cell DNA was isolated by rinsing the mouth various times with a 0.9% saline solution. Approximately, 10mL of saline solution was placed into the mouth and vigorously swished against the cheeks for 10 seconds. The saline solution was expelled into a test tube and centrifuged at 2000 x g for 10 minutes. The supernatant was then discarded, while the pellet was saved. 500ul of 1mM EDTA was added and the pellet was resuspended in the solution. A 500ul aliquot of the cells and resin suspension was then transferred to a clean 1.5mL Eppendorf tube. The samples were then placed in a water bath at 100º C for ten minutes. Exposing the cells to 100º C allowed the cells to lyse and the proteins to denature. After the heat treatment, the samples were transferred to ice. The chilled samples were then placed into a microcentrifuge and spun for 45 seconds at top speed. 200ul aliquots of the supernatant, which contained the DNA, were transferred to 1.5mL Eppendorf tubes (Frankhauser). The isolated DNA was used as the template DNA in the PCR (Polymerase Chain Reaction).

After the template DNA was obtained a PCR (Polymerase Chain Reaction) was to be performed on particular domains of the human gene thrombomodulin, which include EGF4, EGF5, EGF6, N-Terminus and C-Terminus. The following components, listed in the table below, were added to each 0.5-0.6mL-microcentrifuge tube.

Component	**Component Volume**
10X ThermoPol Reaction Buffer	10ul
Mg++ 3mM	3ul
dNTPs 2mM	12ul
Nuclease-Free Water	58ul
Template DNA	8ul
Upstream Primer	4ul
Downstream Primer	4ul
Deep Vent DNA Polymerase	1ul
	100ul Final Volume

The first microcentrifuge tube included primers that would be used in the PCR of domains EGF4 and EGF5, which are TMN1Eco and TMC3. The second included primers TMN1Eco and TMC2 for domains EGF4 and EGF6. The third microcentrifuge tube included TMN1Eco and TMC1 for domains EGF4 and C-Terminus. The last microcentrifuge tube for domains N-Terminus and C-terminus included TMN1Sna and TMC1. After the reagents are added they are briefly vortex and placed in a thermal cycler with a heated lid. The following PCR cycle was used.

Temperature	Time	Number of Cycles
95ºC	5 minutes	2
40ºC	2 minutes	
55ºC	2 minutes	
75ºC	1 minute	30
95ºC	30 seconds	
75ºC	5 minutes	1
4ºC	indefinite	

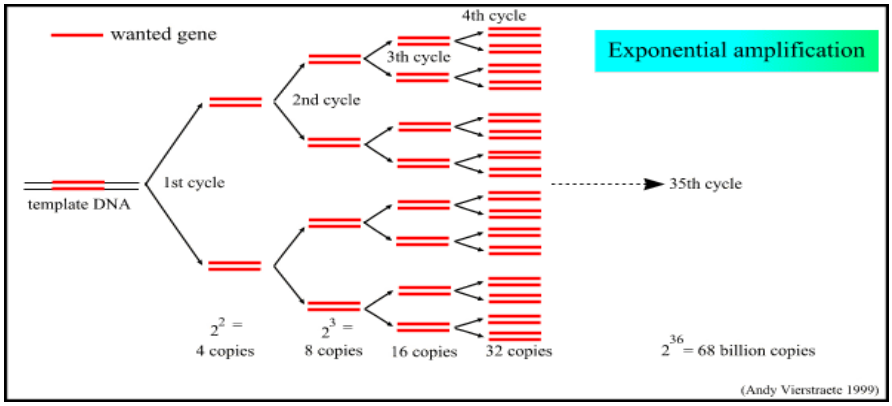

After the PCR cycle is complete 20ul of sample is loaded into a gel. In this case, a DNA agarose gel with a concentration of 1% will be used. The 1% agarose gel is prepared by weighing out 1 gram of agarose and placing it into an Erlenmeyer flask that contains 100mL of 1X TAE buffer. Next, the solution is brought to a boil in the microwave with occasional swirling. The mixture is then cooled to about 50ºC. After the solution has cooled, 10ul of ethidium bromide, a commonly used dye for detecting DNA fragments in agarose gels, should be added. The cooled agar and buffer is then poured into the ready gel box. The comb is then placed into the solution, making sure that there are no bubbles. The comb should not touch the bottom of the gel box. The agarose is then left undisturbed until it completely solidifies. The comb and the dams are then gently removed from the gel. A solution made up of approximately 250mL of 1X TAE buffer and 25ul of ethidium bromide is then poured into the gel box with the solidified agarose gel. The gel is ready to be loaded. 5ul of pGem DNA marker is to be added to one well in the gel. In addition, 16ul of each PCR product is then added to 4ul of 5X glycerol loading buffer for a total of 20ul. Next, each individual sample is added to different wells in the agarose gel. The gel then goes through the process of electrophoresis using 100 V for about 30 minutes. After electrophoresis, the gel is then inspected under an ultraviolet light for the distinctive band. If all goes well, the gene is cut out of the agarose gel and is ready to be cloned into the vector, pPic9k.

The next steps will be to insert the gene from the agarose gel into the plasmid, pPic9k. After that, the vector will be linearized followed by ligation. Then for confirmation, sequencing recombinant clones is necessary to confirm that the gene wanted is in frame with the α-factor secretion signal ATG. Once the insert have been cloned and sequence, it can be transformed into Pichia Pastoris (http://www.invitrogen.com).

Conclusion

Unfortunately, in this work a critical step, the polymerase chain reaction, unexpectedly failed. This led to the troubleshooting of the PCR. Consequently, everything was at a stand still and further work was unable to be accomplished. The cloning of the genes in pPic9k, as well as the transformation of the pPic9k into Pichia Pastoris to acquire the proteins could not be attained in the short extent of time.

Acknowledgements

1. Langston University
2. University of Arkansas
3. Dr. Wes Stites, Mentor
4. Dr. David Paul, Chemistry REU Director
5. George Washington Carver Project
6. Ms. Clark, George Washington Carver Project Director
7. Dr. Jones, Assistant Dean of Graduate Recruitment
8. National Science Foundation
9. Deepika Talla, graduate student
10. Jeff Froude, graduate student
11. Chris Saunders, graduate student
12. Mark Phan, undergraduate

References

1. http://users.ugent.be/~avierstr/principles/pcr.html
2. http://www.invitrogen.com/
3. Frankhauser, David. *Isolation of Buccal Cell DNA*. 2001
4. Stites, Wesley. *Smoking, thrombomodulin oxidation, and thrombosis*.2001

Electron Transfer between Cytochrome C and Cytochrome C Oxidase

Lauren Rogers, Western Carolina University
Cullowhee, North Carolina

Abstract

Cytochrome c oxidase is the terminal electron acceptor within the mitochondria. It is responsible for reducing O_2 into H_2O and in the process providing a proton gradient which powers the production of ATP. Cytochrome c is an electron shuttle which provides oxidase with a supply of electrons. The rates of electron transfer involved in the reduction of cytochrome c oxidase were studied by mutating, growing, and purifying a variant of bovine cytochrome c. The variant was labeled at the 21 position with a ruthenium derivative followed by flash photolysis. The new variant cytochrome c was found to be similar in both the yield and rate of electron transfer in comparison with native like cytochrome c variant Ru-39-Cytc. The fast intramolecular rate was found to be 50,000 sec^{-1}. Binding strengths measured by second order intermolecular rates were raised with increasing ionic strength up a maximum at 70mM NaCl after which increases in ionic strength diminished the rates.

Introduction

"To oxidize food molecules all organisms from yeast to man require a variant of cytochrome c" Richard Dickerson.(4)

Energy for life is derived by combining the energy found from the breakdown of food molecules with oxygen. To maintain life, all organisms must be able to sustain their cells with a supply of ATP. ATP is the energy currency of the cell. The final components of food end up at the electron transport chain. The mitochondrial electron transport chain is made up of four complexes. One of these membrane bound complexes, the enzyme cytochrome c oxidase, is responsible for reducing oxygen to water and through this process a proton gradient is created which powers the production of ATP within the mitochondria(1). Cytochrome c is a heme containing electron shuttle which transports electrons between the outer, inter, and inner membrane spaces within the mitochondria (5). Cytochrome c will donate a total of four electrons, one at a time to oxidase which utilizes these electrons to reduce O_2 in to two water molecules and in the process create an proton gradient within the mitochondria which is responsible for powering the production of ATP(1). Over 96 amino acid sequences have been determined in the past for cytochrome c, leaving it one of the most thoroughly studied proteins within biological sciences(5). Because cytochrome c and oxidase are involved with the production of ATP which powers every aspect of any organisms life, the processes carried by cytochrome c and oxidase when malfunctioning can cause havoc on an organism's life.

Cytochrome c is part of the research in Dr. Deshmunk's lab at the University of North Carolina Chapel Hill. His recent findings have shown that the release of cytochrome c along with other factors such as IAP's leads to neuronal apoptosis which is

relevant in studies regarding neurodegenerative diseases such as Alzheimer's, Huntington's chorea, and Parkinson's.(3)It is thought that the combination of IAP's with cytochrome c is the cause of programmed cell death.

The structure of cytochrome c and cytochrome c oxidase have been known for years through X-ray diffraction techniques. However a thorough study regarding the exact mechanism of electron transfer within oxidase itself has not been accomplished. Based on Riedner and Bosshard's studies it is known that positively charged, acidic lysine groups near the heme crevice on cytochrome c help bind to oxidase and reduce the enzyme(7). Oxidase initially receives an electron at a copper group(CuA) near the binding site to cytochrome c , then passes its electron on to heme a, on to a second heme a3, and then last to a copper (CuB)(6). The transfer of electrons from cytochrome c to oxidase and then through oxidase can be noted in changes in absorption. Understanding the details of the pathway for electrons through oxidase which is responsible for formation of the proton gradient necessary for ATP production will provide better knowledge of the mechanism of cytochrome c oxidase(5).

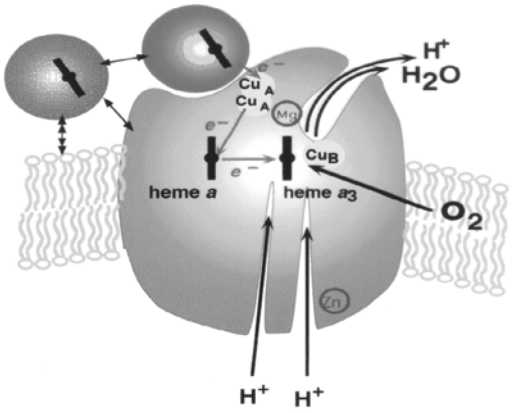

Figure 1.1 Mechanism of Cytochrome c and Cytochrome Oxidase (16)

Previous studies have shown that stopped flow spectrophotometry does not have sufficient resolution time to measure the rate of electron transfer from cytochrome c to oxidase. Dr. Bill Durham and Dr. Francis Millett and Dr. Lois Geren at the University of Arkansas, Fayettville found that a ruthenium-cytochrome c derivative provided a much more rapid method and advanced ability to study the rates of the interaction and electron transfer between cytochrome c and oxidase.(2) By labeling cytochrome c with a ruthenium(II) derivative to form Ru-cytochrome c it was then possible to study the actual transfer of electrons from the heme center of cytochrome c to the CuA group of oxidase, and then from CuA to heme a in oxidase.

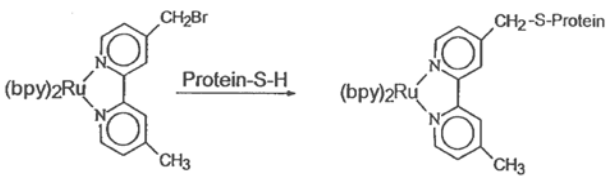

Figure 1.2 Structure of (4-bromomethyl-4'-methylbipyridine) (bisbipyridine)ruthenium-(Br)2 (16)

The ruthenium agent is attached in such a position on cytochrome c so that it does not interfere with binding properties and electron transfer to oxidase. Prior to the discovery of the ruthenium labeling, binding had been studied through stopped flow experiments, but accurate fast rates for electron transfer could not been determined. The ruthenium labeling of the cytochrome c allows it to bind to oxidase, and then with activation/reduction by flash photolysis the rates can be studied without the effects of the initial binding(2). By increasing the concentration of NaCl within the reaction sample both first and second order kinetics can be observed(2).

In past experiments carried out by Millet, Durham, and Geren a bovine cytochrome c mutant was used in which the amino acid residue at position 39, was mutated into a cysteine residue at which the ruthenium agent was attached(6). This

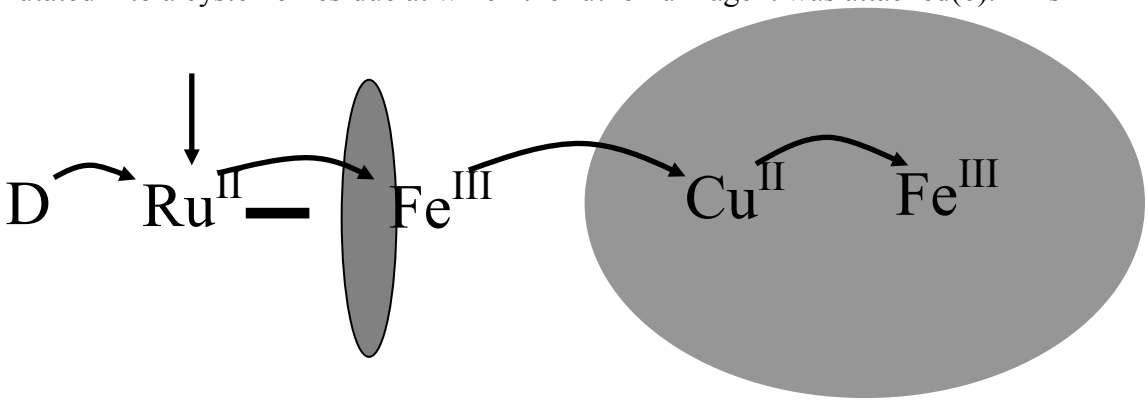

Figure 1.3 Reduction of ruthenium and electron transport from cytochrome c to cytochrome oxidase(16)

mutant cytochrome c provided decent signal for the study of the electron transfer which is discussed in their 1995 paper *Definition of the Interaction Domain for Cytochrome c on Cytochrome c Oxidase.(6)* However, the yields for the activation and the rate of electrons from ruthenium to the heme center of cytochrome c could be increased. The mutation at residue 39, hence the attachment of the Ru agent at position 39 leaves 13 bonds for the electron to pass to reach the heme center of the cytochrome c after laser reduction of the ruthenium. A mutant which lies closer to the heme center of cytochrome c yet does not interfere with the binding or transfer of electrons to oxidase may provide higher activation yields for the Ru-cytochrome c complex. The amino acid residue at position 21 when mutated to a cysteine and labeled with the ruthenium complex may provide a higher yield of electron transfers into the heme center of cytochrome c. The Ru-21-Cytc variant may sustain longer activation periods because of the more direct pathway from reduced ruthenium to the heme c center of the protein. By creating higher yields of transfer of electrons from reduced ruthenium to cytochrome c the yield of electrons to cytochrome c oxidase should also increase hence increasing the ability to study the kinetics of electron transfer to and throughout the oxidase structure.

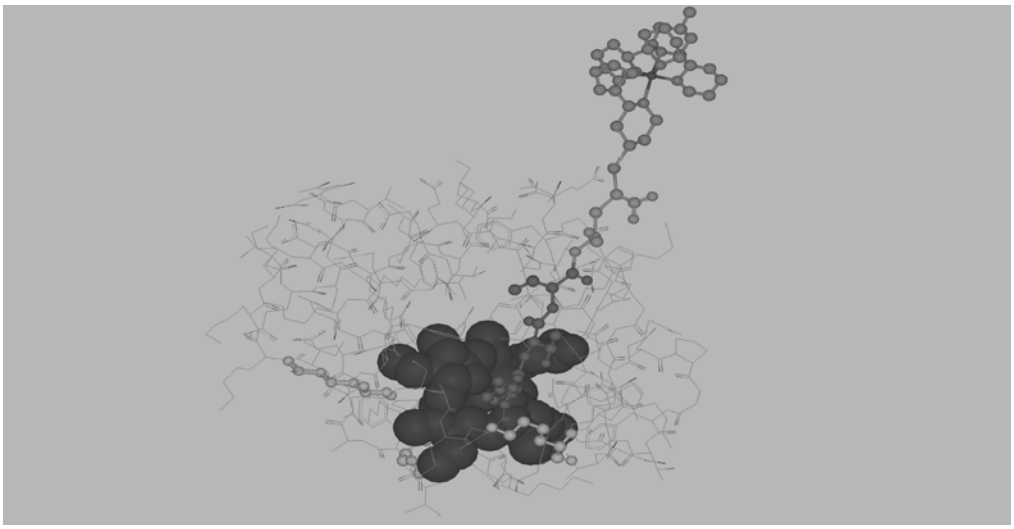

Figure 1.4 Model for the high affinity complex between variant E21C and cytochrome oxidase.(15)

Experimental Procedures

Materials- Beef heart cytochrome c oxidase was prepared as described by Capaldi and Hayashi (3). Horse cytochrome c wild type was supplied by Dr.Gary Pielak from the University of North Carolina at Chapel Hill. Primers were obtained from Integrated DNA Technologies (IDT) and those primers were constructed from the known gene sequence. Site directed mutagenesis using the Stratagene method was carried out with the IDT primers to achieve mutation E21C,C102T. The mutation E21C substituted glutamate at site 21 on the horse cytochrome c with cysteine. The mutation C102T replaced Cys-102 to prevent any unwanted reaction with the ruthenium agent, also to prevent dimerization(7). The E21C, C102T plasmids were sent to the DNA Sequencing Lab, at Poultry Science, University of Arkansas. The sequences did not contain more than the one intended mutation and the plasmids were further used for expression of the mutant protein.

The E21C,C102T variant was treated with 260μM dithiothreitol to reduce any disulfide cross linked dimmers. It was then purified using a BIORAD anion exchange column in high pressure liquid chromatography.

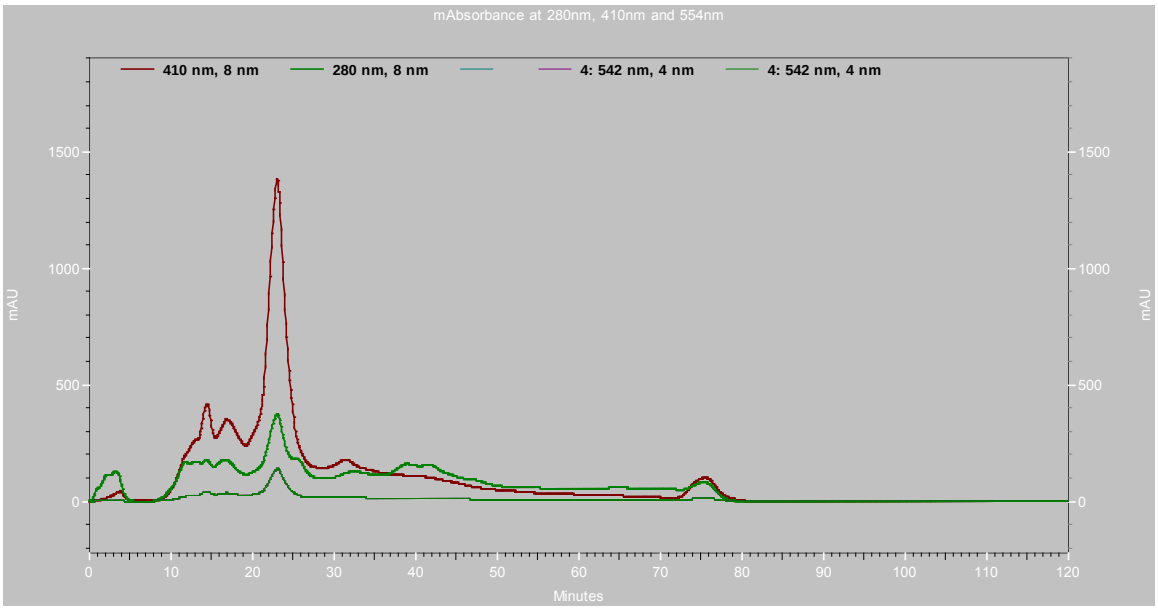

Figure 1.5 E21C Variant Cytochrome c Purification Chromatogram Post-Dithiothreitol Reduction

Once HPLC purified, the sample was collected using a Gilson fractionator, the E21C,C102 variant was concentrated and washed with 200 mM sodium borate pH 9 for a final concentration of 0.17mM. 0.85 mM TCEP solution was added to the variant sample and 0.19mM (4-bromomethyl-4'-methylbipyridine) (bisbipyridine)ruthenium Br_2 was added from a 86.6 mM stock to each variant sample in dry dimethylformamide(8). The sample was left to react over night and then excess ruthenium was washed away using a 200 mM Borate buffer pH 9. The reaction mixture then was oxidized with 10µL of 50mM ferricyanide and passed through a 1 x 10 cm Bio-Gel P-2 column equilibrated with 10 mM sodium phosphate at pH 6 to further purify before high pressure liquid chromatography purification using a BIORAD anion exchange column with the labeled sample. The labeled protein was eluted with a gradient ranging from 5mM to 1M sodium at pH 6.0 with a flow rate of 1 mL/min. A major peak of native protein mixed with labeled protein eluted at 26 minutes, and a minor peak eluted at 45 minutes and was labeled protein and a slight amount of free ruthenium.

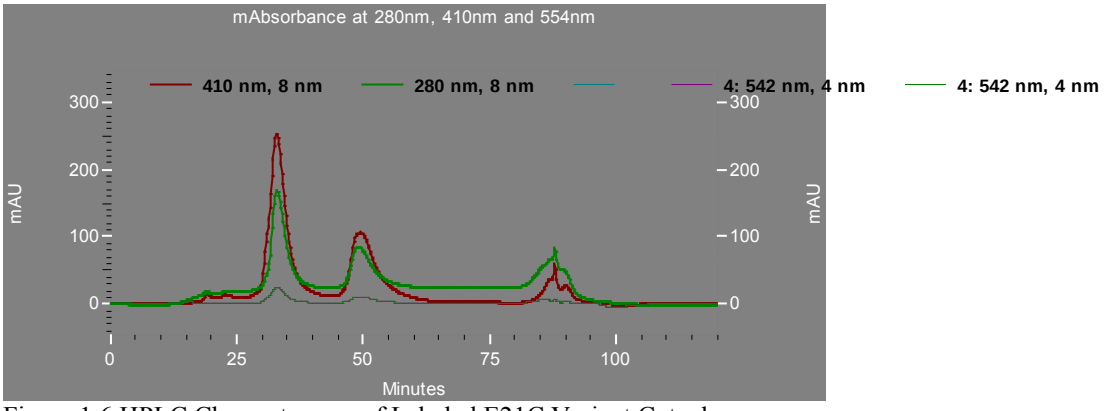

Figure 1.6 HPLC Chromatogram of Labeled E21C Variant Cytochrome c

The first major peak was collected and was combined with the second minor peak for a total labeled sample of 1.5 mL at 8.4 µM labeled Ru-21-Cytc. The samples were concentrated using a centricon concentrator and were washed with 10 mM sodium phosphate buffer pH 7. Absorption spectra of the sample using a diode array was taken to confirm that the sample was both oxidized and labeled.

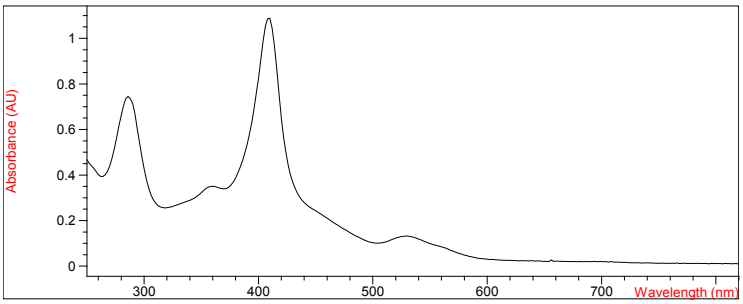

Figure 1.7 Labeled E21C,C102 variant with Ru. Spectra was taken post oxidation with ferricyanide and wash with 10 mM Pi Buffer pH 7.0

Flash Photolysis Experiments- Transient absorbance measurements of the rapid electron transfer between Ru(II) and the heme group in Ru-21-cyt c[1] was carried out as described by Durham *et al*(10). Solutions containing 9.9µM Ru-21-cyt c in 300µL of 5mM Tris pH 8 in 0.1% Lauryl Maltoside and placed in semimicro glass cuvettes. The transient absorbance measurements for the reaction of Ru-21-cyt c with cytochrome oxidase were carried out as described by Pan *et al*(11). The excitation source was a Phase R model DL 1400 flash lamp-pumped dye laser using coumarin 488 to produce a 488nm light pulse of <0.5-µs duration(7). The photomultiplier detector had a response time of 1µs. The reaction of cytochrome c was monitored at 550 nm using an extinction coefficient of $\Delta\acute{\varepsilon}_{550} =$ 18mM^{-1}cm^{-1}(12)The reduction of heme a was measured at 605 nm using $\Delta\acute{\varepsilon}_{604=}$ 16 mM^{-1}cm^{-1} (13) The reaction solutions contained 9.9 µM Ru-21-cyt c, 11.1 µM cytochrome c oxidase, 10 mM aniline, 1mM3-carboxyl-2,2,5,5-tetramethyl-1-pyrolidinyloxy free radical (3CP), and 0.1% lauryl maltoside in 5 mM Tris at pH 8 at 25º C. The ionic strength was increased gradually with additions of sodium chloride in the reaction solution. The reactions were carried out aerobically.

Results

Cytcohrome c was mutated at residue 21 and a cysteine was inserted in place of a glutamate. The purification of the protein can be located in figure 1.5. The large peak responding at 410 nm contained the purified sample of the newly created E21C,C102 mutant. After purification and concentration the sample of variant cytochrome c was labeled with the ruthenium reagent with a 10% yield. Purification of the labeled protein can be found in the HPLC chromatogram in figure 1.6.

Laser flash photolysis of Ru-21-Cyt c revealed rapid electron transfer from activtated Ru(II*) to heme c Fe(III). The yield of heme c which was reduced through flash photolysis using this variant cytochrome c was found to be 5%. The Ru-39-Cyt c yield of heme c reduction is found near 5%.The variant E21C did not provide a yield of

electron transfer higher than variant K39C used in the past, and described in Dr. Francis Millet, Dr. Lois Geren, and Dr. Durham's 1999 paper "*Definition of the Interaction Domain for Cytochrome c on Cytochrome c Oxidase.II: Rapid Kinetic Analyses of Electron Transfer from Cytochrome c to Rhodobacter Sphaeroides Cytochrome Oxidase Surface Mutants.*"(2).

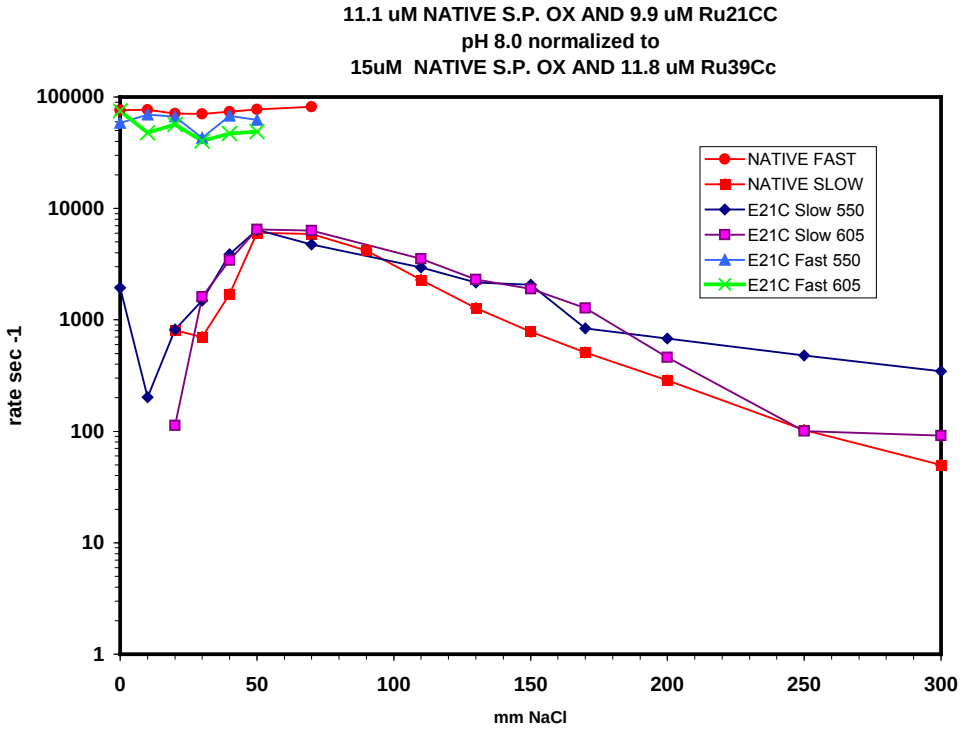

Figure 1.8 Comparison of Cytochome c Variants K39C and E21C Using Ruthenium Derivative Via Flash Photolysis.

When compared to past experiments of the K39C cytochrome c variant, E21C did not improve the yield of transfer of electrons from its attached ruthenium agent to its heme c center. In figure 1.8 E21C is compared to the previously used K39C variant in electron transfer to oxidase. The hypothesized improvement to be made by the E21C variant was for higher rates of electron transfer there by an increase in the yield of electrons through cytochrome c to oxidase.

In figure 1.8 the fast rate found in E21C was similar to native like K39C. In comparison between the fast rates at 605 nm the E21C was within the range of 50,000 $sec^{-1}$and for K39C it was within the range of 60,000 sec^{-1}. Binding strengths measured by second order intermolecular rates were raised with increasing ionic strength up a maximum at 70mM NaCl after which increases in ionic strength diminished the rates. These rates are also represented graphically within figure 1.8.

Discussion

Cytochrome c oxidase is of importance to all life which depends on ATP for energy to power cellular function. This experiment utilized a new variant of cytochrome c which was labeled with a ruthenium derivative with the intention of increasing yields of electron transfer from cytochrome c to R. sphaeroides cytochrome oxidase. If the yield of electrons increased upon laser reduction of the ruthenium agent and corresponding signals increased during the flash photolysis experiment the ability to study the electron pathway throughout oxidase would have improved. Increasing yields of electron transfer corresponds directly with increased signal to noise ratios and increases the ability to study and gain knowledge into the mechanism or pathway through the enzyme oxidase. The variant cytochrome c was mutated at residue 21, where the attachment of a ruthenium complex at position 21 on cytochrome c should not interfere with its binding to R. sphaeroides cyt. c oxidase. The laser activated ruthenium must pass three amino acid residues and 14 bonds to reach the heme c center. The 21 residue does not have any known existing detrimental effects of binding to oxidase and therefore, the pathway to the heme c center with this variant should have provided a faster more successful electron transfer resulting in faster rates and higher yields than the past Ru-39-Cytc.

E21C,C102 was labeled using the same method as with the K39C variant used in the past Geren *et al Biochemistry 1999*. It was successfully labeled as can be seen in figures 1.6 and 1.7. It was successfully reduced by its attached ruthenium derivative based on the resulting absorbance determined during the flash photolysis experiment. Increasing the concentration of NaCl during the flash photolysis experiment found it to behave under second order rate conditions very much like Ru-39-Cyt c. It did not show faster rates in first order kinetic studies, as seen in figure 1.8, neither did it show faster rates in the second order kinetic studies. The Ru-21-Cyt c did not improve in rate or percent yield of reduction of the cytochrome c variants heme c center from Ru-39-Cytc.

Conclusion

The reaction of Ru-21-Cyt c with R. sphaeroides cytochrome c oxidase was determined to be very similar to previous studies involving the variant Ru-39-Cyt c. The kinetics of both first and second order rate studies for the two mutants showed the new E21C variant lacked improvement in the yield of electrons transferred from the ruthenium labeled cytochrome c to oxidase. Based on HPLC and diode array absorption spectra the Ru-21-Cytc variant was assumed to be successfully labeled, however lysine groups lying on the surface of the protein can also be labeled in error. To determine if the correct site was labeled, the 21 residue further analyses on the structure of the labeled Ru-21-Cytc could be helpful. In future studies, ruthenium agents with longer lifetimes which also are limited in back reactions may increase the yield and rate of electron transfer to cytochrome c and on to oxidase. Mutations closer to the heme c center which will not interfere with binding to oxidase or structure of cytochrome c may be possible. The rate of electron transfer when studied in the bound form between cytochrome c and oxidase using ruthenium derivatives provides the most physiologically relevant results as it is a replica of electron transfer within the mitochondria.

Acknowledgements

1. National Science Foundation
2. Dr. David Paul, University of Arkansas, Fayetteville, AR
3. Dr.Frank Millett, Dr. Bill Durham, Dr. Lois Geren, Marilyn Davis, Millett Research Group, University of Arkansas
4. Dr. Gary Pool, Dr. Roger Bacon and Dr. William Kwochka, Western Carolina University, Cullowhee, NC

References

1. Alleyne T; Sampson V. *Cytochrome c/cytochrome c oxidase interaction.*Eur.J.Biochem.268,6534-6544(2001).Biochemistry Unit, Faculty of Medical SciencesUniversity of the West Indies.Eric Williams Medical Sciences Complex.Champs Fleurs, Trinidad and Tobago.
2. Beasley, J.R.; Durham, B; Fine B;Geren, L; Hibdon, S.; Millett, F.; Pielak, G.J.*Design of a Ruthenium-Cytochrome c Derivative to Measure Electron Transfer to the Initial Acceptor in Cytochrome c Oxidase.*The Journal of Biological Chemistry.Vol.270,No.6,Issue of February 10,pp.2466-2472,1995.
3. Capaldi, R.A; and Hayashi, H.(1972)*FEBS Lett.***26**,261-263
4. Deshmukh, Moanish. *Competent to Die* .Cell and Developmental Biology, UNC-Chapel Hill.http://research.unc.edu/endeavors/spr2002/deshmukh.html
5. Dickerson, E. R.; Geis I. *The Structure and History of an Ancient Protein.*Harper and Row Publishers,1969
6. Durham B.; Millet F. *Iron: Heme Proteins and Electron Transport.*University of Arkansas, Fayetteville,AR,USA.
7. Durham, B.; Geren, L.; Grinnell, S.; Millett, F.; Ferguson-Miller, S.; Sadoski, R.; Wang, K.; Zhen Y.;. *Definition of the Interaction Domain for Cytochrome c on Cytochrome c Oxidase.II: Rapid Kinetic Analyses of Electron Transfer from Cytochrome c to Rhodobacter Sphaeroides Cytochrome Oxidase Surface Mutants.*The Journal of Biological Chemistry.1999.Vol 274,No 53,Issue of December 31,pp.38042-38050,1999.
8. Geren,L.,Hahm, S., Durham, B.,and Millett, F. (1991)*Biochemistry* **30**, 9450-9457.
9. Riedner, R. ; Bosshard, H.R. J.Biol.Chem.,1980,255,4732.
10. Durham,B.,Pan, L.P.,Long,J.E. and Millett,F.(1989)Biochemistry28,8659-8665.
11. Pan, L. P., Hibdon, S., Liu, R.-Q., Durham, B., and Millett, F. (1993) *Biochemistry* 32 8492-8498.
12. Margoliash, E.,and Frohwirt,N.(1959)*Biochem*.J.71,570
13. Blair,D.F.,Bocian, D.F.,Babcock, G.T., and Chan, S.T.,.(1982)Biochemistry 21,6928-6935
14. Blair,D.F.,Martin,C.T.,Gelles,J.,Wang,H.,Brudvig,G.W.,Stevens,T.H.,and Cahn,S.I.,(1983)*Chem.Scr*.21,43-53
15. DS Viewer Pro50
16. Millett,F.; *American Chemical Society Presentation Oxidase*.2000.University of Arkansas, Fayetteville, Arkansas.

Investigation of Poly(propylene imine) Dendrimer Host-Guest Complexation with Cu^{2+} and Lipids

Anne St. Martin, Worcester Polytechnic Institute
Worcester, Massachusetts

Introduction

It has been proposed many times that modified dendrimer host-guest interactions have huge potential for use in the area of membrane transport and drug delivery[i]. Different host guest interactions have been investigated with dendrimers for catalytic purposes, namely complexation with copper, palladium, and other inorganic metal ions. However complexation with small organic molecules for biological interests has not been as intensively studied, and non covalent complexation with lipids has to our knowledge never been explored. This paper investigates complexation of 1.5 generation PPI-DAB$(CN)_8$ dendrimers with variously charged lipids, and the competition between these lipids and Cu^{2+} ions for dendritic host interactions.

Guest Host Complexes

Guest host interactions involve multiple non-covalent interactions between a large and geometrically concave organic molecules and inorganic metal ions or simple organic molecules. These host guest complexes differ from supramolecular molecules by their inclusion of the guest compound[ii]. While supramolecular interactions exist between reactants of all shapes and sizes including host guest complexes, they do not necessarily involve inclusion of the guest molecule into the host compound.

Host Guest Interactions and Common Host Molecules

There are many non-covalent supramolecular interactions that contribute to the establishment of guest-host interactions. These include electrostatic interactions between different ions and different dipole moments, hydrogen bonding, π-π stacking interactions, cation-π interactions, Van der Waals forces, and hydrophobic interactions. Common host molecules include cyclodextrins, calixarines, and crown ethers as illustrated in Figure 1.

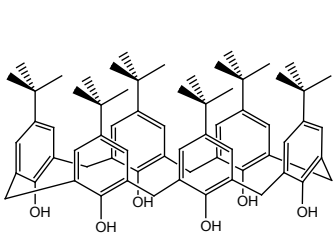

Calixarenes

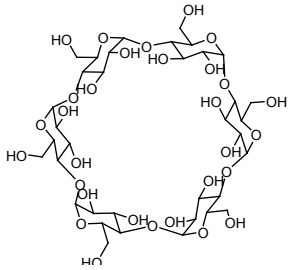

Cyclodextrins

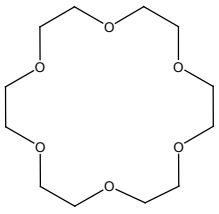

Crown Ethers

Calixarenes are microcyclic oligomers of phenol 4,6 or 8 monomer units. The large hydrophobic cavity is lined by π-electrons of the aromatic rings, and one rim of the cavity is lined by hydroxyl groups. The rings are linked by methylene bridges which results in a degree of freedom for the individual rings. In comparison, cyclodextrins are large cyclic oligosaccharides whose overall bucketshape can incorporate organic species. There are three main generations of cyclodextrins; α, β and γ with 6,7 or 8 monomers respectively. Cavity size ranges from 5.7 to 9.5 angstroms. The internal cavity of cyclodextrins is lined by σ electrons, and hydroxyl groups are situated on both sides of the cavity rim. The cyclodextrin rings are linked by ether groups, which result in greater steric hinderance when compared to calixarenes. Finally, crown ethers are large polyethers whose cavity may encompass metal ions through electrostatic interactions of unshared electron pairs on oxygen atoms. .

Dendrimers as Host Molecules

Dendrimer compounds provide ideal scaffolds for host interactions due to their extensively branched structure[iii]. These branches create several compartments which can encompass guest molecules while increasing the surface area for both inner and outer shell non covalent interactions. Primarily, the multivalent dendrimer surface has a large number of sites which can be functionalized as needed to increase reactivity. As well, the inner cavities created by the dendron branches have well defined microenvironments which are protected from the outside by the surface groups. Finally, in higher generation dendrimers, the core of the molecule is protected by denron branches which shield it from the outside and create a small microenvironment capable of encapsulating guest molecules. An example of host guest binding within the inner cavities of the dendrimer structure is the 'dendritic box', a fifth generation polypropylenimine dendrimer capable of trapping substrates during synthesis[iv]. The diffusion of these molecules out of the dendrimer host was very slow due to the highly packed nature of the dendron branches, and the bulky, tightly packed H-bonding surface groups which blocked escape[v].

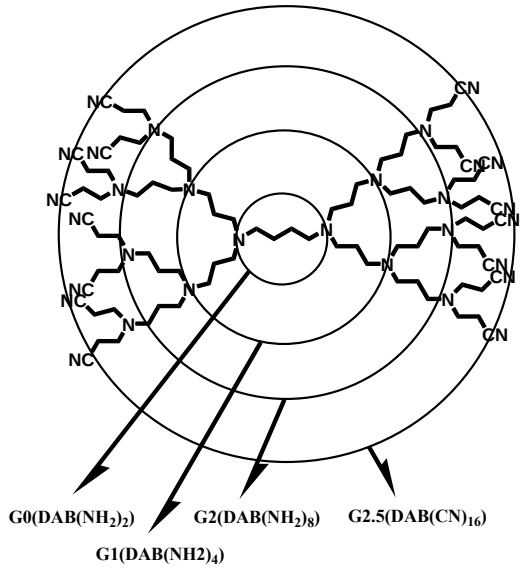

Figure 1 Poly(propylene imine) Dendrimers

Cationic Lipids

Cationic lipids have been studied extensively for their strong biological activity. These lipids are positively charged alkyline lipids of the basic structure illustrated in Figure 3, with two long chain hydrocarbon residues on the C_1 and C_2 positions respectively, and a positively charged cationic group on the C_3. It is also common to see short chain alkoxyl groups on

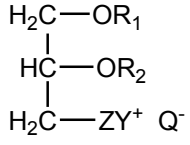

Figure 2 Cationic Lipid Structure

the C_2 hydrocarbon; however if transfection of the lipid is desired it is necessary to have a longer hydrocarbon chain. The hydrocarbon chains on the C_1 and C_2 carbons are attatched by ether, thioether, or amide bonds to the glycerol backbone. The cationic group on the C_3 carbon has a wide variety of spacer groups of acyl, akyl, or amide type of various lengths, and it is common to use a quaternary ammonium salt with shorter spacer groups of one to two carbons in length[vi]. Although the cytotoxicity of cationic lipids containing ammonium salt has been problematic, activity can be increased by involving the heteroatom in the heterocyclic systems of compounds such as aminopyridine, imidazole, or thiazoline to delocalize the positive charge[vii].

Cationic Lipids in Transfection

Cationic lipids have proven to be successful in the delivery of genetic material into cells for the treatment of hereditary and nonhereditary diseases. These cationic amphiphiles are referred to as cytofectin, and form cationic liposomes often with the addition of a helper "structural" lipid to aid in transfection, although the addition of this extra lipid is not always necessary. Complexes with plasmid DNA referred to as genosomes or lipoplexes are produced due to the electrostatic interactions of the positively charged hydrophilic part of the cationic lipid and the negatively charged phosphate groups of the nucleic acid. Once these complexes reach the cell membrane during transfection, the genosome is able to interact with the negatively charged cell membrane due to the positive nature of its cationic lipid interactions. After the genosome aggregates form on the cell membrane they can either fuse with the membrane or more commonly enter through endocytosis, although not all genosomes participate in this process. Following endocytosis, large aggregates of these complexes are formed in the perinuclear compartment and are usually ordered in tubular structures. The rate limiting step in transfection follows with the escape of the genosome into the cytosole. If the helper "structural" lipid is present in the complex it performs its function at this stage by destabilizing the endosomal membrane. Once the genosome has entered the cytosole, the complex dissociates releasing the exogenic DNA into the cell nucleus for expression. The lipofection method of introducing correction genes into targeted cells is not infectious or immunogenic and protects DNA, mRNA, or oligonucleotide molecules from inactivation by cell enzymes making it a preferred method of gene delivery over other exogenic delivery systems[7].

Cationic Polymers

A major concern associated with lipoplex gene transfer is that a large number of the complexes upon endocytocis are delivered to the lysosome and degraded while only small amounts are able to destabilize the endosomal membrane and transfer their associated DNA into the cell nucleus. Certain structural helper lipids such as dioleoylphosphatidylethanolamine (DOPE) have proven to dramatically improve the transfection of these genosomes through fusion with the endosomal membrane. In addition, it has also been shown that cationic polymers including polyamidoamine dendrimers and poly(ethylenimine)[viii] can achieve transfection into human and animal cells, and when combined with DOPE their transfection activity is extremely high.

Dendrimer polymers contain secondary and tertiary amino groups that will protonate under weakly acidic conditions. Thus, it is reasoned that the absorption of protons by these dendron structures restrains the lowering of pH in endosome and prohibits the degredation of DNA in lysosome[ix]. As well, the resulting endosome buffering by the dendrimer compounds is considered to induce swelling of the endosome interior from osmosis, resulting in the rupture of the endosome and release of DNA into cytoplasm. This same type of "proton sponge" reasoning has previously been proposed with polyethylenimine, a mediator to the transfer of genetic material that greatly resembles the PanAm dendrimer structure[x]. Due to its high levels of transfection over a broad range of DNA concentrations, polyethylenimine is used as a vector for the *in vivo* transfer of onglionucleotides into the brain cells of mice. Notably, polyethylenimine improves delivery of genetic material into dense tissues, such as brain tissue, where cationic lipid efficiencies are relatively low. Moreover, polyethylenimines possess low cytotoxicity, and upon investigation the integrity of cell membranes was not deteriorated with their use.

Cationic Lipids with Polyamidoamine Dendron Head Groups

With the goal of increasing the overall delivery of DNA through transfection from endosome to cytoplasm, new types of cationic lipids containing two long alkyl groups on the C1 and C2 carbons, and a polyamidoamine dendron as a head group have been synthesized and their transfection efficiencies have been studied[9]. The large number of tertiary amino groups in the interior of these compounds increases the buffering capacity of the genosome, while the molecular shape and electric balance between the polar head group and the hydrophobic tails may be adjusted by controlling the dendron moiety of the lipid. In addition, the solubility of lipid in water and its ability to form micelles is greatly increased with the presence of the polyamine cationic group. The formation of lipoplexes of dendron bearing lipids with plasmid DNA was studied and it was theorized that the dendron lipids with more amino groups binded to DNA through ionic bonds, while the hydrophobic moiety of the lipid also aids lipoplex formation through hydrophobic interactions. In addition, as the buffering capacity of the dendrons increased with their size, so did the transfection activity of their associated lipoplexes. This supports the aforementioned "proton sponge" theory of dendron bearing lipids as their buffering ability enduces osmotic endosomal swelling and eventual rupture allowing release of exogenic DNA into cytoplasm. The highest rate of transfection during these studies was achieved with a lipolex of third generation dendron bearing lipid combined with DOPE.

Experimental Procedures

Materials

All poly(propylene imine) dendrimers[xi] and lipid materials were synthesized and verified with an Agilent 1100 Series LC/MSD Electrospray Ionization Mass Spectrometor. Materials were also verified by H1 and C13 NMR on either a Bruker AMD-400, Bruker MSL-500, or a Bruker Avance 400 operating with a TMS internal standard.

2.1.1 Dendrimer Synthesis

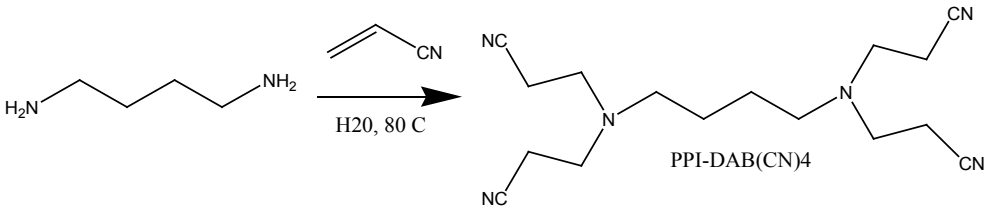

The PPI-DAB$(CN)_4$ dendrimer was obtained through a Michael addition reaction with diaminobutane and acrylnitrile in a 7:1 ratio. Diaminobutane (4.2g, 0.476mol) was dissolved in 100ml distilled H20 and added to acrylnitrile (22.12ml, 0.334mol, 7eq) over a one hour time period with constant stirring. The temperature was then increased to 80°C for an additional two hours. Acrylnitrile was evaporated and product was crystallized in H_20 and filtered. Product was recrystallized from methanol and filtered to yield 11.75g of PPI-DAB$(CN)_4$ at 82%. ^{1}H NMR (Bruker Avance 400MHz, $CDCl_3$): δ = 2.85 (t. 8H. NCH_2CH$_2$CN). 2.57 (m. 4H. NCH_2CH$_2$CH$_2$CH$_2$N). 2.47 (t. 8H. CH_2CN). 1.55 (m. 4H. NCH$_2$CH_2CH$_2$CH$_2$CN); ^{13}C NMR (400MHz, $CDCl_3$): δ = 119 (CN). 53.5 (NCH$_2$CH$_2$CH$_2$CH$_2$N). 49.7 (NCH$_2$CH$_2$CN). 25.2 (NCH$_2$CH$_2$CH$_2$CH$_2$CN). 17.2 (CH$_2$CN); ESI-MS: 300.9 [DAB$(CN)_4$]. 322.9 [DAB$(CN)_4$&Na].

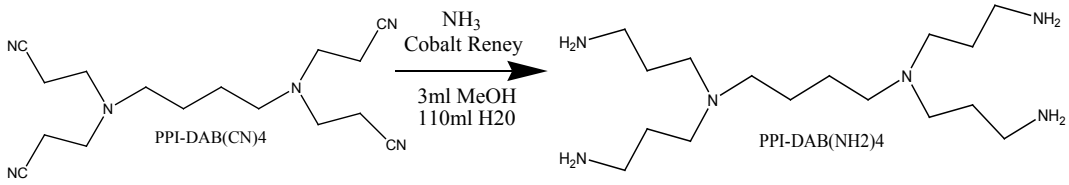

PPI-DAB$(CN)_4$ dendrimer (2.18g, 0.0072mol) dissolved in 3ml MeOH along with Cobalt Reney (4.38g) was combined in an autoclave with 110ml H_20 and 5ml NH_3 (in 25% H_20). The reaction proceeded at 70°C for 55min in autoclave under hydrogen at 50atm. Water was evaporated to yield clear oil product which was redissolved in MeOH, rotovaped, and weighed at 2.5 g, a 17% yield. ^{1}H NMR (Bruker Avance 400MHz, D_2O): δ = 2.57 (t. 8H. CH_2NH$_2$). 2.47 (m. 12H. NCH$_2$CH$_2$CH$_2$CH_2N& NCH_2CH$_2$CH_2NH$_2$). 1.59 (quin. 8H. CH$_2$CH_2NH$_2$). 1.42 (m. 12H. NCH$_2$CH$_2$CH$_2$CH_2N); ^{13}C NMR (400MHz, $CDCl_3$): δ = 53.0 (NCH$_2$CH$_2$CH$_2$CH$_2$N). 50.7 (NCH$_2$CH$_2$CH$_2$NH$_2$). 39.1 (CH$_2$NH$_2$). 28.4 (CH$_2$CH$_2$NH$_2$). 23.5 (NCH$_2$CH$_2$CH$_2$CH$_2$N); ESI-MS: 280.0 [DAB$(NH_2)_4$-CH_2CH$_2$CH_2NH$_2$]. 317.1 [DAB$(NH_2)_4$].

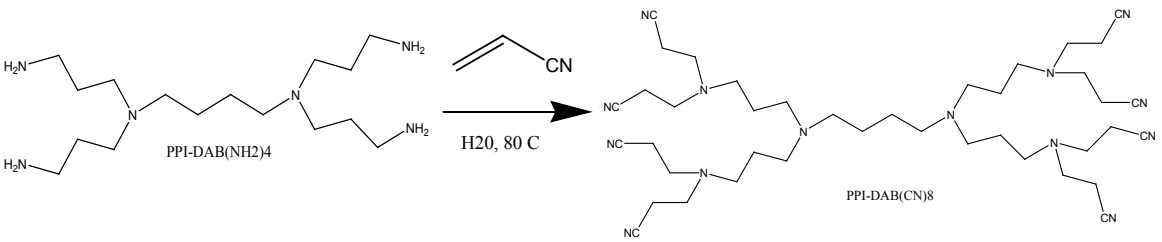

$DAB(NH_2)_4$ (2.5g, 0.0079mol) was put into solution with 150ml distilled H_20. Acrylnitrile (8.73ml, 1:16 molar ratio) was added to the solution drop wise over a 1hr time period at room temperature. Reaction was then heated to 80°C for 2hrs w/ constant stirring. Reaction solution was rotovaped to remove H_20, then reaction solution was redissolved in MeOH, evaporated down and dried to give 4.7g, an 81% yield. Product was verified with MS and ^1H and ^{13}C NMR.

Lipid Synthesis

In order to investigate poly(propylene imine) dendrimer lipid interactions we synthesized one cationic lipid, one neutral lipid and one negatively charged lipid. This range provided a base for comparison between the interactions of $DAB(CN)_8$ and differently charged lipid species.

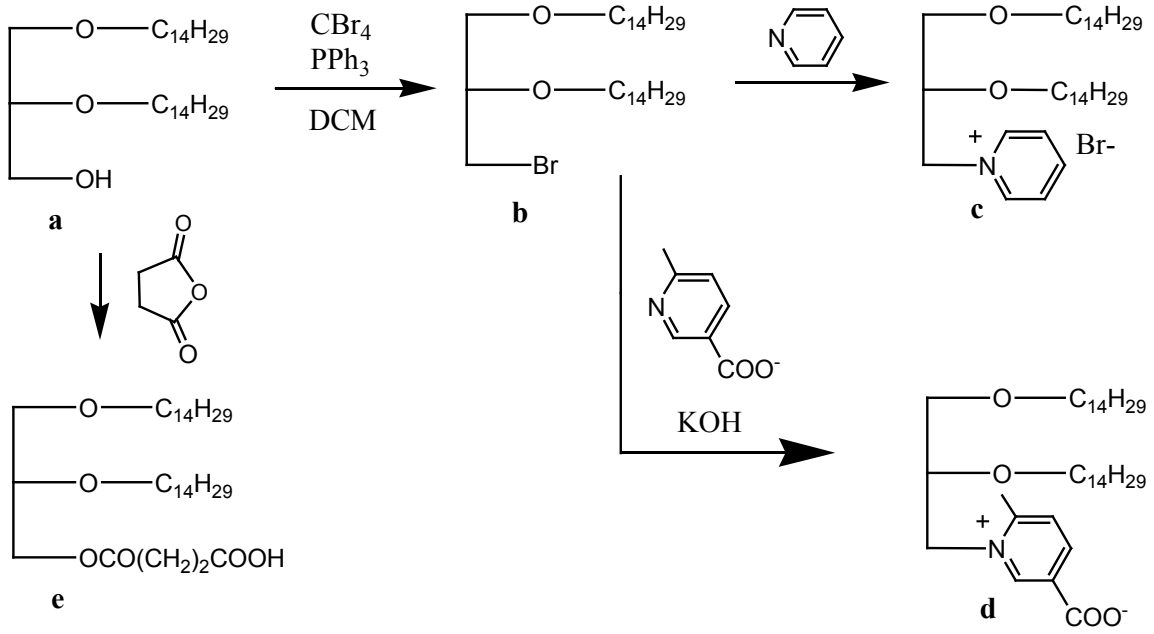

Figure 3 a) 1,2-ditertadecyl-rac-glycerol, b) rac-2,3-ditetradecyloxypropyl-1-bromide, c) rac-N-2,3-ditetradecyloxypropylpyridium bromide, d) rac-N-(2,3-ditetradecyloxypropyl)-6-methylpyridium-3-carboxylate, e) rac-3-O-(3-carboxypropionyl)-1,2-ditetradecyl-glycerol

In the synthesis of rac-2,3-ditetradecyloxypropyl-1-bromide (**b**) from was performed in purified dichloromethane which was refluxed for 1hr 20min w/ calcium hydride and then distilled before reaction. All reagents were dried for 1hr under a vacuum pump to remove the traces of H_20. Then a solution of anhydrous 1,2-ditetradecyl-*rac*-glycerol (**a**) (96.5mg, 0.199mmol) and triphenylphosphine (109.5mg, 0.417mmol, 2.01eq) in 10ml DCM was cooled in an ice bath while a solution of CBr_4 (139.6mg, 0.420mmol, 2.11eq) in 2ml DCM was added drop wise over 1hour. After 1/2 hr, reaction was tested with thin layer chromatography at an 8:1 ratio of petroleum ether to ethyl acetate. The TLC plate was soaked in $Ce(SO_4)_2$ & $H_3[P(Mo_3O_{10}]$ (phosphomolybdic acid) to reveal the R_f of the compounds. Another 1.6 equivalents of CBr_4 was added (106.5mg, 0.321mmol) to the reaction mixture over a 20 min time period. At 17 ½ hrs

product was observed on another TLC, methanol (2 ml) was added and reaction mixture was stirred for 10 min then solvent was evaporated. Product was separated with column chromatography using petrol ether- ethyl acetate (100:2) as an elutant. Combined fractions with desire product (**b**) were evaporated and product was dried to yield 108.0mg, 99%. Product was verified through MS and ^{1}H NMR (Bruker AMD-400).

In the synthesis of 3-O-(3-carboxypropionyl)-1,2-ditetradecyl-*rac*-glycerol (**e**), 1,2-ditertadecyl-*rac*-glycerol (**a**) and succinic anhydride were dried under a vacuum for 1hr prior to reaction, and triethylamine was dried for 2hrs by refluxing with calcium hydride an distilled. A solution of lipid (**a**) (100.8mg, 0.208mmol), succinate anhydride (70.8mg, 0.704mmol, 3.4eq), and NEt_3 (0.01ml, 0.2eq) in anhydrous CH_2Cl_2 was stirred at 50°C for 19hrs. At 19hrs reaction was checked by TLC at a 4:1 petroleum ether to ethyl acetate ratio using aforementioned phosphomolybdic acid solution. Additional 4-dimethylaminopyridine (15mg, 0.6eq) was added as a catalyst to speed up the reaction. After 29 hrs reaction was checked again with TLC and another equivalent of succinic anhydride was added (22.0mg, 1.05eq). After 44 hrs product was verified through TLC, and reaction solution was washed three times with 3ml of 3% HCL aq. solution and dried over Na_2SO_4. Solvent was evaporated, and residue was purified by column chromatography eluated with a 4:1 ratio of petroleum ether to ethyl acetate. Collected fractions were rotovaped and dried on a vacuum to give 71mg, a 58% yield. Product was verified through MS and ^{1}H NMR (Bruker AMD-400).

In the synthesis of *rac*-*N*-2,5-ditetradecyloxypropyl)pyridium bromide (**c**), a solution of *rac*-2,3-ditetradecyloxypropyl-1-bromide (**b**) (108mg, 0.19mmol) in pyridine (1ml, 12.36mmol) was stirred at 90°C for 44hrs. Reaction was checked constantly with TLC against starting material (**b**) using an 8:1 petrolium ether/ethyl acetate solvent ratio, and against desired product with a 6:1 chloroform/MeOH ratio using the aforementioned phosphomolybic acid solution. Pyridine was evaporated and product was dried and recrystalized from diethylether to give 82mg, a 66% yield. Product was verified through MS and ^{1}H NMR (Bruker MSL-500).

In the synthesis of *rac*-*N*-(2,3-ditetradecyloxypropyl)-6-methylpyridinium-3-carboxylate(**d**), rac-2,3-ditetradecyloxypropyl-1-bromide (**b**) (105.1mg, 0.192mmol), 6-methylnicotinic acid (80.6mg, 0.566mmol, 3.06eq), and KOH (33.8mg, 0.603mmol, 3.14eq) were dissolved in 2 ml DMSO. Reaction was heated to 100°C and stirred 23hrs. Reaction mixture was monitored with TLC against in an 8:1 petrolium ether/ethyl acetate solvent ratio. The phosphomolydic acid solution was used to reveal the bromide (**b**), while a Dragendorf solution of $Bi(NO_3)_3$ (20%aq) and KI was used to detect the quaternary amine in the desired product. Chloroform (10ml) was added to the reaction mixture and reaction mixture was washed with H_2O to remove DMSO. Organic layer was dried with Na_2SO_4 and solvent was evaporated. Compound was purified with column chromatography with a gradual gradient from 30:1 to 8:1 PE/EA eluant. Solvent was evaporated from combined fractions and product was dried on a vacuum to give compound (**d**) 86mg (74%). Product was verified through MS and ^{1}H NMR (Bruker MSL-500).

Methods – ESI-MS

Interactions of poly(propylene imine) dendrimers with Cu^{2+} and lipids were investigated using electrospray ionization mass spectrometry (ESI-MS). ESI-MS involves the injection of dilute analyte solution through capillary where a high voltage (2-5kV) is applied. The voltage, which can be either negative or positive depending on the analyte, provides an electrofield gradient necessary for charge separation at the surface of the liquid. The liquid then protrudes form the capillary tip and when it reaches the Rayleigh limit[xii] (where Coulombic repulsion of surface charge is equal to surface tension of the solution), droplets that contain excess of positive or negative charge detach from the capillary tip. The drops then generate charged analyte molecules as they move towards the entrance to the mass spectrometer. There are a few different mechanisms proposed to explain the generation of these charged particles through an increase charge density due to solvent evaporation. Firstly, the coulomb fission mechanism proposes that the increased charge density causes the division of large droplets into smaller droplets[xiii]. Secondly, the ion evaporation mechanism proposes that the increased charge density eventually causes coloumbic repulsion to overcome the surface tension of the liquid, resulting in the release of ions from the droplet surface[xiv]. The droplets formed can be analysed for mass-to-charge ratio within the mass spectrometer[xv].

ESI-MS has proved highly successful in the study of free and complexed species[xvi]. Numerous non-covalent protein assemblies have been studied, including membrane protein-lipid complexes[xvii]. In addition, ESI-MS is highly suited to biomolecule analysis because it allows for the analysis of large, non-volatile molecules directly form the liquid phase. This allows for the combination of ESI-MS with separation techniques in order to ensure the purity of compounds under analysis[xviii]. Namely, during the investigation of PPI-DAB$(CN)_8$ and Cu^{2+} complexation, high performance liquid chromatography was combined with ESI-MS to reduce the complexation of Cu^{2+} with retro-Michael reaction products as explained further in section 3.1.2.

Results

Complexation of Poly(propylene Imine) Dendrimer with Cu^{2+}

3.1.1 DAB$(CN)_4$ & Cu^{2+}

The first generation DAB$(CN)_4$ dendrimer at a concentration of 0.01M in MeOH was injected into the ESI-MS at a flow rate of 0.1ml/min. At the same time, a 0.05M solution of $Cu(CH_3COO)_2$ in MeOH with a trace amount of H_2SO_4 was also injected at a flow rate of 0.1 ml/min. The spectra shown in Figure 5 shows the complexation of the DAB$(CN)_4$

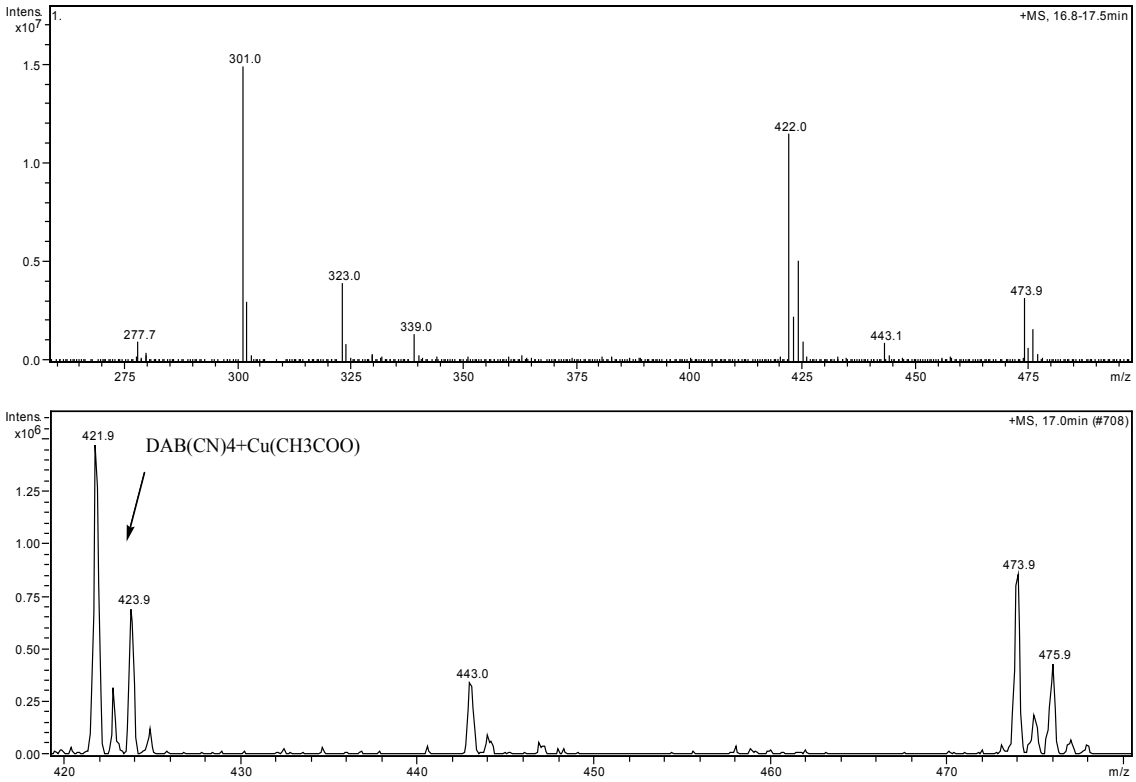

Figure 4 ESI-MS - DAB(CN)$_4$ & Cu^{2+} (positive ion mode, 250-500m/z)

dendrimer with a Cu^{2+} ion and acetate at 422.0m/z. In addition, another peak corresponding to the DAB(CN)$_4$ dendrimer with $CU^{2+}(H20)_6$ can be observed at 473.9m/z.

3.1.2 DAB(CN)$_8$ & Cu^{2+}

When the second generation DAB(CN)$_8$ dendrimer was investigated, a combination of HPLC and ESI-MS was used to ensure that the spectrum observed was the result of the desired dendrimer and not a side product form a retro-Michael addition. As observed in Figure 6, there are two products of retro-Michael addition which involve the absence of

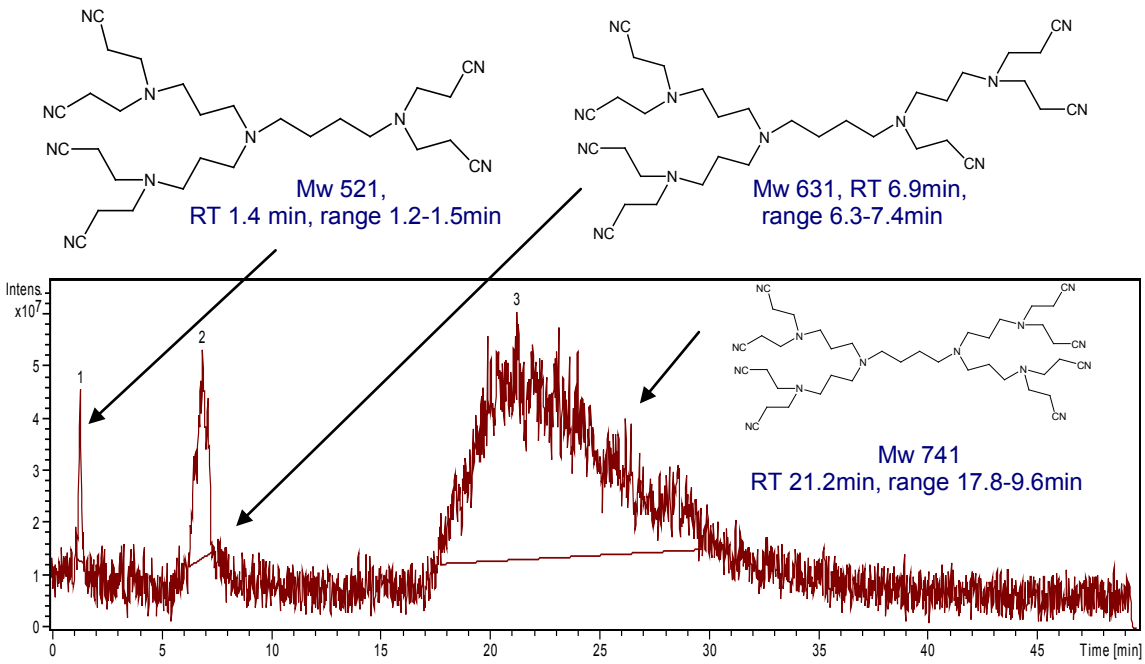

Figure 5 HPLC of DAB(CN)$_8$

one or more acrylnitrile branch additions with peaks of 631m/z and 521m/z respectively. However, after performing HPLC it was observed that the concentration of these side products was not very high, and their interference could be avoided through LC/MS. A solution of DAB(CN)$_8$ (0.1µl, 0.01M) was injected into the HPLC column with an increased elutant ratio of 98% MeOH for the first ten minutes to speed up the investigation. After ten minutes, the elutant ratio was returned again to 80% MeOH. Simultaneously, 0.1ml/min of a 0.05M $CuCl_2$ solution was injected after the HPLC column into the dendrimer solution immediately before it entered into the ESI-MS. A trace amount of formic acid was also added to prevent precipitation of dendrimer with Cu^{2+}. After the first two denrimer side products from the retro-Michael addition had passed through the coloumn, the injection rate of the $CuCl_2$ solution was increased to 0.5ml/min just as the 741 peak of the full DAB(CN)$_8$ dendrimer started to form. As can be seen by the resulting spectrum in Figure 7, complexation of the full DAB(CN)$_8$ dendrimer and Cu_2Cl_2 was found at 470.3m/z. As well, the side products of the dendrimer synthesis remained in the solution and formed their own Cu^{2+} complexes. The first side product with a molecular weight of 631 can be seen in complexation with CuCl at 413.1m/z, with $CuCl_2$ at 449.1m/z, and with Cu_2Cl_2 at 512.2m/z. The second side product with a molecular weight of 521 can be seen in complexation with Cu_2Cl_2 at 456.3m/z.

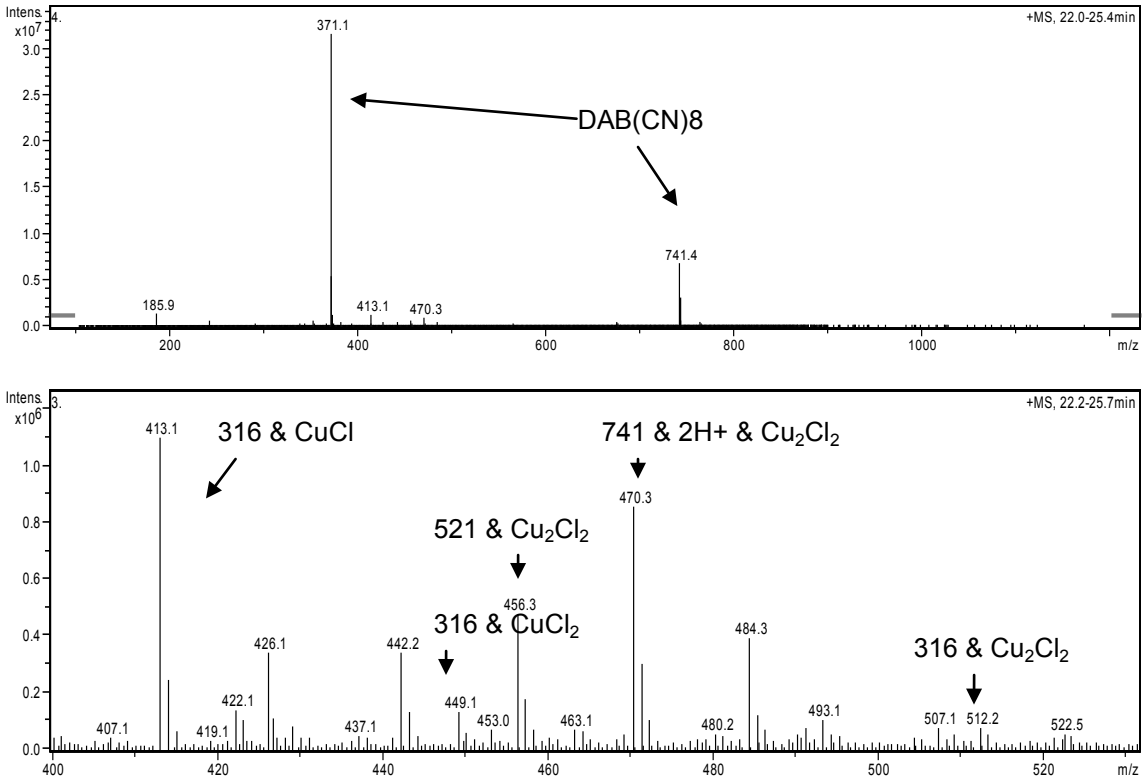

Figure 6 ESI-MS - DAB(CN)$_8$ & Cu^{2+} (positive ion mode; 100-1200m/z & zoom image of 400-530m/z)

The LC/MS approach did not prevent complexation of Cu^{2+} with dendrimer side products. However, the tertiary amine areas of interaction on the side products and the full DAB(CN)$_8$ dendrimer are the same. Therefore, we decided not to continue with HPLC before Mass Spec analysis, but rather keep a careful watch for complexation with side products in further investigations.

Complexation of Poly(propylene Imine) Dendrimer with Lipids

DAB(CN)$_8$ & -3-O-(3-carboxypropionyl)-1,2-ditetradecyl-*rac*-glycerol

A solution of DAB(CN)$_8$ (400µl, 0.005M) in MeOH and 3-O-(3-carbozypropionyl)-1,2-ditetradecyl-*rac*- glycerol (400µl, 0.005M) in $CHCl_3$ was combined with 20µl H_20. In the negative ion mode, 1µl of the solution was injected straight into the ESI-MS, and the obtained spectrum is shown in Figure 8. As can be seen, there was complexation between the full DAB(CN)$_8$ dendrimer and a lipid molecule at peak 1324.3m/z, and complexation between the DAB(CN)$_8$ dendrimer and two lipid molecules at 1905.0m/z. In addition, there was complexation of the first retro-Michael dendrimer side product and one lipid molecule at 1214.1m/z.

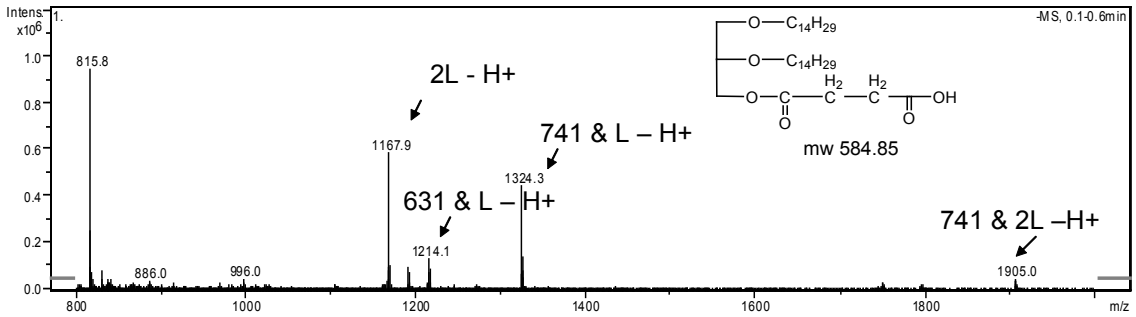

Figure 7 ESI-MS - DAB(CN)$_8$ & rac-3-O-(3-carboxypropionyl)-1,2-ditetradecyl-glycerol (negative ion mode, 800-2000m/z)

3.2.2 DAB(CN)$_8$ & *rac*-N-2,3-ditetradecyloxypropylpyridium bromide

A solution of DAB(CN)$_8$ (200µl, 0.005M) in MeOH and rac-*N*-2,3-ditetradecyloxy-propylpyridium bromide (40µl, 0.005M) in $CHCl_3$ was combined with 20µl H_20. In the positive ion mode, 0.5µl of the solution was injected and the target mass range was increased to 1000-2000m/z. The resulting spectrum is represented in figure 9.

As can be observed, complexation between the DAB(CN)$_8$ dendrimer and one lipid molecule minus one Br ion was found at 1286.2m/z. As well, complexation between the DAB(CN)$_8$ dendrimer and two lipid molecules minus one Br ion was found at 1913.7m/z. In addition, complexation between the two dendrimer side products and the lipid minus one Br ion can be found at 1176.2m/z and 1066.5m/z.

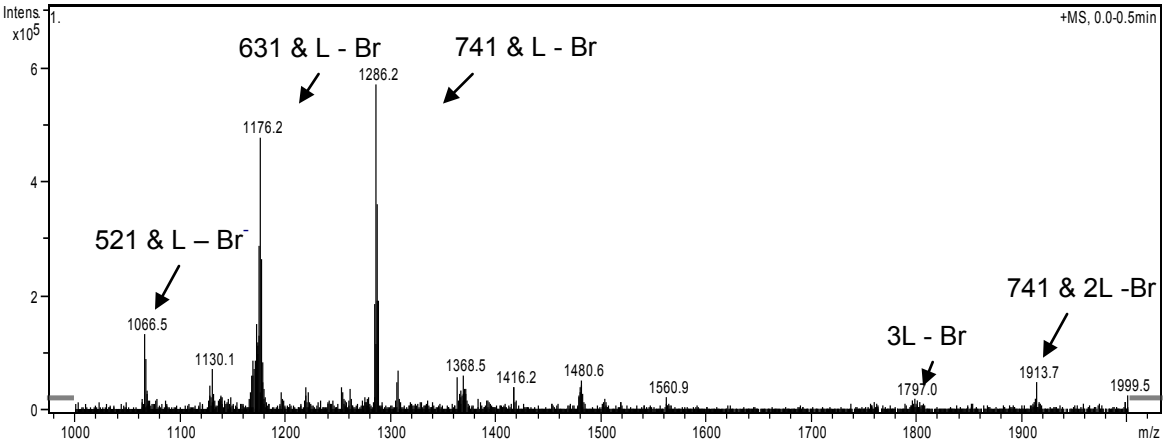

Figure 8 ESI-MS - DAB(CN)$_8$ & rac-N-2,3-ditetradecyloxypropylpyridium bromide (negative ion mode, 1000-2000m/z)

DAB(CN)$_8$ & *rac*-N-(2,3-ditetradecyloxypropyl)-6methylpyridium-3-carboxylate

Complexation between DAB(CN)$_8$ and *rac*-N-(2,3-ditetradecyloxypropyl)-6-methylpyridium-3-carboxylate was not observed. The concentrations and molar ratios of the two compounds were adjusted, and the parameters of the ESI-MS were explored, but no complexes were found.

Competition for $DAB(CN)_8$ Host: Lipid vs. Cu^{2+}

$DAB(CN)_8$ & rac-3-O-(3-carboxypropionyl)-1,2-ditetradecyl-*rac*-glycerol & Cu^{2+}
A solution of $DAB(CN)_8$ (200µl, 0.005M) in MeOH, rac-3-O-(3-carboxypropionyl)-1,2-ditetradecyl-*rac*-glycerol (200µl, 0.005M) in $CHCl_3$ and $CuCl_2$ (100µl, 0.05M) in MeOH was combined with 20µl H_20. In the negative ion mode with a target range of 800-2000m/z, 0.1µl of the solution was injected into the mass spectrometer and the resulting spectrum can be seen in Figure 10. Complexation between two lipid molecules and CuCl is found at 1265.3 m/z, however no complexation between the dendrimer and either the lipid or Cu^{2+} was observed.

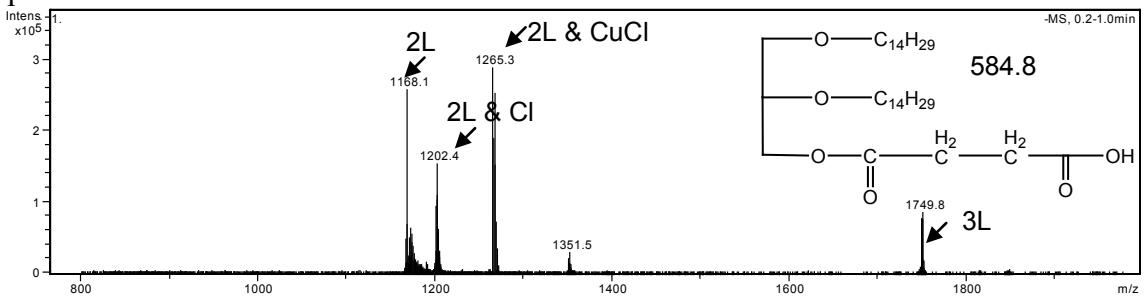

Figure 9 ESI-MS - $DAB(CN)_8$ & rac-3-O-(3-carboxypropionyl)-1,2-ditetradecyl-glycerol & Cu^{2+} (negative ion mode, 800-2000m/z)

The same solution with a 0.1µl injection was observed in the positive ion mode with a target mass range of 700-1000m/z. Complexation between one lipid molecule and CuCl is found at 662.9m/z, between one lipid molecule and Cu^{2+} is found at 646.4m/z, and one lipid molecule with MeOH and Cu^{2+} is found at 725.4m/z. However, again no complexation is observed between $DAB(CN)_8$ and either the lipid molecules or Cu^{2+} ions.

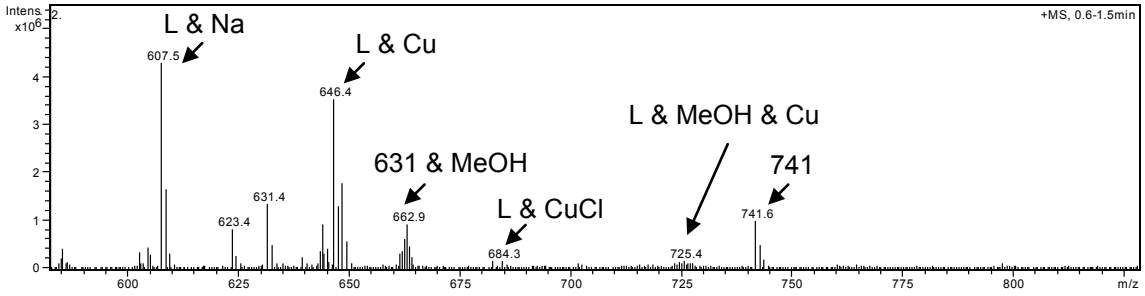

Figure 10 ESI-MS - $DAB(CN)_8$ & rac-3-O-(3-carboxypropionyl)-1,2-ditetradecyl-glycerol & Cu^{2+} (positive ion mode, 550-825m/z)

$DAB(CN)_8$ & *rac*-*N*-2,3-ditetradecyloxypropylpyridium bromide & Cu^{2+}
A solution of $DAB(CN)_8$ (200µl, 0.005M) in MeOH, rac-*N*-2,3-ditetradecyloxy-propylpyridium bromide (60µl, 0.005M) in $CHCl_3$ and $CuCl_2$ (100µl, 0.05M) in MeOH was combined with 20µl H_20. In the positive ion mode, 0.5µl of the solution was injected into the mass spectrometer with a target range of 100-1300m/z. The resulting spectrum is illustrated in Figure 12. Complexation between two lipid molecules and CuCl minus one Br ion was found at 1271.6m/z. In addition, complexation between two lipid molecules and $CuCl_2$ minus two Br ions was found at 1225.7m/z, however no complexation was

observed between the dendrimer and either lipid or Cu^{2+}.

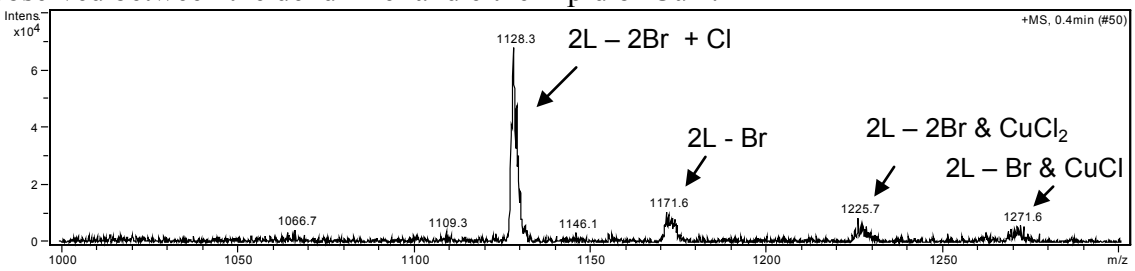

Figure 11 ESI-MS - DAB(CN)8 & rac-N-2,3-ditetradecyloxypropylpyridium bromide & Cu2+ (positive ion mode, 1000-1300m/z)

The same solution with a 0.5µl injection was observed again in the positive ion mode but with a lower target mass range of 200-500m/z. The resulting spectrum is illustrated in figure 13, and this time complexation of one lipid molecule, $DAB(CN)_8$ and two H^+ minus one Br ion was observed at 428.4m/z.

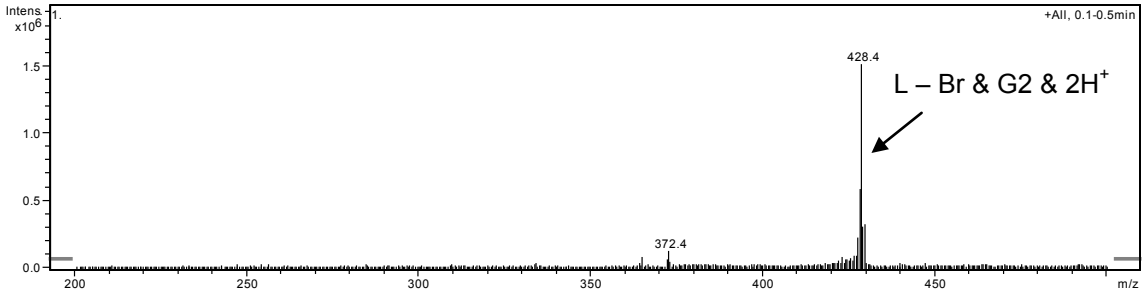

Figure 12 ESI-MS $DAB(CN)_8$ & rac-N-2,3-ditetradecyloxypropylpyridium bromide & Cu^{2+} (positive ion mode, 200-500m/z)

Discussion and Conclusion

Guest host complexation of dendrimers is a very prominent area of research due to its wide scope of possible applications ranging from catalysis to drug delivery. Although the complexation of PPI dendrimers and metal ions has been studied previously, to our knowledge the non covalent interactions of PPI dendrimers and lipids has not been investigated. Therefore, in addition to $DAB(CN)_4$ and $DAB(CN)_8$ host-guest investigation with Cu^{2+} ions, we also investigated the interactions of $DAB(CN)_8$ with three lipid molecules of different charges; 3-O-(3-carboxypropionyl)-1,2-ditetradecyl-*rac*-glycerol, *rac*-*N*-2,3-ditetradecyloxypropylpyridium bromide, and *rac*-*N*-(2,3-ditetradecyloxy-propyl)-6-methylpyridium-3-carboxylate.

Through ESI-MS analysis we established complexation of Cu^{2+} with $DAB(CN)_4$, $DAB(CN)_8$, and the first two retro-Michael addition side products of the $DAB(CN)_8$ compound. In addition, we found strong complexation of $DAB(CN)_8$ with 3-O-(3-carboxypropionyl)-1,2-ditetradecyl-*rac*-glycerol and *rac*-*N*-2,3-ditetradecyloxypropyl-pyridium bromide. The complex between dendrimer and 3-O-(3-carboxypropionyl)-1,2-ditetradecyl-*rac*-glycerol is probably the result of interactions between carbonyl group of lipid and the full orbital of the nitrogen atoms in the dendrimer structure. As well, the complex formed between *rac*-*N*-2,3-ditetradecyloxypropylpyridium bromide is likely the result of the involvement of the dendrimer nitrogen electrons in the positively charged

aromatic pyridium ring. In addition, the lack of complexation of the dendrimer with *rac*-*N*-(2,3-ditetradecyloxypropyl)-6-methylpyridium-3-carboxylate is likely due to the neutral nature of the lipid.

In order to test the strength of the non-covalent dendrimer lipid interactions, we investigated their complexation in the presence of Cu^{2+} ions. While $DAB(CN)_8$ did not form complexes with either the Cu^{2+} ion or the 3-O-(3-carboxypropionyl)-1,2-ditetradecyl-*rac*-glycerol lipid in the mixture, we did find successful complexation between $DAB(CN)_8$ and *rac*-*N*-2,3-ditetradecyloxypropyl-pyridium bromide in the presence of Cu^{2+}. Due to time constraints of this research project further spectral analysis was not possible. However, this observed non-covalent dendrimer-lipid interaction is very interesting and substantiates further investigation. If cationic lipids of similar structure could be made to form complexes with higher generation dendrimers, they could have strong potential for biological applications including drug delivery and transfection.

Acknowledgements

I would like to thank first and foremost Dr. David Paul from the University of Arkansas for working so hard to create the Moscow REU program. Without his vision and hard work I would have never had the opportunity to travel to Russia to do a summer of research. In addition, Dr. Anatoli Ishenko from The Moscow Lomonosov Institute of Fine Chemical Technology was the program organizer from the Russian side and organized our lab placements and cultural experiences. I am very grateful for the effort and care he put into our summer.

From Moscow State University I would like to thank Dr. Anton Maksimov for welcoming me so warmly into his laboratory. Although our time for research was very limited, he was very guiding and extremely helpful which made all the difference. Also, for the patience he showed with me and the constant effort he made to communicate with me in English I will be forever grateful!! I would also like to extend my gratitude to Dean Valery Lunin of the MSU Chemistry Department, and Dr. Edward Karakhanov, Head of the Petrochemistry and Organic Catalysis Department. Their strong support of the program and our research experiences was and always will be very much appreciated.

From the Moscow Lomonosov Institute of Fine Chemical Technology I would like to sincerely thank Dr. Michael Maslov who guided me through the lipid syntheses. Although I was only in his lab for less than two weeks, he was very patient and attentive to my work. I would also like to sincerely thank Dr. Nina Morozova who I shared many good conversations with about Russia and its history over many wonderful cups of tea.

A special note of thanks goes out to Vitaliy Skorkin, my lab mentor and our Russian guide who not only helped me immensely with my research work at MSU, but also accompanied us on the majority of our excursions and worked very hard to make sure our experiences in Russia were very full and enjoyable. He always put the extra effort into making sure we were safe and happy, and we will forever be grateful to him for giving us so many wonderful experiences and lifetime memories.

I also wish to thank my parents for being so supportive of me throughout the years no matter what adventures I choose to pursue. Without their love and support I

would not be where I am today, and would not be so fortunate as to have had so many amazing educational and world travel experiences.

Finally, I sincerely thank the National Science Foundation for recognizing the merit of this international undergraduate research program. I sincerely hope that this program continues for years to come, and that it paves the way for more international research programs and collaborations in the future.

Appendix A – Supporting Data for Synthetic Work

DENDRIMERS

DAB(CN)4: H1 & C13NMR, MS

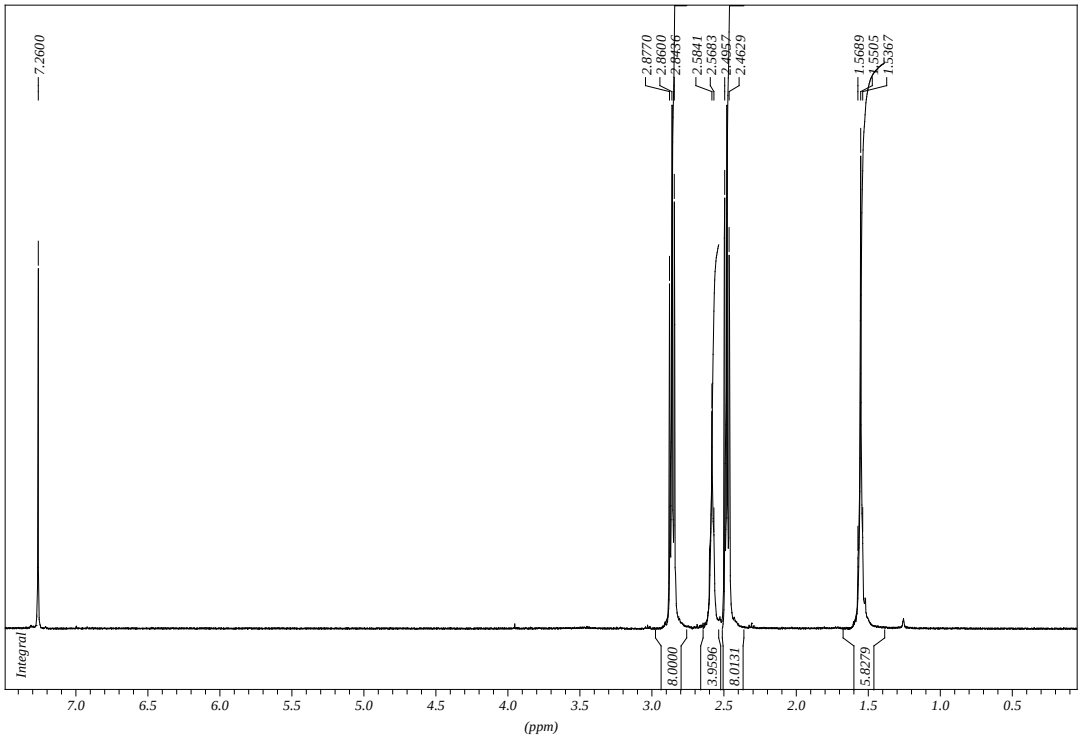

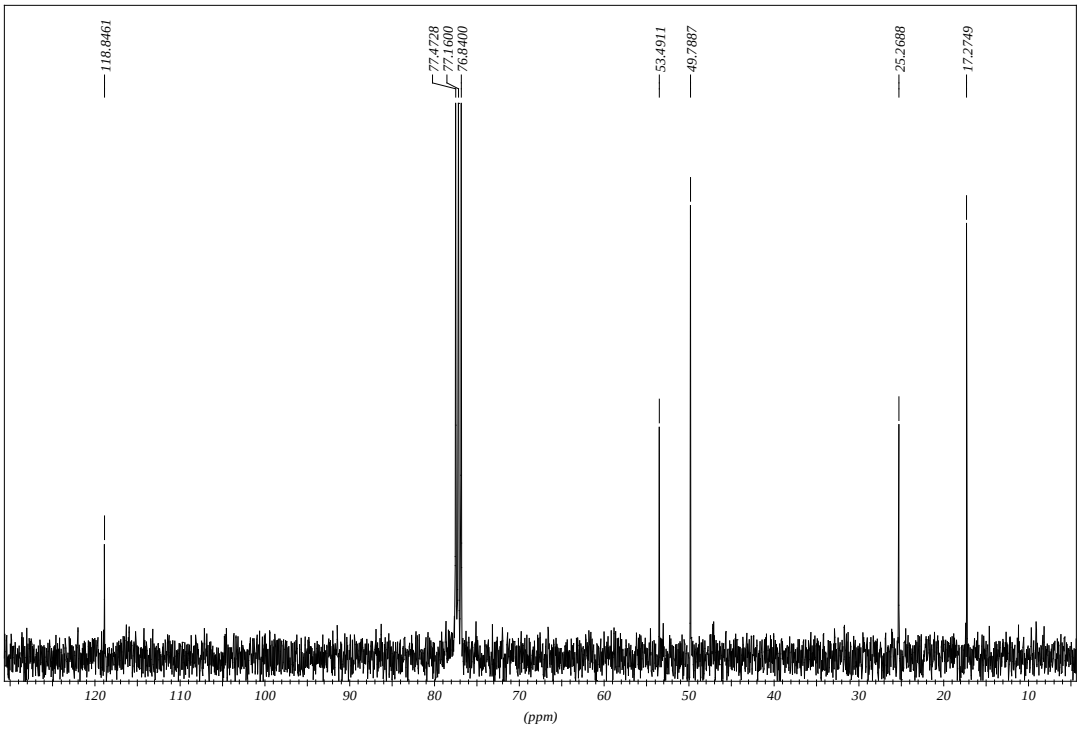

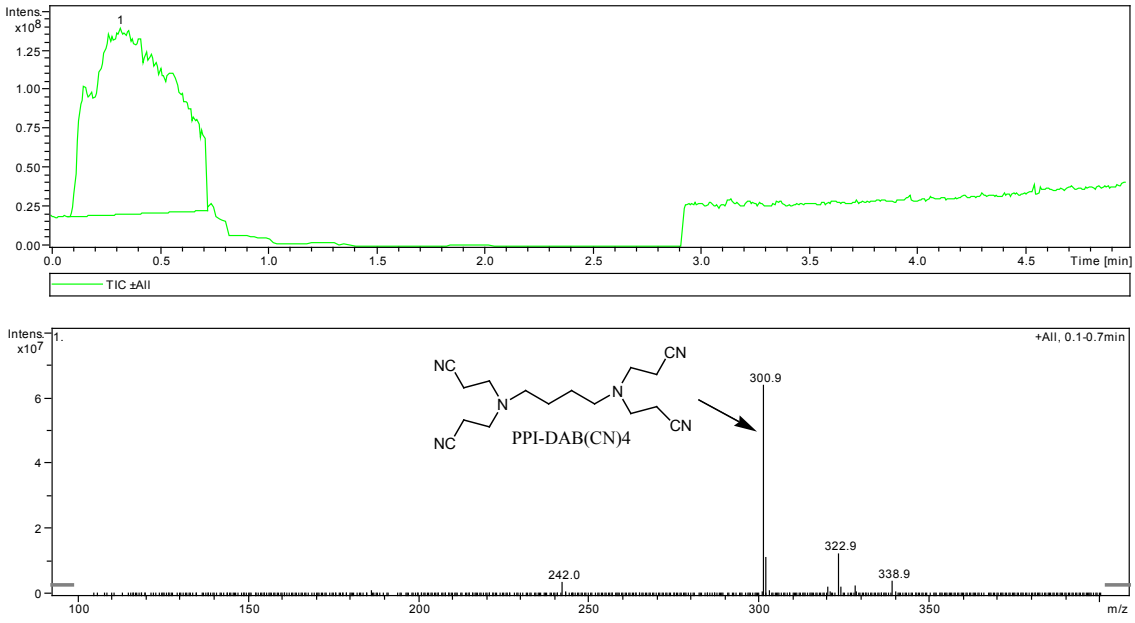

DAB(NH)4: H1 & C13NMR, MS

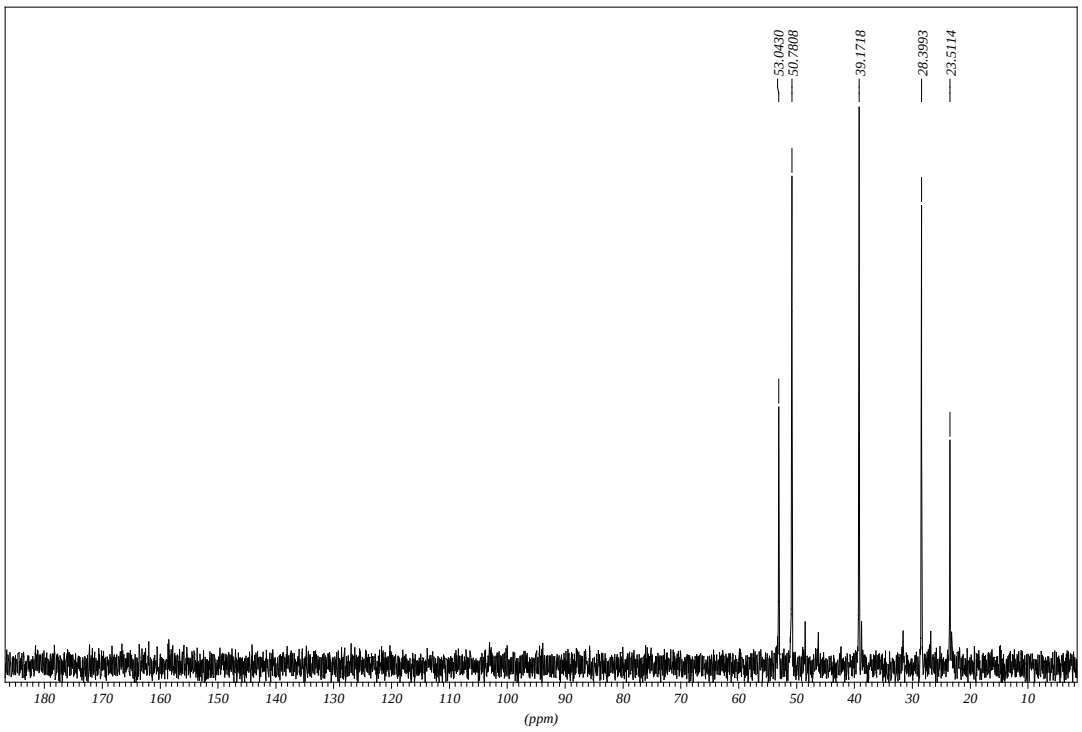
53.0430
50.7808
39.1718
28.3993
23.5114
180 170 160 150 140 130 120 110 100 90 80 70 60 50 40 30 20 10
(ppm)

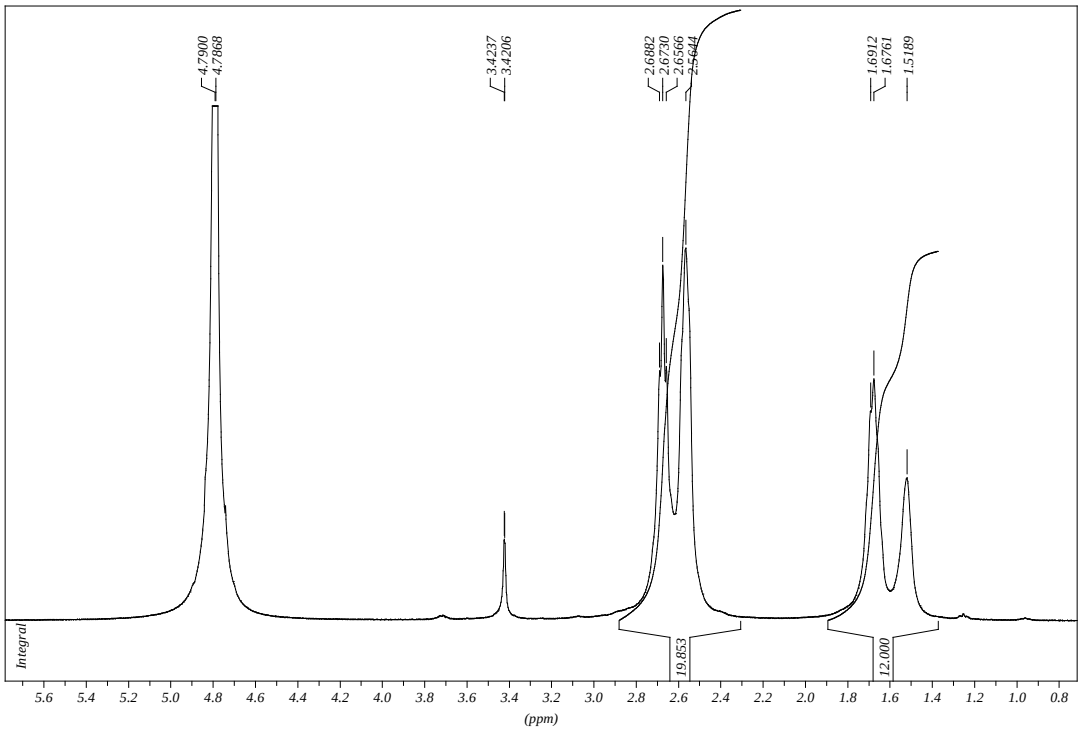
4.7900
4.7868
3.4237
3.4206
2.6882
2.6730
2.6566
2.5644
1.6912
1.6761
1.5189
Integral
19.853
12.000
5.6 5.4 5.2 5.0 4.8 4.6 4.4 4.2 4.0 3.8 3.6 3.4 3.2 3.0 2.8 2.6 2.4 2.2 2.0 1.8 1.6 1.4 1.2 1.0 0.8
(ppm)

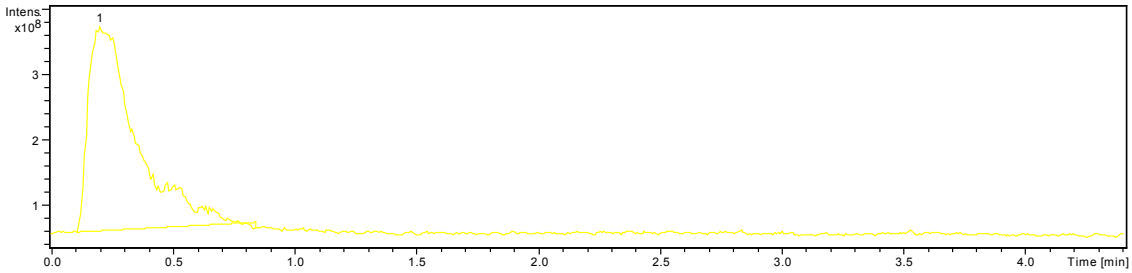
Intens.
x10^8
1
3
2
1
0.0
0.5
1.0
1.5
2.0
2.5
3.0
3.5
4.0
Time [min]

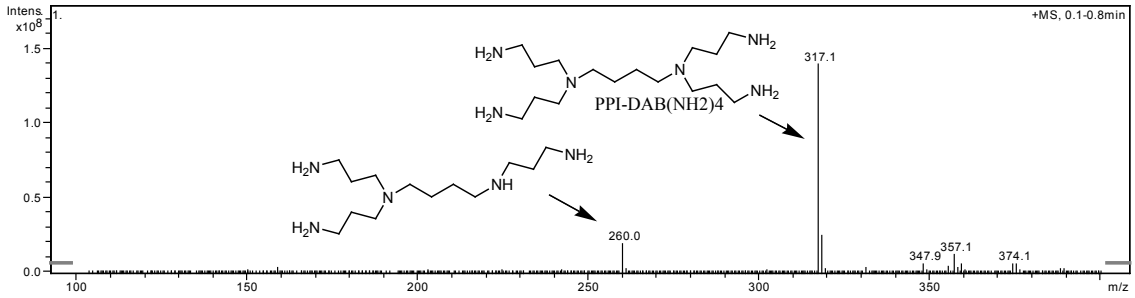
Intens.
x10^8
1.
+MS, 0.1-0.8min
1.5
1.0
0.5
0.0
H2N
NH2
N
NH
PPI-DAB(NH2)4
317.1
260.0
347.9
357.1
374.1
100
150
200
250
300
350
m/z

DAB(CN)$_8$: H^1 & C^{13}NMR, MS

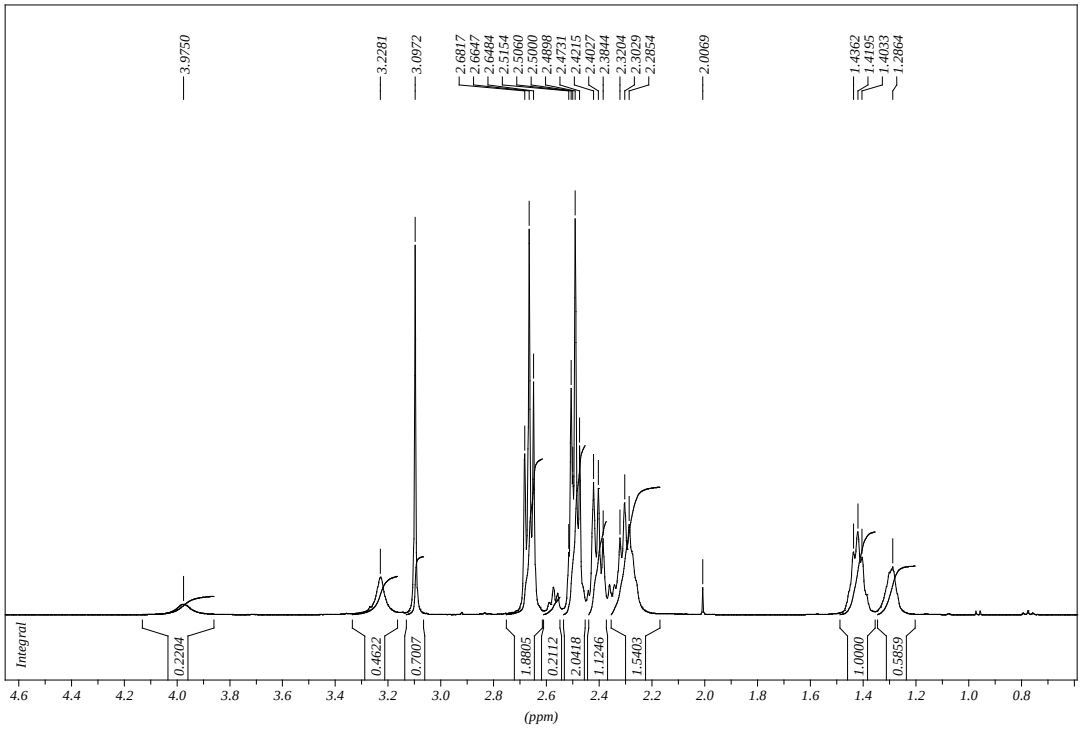

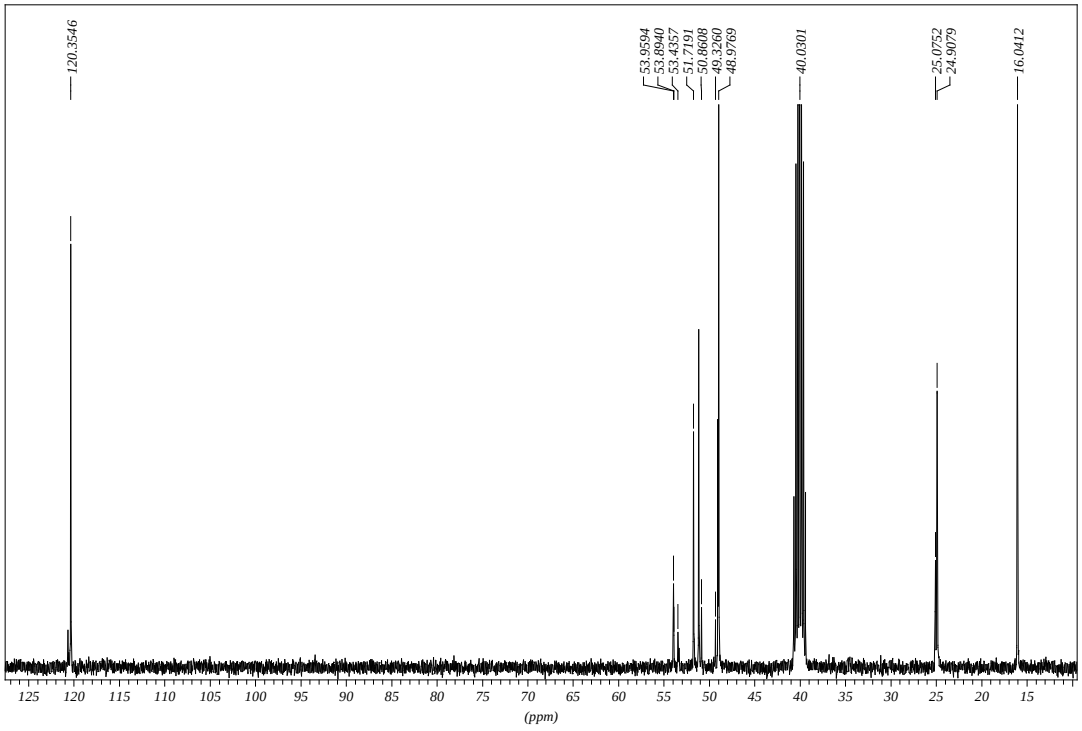

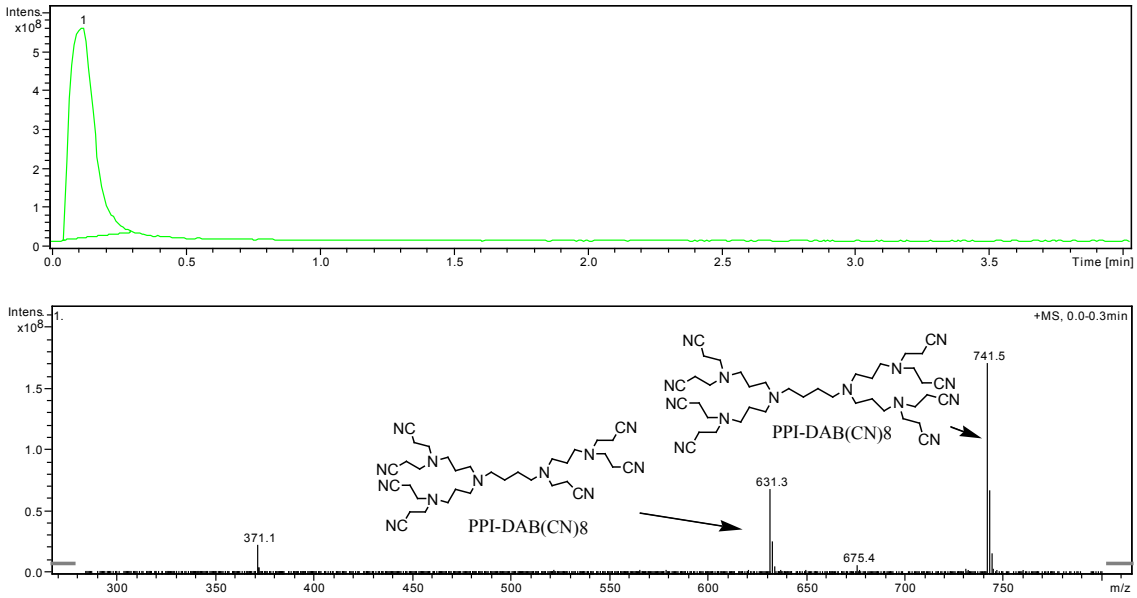
Intens.
x10^8
1
Time [min]
Intens.
x10^8
1.
+MS, 0.0-0.3min
741.5
631.3
371.1
675.4
PPI-DAB(CN)8
PPI-DAB(CN)8
m/z

LIPIDS

Rac-2,3-ditetradecyloxypropyl-1-bromide: : H^1 NMR, MS

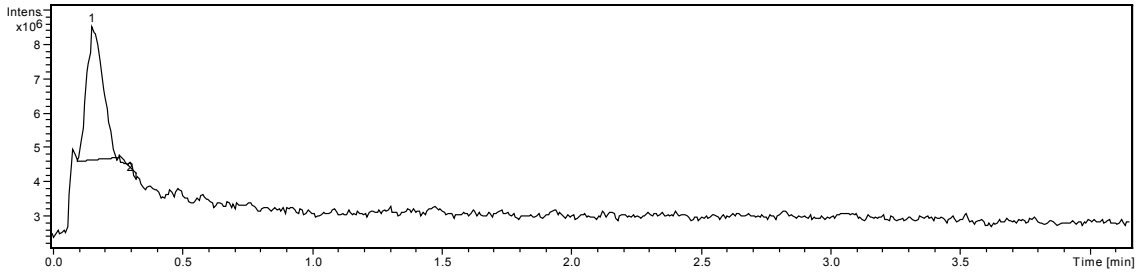

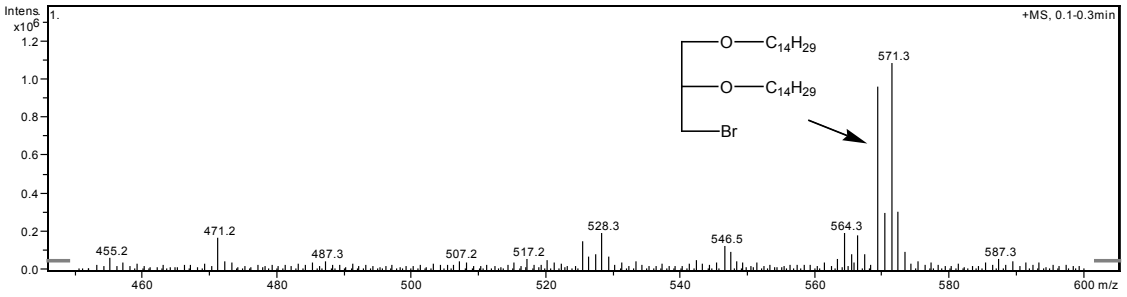

3-O-(3-carboxypropionyl)-1,2-ditetradecyl-*rac*-glycerol: H^1 NMR, MS

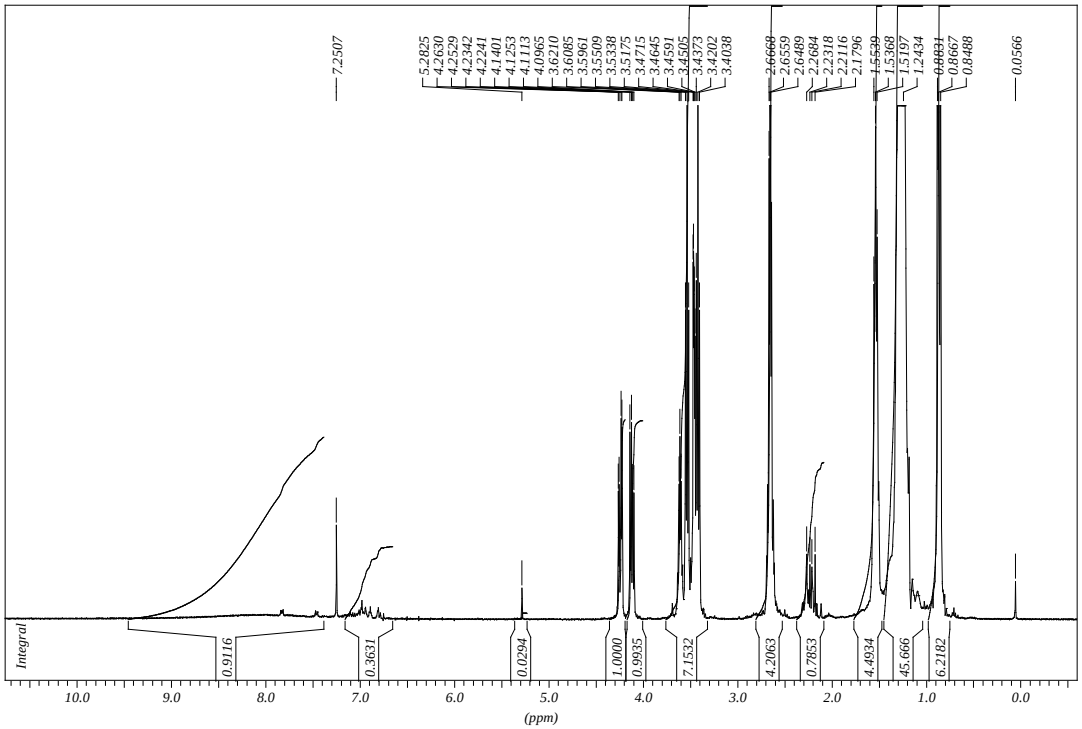

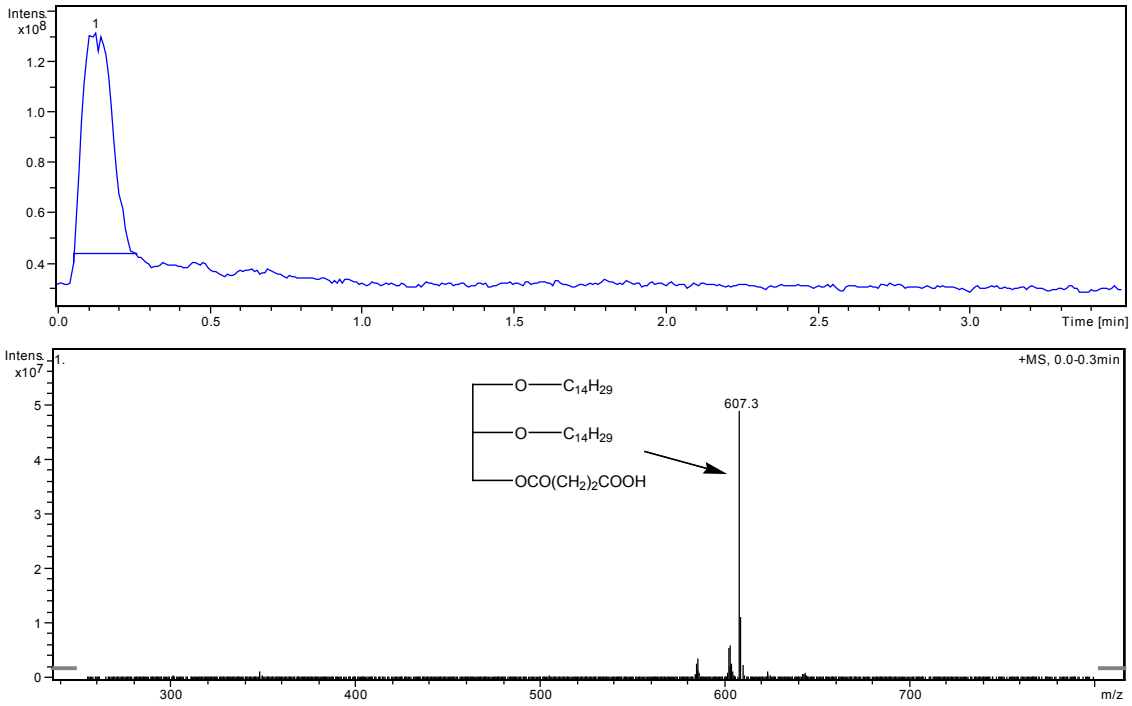

Rac-N-2,3-ditetradecyloxypropylpyridium bromide: H^1 NMR, MS

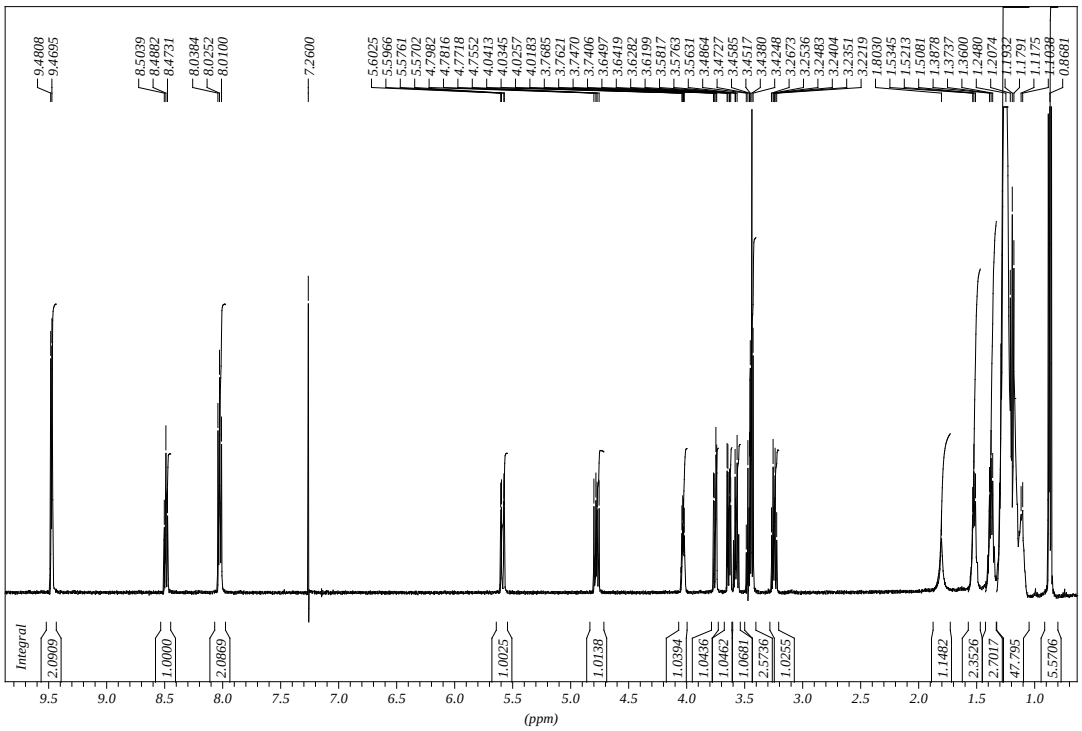

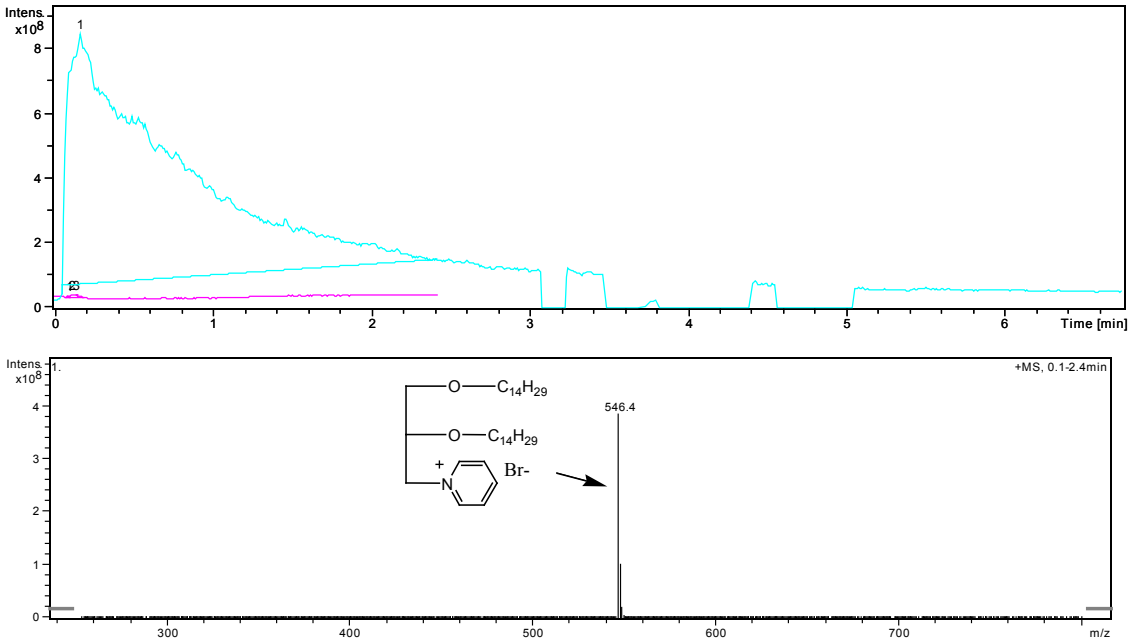

***Rac*-*N*-(2,3-ditetradecyloxypropyl)-6methylpyridium-3-carboxylate: H^1 NMR, MS**

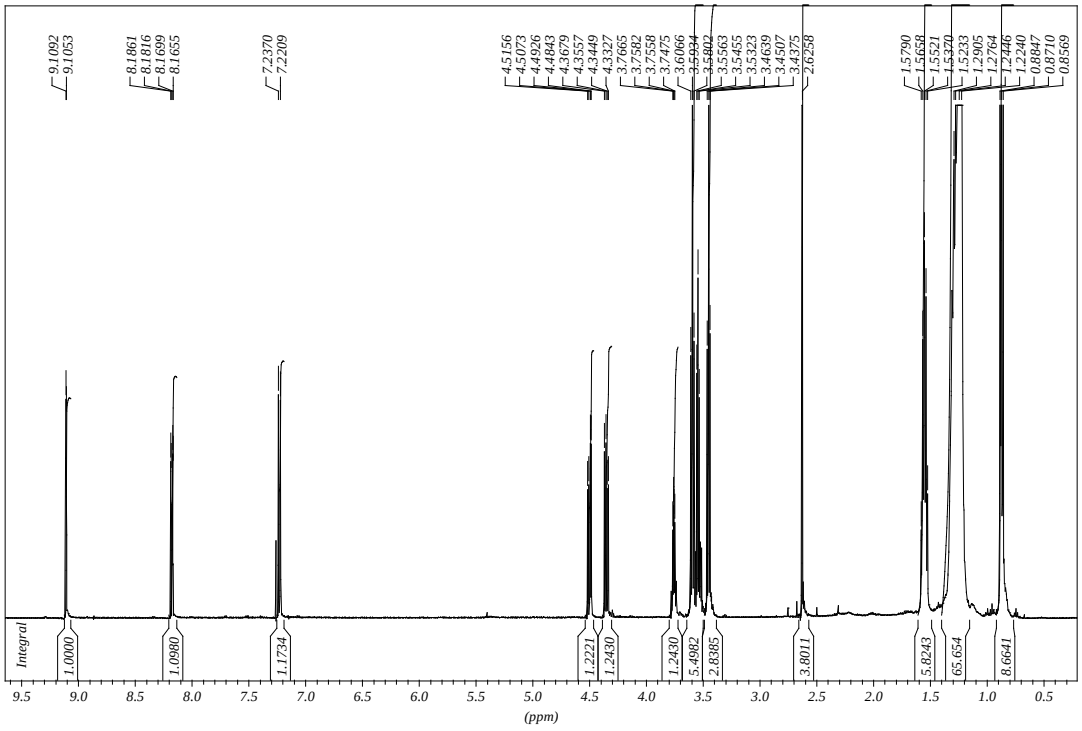

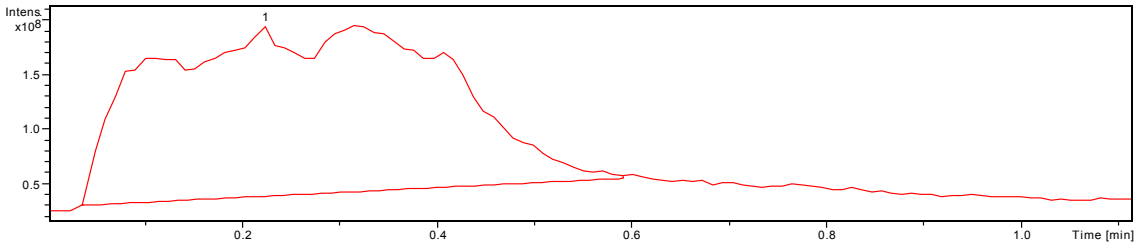
Intens.
x10^8
1.5
1.0
0.5
1
0.2
0.4
0.6
0.8
1.0
Time [min]

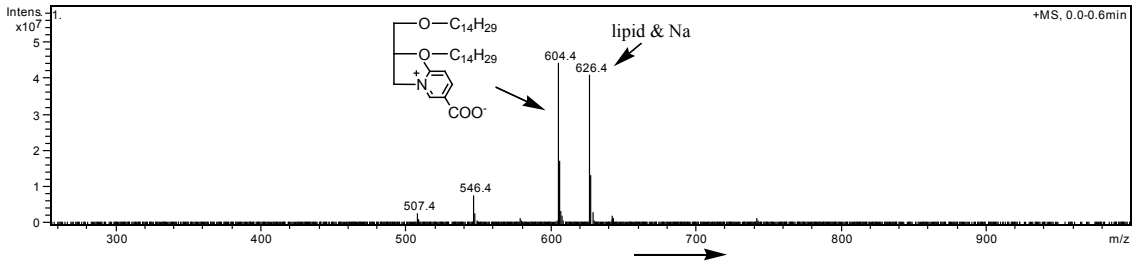
Intens.
x10^7
5
4
3
2
1
0
1.
+MS, 0.0-0.6min
O—C14H29
O—C14H29
N
COO-
lipid & Na
604.4
626.4
546.4
507.4
300
400
500
600
700
800
900
m/z

The Effect of Mutations at Position 160 and 156 on the Redox Potentials of *Chlamydomonas reinhardtii* Cytochrome f

Nicole Vanderbush, Shorter College
Rome, Georgia

Abstract

***Chlamydomonas reinhardtii* cytochrome f is known to have two propionate groups in its heme structure. The interaction of one of these groups with residues Y160 and R156 was investigated through a series of mutagenesis studies. Redox potentials were measured for mutants of Y160. The Y160L mutant reduced the redox potentials by ≈ 35mV whereas the Y160F mutant retained redox values similar to that of the wild type. The Y160L mutant removed both the hydrogen bonding capability of the residue and the aromaticity. The Y160F mutant left the aromaticity intact and removed the hydrogen bonding capability of the residue. Because of the change in redox potentials in the Y160L mutant that are not present in the Y160F mutant, it is surmised that the aromatic character of the residue is what needs to be retained to maintain redox potentials of the wild type. The R156L mutant that was made was air oxidizable and did not allow for accurate measurements of its redox potential. The interaction between the R156 residue and the propionate group of the heme is necessary for the stabilization of the protein.**

Introduction

Cytochrome f is part of the larger membrane bound b_6f complex which acts as a redox partner for the mobile electron carriers plastoquinone and plastocyanin in the electron transport chain of photosynthesis. The electron transfer through cytochrome f drives protons across the thylakoid membrane creating an electrochemical gradient and subsequently resulting in the production of ATP. *Chlamydomonas reinhardtii* cytochrome f is a 26 kDa c-type cytochrome with two surfaced exposed, peripheral propionate groups in its heme. One of these groups interacts with Tyr 160 and Arg 156 (Figure 1). The interaction of the propionate group with Y160 is a hydrogen bond with the phenolic hydrogen of the residue. The interaction of the propionate group with R156 is an electrostatic interaction between the positively charged residue and the negatively charged propionate group. R156 is conserved in all known sequences of cytochrome f, and Y160 is conserved in all but three.

A previous study conducted looked at a mutant of Y160 where the amino acid substitution was a leucine residue. The redox potential of the mutant was affected by about 20mV. This indicates that the interaction of the propionate groups with the protein residues have an affect on the redox potential of the protein. The previous mutant used removed both the hydrogen bonding ability and aromatic characteristics of the residue. In order to determine which characteristic was the one that altered the redox potential a Y160F mutant has been made and its redox potential measured. The replacement of the

tyrosine with a phenylalanine leaves the aromaticity but removes the hydrogen bonding capabilities. An R156L mutant was made and its redox potential measured. The redox

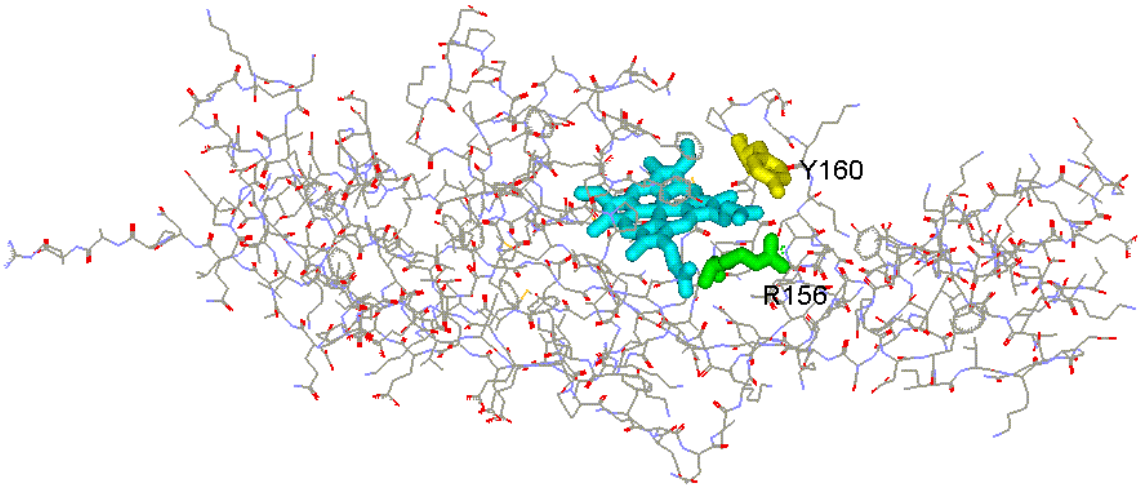

Figure 1: *Chlamydomonas reinhardtii* cytochrome f: file 1CFM downloaded from the Protein Data Bank edited in DS ViewerPro 5.0 by Accelrys Inc. The heme portion and residues Y160 and R156 shown in stick format.

potential of the R156L mutant indicates whether the positive charge of the residue is necessary to maintain redox potentials similar to the wild type.

Experimental Procedures

Mutagenesis for the R156L plasmid was done using the Quickchange II Site-Directed Mutagenesis Kit (1). Complementary primers 5' GGTAATCGTGGTCTTGG TCAAGTATA 3' and 5' GGATATACTTGACCAAGACCACGATT 3' were received from Integrated DNA Technologies and used to mutate the pUCF2 plasmid by means of PCR using the *Pfu* DNA polymerase. The restriction enzyme Dpn1 was added to the plasmid mixture to digest the parent DNA. The Dpn1 treated mixture was transformed into Epicurian Coli XL-1 Blue supercompetent cells and grown selectively on plates containing ampicillin. The plasmids were isolated using the Wizard Plus Minipreps DNA Purification System (2). The presence of the mutation was confirmed by sequencing.

The plasmid Y160F was prepared by Bryan Bishop. A plasmid prep was made from the initial stock of plasmid using the Wizard Plus Minipreps DNA Purification System (2). The plasmids were sequenced to confirm the presence of the mutation. The Y160F plasmid and the R156L plasmid were separately cotransformed along with the pEC86 plasmids into *E. coli* cells (MV1190 strain). The cells were grown according to Soriano et al. (3). The *E. coli* were selectively grown on 2xYT agar plates containing ampicillin and chloramphenicol. They were incubated at 37ºC for 24 hours. Colonies were selected after the 24 hour period, placed in 5mL of 2xYT liquid growth media containing 5µL of 0.027M ampicillin and 2.5µL of 0.15M chloramphenicol, and grown aerobically at 37ºC for 24 hours. The tube cultures were then placed in 1.8 liters of LB medium inoculated with 0.054mM ampicillin, 0.06 mM chloramphenicol, 1mM KNO_3, and 0.25mM IPTG and grown semi-anaerobically for 22 hours at 37ºC. The cells were

harvested and the protein was released by osmotic shock using a TSE buffer (20% sucrose, 30mM Tris-Cl, 1mM EDTA, pH 7.5) according to procedures outlined by Soriano (3).

The soluble fraction recovered from the osmotic shock was applied to a Whatman DE-53 anion exchange column and eluted off with a 0.0- 10mM Tris pH 7.0, 0.2M NaCl gradient. Fractions were collected. The fractions containing cytochrome f were pooled and concentrated to 5mL. The concentrate was put on a G-100 gel filtration column. The fractions were again pooled and concentrated to 10mL then purified further on HPLC using a BioRad Q12 anion exchange column with a 5mM phosphate pH 7.0 to 500mM phosphate pH 7.0 gradient (4). The sample was then exchanged into 5mM phosphate buffer pH 7.0.

Using the ratio of Potassium Ferricyanide (Fe) to Potassium Ferrocyanide (Fo) the midpoint potentials of the mutants were measured. Fe, which oxidizes the sample, was added to 1mL of 5µM purified cytochrome f. Fo was added in increments to reduce the sample. A few crystals of ascorbic acid and dithionite were added at the end to completely reduce the sample. All additions were made according to Table 1. The change in absorbance at 554nm was used to monitor the change in the redox state of cytochrome f. Absorbance was measured with a Hewlett Packard 8452 Diode Array Spectrophotometer each addition of Fe, Fo, ascorbic acid, and dithionite. According to the Nernst Equation (Eh = Eo – 59 log [c(red)/c(ox)]) the plot of log [c(red)/c(ox)] vs. Eh gives a midpoint potential equal to the redox potential where log [c(red)/c(ox)] = 0.0.

Addition	Measured Eh Value
1µL of 100mM Fe	
1µL of 100mM Fo	430mV
1µL of 100mM Fo	412mV
2µL of 100mM Fo	394mV
2µL of 100mM Fo	384mV
2µL of 100mM Fo	371mV
2µL of 100mM Fo	366mV
10µL of 100mM Fo	353mV
10µL of 100mM Fo	343mV
10µL of 100mM Fo	335mV
10µL of 100mM Fo	330mV
A few crystals of ascorbic acid	
A few crystals of dithionite	

Table 1: addition of oxidizing and reducing agents for redox potential measurements and corresponding Eh values.

Results and Discussion

The sequence data for the Y160F mutant showed the correct substitution at position 160 (underlined and bold).

GGTAGTCCTATTTTATCTCCAGATCCTGCTAAAAATAAAAACGTTTCTTACTT
AAAATATCCTATTTATTTTGGTGGTAATCGTGGTCGTGGTCAAGTA**TTT**CCAG
ATGGTAAAAAATCAAACAACACTATTTACAACGCATCAGCAGCTGGTAAAAT
TGTAGCAATCACAGCTCTTTCTGAGAAAAAAGGTGGTTTTGAAGTTTCAATTG
AAAAAGCAAACGGTGAAGTTGTTGTAGACAAAATCCCAGCAGGTCCTGATTT
AATTGTTAAAGAAGGTCAAACTGTACAAGCAGATCAACCATTAACAAACAAC
CCTAACGTTGGTGGTTTCGGTCAGGCTGAAACTGAAATTGTATTACAAAACCC
TGCTCGCTAGAGGATCCCCGGGTACCGAGCTCGAATTCACTGGCCGTCGTTTT
ACAACGTCGTGACTGGGAAAACCCTGGCGTTACCCAACTTAATCGCCTTGCA
GCACATCCCCCTTTCGCCAGCTGGCGTAATAGCGAAGAGGCCCGCACCGATC
GCCCTTCCCAACAGTTGCGCAGCCTGAATGGCGAATGGCGCCTGATGCGGTA
TTTTCTCCTTACGCATCTGTGCGGTATTTCACACCGCATATGGTGCACTCTCAG
TACAATCTGCTCTGATGCCGCATAGTTAAGCCAGCCCCGACACCCGCCAACA

The primer used to sequence the Y160F mutant plasmid encoded for codons 125 through 134 of the cytochrome f gene. This allows accurate sequencing of mutations in the last half of the protein. According to the absorbance spectra the initial A_{554}/A_{280} before purification was between 0.032 and 0.041 for the Y160F mutant (Figures 2 and 3). The Fractions kept after the DE-53 anion exchange column were numbers 11 through 26 (Figure 4). These fractions were concentrated and placed on a G100 gel filtration column. The fractions collected after the G100 were fraction numbers 14 through 28 (Figure 5). The fractions were concentrated and put through HPLC. The fractions collected were those with retention times between 8 and 9 minutes (Figure 6). The final A_{554}/A_{280} was 0.745 (Figure 7).

The sequence for the R156L mutant did show the correct substitution at position 156 (bold and underlined).

GGTAGTCCTATTTTATCTCCAGATCCTGCTAAAAATAAAAACGTTTCTTACTT
AAAATATCCTATTTATTTTGGTGGTAATCGTGGT**CTT**GGTCAAGTATATCCAG
ATGGTAAAAAATCAAACAACACTATTTACAACGCATCAGCAGCTGGTAAAAT
TGTAGCAATCACAGCTCTTTCTGAGAAAAAAGGTGGTTTTGAAGTTTCAATTG
AAAAAGCAAACGGTGAAGTTGTTGTAGACAAAATCCCAGCAGGTCCTGATTT
AATTGTTAAAGAAGGTCAAACTGTACAAGCAGATCAACCATTAACAAACAAC
CCTAACGTTGGTGGTTTCGGTCAGGCTGAAACTGAAATTGTATTACAAAACCC
TGCTCGCTAGAGGATCCCCGGGTACCGAGCTCGAATTCACTGGCCGTCGTTTT
ACAACGTCGTGACTGGGAAAACCCTGGCGTTACCCAACTTAATCGCCTTGCA
GCACATCCCCCTTTCGCCAGCTGGCGTAATAGCGAAGAGGCCCGCACCGATC
GCCCTTCCCAACAGTTGCGCAGCCTGAATGGCGAATGGCGCCTGATGCGGTA
TTTTCTCCTTACGCATCTGTGCGGTATTTCACACCGCATATGGTGCACTCTCAG
TACAATCTGCTCTGATGCCGCATAGTTAAGCCAGCCCCGACACCCGCCAACA

The same primer used for the Y160F mutant was used to sequence the R156L mutant. The initial A_{554}/A_{280} of the crude sample was 0.067 (Figure 8). The sample was put on a DE-53 anion exchange column, and fractions were collected. Fractions 23 through 34 were kept and concentrated(Figure 9).The sample was then placed on a G100 gel filtration column. Fractions were collected and fractions 2 through 15 were kept (Figure 10). The fractions were concentrated and then put on a DEAE HPLC. The fractions kept had a retention time between 6.5 and 8.5 minutes. Fractions with a retention time between 8.5 and 10 minutes were kept separately (Figure 11). The final A_{554}/A_{280} was 0.43 (Figure 12).

The redox potentials measured for the wild type were between 375mV and 380mV (Figures 13 and 14). Previously the redox potential measured for the Y160L-S106C mutant was 356mV. These measurements were for the Y160L-S106C mutant labeled with a Ru complex at the S106C mutated position. New measurements were taken for the Y160L-S106C mutant without the Ru complex attached, and the redox potential was lowered to be 343mV (Figures 15 and 16). This shift has been present in all known Ru cytochrome f derivatives. The redox potentials for the Y160F mutant were found to be between 378mV and 379mV (Figures 17 and 18). This does not significantly vary from the redox potentials of the wild type protein. Because the redox potentials varied with the Y160L mutant and not with the Y160F mutant the aromatic character of cytochrome f residue 160 is what needs to be maintained in order to keep redox potentials comparable to the wild type. The loss of the hydrogen bonding capability of the residue at position 160 was not found to have a substantial effect on redox potentials. It is the aromatic nature of the residue and not the hydrogen bond interaction with the propionate group that retains redox potentials.

The R156L mutant that was created was found to be air oxidizable. Proper redox potentials could not be measured due to this fact. The electrostatic interaction that exists between the positively charged arginine and the negatively charged propionate group of the heme when removed alters the proteins ability to remain in a reduced state. More understanding might arise with repetition of this experiment.

Figures

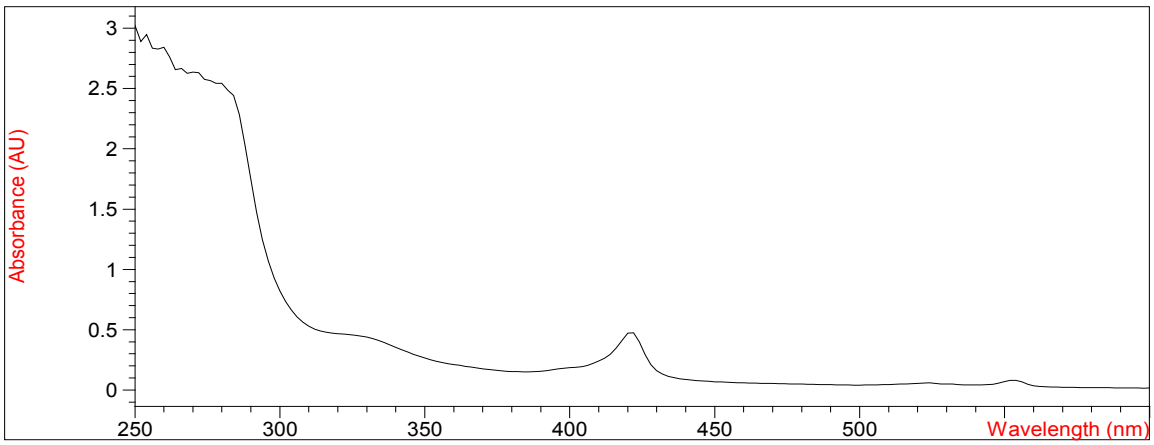

Figure 2: Diode array spectra of crude Y160F showing peaks at 280nm (Abs = 2.54) , 420nm (Abs = 0.47), and 554nm (Abs = 0.081). The peaks at 420nm and 554nm indicate the presence of cytochrome f.

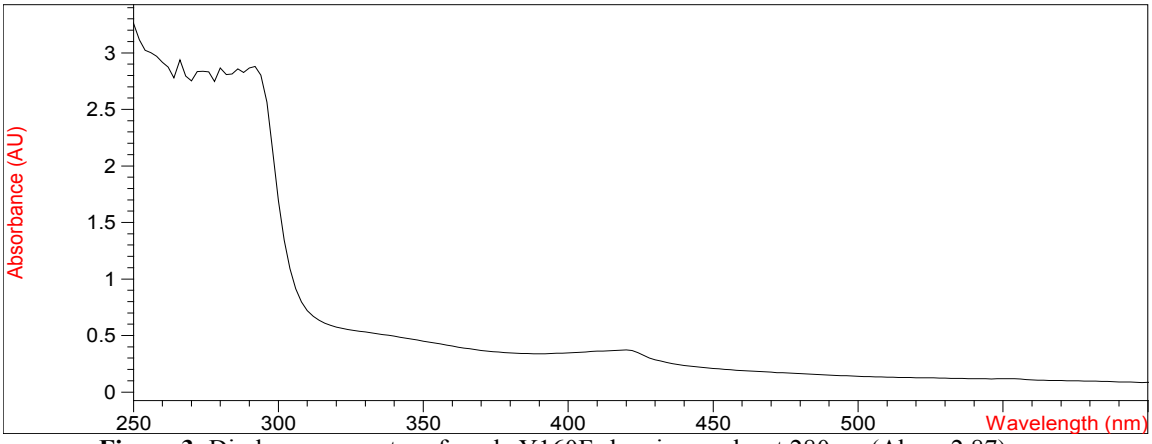

Figure 3: Diode array spectra of crude Y160F showing peaks at 280nm (Abs = 2.87) , 420nm (Abs = 0.37), and 554nm (Abs = 0.12). The peaks at 420nm and 554nm indicate the presence of cytochrome f.

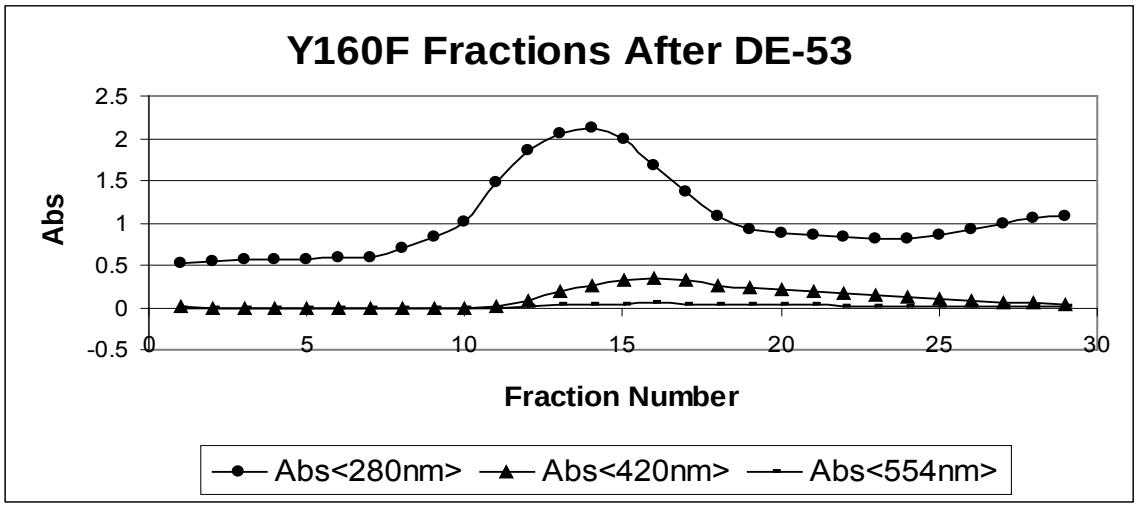

Figure 4: Fractions of the Y160F mutant after DE-53 anion exchange column.

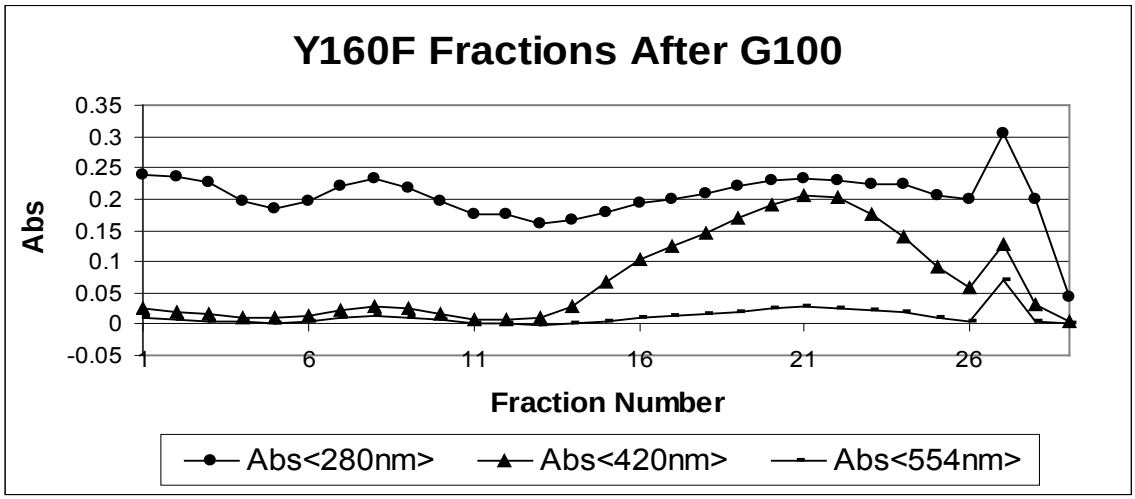

Figure 5: Fractions of the Y160F mutant after G100 gel filtration column. The absorbance at fraction number 21 was due to condensation on the cuvette.

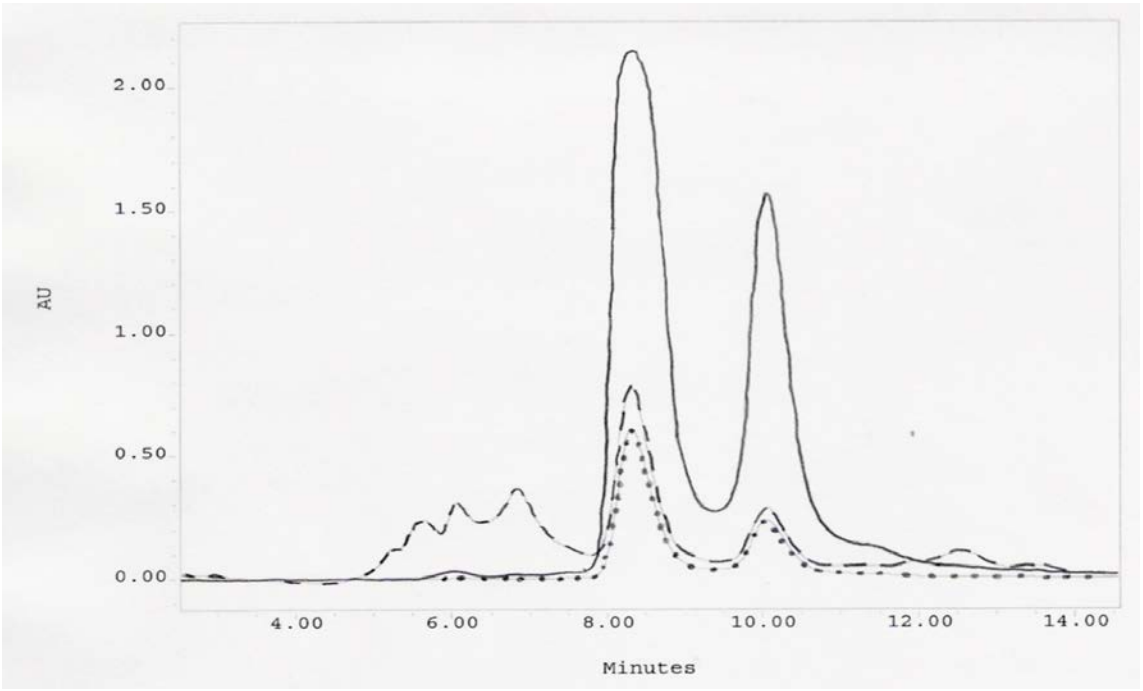

Figure 6: HPLC fraction collection spectra from the Y160F sample showing Abs@ 280(dashed line), Abs@ 420(solid line), Abs@ 554(dotted line).

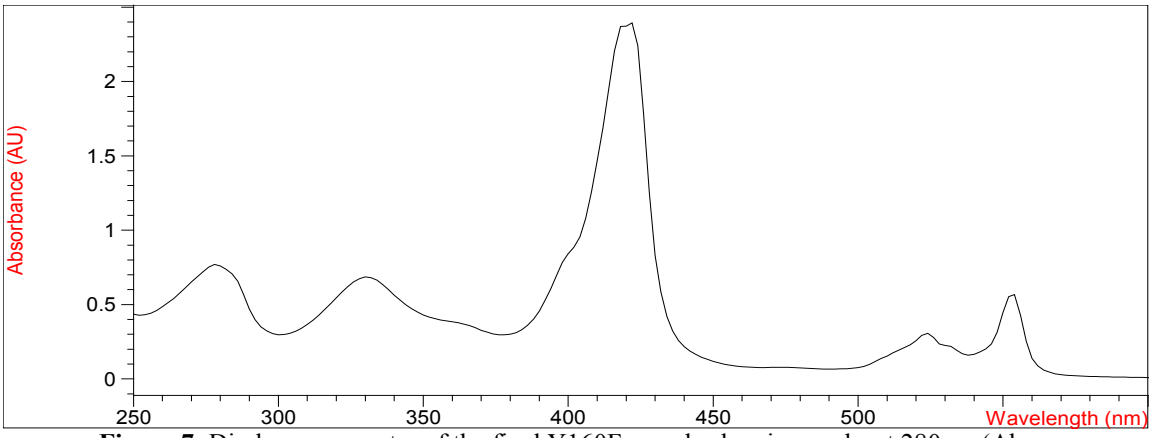

Figure 7: Diode array spectra of the final Y160F sample showing peaks at 280nm (Abs = 0.76) , 420nm (Abs = 2.37), and 554nm (Abs = 0.57). The peaks at 420nm and 554nm indicate the presence of cytochrome f.

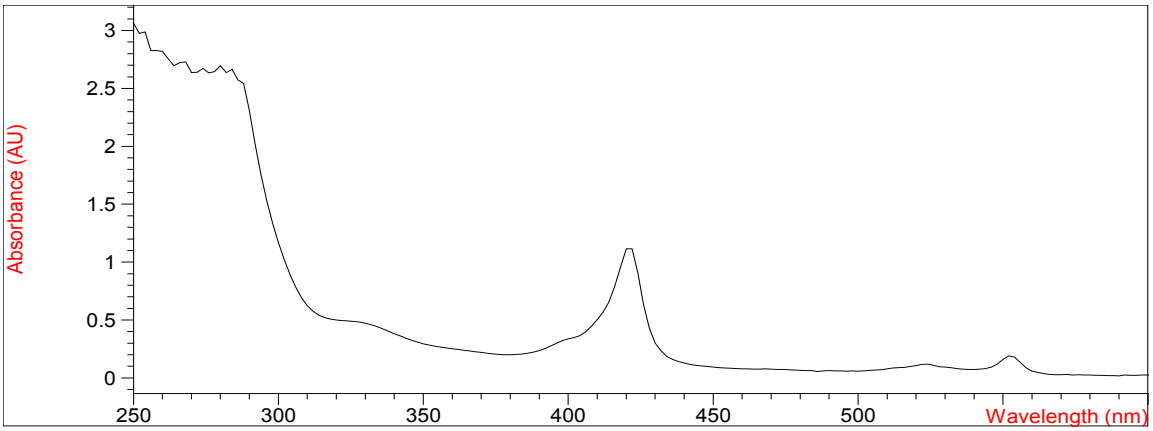

Figure 8: Diode array spectra of crude R156L showing peaks at 280nm (Abs = 2.70), 420nm (Abs = 1.11), and 554nm (Abs = 0.18). The peaks at 420nm and 554nm indicate the presence of cytochrome f.

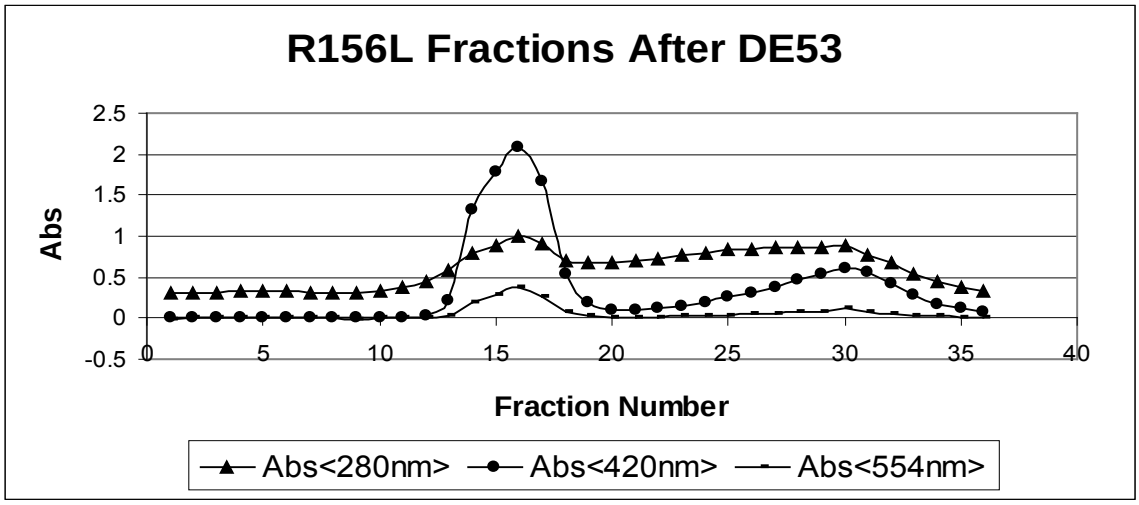

Figure 9: Fractions of the R156L mutant after DE-53 anion exchange column.

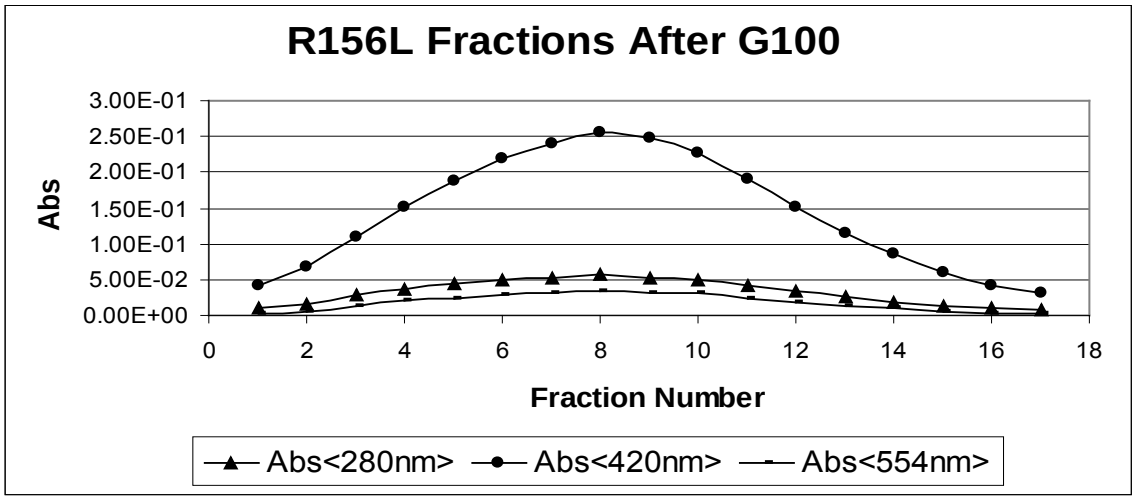

Figure 10: Fractions of the R156L mutant after G100 gel filtration column.

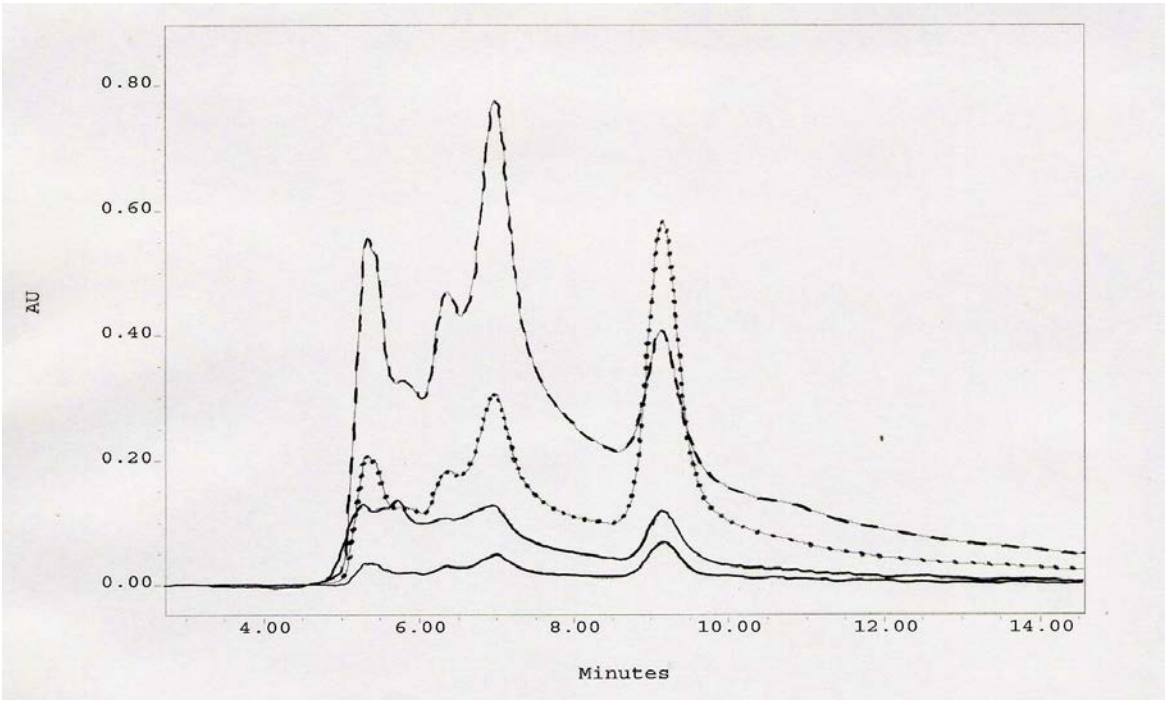

Figure 11: HPLC fraction collection spectra from the R156L sample showing Abs@ 280(upper solid line), Abs@ 410(dashed line), Abs@ 420(dotted line), Abs@ 554(lower solid line).

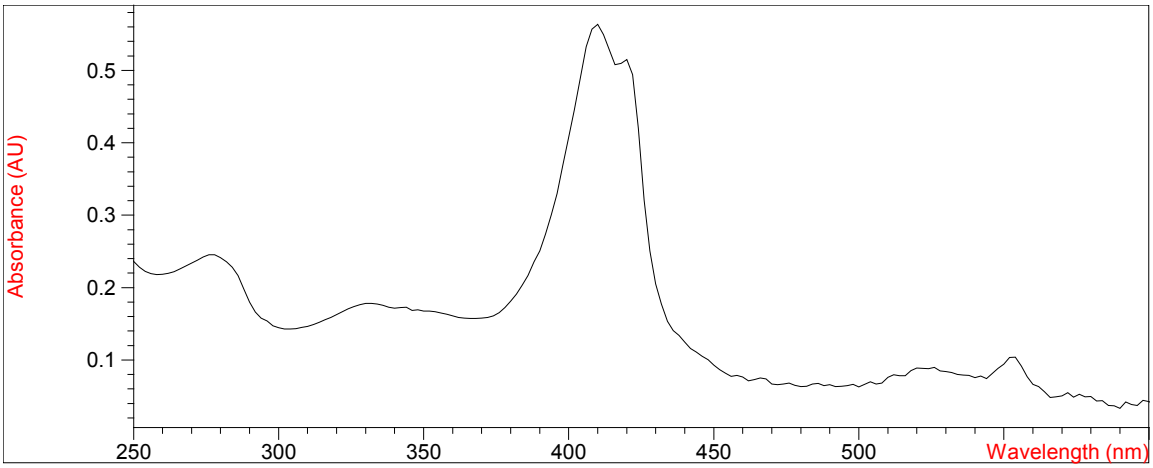

Figure 12: Diode array spectra of the final product of R156L showing peaks at 280nm (Abs = 0.24.), 420nm (Abs = 0.52), and 554nm (Abs = 0.10). The peaks at 420nm and 554nm indicate the presence of cytochrome f.

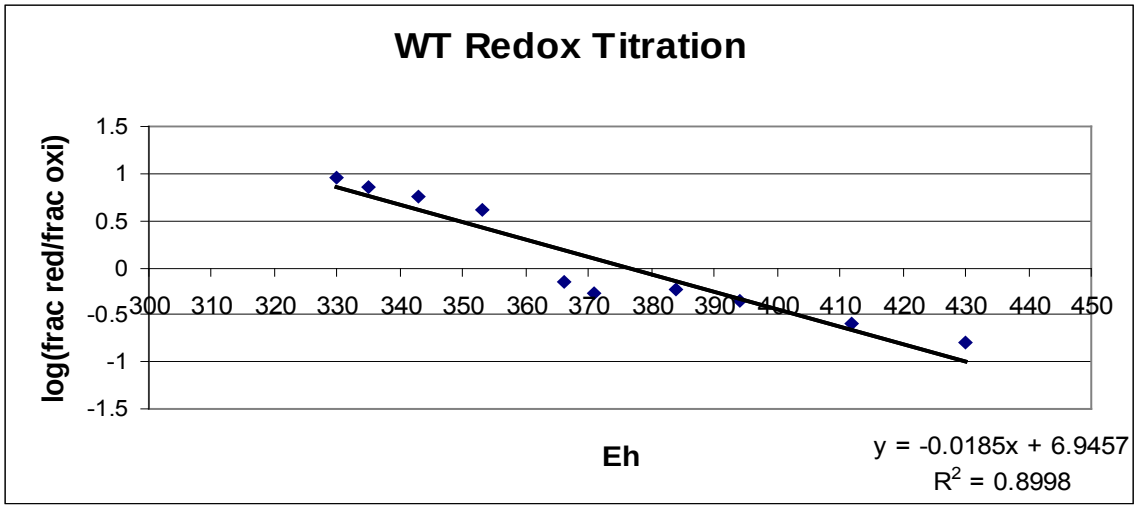

Figure 13: Redox Titration of wild type cytochrome f with a redox potential equal to 375mV.

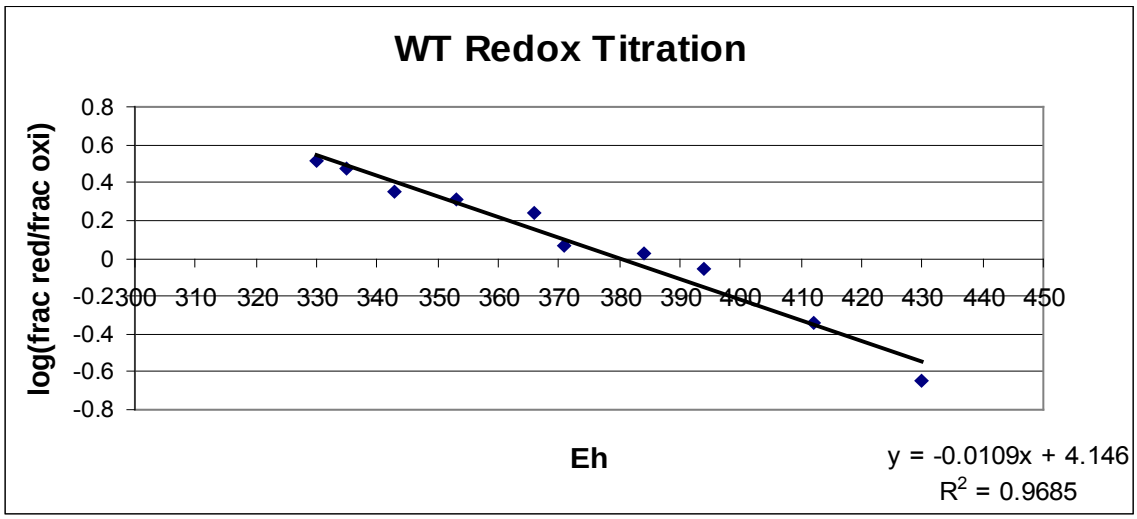

Figure 14: Redox Titration of wild type cytochrome f with a redox potential equal to 380mV.

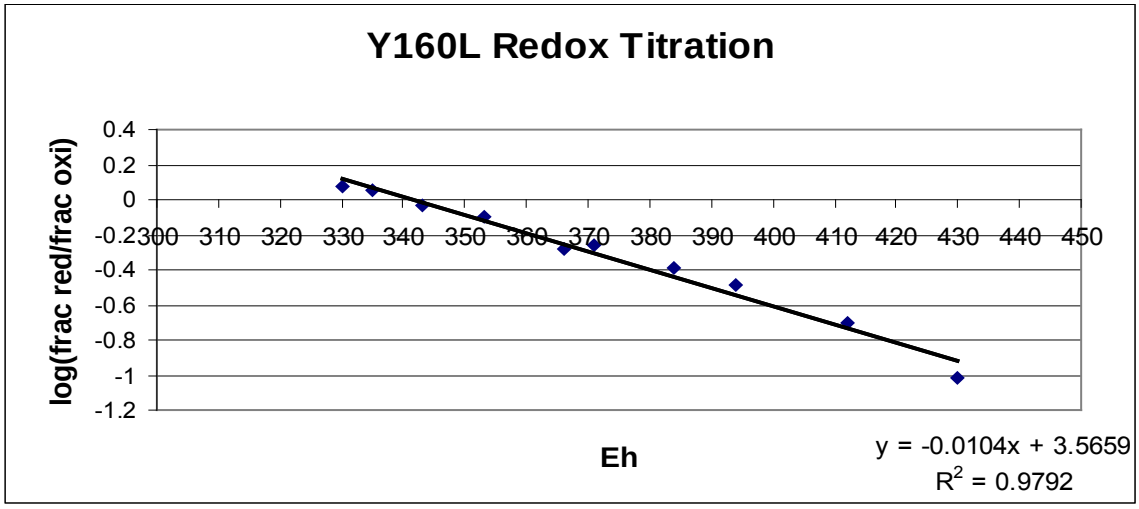

Figure 15: Redox Titration of the unlabeled cytochrome f mutant Y160L-S106C with a redox potential equal to 343mV.

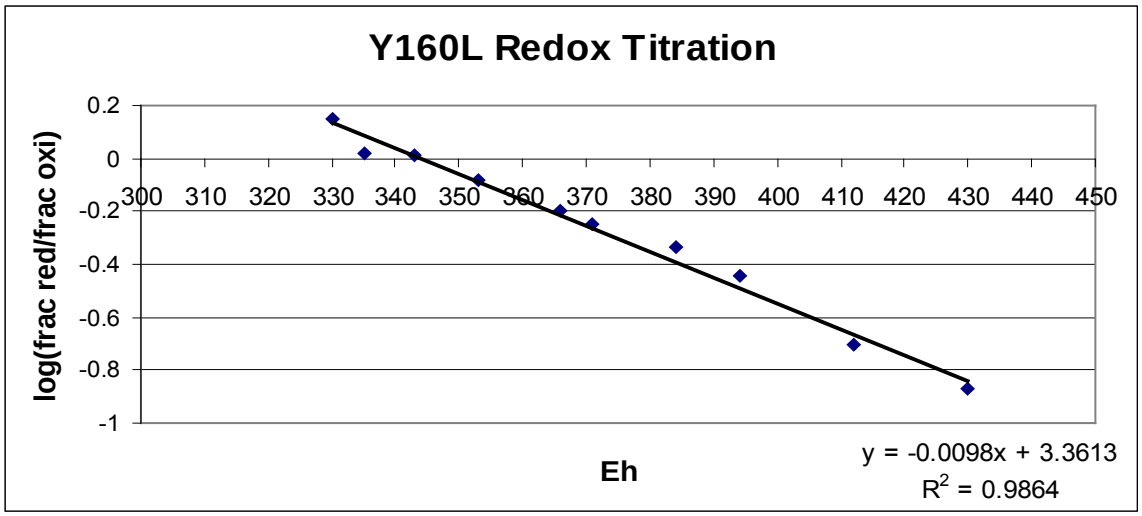

Figure 16: Redox Titration of the unlabeled cytochrome f mutant Y160L-S106C with a redox potential equal to 343mV.

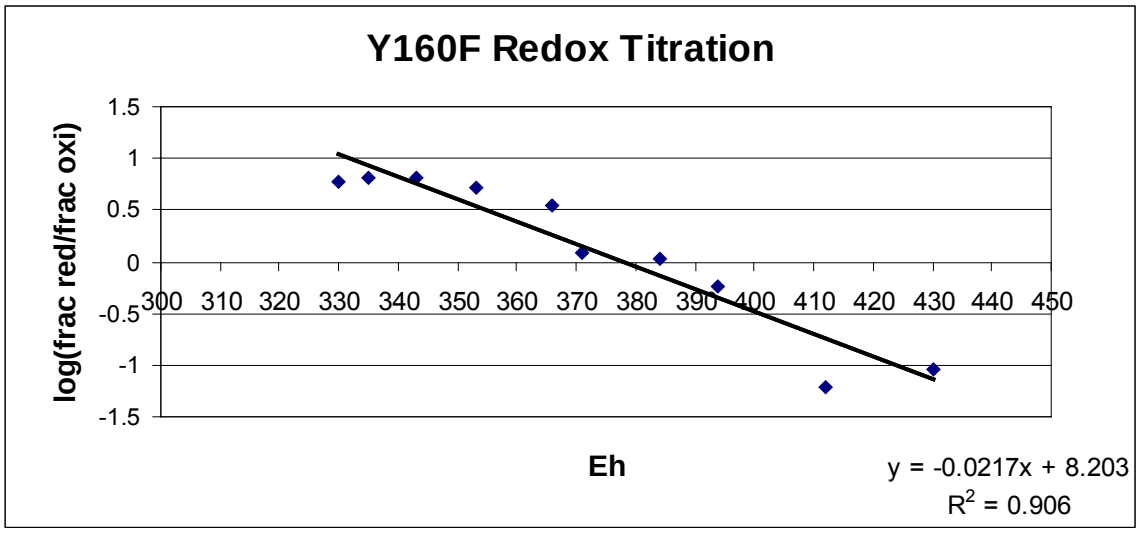

Figure 17: Redox Titration of the cytochrome f mutant Y160F with a redox potential equal to 378mV.

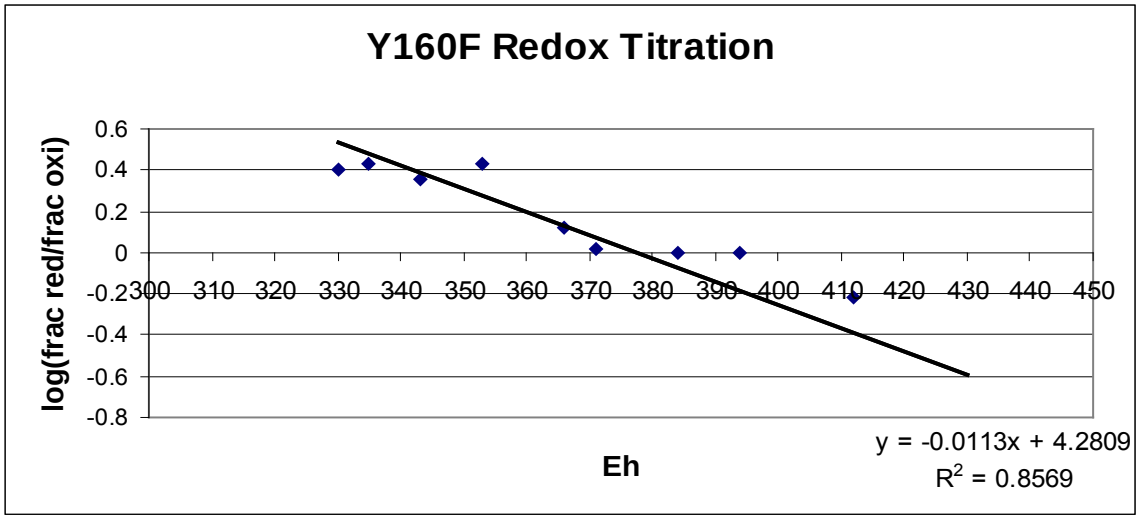

Figure 18: Redox Titration of the cytochrome f mutant Y160F with a redox potential equal to 379mV.

Acknowledgements

1. National Science Foundation for funding
2. Summer REU program, University of Arkansas
3. Dr. David Paul, Associate Professor, University of Arkansas
4. Dr. D.J. Davis, Professor, University of Arkansas
5. Marilyn Davis, Research Assistant, University of Arkansas
6. Dr. Lois Geren, Research Assistant Professor, University of Arkansas
7. Ashwini Bhise, Graduate Research Assistant, University of Arkansas
8. Jay Staiger, Graduate Research Assistant, University of Arkansas
9. Dr. D.C. Pearson, Assistant Professor, Shorter College
10. Dr. Theunis van Aardt, Assistant Professor, Shorter College

References

1. Quickchange II Site-Directed Mutagenesis Kit, Instruction Manual. Stratagene. **2004**.
2. Wizard Plus Minipreps DNA Purification System, Technical Bulletin. Promega. **2002**.
3. Soriano, G.M.; Ponamarev, M.V.; Piskorowski, R.A.; Cramer, W.A. *Biochemistry*. **1998**. 37, 15120- 15128.
4. Ponamarev, M.V.; Cramer W. A. *Biochemistry*. **1998**. 37, 17199- 17208.
5. Ponamarev, M.V.; Schlarb, B.G.; Howe, C.J.; Carrell, C.J.; Smith, J.L.; Bendall, D.S.; Cramer, W.A. *Biochemistry*. **2000**. 39, 5971- 5976.
6. Morand, L.Z.; Frame, M.K.; Colvert, K.K.; Johnson, D.A.; Krogmann, D.W.; Davis, D.J. *Biochemistry*. **1989**. 28, 8039- 8047.

Effect of Relative Humidity on Metalloporphyrin-Based Gas Sensors

Vitaly Vostrikov, Moscow State Academy of Fine Chemical Technology (MITHT)
Moscow, Russia

Abstract

Development of gas sensors that are able to detect sub-ppm concentrations are in high demand in the areas of workplace safety and environment protection. Four metalloporphyrin-based gas sensors with various metals (Co, Cu, VO^+ and Zn) were studied with respect to their response to changes in relative humidity (RH). The Cu metalloporphyrin sensor required the RH to be above 80% to even function. The Zn sensor showed an increase in conductivity with increasing RH. The response of the VO^+ metalloporphyrin sensor showed no correlation with changes in RH.

Introduction

Development of gas sensors able to detect sub-ppm concentrations of toxic gases are essential to ensure workplace safety and environment protection. Although safety regulations allow the concentrations of toxic gases such as HCl and NO_2 to obtain levels up to several ppm, faster detection methods could prevent long-term exposure of personnel to hazardous conditions and therefore minimize potential injuries and casualties.

Current gas-sensing materials are based on semiconductors and include SnO_2 (NO_2 detection [1]), ZnO (NO detection [2]), and $LiTaO_3$ (HCl detection [3]). A conductivity change in the sensor is recorded as the gas interacts with the semiconducting layer. Leo et. al. managed to obtain as much as a 6000% difference in SnO_2 film resistance between a sensor exposed air diluted NO_2 and a blank sample. The problem with the current semiconducting sensors is that they lack selectivity. Because of this, other materials with more promising selectivity, including various metalloporphyrins (NH_3, HCl, NO_2, SO_2 detection [4-6]), have been used. Unlike the semiconducting sensors, most of these sensors have been optically based. Current methods focus on spectral properties, such as photo-reflection [4], fluorescence [5], and optical absorption [6] of porhyrin-based sensors. However, the high cost of optic elements calls for other methods of analysis. It is also possible to measure conductivity changes in a porphyrin film due to the adsorbing gases, thus combining the practicality of an electrical device, and the selectivity of the porphyrin molecule.

One important aspect of porphryin-gas interaction is the presence of water vapor (RH). Itagaki *et al.* studied response of the HCl sensors to different humidities. Sensor response increased with the rise of RH from 5 to 50%. The authors propose that the increase in sensitivity was related to a higher degree dissociation of the sensing molecules and formation of the dicationic form of the porphyrin.

The purpose of this research is to investigate the effects of various conditions (such as light and relative humidity) on the resistance response of porphyrin-based gas sensors (figure 1). Four complexes of etioporphyrins (EP) with metals were chosen for this study: EP -VO^+, EP-Co, EP-Cu and EP-Zn (figure 2).

Experimental Procedures

Pre-coated sensors were kindly loaned from Prof. Anatoli Ischenko of the Moscow State Academy of Fine Chemical Technology (MITHT). Sensors were kept in the dark unless stated otherwise. Data was collected for either 15 minutes with 10 second intervals or for 10-16 hours with 10 minute intervals. Signal stability for the equipment was determined using an 18 MΩ resistor and collecting ohmic data over several hours (data not shown). A long term drift of 0.003MΩ/h was noted with short term drift (20 minute duration) of ±0.12% and a short term noise of 0.03%. Signals outside this range can be attributed to the effects of humidity.

Experiments were performed using a Keithley model 617 programmable electrometer (Keithley Instruments Inc., U.S.A.) in DC mode. Resistance values were calculated internally by determining the current from a 1.00 V applied potential. The electrometer was set into "ohms" mode, zero check was performed, and zero correction enabled. The sensor was attached to the electrometer's contacts and placed into an Erlenmeyer flask covered with a dark mask (figure 3). Zero check mode was switched off and after 1 minute data acquisition was initiated. Different RH was achieved by exposing the sensor to various saturated salt solutions (Table 1). According to Hong *et al.* [7] the effect of temperature on solvent-vapor equilibrium (and therefore RH) is negligible, allowing the experiments to be conducted over a small range of room temperatures (22-24 ^{0}C). Sensors were left in air for at least 12 hours between measurements to re-equilibrate.

Salt solution	Relative humidity, %
$MgCl_2$	33
K_2CO_3	44
$Mg(NO_3)_2$	55
NH_4NO_3	65
NaCl	76
$(NH_4)_2SO_4$	81
KCl	87
KNO_3	94
K_2SO_4	97

Table 1. Saturated salt solutions employed.

In order to study the influence of light on the sensors' conductivity, some experiments were performed without the dark cover.

Results and Discussion

The long-term stability of the conductivity of the EP - Zn sensor is shown in figure 4. The same sensor was used with a 12 hour gap between experiments during which time the sensor was allowed to dry. The signals appear to be drifting with time with occasional step changes. The step changes could be an instrumental artifact caused by poor electrical connections to the sensor, but the short-term instability in the signal is

± 12%, which can not be accounted for by instabilities in the instrumentation (0.12%). In previous work by Itagaki, he postulated the sensing mechanism for HCl (gas) as a two-step process (reactions 1 and 2 below).

$$[HCl]_{gas} \Leftrightarrow [HCl]_{film} \quad (1)$$

$$2[HCl]_{film} + [TPPH_2] \Leftrightarrow [TPPH_2 \cdot 2HCl] \quad (2)$$

Response of porphyrin coated gas sensors at different RH was studied. The effects of RH on the response of porphyrin films has been reported to be significant with differences in resistance reaching up to 1000%. In the first stage of the mechanism the sensing gas adsorbeds to the tetraphenylporphyrin (TPPH) film; in the second stage the reaction between the gas and TPPH occurs. It is the second reaction that causes a change in the resistance, but in order to get reproducible results desorption of gas from the porhyrin film must occur. In our experiments we did not have a test gas but we hypothesized that the difference in the experiments (under identical condition) could be the result of differing initial saturation levels of the porphyrin film. The assumption would be that full desorption is not achieved during the 12 hour gap between the experiments.

In order to test this hypothesis an EP-Zn sensor (figure 5) was left in the open air and data collected over 53 hours. It took approximately 2-3 hours for the system to equilibrate, and during the remaining time the resistance oscillated between 7.1 and 10.0 GΩ. We can conclude from this that drying time should have been sufficient to start the sensor out in a known state. The instability of ± 25% indicates that hydration is critical to the sensor. It could also mean that the absolute amount of water available is also a determining factor in determining the stability of the sensor. The resistance of the EP - Zn sensor is much lower in the presence of water vapor, 0.1 G Ω vs 7.1 to 10.0 GΩ dry. Evidently the water vapor is in a slow equilibrium between the air and the porphyrin film. This exchange of water is slow and unpredictable at room temperature.

Effect of light was tested for the EP – Co sensor. If the experiment was carried out with dark cover, the resistance would settle at 1.4-1.8 GΩ. If the dark cover was removed and the sensor was exposed to light, the resistance falls to 0.6-0.8 GΩ (figure 6). In semi-conducting materials light promotes an increase of the charge carriers in the conduction band, which is the case here. Another striking point is that when exposed to light the signal becomes much more stable. Instability is ± 20% in the dark, but only ± 0.1% in the light. It seems that high resistances are inherently unstable. Some minimum conductivity must be reached before a stable response is achieved. For the Co-EP sensor this conductivity can be achieved by exposure to light.

Resistance of the EP - Cu sensor was beyond the limits of measurement of the multimeter (200 GΩ). Effect of RH on the EP - Cu sensor was complicated: it was possible to collect data for RH=33, 81, 87, 94 and 97% but at RH=44, 55, 65 and 76% resistance went over 200 GΩ (figure 7). It can be proposed that EP - Cu sensor works only in high RH environment but this cannot explain results for RH=33%.

The effects of RH on the EP – Co, EP – VO+, EP- Zn are all similar to the EP – Cu sensor. Resistance of the dry sensor is quite high, but it is difficult to observe a simple relationship between RH and conductivity. In general higher RH lowers the resistance of the film.

Conclusion

Sensors composed of highly resistive films are extremely noisy. Conduction through these films is postulated to be described by percolation theory. In this theory conduction is achieved by a hopping mechanism between conductive sites. There is a threshold number for sites that must be achieved before conduction can proceed. Evidently near this threshold level, the conduction pathways are ill defined resulting in noise. It is expected that once this threshold is exceeded, the noise should diminish. Conduction proceeds via a complex mechanism that includes RH, light, and morphology of the porphyrin layer. The effect of temperature on conductivity of the porphyrin layer is also known to have a considerable effect. Further investigation should be carried out in this area.

Acknowledgements

The author would like to thank National Science Foundation Grant NSF/CHE/REU 0243978 for the financial support of this research.

References

1. Leo, G.; Rella, R.; Siciliano, P.; Capone, S.; Alonso, J.C.; Pankov, V.; Ortiz, A. *Sprayed SnO thin films for NO sensors*. **1999**. Sensors and Actuators B, 58, 370-374.
2. Boccuzzi, F.; Guglielminotti, E.; Chiorino, A. *IR study of gas-sensor materials: NO interaction on ZnO and TiO_2, pure or modified by metals*. **1992**. Sensors and Actuators B, 7, 645-650.
3. Faccio, M.; Ferri, G.; Ponti, P.P.; Savelli, G.; D'Amico, A. *Hydrogen chloride detection by $LiTaO_3$*. **1992**. Sensors and Actuators B, 7, 677-681.
4. Itagaki, Y.; Deki, K.; Nakashima, S.-I.; Sadaoka, Y. *Toxic gas detection using porphyrin dispersed polymer composites*. **2005**. Sensors and Actuators B, 108, 393-397.
5. Vaughan, A.A.; Baronb, M.G.; Narayanaswamya, R. *Optical Ammonia Sensing Films Based on an Immobilized Metalloporphyrin*. **1996**. Analytical Communications, 33, 393-396.
6. Umar, A.A.; Salleh, M.M.; Yahaya, M. *Self-assembled monolayer of copper(II) meso-tetra(4-sulfanatophenyl) porphyrin as an optical gas sensor*. **2004**. Sensors and Actuators B, 101, 231-235.
7. Hong, T.D.; Edgington, S.; Ellis, R.H.; de Muro, M.A.; Moore, D. *Saturated salt solutions for humidity control and the survival of dry powder and oil formulations of Beauveria bassiana conidia*. **2005**. Journal of Invertebrate Pathology, in press.

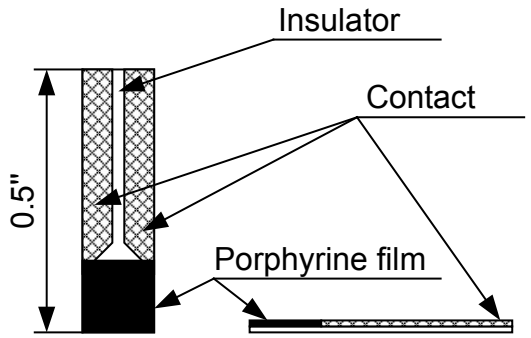

Figure 1. Structure of the sensors employed.

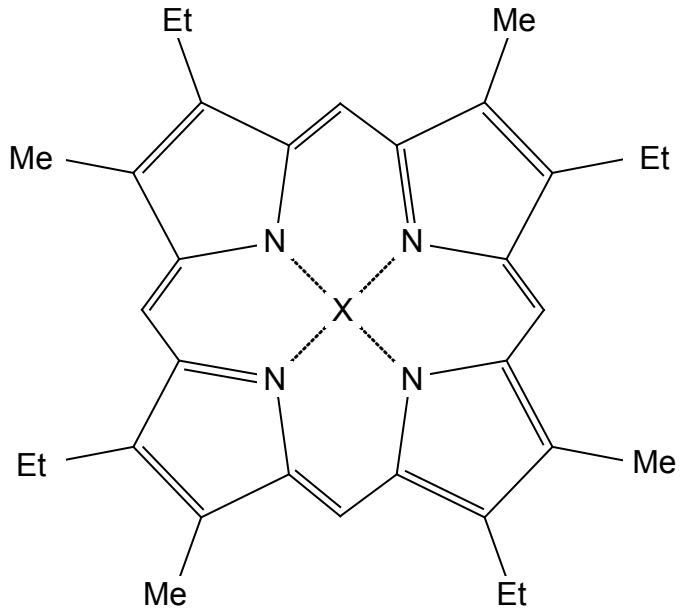

Figure 2. Structure of porphyrins used in this research. X refers to various metals: Co, Cu, VO^{+} and Zn.

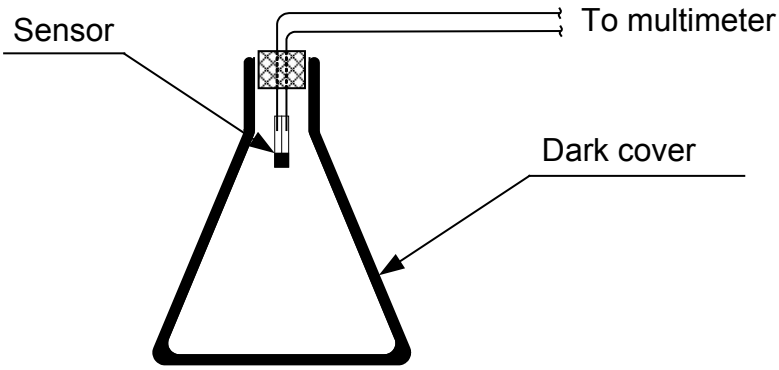

Figure 3. Experimental Set-up.

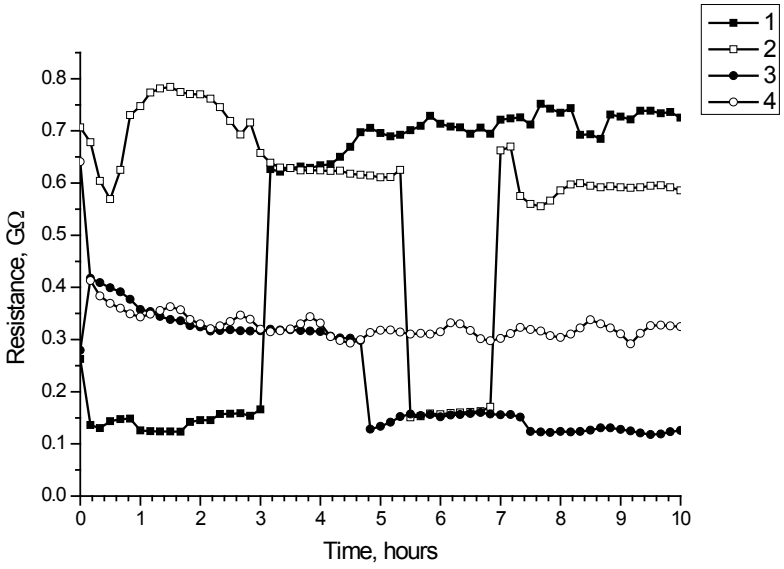

Figure 4. EP- Zn sensor, RH=76%. Four independent collections at the same experimental conditions.

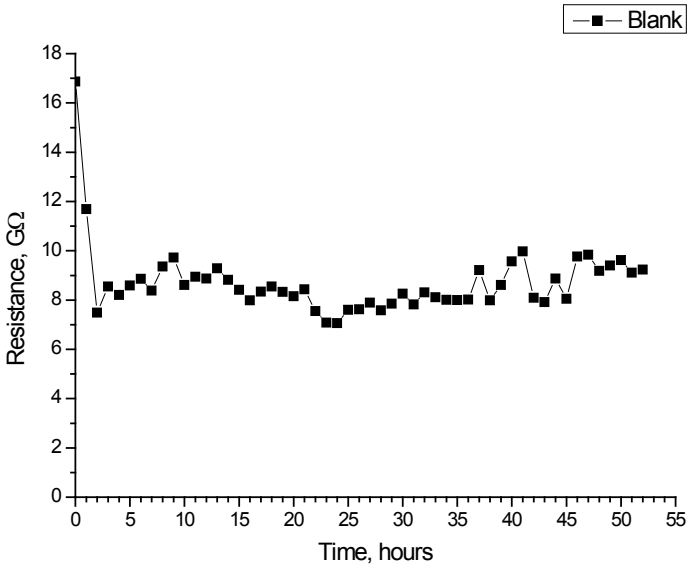

Figure 5. 53-hours experiment for EP - Zn sensor. Data acquisition interval – 1 hour.

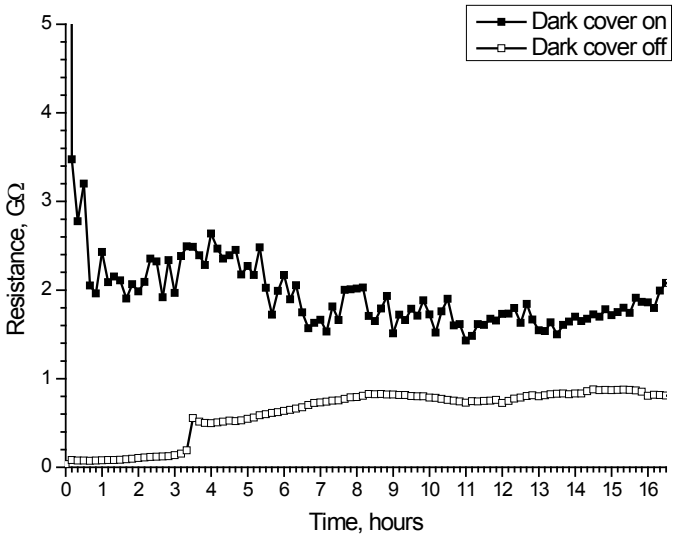

Figure 6. Effect of light on EP - Co sensor. No salt solution was used.

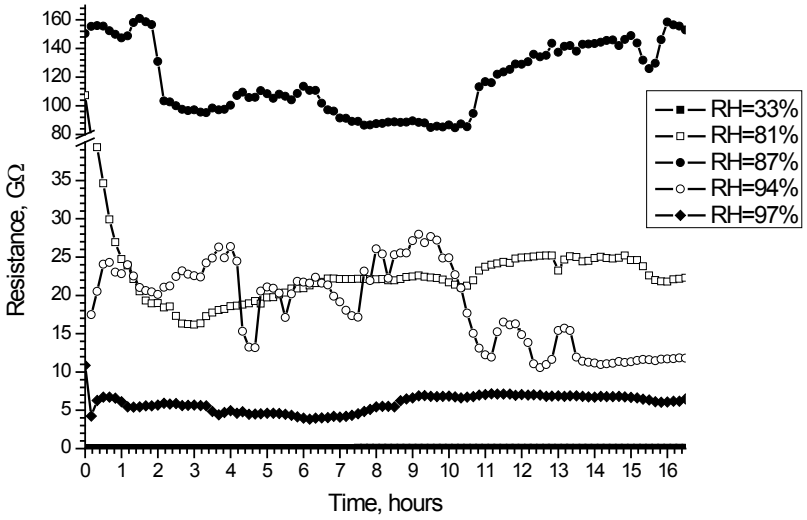

Figure 7. Effect of RH on EP - Cu sensor.

Redox Magnetohydrodynamic Enhancement of Stripping Analysis Using Screen-Printed Carbon Electrodes

Melissa Weston, Colorado State University
Fort Collins, Colorado

Abstract

The use of redox magnetohydrodynamics (MHD) to enhance the stripping analysis response to heavy metals has been investigated. The utility of low temperature co-fired ceramic (LTCC) screen-printed carbon (SPC) electrodes for redox MHD enhanced stripping analysis has also been evaluated. The analytes tested were Cd^{2+}, Cu^{2+}, and Pb^{2+} at concentrations ranging from each metal's individual detection limit to 2 μM. Analytes were codeposited with Hg^{2+}, which formed a Hg thin film on the electrode surface. High concentrations of Fe^{3+} were used to produce a high cathodic current which generates a significant Lorentz force in the presence of a magnetic field. The Lorentz force induces solution convection, enhancing the mass transport of analytes to the electrode, which increases the quantities of analytes preconcentrated into the mercury thin film. The result is larger observed anodic stripping peaks and improved sensitivity when compared to analyses performed in the absence of a magnetic field. The effects on ASV signal of varying Hg^{2+} concentration (0.1 and 1 mM), deposition time (10- 600 s), and electrode surface were investigated. Using disposable LTCC-SPC working electrodes, small volumes (150 μL), and small permanent magnets (0.78 T), peak areas from linear sweep voltammetry were increased by 75% when compared to the signal obtained in the absence of a magnetic field. Limits of detection on the order of 10^{-9} M were achieved with only a 1 min preconcentration time. Use of disposable electrodes, small permanent magnets, and small volumes improved potential for this method to be used in portable devices.

Introduction

We have previously reported the use of high concentrations of Fe^{3+} to enhance anodic stripping voltammetry (ASV) by redox magnetohydrodynamics (MHD).[1] High concentrations of Fe^{3+} in the presence of a magnetic field are used to generate convection near the electrode surface due to the Lorentz force and low concentrations (~1 mM) of Hg^{2+} are used to form the Hg film electrode[2] while codepositing with the analytes. The analyses reported here use these previously reported parameters with low temperature co-fired ceramic (LTCC) screen-printed carbon (SPC) electrodes to perform redox MHD enhanced stripping analysis. In this work, we have determined the detection limits of the method, performed analyses on real samples and reported accuracy, and demonstrated the potential of using redox MHD in portable devices for the analysis of small volumes.

Linear scan ASV is commonly used to analyze metals (e.g. lead, cadmium, copper, thallium, zinc, indium, etc.) in environmental samples, such as sediments[3, 4] and natural waters,[5-9] and in biological samples, such as blood[10-13] and urine.[14-16] It has also been used to detect DNA hybridization.[17-20] In ASV, a deposition (preconcentration) step

reduces chemical species of interest at an electrode and a second step applies a potential function that reoxidizes (or strips) the species.[21] The magnitude of the resulting anodic peak current is proportional to the amount of analyte reduced in the preconcentration step, and therefore, the concentration of analyte in the sample.[5, 21, 22]

In ASV, mercury is widely used as the electrode material of choice due to its large hydrogen overpotential, uniform surface, and suppression of multiple peaks and distorted signals when compared to the direct use of solid electrodes.[23] In this work, a mercury film formation was employed at a solid electrode composed of LTCC that was screen-printed with carbon paste. LTCC is manufactured in the form of flexible tapes and marketed in the form of unfired flexible sheets. It is composed of aluminum oxide, glass frit binder and organic materials.[24] LTCC possesses several advantages, which make it attractive for use as a base for solid electrochemical sensors. LTCC is compatible with high conductivity metals such as silver and gold[24] and can be readily screen printed with resistive materials including carbon paste, as done in this work. LTCC that is screen printed with carbon can be easily mass produced and inexpensive. This makes these LTCC-SPC electrodes attractive for routine, low-cost procedures. The ability of the LTCC-SPC electrodes for use in stripping analysis of trace metals is reported.

In the work described here, the codeposition of analytes with Hg^{2+} (to form a Hg thin film electrode) occurs along with the reduction of a high concentration of Fe^{3+}, to generate a large cathodic current, $\mathbf{J}$ (A/m^2), in the presence of an external magnetic field, $\mathbf{B}$ (T). The resulting Lorentz force, $\mathbf{F_L}$ (N/m^3) acts on the charge-carrying ions to induce solution convection.[25-27] Its magnitude and direction are governed by the right-hand rule.

$$\mathbf{F_L} = \mathbf{J} \times \mathbf{B}$$

The resulting MHD convection enhances the mass transport of analytes to the electrode, resulting in higher quantities of analytes preconcentrated into the mercury thin film. Therefore, larger anodic stripping peaks are observed and sensitivity improves when compared to analyses performed in the absence of a magnetic field. This method of convection is an attractive alternative for applications involving sample volumes too small to allow mechanical stirring or for in-field applications using portable devices that cannot be complicated by the instrumentation required for mechanical stirring.

Experimental detection limits as low as 25 nM are achieved with only a 60 s preconcentration time and small permanent magnets. This analysis time to achieve comparable detection limits is much faster than many devices on the market. There are commercially available devices that can achieve slightly lower limits of detection, but at either lengthy deposition times of 10-20 min,[28] or by use of expensive, specialized electrodes that can cost ~$2000 for an iridium nanoelectrode array alone.[29]

In contrast to the specialized electrodes required for most portable systems with low detection limits, the method reported in this paper uses an inexpensive, readily manufactured electrode. To determine the effectiveness of MHD convection on ASV, we compared results from experiments performed in the absence and presence of a magnetic field. The analytes tested are Cd^{2+}, Cu^{2+}, and Pb^{2+} at concentrations ranging from the individual detection limits to 2 μM. To demonstrate the portability of the redox MHD

enhanced analysis method, small volume analyses (150 μL) was performed using compact NdFeB sintered magnets (~0.78 T). Signal enhancements of ~75% are observed when using the disposable LTCC-SPC electrodes. The effects of varying Hg^{2+} concentration (0.1 and 1 mM), deposition time (10- 600 s), and electrode surface were investigated. Detection limits and studies with a real sample lake matrix were also performed and evaluated for accuracy.

Experimental Procedures

Chemicals and materials. All chemicals were of analytical grade and were used as received. Aqueous solutions were prepared with high purity deionized (DI) water (Milli-Q, model RG). Nitric acid, potassium nitrate, and copper II nitrate pentahemihydrate (all certified ACS grade) were obtained from Fisher Scientific (Fair Lawn, NJ). Mercury II nitrate monohydrate (99.99+%), cadmium nitrate tetrahydrate, and ferric nitrate nonahydrate (99.999+%) were purchased from Aldrich Chemical Co. (St. Louis, MO). Lead II nitrate (99.2%) was acquired from JT Baker Chemical Co. (Phillipsburg, NJ).

Fabrication of carbon paste electrodes on LTCC. The carbon paste (7102, E.I.Dupont and Co) was screen-printed on multi-layered low temperature co-fired ceramic (LTCC) sheets to form the electrodes. For better adhesion, Au paste (5734 conductor paste, E.I.Dupont and Co) was printed as a seed layer onto LTCC tapes. Briefly, the electrode designs were drawn in AutoCAD software (2000 version). Six unpatterned LTCC tapes served as supporting layers for the base of the electrodes. The seventh layer contained the carbon electrode with Au as seed layer. The pre-fired "green" tape 951 AT (E.I.Dupont and Co., Wilmington, DE) was initially cured at 120 ^{0}C for 30 min. Computer numerically-controlled punching was then used to form the registration holes. Stainless steel screens (325.0009 mesh, Hybrid Screen Technologies, Inc.) were used to print the Au. All layers were aligned, stacked, and laminated at 950 psi at 70 ^{0}C for 10 min, and then co-fired in one step with a temperature cycle recommended by Dupont Co. Then the carbon electrodes were formed as a post-fired process on the gold electrodes. A 325.0009 mesh screen was used to screen-print the carbon and cured at 125 ^{0}C for 10 min in a box oven. Then, the electrodes were diced using a silicon carbide saw to appropriate dimensions. Electrical contact to the chip was made with copper wire affixed to the screen-printed carbon (SPC), secured by epoxy, and sealed with heat shrink tubing. The active area on the chip was isolated using a single coat of nail polish (Cover Girl, Noxell Corp.). Electrode area was made to be approximately 2 mm × x 2.5 mm. For the large volume experiments, a platinum flag counter electrode was constructed from a Pt sheet (99.99%, 0.1 mm thick, Alfa AESAR) and spot welded to a Pt wire, the free end of which was sealed in a glass tube where connection was made to a copper wire, and a homemade Ag/AgCl (saturated KCl) was used as the reference electrode. For the small volume experiments, a Pt wire (99.95%, 0.5 mm diameter, Alfa AESAR) was used as the counter electrode, and a 1 mm diameter Ag/AgCl (saturated KCl) (Microelectrodes, Inc., Bedford, NH) was used as the reference electrode.

Electrochemical measurements. An Electrochemical Workstation model 750A (CH Instruments, Inc., Austin, TX) was controlled by a PC computer running CHI-750A software. A Ag/AgCl (saturated KCl) electrode served as a reference. Between

experiments, the potential at the working electrode was held at 0.7 V in electrolyte (30 mM HNO_3 / 0.1 M KNO_3) until mercury from previous experiments was oxidized as indicated by chronoamperometry. The working electrode was then rinsed with DI water. The counter and reference electrodes were rinsed with DI water between experiments.

Large volume experiments. The experimental setup for large volume experiments is shown in Figure 1. An electromagnet (New England Techni-Coil), powered by an EMS 100-50 power supply (Lambda EMI) and cooled by an Affinity F-series chiller (Lydall) was used; magnet poles, with 7.5 cm diameter each were separated by 2.5 cm. A tunable magnetic field strength was obtainable, from 0 to 1.77 T by adjusting the current in the magnet power supply from 0 to 50 A. The electrochemical cell was a round bottom culture tube (14 mL, VWR), to which a hole was drilled in the bottom and Tygon tubing attached. A pinch clamp was secured on the tubing to control flow. The working electrode was placed in the cell so that the surface normal was perpendicular to the magnetic field to achieve a maximum Lorentz force, inducing MHD convection parallel to the electrode surface. The counter electrode was positioned on the bottom of the culture tube, ~1 cm below the working and reference electrodes.[30]

To perform analyses, 1 mL of deposition solution containing analytes (Cd^{2+}, Cu^{2+}, Pb^{2+}), Hg^{2+}, Fe^{3+}, and electrolyte (30 mM HNO_3 and 0.1 M KNO_3) was placed in the culture tube. Analyte solution was deposited for a specific deposition time at –0.8 V. After the deposition, 3 mL of electrolyte were added to the tube, the pinch clamp was opened and solution was drained back to the original, 1 mL, level. This procedure was repeated at 70 and 80 s, with the potential still held at –0.8 V. This rinsing procedure lowers the concentration of Fe^{3+} in solution, which reduces the cathodic background current that results from reduction of the high concentration of Fe^{3+}. A positive potential at 2 V/s for linear sweep ASV is applied at 90 s from –0.8 to 0.4 V to strip the metals.

Small volume experiments. The experimental setup for small volume experiments is shown in Figure 2. The magnetic field was induced from utilization of two permanent magnets oriented in the attracting position at a separation of 0.4 in.. The magnets used were 1” × 1” × 0.5” NdFeB sintered magnets (1.23 T residual induction, 0.55 T on the surface, Magnet Sales Co.). To enhance the magnetic field, a block of 1006 low carbon steel from New England Techni-coil was cut into a U-shape to hold magnets in place. This resulted in a magnetic field strength of 0.78 T. The electrochemical cell was a 2 mL centrifuge tube (VWR), which was positioned between the magnets to achieve maximum magnetic field strength. The working electrode was placed in the cell so that the surface normal was perpendicular to the magnetic field. To perform analyses, 150 μL of the analyte deposition solution was placed in the tube. A deposition potential of –0.8 V was held for 60 s at –0.8 V. After deposition, 1.5 mL of electrolyte was added to dilute the analyte solution, maintaining a potential of -0.8 V. A potential was applied from –0.8 to 0.4 V at a scan rate of 2 V/s to strip the metals.

Results and Discussion

Redox MHD enhancement. A stripping voltammogram of a solution containing 2 μM Cd^{2+}, Cu^{2+}, and Pb^{2+} was obtained using the small volume setup with the 5 mm^2 SPC working electrode and is shown in Figure 3. The analytes are distinguished by their unique redox potentials. At 0.78 T, there is a 75 ± 1.5% (N=3) increase in peak areas

compared to 0 T. The enhancement was calculated based on the anodic peak area for the Pb species. These results indicate that redox MHD could be used with disposable SPC electrodes to enhance stripping signals, which would be useful in a portable device for on-site analyses.

Deposition times and Hg film. The anodic stripping peaks that result from linear scan ASV of solutions containing 2 μM concentrations of Cd^{2+}, Cu^{2+}, and Pb^{2+}, at varying deposition times are shown in Figure 4. Experiments were performed using the large volume setup with a 5 mm^2 SPC working electrode at 0 and 1.77 T. At 10 s deposition times, there is an 80% increase in peak area (based on Pb peak) at 1.77 T, compared to 0 T. The enhancement increases as deposition times increase until it reaches a maximum enhancement at 300 s. There is a 105% increase with 30 s depositions, 189% increase at 60 s depositions, 240% at 300 s, and 212% increase at 600 s deposition times. A more uniform Hg film is formed on the electrode surface at longer deposition times allowing for increased metal deposition and enhanced signals. Increasing the deposition period past 300 s does not increase stripping peaks further. The Hg film thickness, *l*, could be determined by deposition of a solution of 1 mM Hg^{2+} and electrolyte onto the electrode using chronoamperometry at –0.8 V for varying times at 0 T. The peak area was used to calculate the volume of Hg deposited, which was divided by the electrode area to calculate film thickness, *l*. The electrode area used in all calculations was 5 mm^2 for the SPC working electrode. For 10 s depositions, $l = 3.1$ nm; for 30 s depositions $l = 6.9$ nm; for 60 s depositions $l = 12$ nm; for 300 s depositions $l = 47.6$ nm; and for 600 s depositions $l = 89.3$ nm. The mercury film is considered thin film when $l \leq 120$ nm.<reference?> It can be assumed that at 600 s under a magnetic field of 1.77 T, the Hg will form a thick film due to the increased convection enhancing the transport of Hg^{2+} to the electrode surface. Deposition times of 600 s, therefore, result in mercury film electrodes that are thick enough to display semi-infinite behavior. This supports the MHD enhancement reaching a maximum at 300 s deposition time.

The effect of a different concentration of Hg^{2+} on the anodic stripping peaks that result from linear scan ASV is observed in Figure 5. The large volume experimental setup was used with the 5 mm^2 SPC working electrode in a solution of 2 μM Cd^{2+}, Cu^{2+}, and Pb^{2+}, electrolyte, and 100 mM Fe^{3+} at 0 and 1.77 T with a 600 s deposition. An approximate 215% increase in peak area is observed in both the 0.1 and 1 mM concentrations of Hg^{2+}. However, the presence of Cd is only observed with the higher Hg^{2+} concentration due to the increased Hg film coverage.

Electrode type. The effect of the working electrode type and mercury concentration on ASV is shown in Figure 6. A 5 mm^2 SPC and 3 mm GC working electrode were used in the small and large volume experimental setups with 60 s deposition times at 0 T. In the solutions containing 2 μM Cd^{2+}, Cu^{2+}, and Pb^{2+}, 100 mM Fe^{3+}, 1 mM Hg^{2+}, and electrolyte, a fourth peak on the anodic stripping voltammogram is observed at 0.1 and –0.1 V for the GC and SPC electrodes, respectively. This same peak can be seen in solutions containing only electrolyte and 100 mM Fe^{3+}, in which the strip was from bare carbon rather than from a mercury film electrode. These findings indicate that this peak is the Fe^0 stripped from bare carbon. This occurs with the GC electrode when adequate polishing has not been performed, due to a non-uniform Hg film forming on the electrode surface; and with the SPC electrode after many uses when the same non-uniform Hg film begins to form.

Optical microscope images of the GC and SPC electrodes, both bare and with a mercury film, are shown in Figure 7. A 60 s deposition time at –0.8 V in a solution containing 1 mM Hg and electrolyte was performed on new and used SPC working electrodes. It can be observed, from the optical images, that there is poor Hg coverage on the used electrode compared to that of the new electrode. A smooth Hg film covers the surface of the new electrode. The differences seem to be a result of the differences in roughness of the electrode surfaces. Therefore, for the Fe peak becomes more apparent as the uniformity of the Hg coverage decreases, with the number of uses (and increased roughness) of the electrode. When compared to the surfaces of GC electrodes, there are some differences. The Hg film on the GC forms around the edges because of radial diffusion due to the disk shape of the electrode. The effect of increasing Hg^{2+} concentrations can also be seen from the GC images. The Hg film becomes much thicker with the 60 mM Hg^{2+} when compared to that of the 1 mM Hg^{2+}.

Detection Limits. Calibration curve and detection limit data for linear sweep ASV of Cd^{2+} and Pb^{2+} are provided in Table 1. The calibration curve was produced by performing experiments using the small volume experimental setup and a 5 mm^2 SPC working electrode at 0 and 0.78 T. The calibration curves (not shown) were linear in the concentration range from the limit of detection of each species through 1 μM for Cd^{2+} and Pb^{2+}. The experimental limits of detection were calculated based upon the sensitivities of the peak current, determined from linear regression, and the charging current. The limits were the lowest concentrations of the analytes, which resulted in peak currents that were greater than three times the standard deviation of the noise in the current. The equation $C_L = 3\sigma_b/g$, where C_L is the detection limit; σ_b is the standard deviation of the background current; and g is the sensitivity of the peak current (the slope of the calibration curve) was used to obtain the calculated limits of detection. For the Pb species, under a magnetic field strength of 0.78 T, sensitivities were increased by 38% and limits of detection were decreased by 27%; for the Cd species, sensitivities were increased by 33% and limits of detection were decreased by 37% using a magnetic field strength of 0.78 T. Limits of detection for Pb and Cd were found to be 20 and 25 nM, respectively; because this is well below EPA regulated values of 44 and 72 nM for Cd and Pb, respectively, for the highest level of those contaminants allowed in drinking water, makes redox MHD enhanced ASV, using only 60 s deposition times and disposable LTCC SPC electrodes, competitive with other commercially available analysis systems.

Standard Addition. Analyses of pristine simulant samples for lead and cadmium using redox MHD enhanced ASV were performed through calibration via the method of standard additions. The simulated standard addition analyses are shown in Figures 8 and 9. In both Pb and Cd analyses, the small volume experimental setup was used with a 5 mm^2 SPC working electrode in solutions containing the simulant (DI water spiked with 200 nM analyte), 1 mM Hg^{2+}, 100 mM Fe^{3+}, electrolyte, and increasing concentrations of added standard analyte with 60 s deposition times at 0.78 T. Concentrations for the simulants, determined from linear regression, were 197 ± 17 and 212 ± 69 nM for Pb and Cd, respectively. These values have relative standard errors of 1.5% and 6% for Pb and Cd. This indicates that calibration directly via standard addition at 60 s depositions provides accurate results.

A similar standard addition analysis was performed on a real sample water matrix for cadmium and lead. Results of the ASV standard addition analysis of solutions containing lake matrix spiked with 200 nM Pb^{2+} and Cd^{2+}, 1 mM Hg^{2+}, 100 mM Fe^{3+}, electrolyte and added standards for Pb^{2+} and Cd^{2+} are shown in Figure 9. Elemental analysis of the lake water by ICP-MS emission by an outside laboratory using EPA Method 200.8 verified that it did not contain existing Pb or Cd above 1 ppb. Experiments were performed using the small volume setup with 60 s depositions and a 5 mm^2 SPC working electrode. The concentration of the spiked matrix determined from linear regression was 237 ± 40 nM Pb^{2+}. The ability to achieve results for real samples within a reasonable error with only a 60 s preconcentration time and a disposable electrode makes redox MHD enhanced ASV attractive for use as a portable analytical device for environmental applications.

Figure Captions

Figure 1. Experimental setup for large volume (1 mL) experiments with electromagnet. The pinch clamp allows for flow-through mechanism. The Lorentz force is generated by the interaction of the current and magnetic field, which are perpendicular to each other.

Figure 2. Experimental setup for small volume (150 μL) analyses with permanent magnets centered in a 1006 low carbon steel ring. The Lorentz force is generated by perpendicular interaction of the current and magnetic field.

Figure 3. ASV analysis of analyte solution using a 5 mm^2 SPC working electrode in the small volume (150 μL) stripping setup at 0 T (dashed curve) and 0.78 T (solid curve). Linear sweep (2 V/s) was performed after 60 s deposition in solutions containing 1 mM $Hg(NO_3)_2$, 100 mM $Fe(NO_3)_3$, 30 mM HNO_3, 0.1 M KNO_3, 2 μM $Cd(NO_3)_2$, 2 μM $Cu(NO_3)_2$, and 2 μM $Pb(NO_3)_2$ and after dilution with 1.5 mL of electrolyte.

Figure 4. Effect of deposition times on ASV using a 5 mm^2 SPC working electrode and the large volume (1 mL) stripping setup at 0 T (dashed curve) and 1.77 T (solid curve). Linear sweep (2 V/s) was performed after varying deposition times in solutions containing 1 mM $Hg(NO_3)_2$, 100 mM $Fe(NO_3)_3$, 30 mM HNO_3, 0.1 M KNO_3, 2 μM $Cd(NO_3)_2$, 2 μM $Cu(NO_3)_2$, and 2 μM $Pb(NO_3)_2$ and after rinsing three times (3 mL each) over 30 s with electrolyte. Peak areas, based on Pb peaks, increased by 189, 240, and 212%, at 60, 300, and 600 s, respectively, in the magnetic field when compared to that in the absence of the field.

Figure 5. Effect of different concentrations of $Hg(NO_3)_2$ on ASV using a 5 mm^2 SPC working electrode and the large volume (1 mL) stripping setup at 0 T (dashed curve) and 1.77 T (solid curve). Linear sweep (2 V/s) was performed after 600 s deposition in solutions containing varying $Hg(NO_3)_2$ concentrations and 100 mM $Fe(NO_3)_3$, 30 mM HNO_3, 0.1 M KNO_3, 2 μM $Cd(NO_3)_2$, 2 μM $Cu(NO_3)_2$, and 2 μM $Pb(NO_3)_2$ and after rinsing three times (3 mL each) over 30 s with electrolyte.

Figure 6. Effect of electrode type and mercury concentration on ASV; linear sweep (2 V/s) was performed after 60 s deposition time at 0 T. (**a**) 5 mm^2 used SPC working electrode and the small volume (150 μL) stripping setup for a solution containing 1 mM $Hg(NO_3)_2$, 100 mM $Fe(NO_3)_3$, 30 mM HNO_3, 0.1 M KNO_3, 2 μM $Cd(NO_3)_2$, 2 μM $Cu(NO_3)_2$, and 2 μM $Pb(NO_3)_2$ and dilution with 1.5 mL of electrolyte; (**b**) 3 mm GC working electrode and the large volume (1 mL) stripping setup for a solution containing 60 mM $Hg(NO_3)_2$, 100 mM $Fe(NO_3)_3$, 30 mM HNO_3, 0.1 M KNO_3, 2 μM $Cd(NO_3)_2$, 2 μM $Cu(NO_3)_2$, and 2 μM $Pb(NO_3)_2$ and a three times dilution over 30 s with electrolyte (3 mL each time); (**c**) 5 mm^2 new SPC working electrode and the large volume stripping setup for a solution containing 1 mM $Hg(NO_3)_2$, 100 mM $Fe(NO_3)_3$, 30 mM HNO_3, 0.1 M KNO_3 and a three times dilution over 30 s with electrolyte; (**d**) 3 mm GC working electrode and the large volume stripping setup for a solution containing 1 mM $Hg(NO_3)_2$, 100 mM $Fe(NO_3)_3$, 30 mM HNO_3, 0.1 M KNO_3 and a three times dilution over 30 s with electrolyte.

Figure 7. Optical microscope images of: (a) 5 mm^2 SPC electrode before use; (b) used 5 mm^2 SPC electrode after 60 s deposition at -0.8 V in a solution containing 1 mM $Hg(NO_3)_2$, 30 mM HNO_3, and 0.1 M KNO_3; (c) new SPC electrode after 60 s deposition at -0.8 V in a solution containing 1 mM $Hg(NO_3)_2$, 30 mM HNO_3, and 0.1 M KNO_3; (d) 3 mm GC electrode after 60 s deposition at -0.8 V in a solution containing 1 mM $Hg(NO_3)_2$, 30 mM HNO_3, and 0.1 M KNO_3; (e) 3 mm GC electrode after 60 s deposition at -0.8 V in a solution containing 60 mM $Hg(NO_3)_2$, 30 mM HNO_3, and 0.1 M KNO_3.

Figure 8. Standard addition analysis of pristine simulant sample for lead via ASV using a 5 mm^2 SPC working electrode in the small volume stripping setup at 0.78 T. Linear sweep (2 V/s) was performed after 60 s deposition in solutions containing DI water spiked with 200 nM $Pb(NO_3)_2$ and 1 mM $Hg(NO_3)_2$, 100 mM $Fe(NO_3)_3$, 30 mM HNO_3, 0.1 M KNO_3, and varying concentrations of added standard Pb^{2+}.

Figure 9. Standard addition analysis of pristine simulant sample for cadmium via ASV using a 5 mm^2 SPC working electrode in the small volume stripping setup at 0.78 T. Linear sweep (2 V/s) was performed after a 300 s deposition in solutions containing DI water spiked with 200 nM $Cd(NO_3)_2$ and 1 mM $Hg(NO_3)_2$, 100 mM $Fe(NO_3)_3$, 30 mM HNO_3, 0.1 M KNO_3, and varying concentrations of added standard Cd^{2+}.

Figure 10. Standard addition analysis on Fayetteville Lake water matrix for cadmium and lead via ASV using a 5 mm^2 SPC working electrode in the small volume stripping setup at 0.78 T. Linear sweep (2 V/s) was performed after a 300 s deposition in solutions containing lake matrix spiked with 200 nM $Pb(NO_3)_2$ and 200 nM $Cd(NO_3)_2$, and 1 mM $Hg(NO_3)_2$, 100 mM $Fe(NO_3)_3$, 30 mM HNO_3, 0.1 M KNO_3, and varying concentrations of added standards for $Cd^{2+}$and Pb^{2+}.

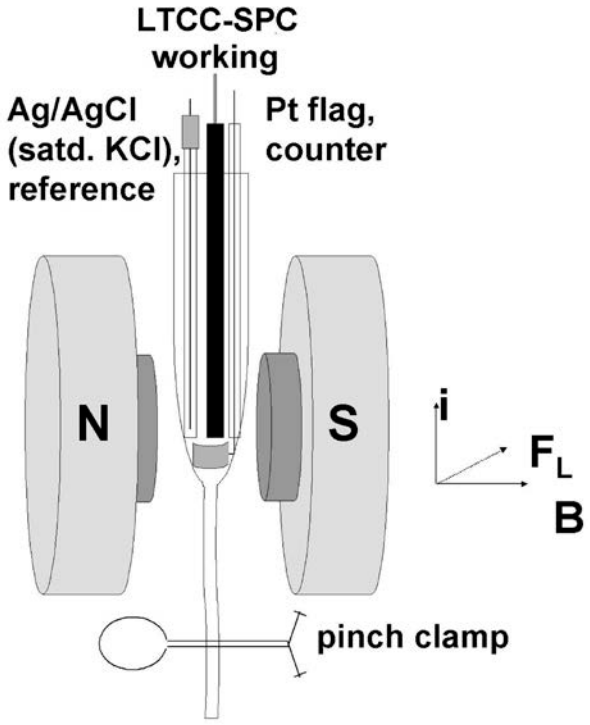
LTCC-SPC
working
Ag/AgCl
(satd. KCl),
reference
Pt flag,
counter
N
S
i
F_L
B
pinch clamp

Figure 1

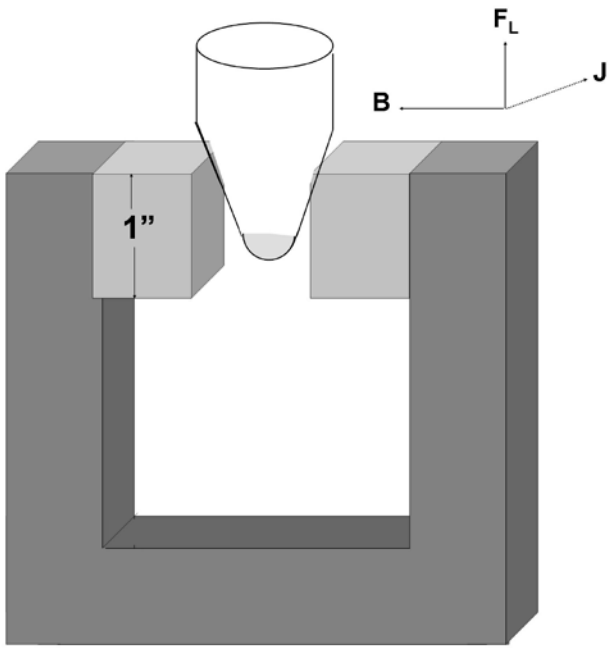

Figure 2

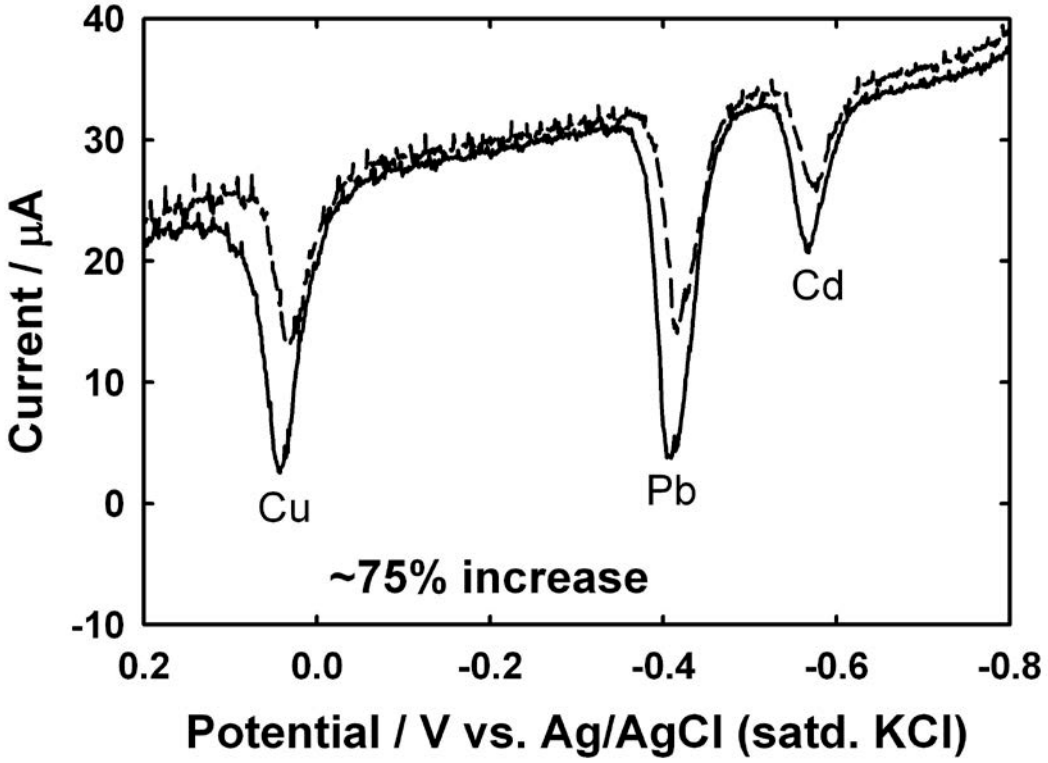
40
30
20
10
0
-10
Current / µA
Cu
Pb
Cd
~75% increase
0.2
0.0
-0.2
-0.4
-0.6
-0.8
Potential / V vs. Ag/AgCl (satd. KCl)

Figure 3

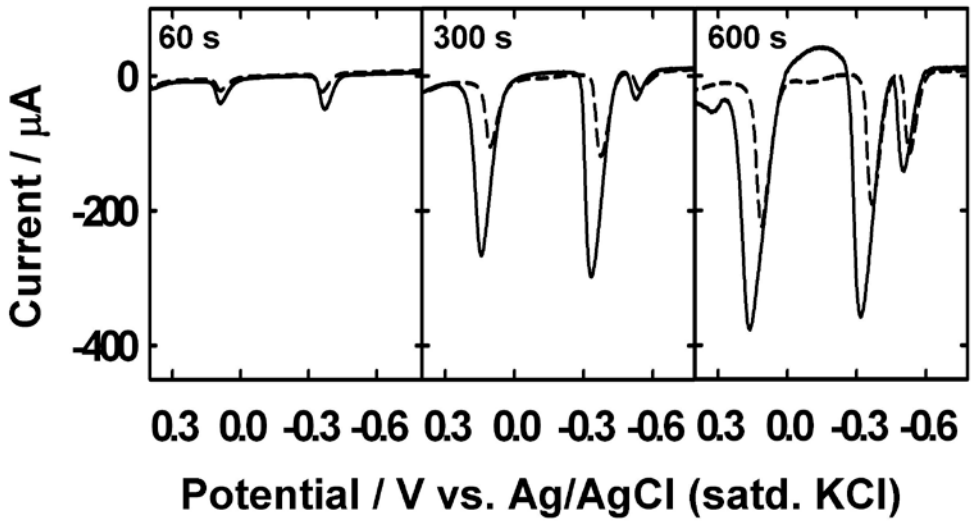
60 s
300 s
600 s
0
-200
-400
Current / µA
0.3 0.0 -0.3 -0.6 0.3 0.0 -0.3 -0.6 0.3 0.0 -0.3 -0.6
Potential / V vs. Ag/AgCl (satd. KCl)

Figure 4

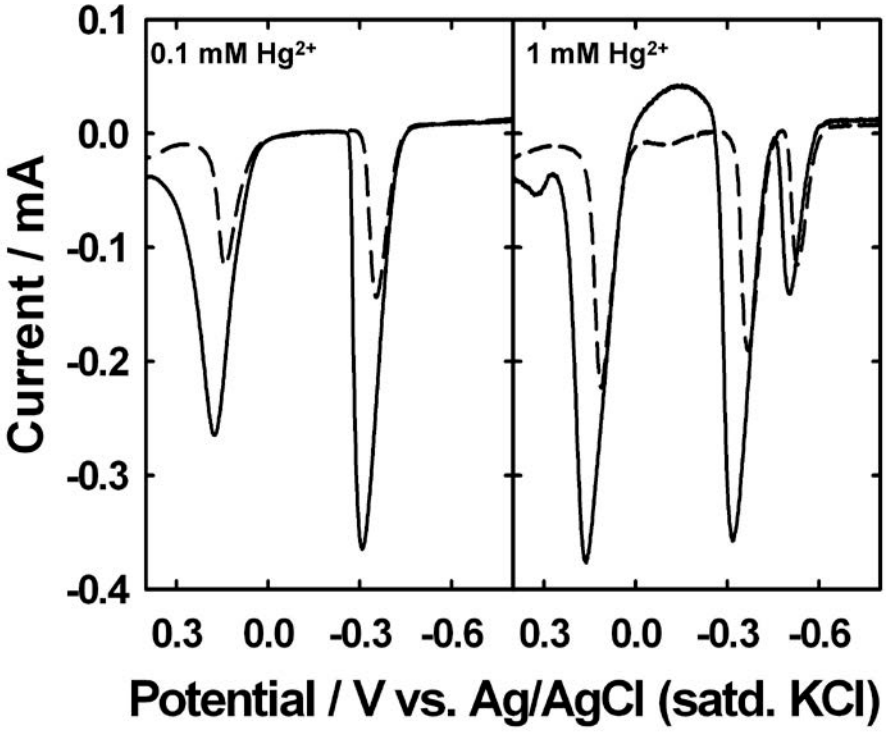
0.1 mM Hg2+
1 mM Hg2+
Current / mA
0.1
0.0
-0.1
-0.2
-0.3
-0.4
0.3
0.0
-0.3
-0.6
0.3
0.0
-0.3
-0.6
Potential / V vs. Ag/AgCl (satd. KCl)

Figure 5

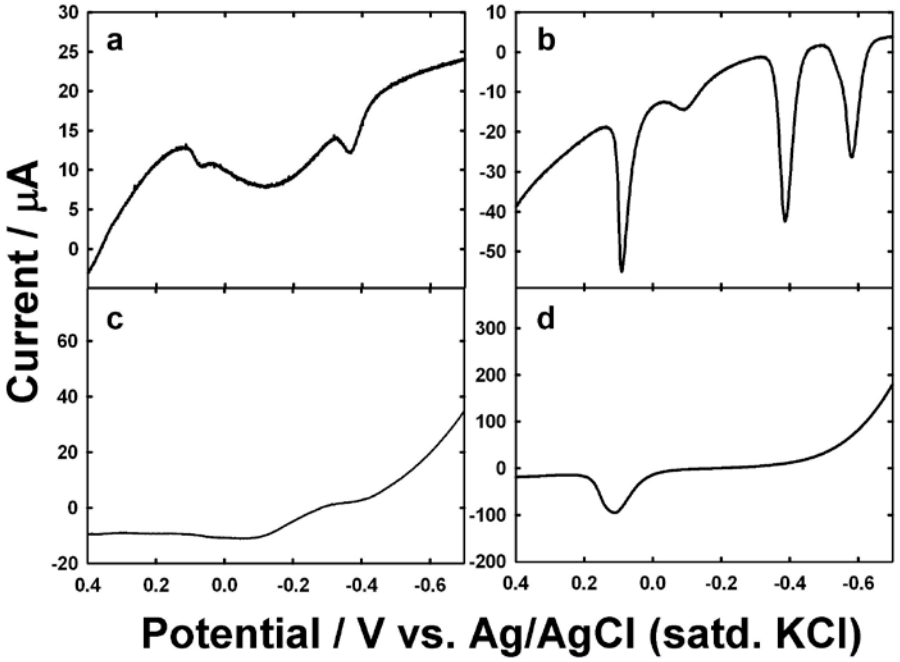

Figure 6

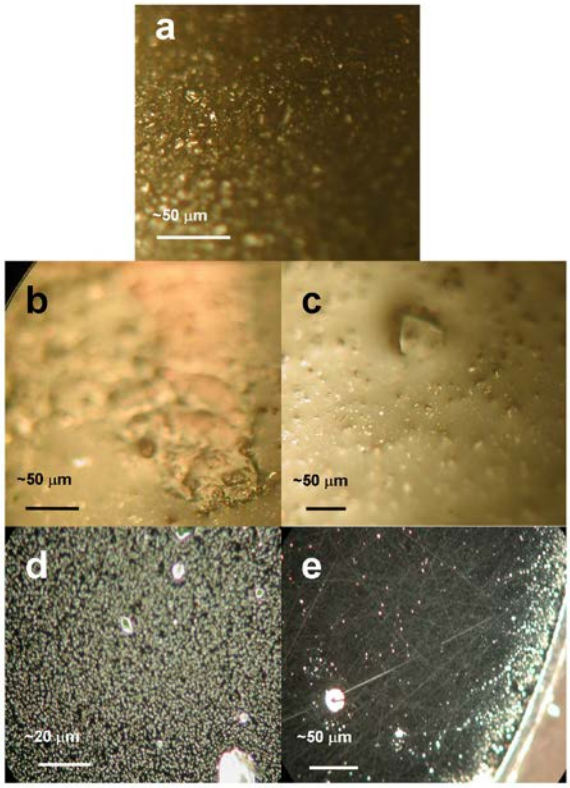

Figure 7

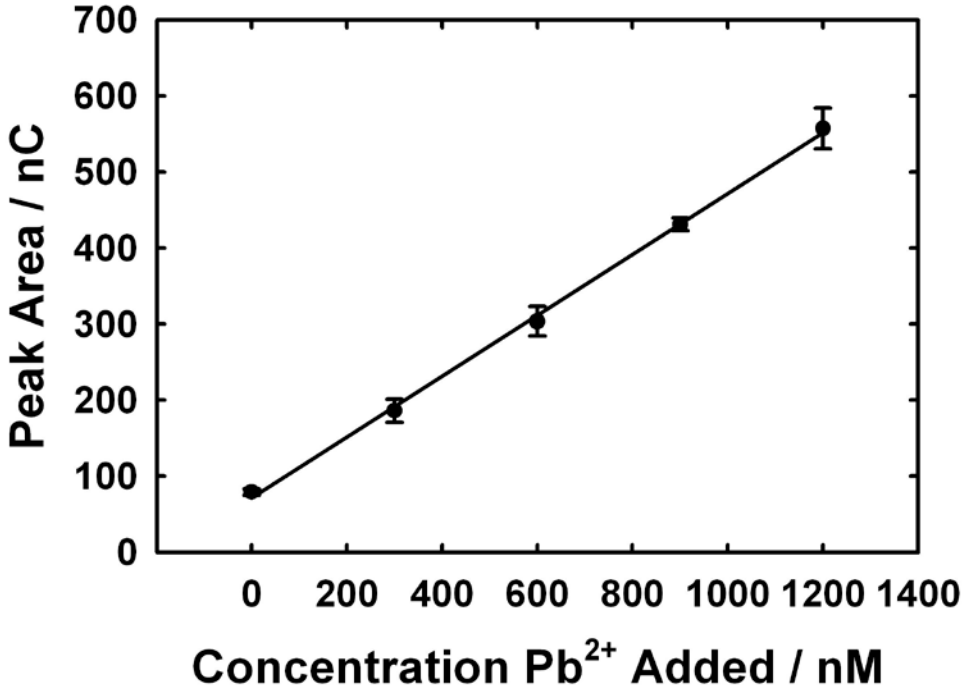
Peak Area / nC
700
600
500
400
300
200
100
0
0
200
400
600
800
1000
1200
1400
Concentration Pb2+ Added / nM

Figure 8

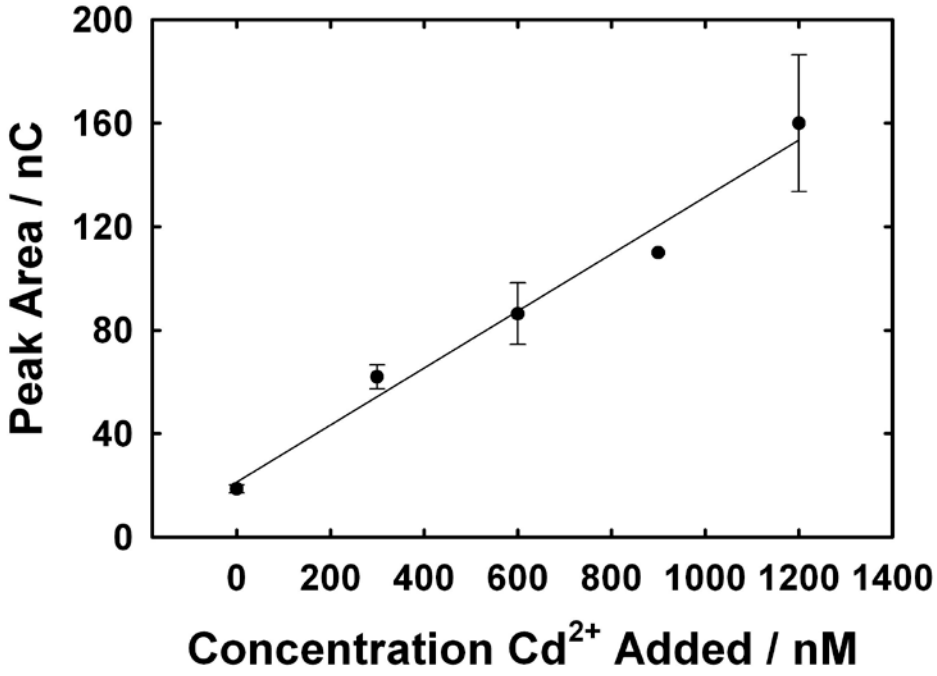
Peak Area / nC
200
160
120
80
40
0
0
200
400
600
800
1000
1200
1400
Concentration Cd2+ Added / nM

Figure 9

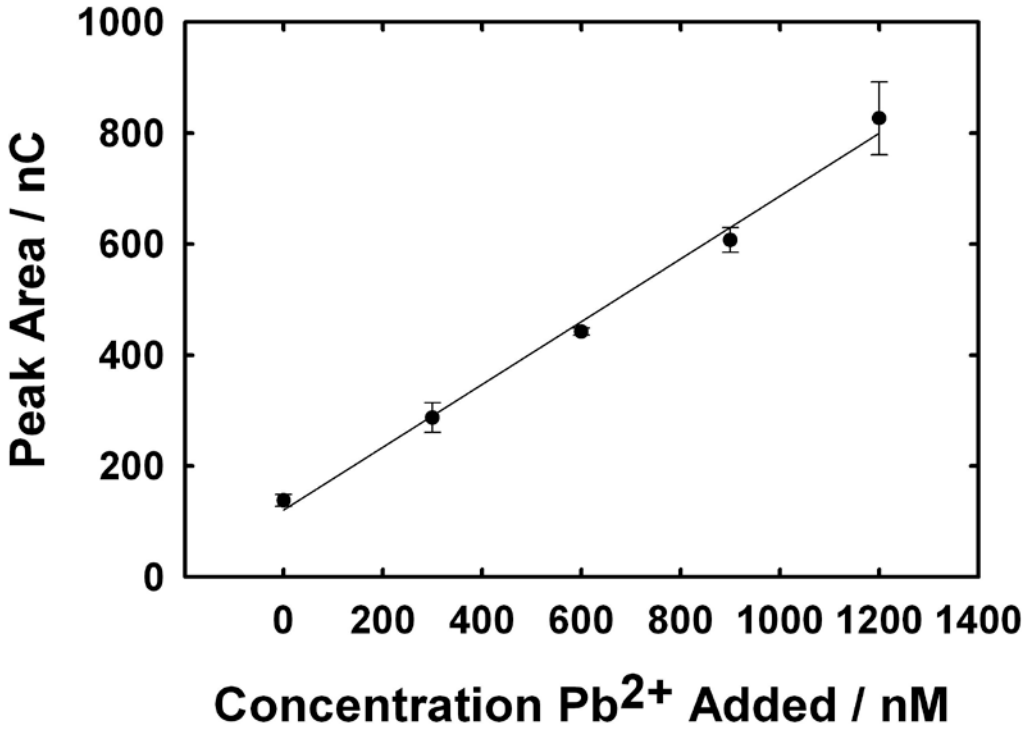
1000
800
600
400
200
0
Peak Area / nC
0
200
400
600
800
1000
1200
1400
Concentration Pb2+ Added / nM

Figure 10

Analyte	Cd^{2+}		Pb^{2+}	
Magnetic Field Strength	**0 T**	**0.78 T**	**0 T**	**0.78 T**
Sensitivity (nC/nM)	0.29	0.57	0.13	0.18
R^2 based on Peak Area	0.999	0.976	0.976	0.988
Sensitivity (mA/nM)	0.011	0.015	5.7×10^{-3}	7.5×10^{-3}
R^2 based on Peak Current	0.998	0.982	0.975	0.989
Experimental Limit of Detection (nM)	50	25	n/a	n/a
Calculated Limit of Detection (nM)	83	63	28	20

Table 1

References

1. Clark, E. A.; Fritsch, I. Anal. Chem. 2004, 76, 2415-2418.
2. Florence, T. M. J. Electroanal. Chem. 1970, 27, 273-281.
3. Olsen, K. B.; Wang, J.; Setladji, R.; Lu, J. Environ. Sci. Technol. 1994, 28, 2074-2079.
4. da Silva, C. L.; Masini, J. C. Fres. Z. Anal. Chem. 2000, 367, 284-290.
5. Petrie, L. M.; Baier, R. W. Analytical Chemistry 1978, 50, 351-357.
6. Emons, H.; Baade, A.; Schoning, M. J. Electroanalysis 2000, 12, 1171-1176.
7. Davison, W. J. Electroanal. Chem. 1978, 87, 395-404.
8. Mart, L.; Nuernberg, H. W.; Valenta, P. Fres. Z. Anal. Chem. 1980, 300, 350-362.
9. Richter, P.; Toral, M. I.; Abbott, B. Electroanalysis 2002, 14, 1288-1293.
10. Prakash, R.; Srivastava, R. C.; Seth, P. K. Electroanalysis 2001, 14, 303-308.
11. Hardcastle, J. L.; Compton, R. G. Electroanalysis 2002, 14, 753-759.
12. Liu, T. Z.; Lai, D.; Osterloh, J. D. Anal. Chem. 1997, 69, 3539-3543.
13. Kruusma, J.; Nei, L.; Hardcastle, J. L.; Compton, R. G.; Lust, E.; Keis, H. Electroanalysis 2004, 16, 399-403.
14. Horng, C.-J. Analyst 1996, 121, 1511-1514.
15. Golimowski, J.; Valenta, P.; Stoeppler, M.; Nurnberg, H. W. Talanta 1979, 26, 649-656.
16. Levit, D. L. Anal. Chem. 1973, 45, 1291.
17. Wang, J.; Liu, G.; Polsky, R.; Arben, M. Electrochem. Comm. 2002, 4, 722-726.
18. Wang, J.; Liu, G.; Merkoci, A. J. Am. Chem. Soc. 2003, 125, 3214-3215.
19. Zhu, N.; Zhang, A.; He, P.; Fang, Y. Electroanalysis 2004, 16, 1925-1930.
20. Authier, L.; Grossiord, C.; Brossier, P. Anal. Chem. 2001, 73, 4450-4456.
21. Bard, A. J.; Faulkner, L. R. Electrochemical Methods: Fundamentals and Applications, 2nd ed.; John Wiley & Sons, Inc.: New York, 2001.
22. Wang, J. Analytical Electrochemistry, 2nd Edition; Wiley-VCH: New York, 2000.
23. Kounaves, S.; Nolan, M. Anal. Chem. 1999, 71.
24. Fakunle, E.; Fritsch, I.; Aguilar, Z. P. Lab on a Chip.
25. Leventis, N.; Gao, X. Journal of Physical Chemistry B 1999, 103, 5832-5840.
26. Grant, K. M.; Hemmert, J. W.; White, H. S. Journal of the American Chemical Society 2002, 124, 462-467.
27. Lee, J.; Gao, X.; Hardy, L. D. A.; White, H. S. J. Electrochem. Soc. 1995, 142, L90-L92.
28. GAT-TEA 4000MP, B., Germany;, 2004.
29. TraceDetect;; Nano-BandTM Electrodes product specifications. Seattle, WA., 2003.
30. Leventis, N.; Chen, M.; Gao, X.; Canalas, M.; Zhang, P. Journal of Physical Chemistry B 1998, 102, 3512-3522.

Analysis of TFA Cleavage Protocols and NMR spectroscopy of RWALP Peptides

Jamesha Wills, Grambling State University
Grambling, LA 71245

Abstract

The objective for this experiment was to investigate the interaction of WALP peptides with arginine head and tail groups. Peptides were synthesized using Solid Phase Peptide Synthesis (SPPS). Three peptides were constructed and consisted of 15 amino acids in which a core of repeating Leu-Ala residues was flanked by Trp and Arg at both ends. The first peptide was RWALP15, acetyl-GRW$(LA)_4$LWRA-amide, the second peptide was an identical RWALP15 having different percentages of deuterated alanines at the $7^{(100\%)}9^{(50\%)}11^{(75\%)}$ positions, and the third peptide was an RWALP15 peptide with the tryptophan tail groups moved into the hydrophobic region at positions 5 and 11 and deuterated alanines at positions $7^{(100\%)}9^{(50\%)}$. These peptides were analyzed using different methods such as NMR, MS, and RP-HPLC. The data from these methods yielded the necessary data to indicate if a harsher cleavage method of the peptides was needed. Cleavages of these peptides were conducted using trifluoroacetic acid (TFA) in different cleavage cocktails to scavenge the peptide's protecting groups. The cocktails increased in scavenger properties as thiols were incorporated to aid in the removal of the protecting groups. Previous analysis of adding arginine (Arg) to a WALP peptide using pentamethylchroman-6-sulfonyl (Pmc) proved difficult to cleave and synthesize. Therefore, a goal for the three peptides that were synthesized and analyzed was to use a different protecting group. The arginine was protected with a pentamethyldihydrobenzofuran-5-sulfonyl (Pbf) group. The cleavage of RWALP15 proved to initially yield desirable results using the less harsh cleavage cocktails. Upon further investigation, it was noticed that the HPLC spectra showed possible degradation or contamination of the peptide when the cleaved sample was re-injected the next day or a few days later. Therefore a harsher cleavage cocktail containing thiols was selected that yielded the desired results shown in figure 4 JW23-26 in the results section.

Introduction

The research being conducted in Dr. Koeppe's lab deals with synthesizing hydrophobic membrane-active peptides of different lengths and amino acid composition to analyze their intrinsic properties. This lab studies several different peptides such as WALP peptides, which were first made by Dr. Denise Greathouse within this lab, and gramicidin A and antimicrobial peptides known as lactoferricin peptides. WALP peptides are named for the amino acid residues that compose the peptide. Therefore, WALP peptides (P) are composed of tryptophan (W) at both ends and poly alanine (A) and leucine (L) centers (5). These peptides have been found to play a role in modulating

the phase behavior of the lipid bilayer. These membrane proteins are able to span the lipid bilayer through interactions of their exposed hydrophobic segments with the lipid hydrocarbon acyl chains (1). By studying the interaction of the side chains, predictions can be made as to the function a particular residue may perform within the lipid bilayer. By knowing the function of a particular protein, predictions can be made about a certain protein and its behavior. This information can help to "typecast" certain medicines or medical applications according to a protein's structure.

Previous research has studied the interaction of synthetic peptides within a lipid bilayer (3). Peptides of different length ranging anywhere from 8 amino acids to >25 were inserted into a bilayer and changes to the lipid's configuration and other properties were studied. It has been shown that when a membrane protein has one or more hydrophobic segments it may span the membrane in an alpha-helical configuration (3). The proteins interact with their environment through hydrophobic interaction within the inner regions of the bilayer, and hydrogen bonding, dipolar and electrostatic interactions within the interfacial region (3). These interactions are being studied to understand the specific roles they may play.

This paper focuses on the synthesis the RWALP15 peptide. As previously stated WALP peptides have already been developed and analyzed. A different angle of the WALP peptide was investigated by adding a charged amino acid (arginine) to each end of the peptide. The initial peptide was fifteen amino acid residues long and has arginines (arg) attached in positions two and fourteen on the peptide with the tryptophan groups attached at positions three and thirteen. Modifications previously stated were made to the peptide and further analysis was conducted. Table1 shows the model WALP15 peptide and the noted modifications for the RWALP15 peptide.

Experimental Procedure

Materials and Methods

Synthesis of 9-Fluorenylomethoxycarbonyl-Alanine (Fmoc-Ala) and Fmoc-Ala deuterated (Fmoc-Ala-d4)

Materials- Fmoc-oxysuccinimide (Fmoc-ONSu), triethylamine (TEA), hydrochloric acid (HCl), sodium hydroxide (NaOH), L-alanine, L-alanine 2,3,3-d4 98%, acetonitrile (ACN), methyl t-butyl ether (MtBE), ethyl acetate (EA), methanol (MeOH), hexane. The chemicals used for synthesis were purchase from Aldrich, NovaBiochem, and solvents were purchased from Burdick & Jackson.

Method- Using a previous outlined protocol within the Koeppe lab, fmoc-Ala was successfully synthesized (4). This protocol is a six-step process revised by a graduate student, which yielded the desired product. The final product was white crystals that tend to aggregate into a thin plate at the bottom of the crystallization vial. During the crystallization step, it was necessary to reduce the volume of the solution with N_2 to promote the formation of crystals. This protocol was repeated for the synthesis of fmoc-Ala-d4. The deuterated version of alanine was inserted where alanine was previously used. Again the synthesis was successful. An NMR sample was prepared to insure desired product was obtained. The ^1H solution NMR spectrum for this sample is shown in NMR appendix figure 1.

Solid Phase Peptide Synthesis (SPPS) for RWALP15 peptides

Materials - Fmoc-Ala-OH, Fmoc-Leucine-OH (Fmoc-Leu-OH), Arginine-Pbf, Tryptophan-Boc, Acetyl-Glycine, Fmoc-Ala-d4, Rink Amide Resin, 433A Peptide Synthesizer. All chemicals used for this synthesis were purchased from AdvancedChem Tech and NovaBiochem; the synthesizer is from PE Applied Biosystems. The deuterated alanine used was from above synthesis.

Method -There is a four-step process used to prepare a synthetic peptide. The initial step is known as Solid Phase Peptide Synthesis. The basic analogy is that a growing peptide is covalently attached to insoluble polystyrene resin beads. This process decreases the probability of peptide being loss during filtration and washing. The pre-step is known as loading. During this step the resin beads are "loaded" with a peptide specific amino acid. For synthesizing the RWALP15 peptides, the rink resin was loaded with Fmoc-Ala for use. The resin was tested for the concentration of amino acid that bonded to the bead. From the calculations a 0.61 mmol/g substitution was shown for this resin load. This particular peptide takes approximately three days to make before analysis can be performed. The first step is placing the loaded resin into the peptide synthesizer cartridge where the specific amino acids are added covalently during specific cycles to the resin, as the cycles repeat the chain increases in length. The table below shows the peptides that synthesized for analyses, these peptides differ in their primary structures. 638B was a straight chain RWALP15 peptide. The second peptide 638C incorporated deuterated alanines at the indicated places. Peptide 643 was synthesized to analyze changes due to moving the anchoring tryptophan groups from the tails of the molecule to the hydrophobic core. MALDI-TOF MS was conducted on the first two peptides and a sample was prepared on the third peptide for future MS analysis.

Model:
WALP15 Ac-GWWLALALALALWWA-ethanolamide
Sequences:
RWALP15a Ac-G*R*WLALALALALW*R*A-amide
RWALP15a Ac-G*R*WLAL*A*L*A*LA*A*LW*R*A-amide
RWALP15b Ac-G*R*ALWL*A*L*A*LWLA*R*A-amide

			1	2	3	4	5	6	7	8	9	10	11	12	13	14	15	
Model Peptide:																		
WALP15		Ac	G	W	W	L	A	L	A	L	A	L	A	L	W	W	A	
RWALP15	638B	Ac	G	R	W	L	A	L	A	L	A	L	A	L	W	R	A	NH
RWALP15	638C	Ac	G	R	W	L	A	L	Ad4 100%	L	Ad4 50%	L	Ad4 75%	L	W	R	A	NH
RWALP15	643	Ac	G	R	A	L	W	L	Ad4 100%	L	Ad4 50%	L	W	L	A	R	A	NH

Table 1: Synthesized WALP15 peptides

Cleavage of Peptides

Materials- Trifluoroacetic acid (TFA), distilled H_2O, phenol, triisopropylsilane (TIPS), thioanisole, ethanedithiol (EDT), 2,2,2 trifluoroethanol (TFE) and methyl-t-butyl ether/hexane (50:50). All chemicals used were ordered from Aldrich unless otherwise noted. The TFA was purchased from Pierce. The phenol used was re-crystallized in the lab, as well as the water was distilled in house.

Method- The second step is the cleavage step. During this phase the protecting groups that were placed on the amino acid residues to minimize side-reactions will be removed using cocktails. The peptide is also cleaved from the resin during this process. There are several "cleavage cocktails" used and the cocktails generally are peptide specific at certain chain lengths and residues. Table 2 shows the cleavage cocktails used for these peptides.

Reagent B	Reagent K
88% Trifluoroacetic Acid (TFA)	82.5% Trifluoroacetic Acid (TFA)
5% dH_2O	5% dH_2O
2% Triisopropylsilane (TIPS)	5% Thioanisole
5% Phenol	2.5% Ethanedithiol (EDT)
	5% Phenol

Table 2: Cleavage cocktails used

There are two types of cleavages, a small scale and a large scale. For the small-scale cleavage, reagent B cocktail was prepared and place on motomixer to stir continuously for a total of 24 hours at room temperature 25^{o}C. A dilution of the peptide from the cleavage solution was made at one, two, three, four, six, and twenty-four hours. The data yielded from RP-HPLC showed a peak at ~4.0 minutes for each of the samples. This indicates that the peptide is eluting off the column at around the same time. The only noticeable change was the intensity of the peak. The data shown in the HPLC Appendix indicated that at the 3rd hour sample had the greatest elution peak (Figure 4 JW9). Because these results were favorable, an upscale cleavage was the next step. Cleaving on a larger scale helps to check the data and see if it is reproducible. Large-scale cleavage is also necessary to produce sufficient quantities of the peptide for experiments. The first large-scale cleavage of RWALP15 638B used the same reagents but was a two-step process. The peptide was added to cocktail reagent B and allowed to stir for 3 hours on a mechanical stirrer wrapped in foil. This solution was filtered and washed with 2 ml neat TFA and the volume of the solution was reduced to ¼ by blowing N_2 over it. This reduced solution was added drop-wise to cold MtBE/Hexane (in an ice bath) and allowed to sit for 30 minutes. A white precipitate formed and was centrifuged for 10 minutes at 1500 rpm's at 4^{0}C to get a pellet. The precipitation process was repeated 3 times adding fresh cold MtBE/Hexane each time and increasing the rpm of the centrifuge by 100 rpms. The pellet was then dissolved in TFE and N_2 was used to evaporate the solution to a film. 500µL of ACN and 500µL dH_2O was added to the film. The solution was then freeze dried with liquid nitrogen to a white powder and placed on the vacuum line overnight. The powder was dissolved for quantitation analysis in TFE and a 1mg/mol HPLC sample was made to confirm purity. The data from cocktail B initially yielded similar results as the small-scale analysis. Upon further analysis the cleavage seem to degrade when solution was left in the refrigerator for a couple of days and re-injected onto HPLC (See

figure 4 JW16-22). Therefore cleavage cocktail K was used and following the high-scale cleavage outlined above yielded more favorable results for cleavage (See figure 4 JW 23-26).

Characterization

Materials- Hitachi Pump L-7100 column Zorbax SB-C8 (4.6*5.00mm)-HPLC, Hewlett Packard 8452A Diode Array Spectrophotometer-UV-Vis, Bruker NMR (^{2}H probe, ^{31}P probe, NMR tubes)

Method-The third step is known as the characterization step; at this point the synthesized peptide is checked to make sure the right product was yielded. The most common methods used for characterization are UV spectroscopy, reversed-phase high performance liquid chromatography (RP-HPLC), sequence analysis, ^{31}P and ^{2}H NMR (only for certain peptides), and matrix-assisted laser desorption ionization time-of-flight mass spectrometry (MALDI/TOF MS). All of these methods were used excluding sequence analysis. UV was used to quantitate the peptide by detection of absorbance of tryptophan groups at 280 nm. Beer's Law was used to calculate dilution factors for HPLC analysis. RP-HPLC was used for analysis purposes to show eluted peptide peak and impurities. ^{31}P and ^{2}H NMR was used to analyze the phospholipid bilayer and peptide respectively. Using DMPC and DLPC liquid-crystalline lipid bilayers, oriented hydrated samples of the peptide was made. The oriented sample was from peptide RWALP15-638C. The results shown in figure 5 indicate a small tilt of the peptide. The MALDI-TOF MS was used to insure that the correct mass of the peptides was obtained. From the spectra shown in figure 6 the correct molecular mass of 1722 grams/mole was obtained.

Purification

Materials- HPLC apparatus

Method-The fourth step is the purification step and is performed using the preparative HPLC and is only used when needed. I did not need to purify my samples using this method.

Results and Discussion

The spectra for all methods are listed in the Appendices. The data from these spectra support the results discussed in the methods section of each procedure.

Using SPPS, the peptides were successfully synthesized. This is confirmed through the mass spectrum which indicated the correct molar masses for the 638B and 638C peptides. The chromatograms showed few impurities.

For the cleavage process, the thiol cocktail was preferred over the TIPS cocktail for these peptides containing Arg groups with the Pbf protecting group. The advantages for using thiols were sharper peptide peaks, less unknown peaks, and better results upon further analysis.

From the ^{31}P-NMR it was determined that the incorporated 638C peptide was compatible with the DMPC lipid bilayer. The spectrum also showed an 85% orientation of the bilayer. The small shoulder on the $\beta = 0$ spectrum could be due to the lack of complete orientation or overlapping of the bilayer.

The ^{2}H-NMR showed that the peptide did insert into the bilayer. Also, the peptide rotates rapidly about a line normal to the lipid bilayer. This fact is known from the factor of two reduction in the quadrupolar splitting when the sample is changed from $\beta = 0$ to $\beta = 90^{o}$. The peptide most likely has a helical secondary structure; noted from the repeated pattern of large and small quadrupolar splittings. A defined average orientation is noted in which the peptide's helical axis is somewhat tilted with respect to the bilayer normal. The tilt is not random but has a particular direction with respect to Arg-2 and Trp-3 groups in the 638C peptide. The tilt was estimated to be approximately 10^{o}; precise calculations will be established upon further measurements.

Conclusion

In conclusion, synthesis of the RWALP15 peptide was successfully obtained. It was determined from the results; that better purity was achieved using Arg-Pbf as opposed to using Arg-Pmc. The cleavage of RWALP peptides with Arg-Pbf is more effective using thiols than TIPS. For preparing large-scale cleavages, a mixing time of 3hours produced the maximum yield of cleaved peptide using TIPS cleavage. Also, for the oriented ^{31}P and ^{2}H NMR spectra it was determined that RWALP15 peptides have a distinct yet relatively small tilt. This realization holds because of the small size of this particular peptide. These methods pave the way for many new experiments concerning the interactions of (Arg, Trp)-anchored peptides with lipid bilayer membranes. My advisor therefore has said that these are "ground-breaking" experiments.

References

1. De Planque, M.; Kruijtzer J.; Liskamp, R.; Marsh, D.; et al. *The Journal of Biological Chemistry.* **1999**. Vol. 4, No.30. 20839-20846.
2. Greathouse, D., *FMOC-Solid Phase Peptide Synthesis.* Spring **1998**. CHEM 4853; *Methods Enzymology.* **1999.** 294. 525-550.
3. Killian, J. A., *FEBS Letters 555.* **2003**. FEBS 27772. 134-138.
4. Rankenberg, A., *Anne's Revised Method for Preparation of Fmoc-Amino Ala.* 2005. Method revised from Kortenaar, P., et al., Int. J. Pep. Prot. Res. **1998**. 27. 398-400.
5. Killian, J. A., et al. *Biochemistry.* **1996.** *35. 1037-1045.*

[i] Watkins,D.M.; Sayed-Sweet, Y.; Kilmash, J.W.; Turro, N.J., Tomalia,D.A. (1997) Dendrimers With Hydrophobic Cores and the Formation of Supramolecular Dendrimer-Surfactant Assemblies. *Langmuir.* 13, 3136-3141

[ii] Karakhanov, E.A.; Maksimov, A.L.; Runove, E.A. (2005) Design of supramolecular metal complex catalytic systems for organic and petrochemical synthesis. *Russian Chemical Reviews.* 74, 97-111

[iii] Boas, U.; Heegaard, P.M.H. (2003) Dendrimers in Drug Research. *Chem. Soc. Rev*. 33, 43-63

[iv] Jansen, J.F.G.A.; de Brabander-van den Berg, E.M.M.; Meijer, E.W. (1994) *Science*. 226, 1226-1229

[v] Smith, D.K.' Diederich. F.; (1998) Functional Dendrimers: unique Biological Mimics. *Chem. Eur. J.* 8, 1353-1361

[vi] Konstantinova, I.D.; Zaitseva, I.P.; Ushakova, I.P.; Serebrennikova, G.A. (1994) Synthesis of cationic ether lipids of alkyl type with short-chain substituents at the 2-position of the glycerol backbone. *Russian Chemical Bulletin. Vol 43, No. 10,* 1731-1735

[vii] Maslov, M.A.; Syicheva, E.V.; Morozova, N.G.; Serebrennikova, G.A. (2000) Cationic amphiphiles of both lipid and nonlipid nature in gene therapy. *Russian Chemical Bulletin, Vol. 49, No. 3.* 385-401

[viii]Pollard, Helene.; Remey, Jen-Serge.; Loussouarn, Gildas.; et. al (1998). Polyethlenimine but not Cationic Lipids Promotes Transgene Delivery to the Nucleus in Mammalian Cells *J Biol Chem.* 213, 7507-7511

[ix] Takahashi, Toshinari.; Kono, Kenji.; Itoh, Toshihide.; Emi, Nobuhiko.; Takagishi, Toru. (2003) Synthesis of novel cationic lipidshaving polyamidoamine dendrons and their transfection activity. *Bioconjugate Chem. 14,* 764-773

[x] Denmeneix, B.A,; Goula, D.; Benoist, C.; Remy, J.S.; Behr, J.P. *GeneTherepy*, Ed, K. G. Xanthopoulos, Springer, 1998, 195.

[xi] de Brabander-van den Berg, E.M.M; Maijer, E.M. Poly(propylene imine) Dendrimers: Large-Scale Synthesis by Heterogeneously Catalyzed Hydrogenations. *Angew. Chem. Int. Ed. Engl*. 32, No 9, 1308-1311

[xii] Taflin, D.C.; Ward, T.L.; Davis, E.J. (1989) Electrified Droplet Fission and the Rayleigh Limit. *Langmuir*. 5, 376-384

[xiii] Dole, M.; Mack, L.L.; Hines, R.L.; Mobley, R.C.; Ferguson, L.D., Alice, M.B. (1968) Molecular Beams of Macroions. *J. Chem. Physics*. 49, 2240-2249

[xiv] Iribarne, J.V.; Dziedzic, P.J.; Thomson, B.A. (1983) Atmospheric Pressure Ion Evaporation-Mass Spectrometry. *Int. J. Mass. Spectrom. Ion. Phys.* 50, 331-347

[xv] Cech, N.B.; Enke, C.G. (2001) Practical Implications of Some Recent Studies in Electrospray Ionization Fundamentals. *Mass Spectrometry Reviews*. 20, 362-387

[xvi] Oldham, N.J.; Lissina,O.; Nunn, M.A.; Paesen, G.C. (2003) Non-Denaturing Electrospray Ionization-Mass Spectrometry Reveals Ligand Selectivity in Histamine-Binding Protien RaHBP2. *Org. Biomol. Chem*. 1, 3645-3646

[xvii] Demmers, J.A.A.; van Dalen, A.; de Kruijff, B.; Heck, A.J.R. ; Killian, J.A. (2003) Interaction of the K+ Channel KcsA With Membrane Phospholipids as Studied by ESI Mass Spectrometry. *Federation of European Biochemical Societies*. 541, 28-32

[xviii] van der Wal, Sj.; Mengerink, Y.; Brackman, J.C., de Brabander, E.M.M.; Jeronimus-Stratingh, C.M.; Bruins, A.P.; (1998) Compositional Analysis of Nitrile Terminated Poly(propylene imine) Dendrimers by High-Performance Liquid Chromatography Combined With Mass Spectrometry. *Journal of Chromatorgraphy*. 825, 135-147